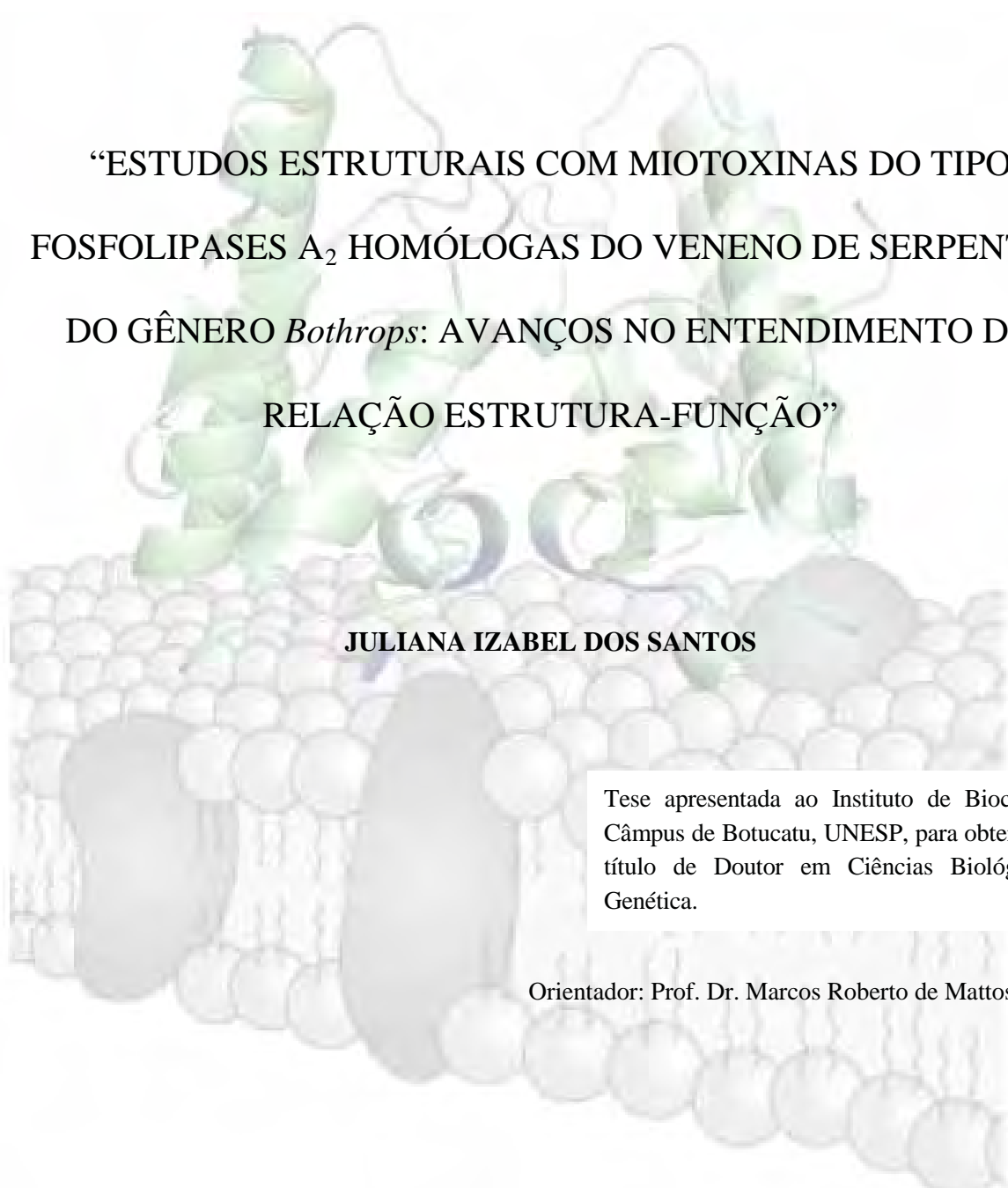


UNIVERSIDADE ESTADUAL PAULISTA

“Júlio de Mesquita Filho”

INSTITUTO DE BIOCÊNCIAS DE BOTUCATU



“ESTUDOS ESTRUTURAIS COM MIOTOXINAS DO TIPO
FOSFOLIPASES A₂ HOMÓLOGAS DO VENENO DE SERPENTES
DO GÊNERO *Bothrops*: AVANÇOS NO ENTENDIMENTO DA
RELAÇÃO ESTRUTURA-FUNÇÃO”

JULIANA IZABEL DOS SANTOS

Tese apresentada ao Instituto de Biociências,
Câmpus de Botucatu, UNESP, para obtenção do
título de Doutor em Ciências Biológicas –
Genética.

Orientador: Prof. Dr. Marcos Roberto de Mattos Fontes

**BOTUCATU - SP
2011**

UNIVERSIDADE ESTADUAL PAULISTA

“Júlio de Mesquita Filho”

INSTITUTO DE BIOCÊNCIAS DE BOTUCATU

“ESTUDOS ESTRUTURAIS COM MIOTOXINAS DO TIPO
FOSFOLIPASES A₂ HOMÓLOGAS DO VENENO DE SERPENTES
DO GÊNERO *Bothrops*: AVANÇOS NO ENTENDIMENTO DA
RELAÇÃO ESTRUTURA-FUNÇÃO”

JULIANA IZABEL DOS SANTOS

PROF. DR. MARCOS ROBERTO DE MATTOS FONTES

Tese apresentada ao Instituto de Biociências,
Câmpus de Botucatu, UNESP, para obtenção do
título de Doutor em Ciências Biológicas –
Genética.

**BOTUCATU - SP
2011**

Tese de doutorado

dos Santos, Juliana Izabel.

Estudos estruturais com miotoxinas do tipo fosfolipases A₂ homólogas do veneno de serpentes do gênero *Bothrops*: Avanços no entendimento da relação estrutura-função / Juliana Izabel dos Santos. - Botucatu, 2011

Tese (doutorado) - Instituto de Biociências de Botucatu, Universidade Estadual Paulista, 2011

Orientador: Marcos Roberto de Mattos Fontes

Capes: 20901003

1. Biofísica Molecular.

Palavras-chave: Miotoxina; fosfolipase A₂ homóloga; Ácido rosmarínico; Veneno Botrópico; Cristalografia de proteínas

Às vítimas de envenenamento botrópico

Agradecimentos

Ao professor Dr. Marcos Roberto de Mattos Fontes, por me confiar este trabalho, pelas oportunidades e também pelas conversas que me propiciaram crescimento científico;

Ao prof. Dr. Andreimar Martins Soares, pelo fornecimento das amostras que foram utilizadas neste trabalho;

À Fundação de Amparo à pesquisa do Estado de São Paulo (FAPESP) pela bolsa concedida (processo nº 2007/59084-8);

Ao Laboratório Nacional de Luz Síncrotron (LNLS), por disponibilizar suas instalações para as coletas de dados;

Ao mestrando Rafael Junqueira Borges, com quem dividi a realização de parte deste trabalho;

À Cilene do Carmo Frederici Padilha, pelas ajudas quando necessitei;

Ao prof. Dr. Pedro Padilha, pelas valiosas explicações sobre coordenação de compostos;

Ao Dr. André Ambrosio, pelo auxílio no início do processamento dos dados anômalos;

À minha família, em especial minha mãe que esteve presente em todos os momentos;

Ao prof. Dr. Paulo Ramos e aos funcionários Cilene, Meire, Silvia e Edson, pelas conversas e cafezinhos;

Aos colegas e amigos do Laboratório de Biologia Molecular Estrutural e Depto. de Física e Biofísica pelas ajudas e brincadeiras que tornaram o dia-a-dia mais agradável;

Aos amigos que estiveram presente nestes dois anos.

À turma do voleibol, em especial à Juliana, ao Amauri, à Eneida, ao Heraldo e Erika, que propiciaram momentos de descontração neste período.

“Para ser grande, sê inteiro.

Nada teu exagera ou exclui.

Sê todo em cada coisa.

Põe quanto és no mínimo que fazes.

Assim em cada lago a lua toda brilha, porque alta vive.”

(Fernando Pessoa)

Resumo

O envenenamento por picadas de serpentes é um importante problema de saúde pública em muitos países tropicais e subtropicais. Aspectos científicos, médicos e sociais relacionados ao envenenamento por serpentes do gênero *Bothrops* são especialmente importantes no Brasil já que estes animais são responsáveis por aproximadamente 90% dos acidentes ofídicos relatados em nosso país. Um dos principais problemas relacionados ao acidente botrópico é o proeminente dano tecidual local cuja patogênese é complexa e envolve a ação combinada de uma variedade de componentes do veneno. As fosfolipases A₂ (PLA₂s) são os componentes mais abundantes no veneno e tem papel fundamental quando se trata do estabelecimento de lesão muscular. O presente trabalho descreve estudos estruturais com miotoxinas que adotam enovelamento de PLA₂s (PLA₂s homólogas) com o objetivo de melhor entender a relação estrutura – função destas toxinas. Para tanto, estudos estruturais por cristalografia de difração de raios X com Lys49-PLA₂s de venenos botrópicos complexadas com os inibidores manganês e ácido rosmarínico (AR) foram realizados. A estrutura cristalográfica de uma miotoxina Asp49-PLA₂ homóloga complexada com cálcio também foi elucidada. Adicionalmente, o arranjo quaternário de miotoxinas Asp49-PLA₂s homólogas do gênero *Bothrops* foi revisado e características estruturais relevantes para a expressão da miotoxicidade destas proteínas foram apontadas. A estrutura cristalográfica do complexo formado entre uma Lys49-PLA₂ e o inibidor AR evidencia que este inibidor interage com a proteína na entrada de uma dos canais hidrofóbicos do dímero protéico, estabelecendo ligações de hidrogênio com átomos dos resíduos Phe3, Lys7, Leu10, Gln11 e Gly15 do monômero com a qual interage. Já no complexo formado entre uma Lys49-PLA₂ e o inibidor Mn²⁺, fica demonstrado que o Mn²⁺ é coordenado por átomos dos resíduos de ambos os monômeros da toxina (resíduos Asn17 e Ala19 de um monômero e His120 e Lys122 do outro), interagindo diretamente no canal hidrofóbico. Desta forma, apesar de a região C-terminal das Lys49-PLA₂s ser bem definida como o sítio miotóxico destas proteínas, nossos resultados enfatizam a importância do canal hidrofóbico para o mecanismo de ação das mesmas. O estudo do complexo formado entre a Asp49-PLA₂ homólogas e íons cálcio demonstrou que esta miotoxina não é capaz de coordenar Ca²⁺ no *loop* de ligação de cálcio, dando suporte para um recente estudo que demonstra a não-atividade catalítica destas proteínas. Uma revisão da estrutura quaternária destas Asp49-PLA₂s diméricas utilizando ferramentas de bioinformática indicou que a disposição dos monômeros destas proteínas em solução é diferente daquela adotada na resolução de suas estruturas cristalográficas. Nesta configuração alternativa, os *loops* de ligação de cálcio destas miotoxinas estão na interface. Esta observação provavelmente é uma consequência da distorção do *loop* de cálcio observado em Asp49-PLA₂s miotóxicas que, além de propiciar a formação de uma nova interface, também confere suporte mecânico para a provável região responsável pela expressão da miotoxicidade nestas PLA₂s homólogas (região C-terminal). Estes achados evidenciam um avanço no conhecimento do modo de atuação das miotoxinas do tipo PLA₂s homólogas, podendo inclusive ser úteis para o desenvolvimento de novas drogas baseadas em estrutura no intuito de complementar a soroterapia convencional.

Palavras-chave: Ácido rosmarínico; Cristalografia de proteínas; Fosfolipase A₂ homóloga; Miotoxina; Veneno botrópico.

Abstract

Envenoming resulting from snakebites is an important public health problem in many tropical and subtropical countries. Scientific, medical and social aspects related to envenoming by snakes from *Bothrops* genus are especially important in Brazil because these animals are responsible for approximately 90 % of all ophidian accidents reported in our country. One of the main problems regarding bothropic accidents is a prominent local tissue damage whose pathogenesis is complex and involves the combined action of a variety of venom components. Phospholipases A₂ (PLA₂s) are the most abundant muscle-damaging components of these venoms playing a central role in the muscle damage establishment. The present work reports structural studies with myotoxins that adopt a PLA₂ fold (PLA₂-like myotoxins) aiming a better understanding of their structure-function relationship. For this purpose, X-ray crystallographic studies of Lys49-PLA₂s from bothropic snake venoms complexed to the inhibitors manganese and rosmarinic acid (RA) were performed. The crystallographic structure of the complex formed between an Asp49-PLA₂-like myotoxin and calcium was also solved. Additionally, the quaternary assembly of Asp49-PLA₂-like myotoxins from *Bothrops* genus was reviewed and relevant structural features for their myotoxicity expression were pointed out. The crystallographic structure of the complex formed between a Lys49-PLA₂ and the inhibitor RA demonstrates that the inhibitor interacts with the protein in the entrance of one of its hydrophobic channel, establishing hydrogen bonds with atoms of the residues Phe3, Lys7, Leu10, Gln11 and Gly15 of the monomer with which it interacts. For the complex formed between a Lys49-PLA₂ and the inhibitor Mn²⁺ the manganese ion is coordinated by atoms of the residues of both monomers of the toxin (residues Asn17 and Ala19 of one of the monomers, and His120 and Lys122 of the other), interacting inside the hydrophobic channel. Therefore, although the C-terminal region of Lys49-PLA₂s is well-defined as containing their myotoxic site, our results emphasizes the importance of the hydrophobic channel of these myotoxins for their mechanism of action. Regarding the Asp49-PLA₂s-like / calcium complex, it is shown that this myotoxin do not bind calcium in the calcium-binding-loop region. This knowledge supports a recent study that shows the catalytic inactivity of these proteins. A review of these dimeric Asp49-PLA₂s quaternary structure using bioinformatics tools points that the disposition between their monomers in solution is probably different from that observed for their crystallographic structures. In this alternative configuration, the calcium binding loop of these myotoxins is at the interface. This observation is probably a consequence of the calcium binding loop distortion observed in Asp49-PLA₂-like myotoxins which besides leading to a new interface formation also provides mechanical support to the probable region responsible for myotoxicity expression in these homologue PLA₂s (C-terminal region). These findings bring an advance in the knowledge of PLA₂-like myotoxins' mode of action, and may even be useful to guide the development of new structure-based drugs in order to supplement the conventional serum therapy.

Keywords: Rosmarinic acid; Protein Crystallography; Homologue phospholipases A₂; Miotoxin; Bothropic venom.

Lista de Figuras

Figura 1. Enovelamento típico de uma PLA ₂	15
Figura 2. Sítio catalítico de Asp49-PLA ₂ s e região análoga em Lys49-PLA ₂ s.....	17
Figura 3. Conformações diméricas possíveis para as Lys49-PLA ₂ s.....	20
Figura 4. Localização do sítio miotóxico das Lys49-PLA ₂ s em ambas as conformações possíveis. ...	22
Figura 5. Modelo de interação entre Lys49-PLA ₂ s botrópicas e membranas musculares proposto por dos Santos e colaboradores, em 2009	22
Figura 6. Árvore filogenética de fosfolipases A ₂ de venenos de serpentes da família Viperidae, subfamília Crotalinae.	24
Figura 7. Cristais da proteína PrTX-I na presença do inibidor ácido rosmarínico (AR).....	34
Figura 8. Mapa de densidade eletrônica $2 F_{\text{obs}} - F_{\text{c}} $ (corte de 1σ) mostrando a região de entrada do canal hidrofóbico onde pode-se observar densidade eletrônica compatível com a de uma molécula de ácido rosmarínico nas proximidades dos aminoácidos Lys7 e Lys122.	34
Figura 9. Interações entre a PrTX-I e seu inibidor ácido rosmarínico (AR).	37
Figura 10. Sobreposição entre a PrTX-I nativa e PrTX-I/AR.	37
Figura 11. Estudos estruturais comparativos entre a PrTX-I/AR e duas outras estruturas de Lys49-PLA ₂ s complexadas com ácidos graxos.	39
Figura 12. Modelo de inibição de Lys49-PLA ₂ s botrópicas pelo ácido rosmarínico (AR).	40
Figura 13. Cristais do complexo PrTX-I/Mn ²⁺ que difratam a 1,9 Å de resolução.....	42
Figura 14. Cristal de PrTX-I/Mn ²⁺ crescido em presença de MnSO ₄	44
Figura 15. Cristais do complexo PrTX-I/Mn ²⁺ submetidos a testes de fluorescência.....	47
Figura 16. Regiões de coordenação do Mn ²⁺ na estrutura da PrTX-I complexada com íons manganês obtida em grupo espacial P3 ₁ 21.	49
Figura 17. Estrutura da BthTX-I complexada com Mn ²⁺ obtida no grupo espacial P2 ₁	52
Figura 18. Testes de fluorescência realizados com feixe colimado (0,1 mm) em λ de 1,8961 (E=6.5389 eV) para os cristais coletados no NSLS.	55

Figura 19. Sobreposição entre a estrutura <i>P3-PrTX-I/Mn²⁺</i> e outras <i>Lys49-PLA₂s</i> de grupo espacial <i>P3₁21</i>	57
Figura 20. Comparação da estrutura <i>BthTX-I</i> complexada com manganês e outras estruturas cristalográficas de <i>Lys49-PLA₂s</i> de grupo espacial <i>P2₁</i> e <i>P2₁2₁2₁</i>	58
Figura 21. Rearranjo quaternário observado em <i>Lys49-PLA₂s</i> botrópicas após interação com ligantes.....	59
Figura 22. Comparação da estrutura <i>P3-PrTX-I/Mn²⁺</i> (grupo espacial <i>P3₁21</i>) e <i>Lys49-PLA₂s</i> botrópicas de grupo espacial <i>P2₁</i> e <i>P2₁2₁2₁</i> com ligantes presentes no canal hidrofóbico.....	60
Figura 23. Modelo de inibição de <i>Lys49-PLA₂s</i> botrópicas por íons manganês.....	61
Figura 24. Estrutura cristalográfica do complexo <i>BthTX-II/Ca²⁺</i>	64
Figura 25. Sítios de coordenação dos íons cálcio no complexo <i>BthTX-II/Ca²⁺</i>	66
Figura 26. Sobreposição entre as estruturas cristalográficas <i>BthTX-II</i> nativa e <i>BthTX-II/Ca²⁺</i>	68
Figura 27. Possíveis conformações diméricas para a resolução das estruturas de <i>Asp49-PLA₂s</i> miotóxicas quando observam-se seus contatos na rede cristalina.	69
Figura 28. Conformação adotada pelo <i>loop</i> de ligação de cálcio de algumas estruturas cristalográficas de <i>PLA₂s</i> de serpentes da família <i>Viperidae</i>	72
Figura 29. Conformação quaternária mais provável de ocorrer em solução para as estruturas <i>BthTX-II</i> (<i>A₁</i>), <i>PrTX-III</i> (<i>B₁</i>) e <i>DacuTX</i> (<i>C₁</i>) <i>A₁</i> também representa a estrutura do complexo <i>BthTX-II/Ca²⁺</i> , conforme indicado por análises no programa <i>PISA</i> (Tabela VIII).....	73
Figura 30. Conformações diméricas possíveis para as <i>Lys49-PLA₂s</i>	78
Figura 31. Sítio miotóxico de <i>Lys49-PLA₂s</i> e interação com membranas.....	79
Figura 32. Diferenças estruturais entre o arranjo quaternário sugerido pelo <i>PISA</i> para <i>Asp49-PLA₂s</i> miotóxicas e <i>Lys49-PLA₂s</i>	80
Figura 33. Árvore filogenética de fosfolipases <i>A₂</i> de venenos de serpentes da família <i>Viperidae</i> , subfamília <i>Crotalinae</i>	82

Lista de Tabelas

Tabela I. Estatísticas de coleta de dados de difração de raios X e de refinamento para a estrutura do complexo PrTX-I/AR.....	35
Tabela II. Estatísticas de refinamento e dos dados de difração de raios X para o complexo PrTX-I / Mn ²⁺ a 2,1Å e 1,9Å	43
Tabela III. Estatísticas de refinamento e dos dados de difração de raios X para o complexo PrTX-I / Mn ²⁺ crescido em presença de MnSO ₄	45
Tabela IV. Estatísticas dos dados de difração de raios X e refinamento para o complexo PrTX-I/Mn ²⁺ coletados nos comprimentos de onda referentes ao pico e remoto no grupo espacial P3 ₁ 21.	48
Tabela V. Estatísticas dos dados de difração de raios X e refinamento para o complexo BthTX-I/Mn ²⁺ coletados nos comprimentos de onda referentes ao pico e remoto no grupo espacial P2 ₁	51
Tabela VI. Estruturas cristalográficas de Lys49-PLA ₂ s botrópicas utilizadas nas comparações dos complexos de manganês obtidos neste trabalho.....	56
Tabela VII. Estatísticas da coleta de dados e refinamento do complexo BthTX-II/Ca ²⁺	63
Tabela VIII. Valores de área de interface e energia livre de solvatação segundo análises do programa <i>online</i> PISA (Krissinel eHenrick, 2007) disponível no servidor do <i>European Bioinformatics Institute server</i> (http://www.ebi.ac.uk).....	70
Tabela IX. Distribuição de resíduos carregados positivamente (arginina, lisina e histidina) na região C-terminal* de PLA ₂ s de venenos de serpentes da subfamília Crotalinae (família Viperidae)	74
Tabela X. Distribuição de resíduos aromáticos (fenilalanina, triptofano, tirosina e histidina) na região C-terminal* de PLA ₂ s de venenos de serpentes da subfamília Crotalinae (família Viperidae)	75
Tabela XI. Distância (<i>d</i>) entre o átomo O η da Tyr28 e o grupamento amino do resíduo Gly35 em estruturas de Asp49-PLA ₂ s.....	77

Sumário

1. Introdução.....	11
1.1. Patogênese do envenenamento botrópico: algumas proteínas envolvidas	13
1.2. PLA ₂ s e PLA ₂ s homólogas	14
1.3. Lys49-PLA ₂ s.....	16
1.4. Estrutura de Lys49-PLA ₂ s e a importância do seu arranjo quaternário	19
1.5. Outras PLA ₂ s miotóxicas conhecidas	23
2. Objetivos	25
3. Material e Métodos.....	26
3.1. Amostras utilizadas nos experimentos de cristalização	26
3.1.1. A Proteína PrTX-I.....	26
3.1.2. A Proteína BthTX-I.....	26
3.1.3. A Proteína BthTX-II	27
3.1.4. Ácido rosmarínico	27
3.1.5. Íons manganês.....	28
3.1.6. Íons cálcio	28
3.2. Estudos estruturais por cristalografia de raios X com o complexo PrTX-I/AR	28
3.3. Estudos estruturais por cristalografia de raios X com complexos Lys49-PLA ₂ s/Mn ²⁺	29
3.4. Estudos estruturais por cristalografia de raios X com o complexo BthTX-II/Ca ²⁺	30
3.5. Estudos estruturais comparativos entre as estruturas quaternárias de Asp49-PLA ₂ s miotóxicas e Lys49-PLA ₂ s.....	32
4. Resultados e Discussão.....	33
4.1. Estudos estruturais do complexo PrTX-I/AR por cristalografia de raios X.....	33
4.1.1. Dificuldades encontradas para a obtenção da estrutura do complexo.....	41
4.2. Estudos estruturais com o Lys49-PLA ₂ s complexadas com Mn ²⁺ por cristalografia de raios X41	
4.2.1. Experimentos com MnCl ₂ na condição de cristalização como fonte de íons manganês.....	42
4.2.2. Experimentos com MnSO ₄ na condição de cristalização como fonte de íons manganês....	44
4.2.3. Experimentos de espalhamento anômalo para o elemento manganês	46
4.2.3.1. Dificuldades encontradas para o trabalho com dados anômalos.....	53
4.2.4. Inibição de Lys49-PLA ₂ s por íons manganês	55
4.3. Estudos estruturais por cristalografia de raios X com o complexo BthTX-II/Ca ²⁺	62

4.3.1. Dificuldades encontradas durante a resolução da estrutura do complexo.....	67
4.3.2. Comparação entre a BthX-II/Ca ²⁺ e sua forma nativa	67
4.4. Arranjo quaternário da BthTX-II/Ca ²⁺ e outras Asp49-PLA ₂ s miotóxicas.....	68
4.4.1. Estrutura quaternária mais provável para Asp49-PLAs miotóxicas	68
4.4.2. Expressão da miotoxicidade e ausência de atividade catalítica das Asp49-PLA ₂ s miotóxicas do ponto de vista estrutural.....	70
4.5. Arranjo quaternário das PLA ₂ s homólogas Asp49 e Lys49: estudo comparativo e implicações funcionais	77
5. Considerações Finais.....	84
6. Referências Bibliográficas	86
7. Apêndice.....	107
8. Anexo I	Error! Bookmark not defined.20
9. Anexo II.....	Error! Bookmark not defined.
10. Anexo III	Error! Bookmark not defined.46
11. Anexo IV	Error! Bookmark not defined.

1. Introdução

O envenenamento ofídico é um problema de saúde pública em muitos países tropicais e subtropicais (Theakston e Warrell, 2000; Kasturiratne *et al.*, 2008). Um recente estudo estima que no mínimo 421.000 envenenamentos e 20.000 mortes relacionadas a acidentes ofídicos ocorrem anualmente, podendo estes números se estender a 1.841.000 envenenamentos e 94.000 mortes (Kasturiratne *et al.*, 2008). A maioria das mortes ocorre no Sul e Sudeste da Ásia e na África Subsaariana (Kasturiratne *et al.*, 2008), sendo que este problema é particularmente importante nas regiões rurais, já que a população destes locais geralmente tem difícil acesso a sistemas de saúde e, em alguns casos, à soroterapia (Theakston e Warrell, 2000; Gutierrez *et al.*, 2006). Um grande número de vítimas sobrevive com sequelas físicas e psicológicas (Gutierrez *et al.*, 2006). Jovens trabalhadores da agricultura, em especial do sexo masculino, constituem o grupo mais afetado, o que permite a classificação do envenenamento por serpentes como uma doença ocupacional (Gutierrez *et al.*, 2006). Diante das estatísticas mais recentes, o envenenamento de serpentes passou a ser considerado uma doença tropical negligenciada pela Organização Mundial de Saúde (OMS) (http://www.who.int/neglected_diseases/diseases/snakebites/en/index.html).

Apesar de a maioria das mortes por envenenamento de serpentes ocorrerem na Ásia e África (Kasturiratne *et al.*, 2008), este problema é também importante na América Latina, onde as serpentes do gênero *Bothrops* (família Viperidae, subfamília Crotalinae) são responsáveis por mais de 85% de todos os acidentes ofídicos reportados (Ministério Da Saúde, 2001; De Oliveira, 2009). No Brasil, estima-se que ocorra cerca de 20.000 acidentes com serpentes por ano, sendo que 73,5% destes é dado por serpentes do gênero *Bothrops* (Ministério Da Saúde, 2010).

Um dos principais problemas associados ao envenenamento botrópico é o proeminente dano local causado pela picada destas serpentes que, em casos mais severos, pode evoluir para necrose do músculo esquelético do local afetado (Gutierrez *et al.*, 2006). A demora no atendimento às vítimas frequentemente resulta em dano tecidual considerável e por vezes irreversível, podendo até mesmo causar invalidez permanente, já que o dano local se estabelece rapidamente após o envenenamento (Nishioka Sde e Silveira, 1992; Cardoso *et al.*, 1993; Fan e Cardoso, 1995; Warrell, 1996; Otero *et al.*, 2002; Gutierrez *et al.*, 2006).

Atualmente, a administração parenteral de antivenenos de origem animal (soro antiofídico) consta como único tratamento específico disponível para o envenenamento de serpentes (Gutierrez *et al.*, 2006). Estes antivenenos são compostos por imunoglobulinas, sendo constituídos de moléculas de IgG inteiras (~150kDa), ou seus fragmentos F(ab')₂ ou Fab (Lalloo e Theakston, 2003; Theakston *et al.*, 2003; Otero *et al.*, 2006; Gutierrez *et al.*, 2009; Gutierrez *et al.*, 2010). Apesar do sucesso dessa terapia na neutralização das toxinas responsáveis pelos efeitos sistêmicos do envenenamento por serpentes do gênero *Bothrops*, o soro apresenta limitada eficácia na proteção do estabelecimento da mionecrose (Warrell, 1992). Esta limitação se explica pelas propriedades farmacocinéticas e farmacodinâmicas destes anticorpos *in vivo* (Gutierrez *et al.*, 2003) já que há comprovação da presença de imunoglobulinas com capacidade de neutralização das toxinas que atuam localmente no soro (Gutierrez *et al.*, 1998). Assim sendo, possíveis alternativas para o avanço no tratamento deste problema são: i) a elucidação dos componentes envolvidos no processo e as bases moleculares de seu mecanismo de ação, e ii) o conhecimento de moléculas com propriedades farmacocinéticas e farmacodinâmicas mais adequadas para a neutralização das toxinas de ação local.

Centenas de plantas utilizadas na medicina tradicional para o tratamento do envenenamento ofídico já foram descritas e nos últimos anos muitas delas têm sido alvo de investigações científicas (Gomes *et al.*; Martz, 1992; Mors *et al.*, 2000; Otero *et al.*, 2000; Soares *et al.*, 2005; Marcussi *et al.*, 2007). A validação científica da eficácia destas plantas bem como o conhecimento de seus princípios ativos é um importante passo na busca de possíveis novos agentes neutralizadores de toxinas em geral, e em especial das que atuam localmente, no caso do envenenamento botrópico, por exemplo. No que diz respeito ao envenenamento botrópico, alguns extratos de plantas utilizados para contornar a hemorragia e a miotoxicidade já foram validados (Izidoro *et al.*, 2003; Januario *et al.*, 2004; Esmeraldino *et al.*, 2005; Nunez *et al.*, 2005; Veronese *et al.*, 2005; Cavalcante *et al.*, 2007; Da Silva *et al.*, 2007; Vale *et al.*, 2008). Um exemplo bem sucedido deste tipo de estudo é o publicado por Ticli e colaboradores em 2005, onde os autores demonstraram que o extrato metanólico de *Cordia verbenacea* é capaz de inibir o edema provocado tanto pelo veneno bruto de *Bothrops jararacussu* quanto o provocado por duas de suas principais PLA₂s homólogas (BthTX-I e BthTX-II) (Ticli *et al.*, 2005). Após isolamento do ácido rosmarínico (AR), os autores demonstraram que o mesmo foi capaz de inibir significativamente o efeito miotóxico induzido pelas

proteínas básicas BthTX-I e BthTX-II e também demonstraram que o AR potencializa o efeito de um soro comercial polivalente na neutralização de miotoxinas ou mesmo do veneno bruto (Ticli *et al.*, 2005). O possível mecanismo de ação para a atuação do AR é a interação com as PLA₂s miotóxicas citadas, já que a possibilidade de degradação da toxina foi descartada após estudos de eletroforese e dicroísmo circular (Ticli *et al.*, 2005).

Interessantemente, Soares e colaboradores demonstraram que alguns íons também são capazes de interferir com a atividade miotóxica de Lys49-PLA₂s, sendo que íons manganês demonstraram maior proteção contra a atividade da miotoxina bothropstoxina-I (BthTX-I) (Soares *et al.*, 2002). Além disso, a atividade anti-miotóxica de alguns outros ligantes como o PEG 400, a suramina e derivados de heparina também já foi demonstrada experimentalmente (Lomonte, Moreno *et al.*, 1994; Lomonte, Tarkowski *et al.*, 1994; Murakami *et al.*, 2005; Murakami *et al.*, 2007).

1.1. Patogênese do envenenamento botrópico: algumas proteínas envolvidas

A patogênese da mionecrose é complexa e envolve a ação combinada de uma variedade de componentes do veneno, dentre aos quais podemos citar as miotoxinas e as metaloproteases (Oliveira *et al.*; Wallnoefer *et al.*; Rosenberg, 1990; Gutierrez, 2002; Gutierrez e Ownby, 2003; Lomonte, Angulo e Calderon, 2003; Soares *et al.*, 2004; Gutierrez *et al.*, 2005; Ramos e Selistre-De-Araujo, 2006; Gutierrez *et al.*, 2008; Mora *et al.*, 2008). O papel das metaloproteases no estabelecimento da mionecrose se deve à ação destas enzimas sob a membrana basal de vasos sangüíneos, culminando com o rompimento destas e conseqüente deficiência do suprimento sangüíneo da região afetada (Oliveira *et al.*; Wallnoefer *et al.*; Mora *et al.*, 2008). Dentre as miotoxinas que contribuem para o estabelecimento da lesão muscular, podemos citar três grupos principais: i) o formado pelas “pequenas” miotoxinas, um grupo constituído por peptídeos (42 a 45 aminoácidos) básicos não-enzimáticos, ii) o composto pelas cardiotoxinas, que são proteínas básicas, não-enzimáticas, de cerca de 60 aminoácidos, e iii) os constituídos pelas PLA₂s miotóxicas, proteínas básicas, de cadeia simples ou multiméricas, que podem ou não apresentar atividade neurotóxica (Harris e Cullen, 1990). A PLA₂s não-neurotóxicas são comumente encontradas em venenos de serpentes da família Viperidae, sendo as Asp49-PLA₂s e as Lys49-PLA₂s duas classes de proteínas presentes nestes venenos (Lomonte, Angulo e Calderon, 2003).

As fosfolipases A2 (PLA₂s) são proteínas com atividade fosfolipásica já bem caracterizada em mamíferos (Van Deenen e De Haas, 1963); porém, nos venenos de serpentes, elas são conhecidas pelo amplo espectro de efeitos tóxicos e propriedades farmacológicas manifestados (Doley e Kini, 2009), atividades estas que podem ser explicadas pelo modo particular de evolução destas toxinas (Ogawa *et al.*, 1992; Nakashima *et al.*, 1993; Nakashima *et al.*, 1995; Kini e Chan, 1999). Um recente estudo filogenético mostra que as fosfolipases A2 presentes no veneno de serpentes da família Viperidae podem ser classificadas em dois grupos, de acordo com seu curso evolutivo: i) PLA₂s cataliticamente ativas dependente de cálcio, como as Asp49-, Asn49- e Gln49-PLA₂s; e ii) PLA₂s homólogas cataliticamente inativas, como as Lys49-, Arg49- e algumas Asp49-PLA₂s, que atuam por um mecanismo independente de cálcio ainda não bem esclarecido (Dos Santos *et al.*, 2011).

As Lys49-PLA₂s, apesar de não apresentarem atividade catalítica, desempenham um papel crucial no estabelecimento do dano muscular após envenenamento botrópico já que quando estas proteínas são seletivamente neutralizadas, a maior parte do dano muscular de venenos brutos não ocorre (Lomonte *et al.*, 1987; Lomonte *et al.*, 1990; Moura-Da-Silva *et al.*, 1991; Lomonte *et al.*, 1992; Melo e Ownby, 1999; Trento *et al.*, 2001).

1.2. PLA₂s e PLA₂s homólogas

As PLA₂s clássicas (E.C. 3.1.1.4.) de venenos de serpentes são proteínas pequenas (14-18 kDa), com um alto grau de similaridade seqüencial e estrutural, e possuem geralmente 5 a 8 pontes dissulfeto; necessitam de Ca²⁺ para catálise e apresentam, em sua seqüência primária, cerca de 122 aminoácidos que seguem o modelo de numeração de uma PLA₂ de pâncreas bovino (resíduos 1 ao 133) (Renetseder *et al.*, 1985). A estrutura terciária destas proteínas é composta por uma α -hélice na região N-terminal (“h1”), cujos resíduos formam a canal hidrofóbico das PLA₂s, uma hélice curta (*short helix*), um *loop* de ligação de cálcio, uma segunda α -hélice (“h2”), duas folhas β -pregueadas antiparalelas, uma outra α -hélice (“h3”) e por fim, uma região bastante flexível, denominada C-terminal (Figura 1). As regiões “h2” e folhas- β formam o sítio catalítico das PLA₂s (Arni e Ward, 1996; Ward, De Azevedo *et al.*, 1998). Esse “enovelamento” típico é determinado, em grande parte, pelas pontes dissulfeto.

Estas PLA₂s são conhecidas ainda por apresentarem em sua estrutura básica os resíduos His48, Tyr52, Asp73 e Asp99, que formam a rede catalítica, e os resíduos Asp28, Gly30, Gly 32 e Asp49, que estão envolvidos na coordenação do co-fator cálcio (Arni e Ward, 1996; Ward, De Azevedo *et al.*, 1998). Esses resíduos são altamente conservados nas PLA₂s em geral, sendo que o resíduo Asp49 é considerado fundamental para atividade catalítica, já que substituições deste resíduo por Glu, Ala, Asn, Gln e Lys levam à perda dessa atividade (Yu *et al.*, 1993). Os resíduos Asp28, Gly30 e Gly32 que coordenam o íon cálcio se encontram numa região denominada *loop* de ligação de cálcio, cuja arquitetura preservada é fundamental para a atividade enzimática destas PLA₂s (Arni e Ward, 1996; Ward, Alves *et al.*, 1998).

Nos venenos de serpentes da família Viperidae, encontramos alguns grupos de PLA₂s que são geralmente classificados de acordo com o aminoácido presente na posição 49 de suas seqüências primárias (ex.: Arg49-PLA₂s, Asp49-PLA₂s, Asn49-PLA₂s, Gln49-PLA₂s, Lys49-PLA₂s, Ser49-PLA₂s). Dentre esses grupos, diferentes conformações oligoméricas são observadas: monômeros (Holland *et al.*, 1990; Scott *et al.*, 1992), dímeros (Brunie *et al.*, 1985; Arni *et al.*, 1995; Marchi-Salvador *et al.*, 2009), trímeros (Fremont *et al.*, 1993) e tetrâmeros (Marchi-Salvador *et al.*, 2008).

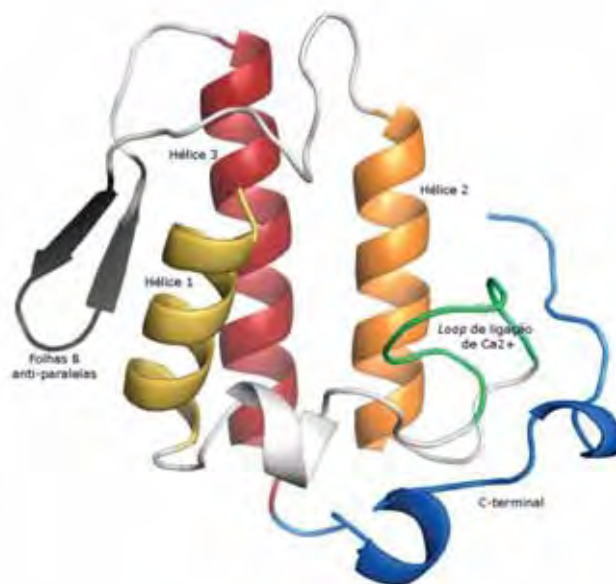


Figura 1. Enovelamento típico de uma PLA₂. A estrutura terciária destas proteínas é composta por uma α -hélice na região N-terminal (“h1”, em amarelo), cujos resíduos formam a canal hidrofóbico das PLA₂s, uma hélice curta (*short helix*, em branco), um *loop* de ligação de cálcio (em verde), uma segunda α -hélice (“h2”, em alaranjando), duas folhas β -pregueadas antiparalelas (em cinza), uma outra α -hélice (“h3”, em vermelho) e por fim, uma região bastante flexível, denominada C-terminal (em azul). Figura gerada no programa *Pymol* (Delano, 2002).

1.3. Lys49-PLA₂s

Um grupo que merece destaque dentre os grupos de PLA₂s de venenos de serpentes conhecidos é o formado pelas Lys49-PLA₂s homólogas, proteínas que apresentam atividade miotóxica (Maraganore *et al.*, 1984; Dos Santos, Fernandes *et al.*, 2009) e são bastante importantes quando consideramos a patofisiologia do envenenamento viperídico, conforme descrito previamente. Essas PLA₂s homólogas foram caracterizadas, num primeiro momento, por apresentarem uma substituição natural do ácido aspártico na posição 49 (D49K) (Maraganore *et al.*, 1984; Homs-Brandeburgo *et al.*, 1988; Francis *et al.*, 1991; Ward *et al.*, 1995; Dos Santos, Fernandes *et al.*, 2009). A análise de estruturas cristalográficas de Lys49-PLA₂s demonstraram que a perda da atividade catalítica neste grupo de PLA₂s se deve ao fato de o átomo Nε da lisina 49 ocupar a posição do cálcio na região do sítio catalítico das Asp49-PLA₂s (Holland *et al.*, 1990; Scott *et al.*, 1992; Arni *et al.*, 1995), o que torna impossível a coordenação do íon Ca²⁺ e, conseqüentemente, inviabiliza a ocorrência da reação catalítica nas Lys49-PLA₂s (Scott *et al.*, 1990; Arni e Ward, 1996; Ward, Alves *et al.*, 1998) (Figura 2). Apesar destas evidências estruturais que corroboram para uma ausência de atividade catalítica nas Lys49-PLA₂s, alguns autores demonstraram que estas proteínas apresentam uma reduzida (quando comparada à ação de uma Asp49-PLA₂) capacidade de hidrolisar fosfolípidios (Liu *et al.*, 1990; Yoshizumi *et al.*, 1990; Rodrigues-Simioni *et al.*, 1995; Shimohigashi *et al.*, 1995; Yamaguchi *et al.*, 1997).

Em 2002, Lee e colaboradores (Lee *et al.*, 2001) tentaram explicar o porquê da reduzida ou inexistente atividade fosfolipídica das Lys49-PLA₂s através do estudo da estrutura cristalográfica de uma Lys49-PLA₂ complexada com um ácido graxo. Segundo os autores, a retenção do produto da catálise (ácido graxo) no sítio ativo da proteína explicaria a reduzida ou inexistente atividade catalítica das mesmas (Lee *et al.*, 2001).

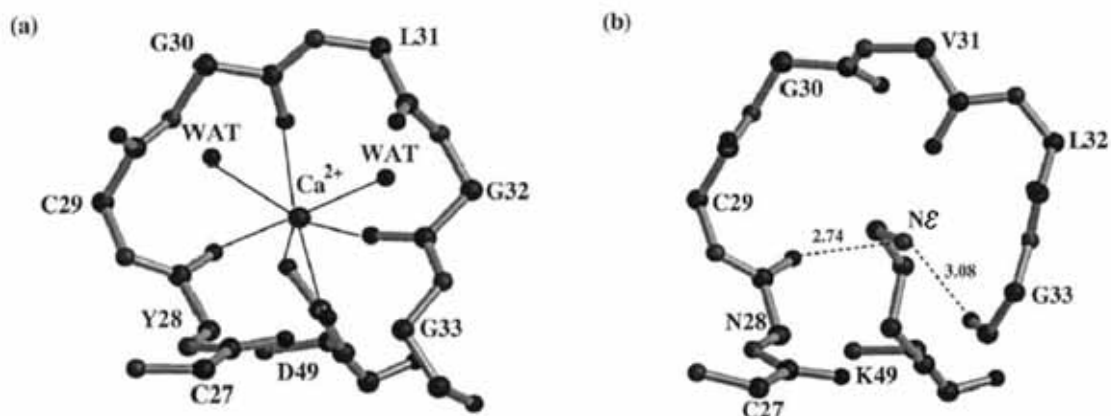


Figura 2. Sítio catalítico de Asp49-PLA₂s e região análoga em Lys49-PLA₂s. **(a)** Região de coordenação do Ca²⁺ (*loop* de ligação de cálcio) de uma PLA₂ cataliticamente ativa de *Naja naja naja* (Asp49-PLA₂) mostrando coordenação do íon cálcio pelos resíduos do *loop* de ligação de cálcio Tyr28, Gly30 e Gly32, pelo resíduo Asp49 e uma molécula de água. **(b)** Região análoga ao sítio catalítico de PLA₂s enzimaticamente ativas em uma miotoxina II (PLA₂ homóloga) cataliticamente inativa de *Bothrops asper* (Lys49-PLA₂). Nesta figura, nota-se que o átomo N impede a coordenação do íon por ocupar fisicamente a região de coordenação do co-fator (Arni e Ward, 1996).

Ainda em 2002, experimentos de mutação sítio-dirigida onde a lisina da posição 49 da proteína BthTX-I (uma Lys49-PLA₂ presente no veneno de *Bothrops jararacussu*) foi substituída (mutada) por um ácido aspártico (K49D) demonstraram que esta proteína continuou não apresentando atividade catalítica (Ward *et al.*, 2002). Estes estudos provaram que as Lys49-PLA₂s realmente não possuem atividade catalítica e sugeriram ainda que a perda da atividade catalítica neste grupo de PLA₂s não está somente relacionada à mutação D49K e sim um conjunto de outros fatores estruturais (Ward *et al.*, 2002; Dos Santos, Fernandes *et al.*, 2009). Desta forma, demonstrou-se que as Lys49-PLA₂s são proteínas desprovidas de atividade enzimática, passando então a ser denominadas PLA₂s homólogas, e o foco de atenção sobre elas passou a ser no sentido de explicar o mecanismo pelo qual estas proteínas estabelecem a atividade danificadora de membranas musculares (Gallacci e Cavalcante, 2010).

A atividade miotóxica de Lys49-PLA₂s foi primeiramente descrita em 1984 (Maraganore *et al.*, 1984) e, desde então, vários estudos vêm sendo realizados com este grupo de PLA₂s homólogas. É de consenso na literatura que o C-terminal destas proteínas (região 115 a 129) é a região responsável pela expressão da atividade miotóxica das mesmas (Nunez *et al.*, 2001; Chioato *et al.*, 2002; Lomonte, Angulo e Calderon, 2003; Lomonte, Angulo e Santamaria, 2003; Ambrosio *et al.*, 2005; Chioato

et al., 2007). A partir deste conhecimento, algumas hipóteses sobre o mecanismo de ação para as Lys49-PLA₂s foram elaboradas. Em um delas, foi proposto que as regiões C-terminais dos monômeros das Lys49-PLA₂s, ricas em resíduos hidrofóbicos e básicos, se insinuam através das membranas (celulares ou artificiais), promovendo a desestabilização destas, ou atuam como “âncoras”, possibilitando o contato de sítios protéicos reativos desconhecidos (Lomonte, Tarkowski *et al.*, 1994; Gutierrez e Lomonte, 1995). Mais recentemente, Ambrosio e colaboradores sugeriram que a retenção do ácido graxo no sítio ativo da Lys49-PLA₂s provoca uma mudança conformacional no C-terminal da proteína, propiciando a adequada orientação de alguns resíduos para o estabelecimento da lesão muscular (Ambrosio *et al.*, 2005). Esta mudança conformacional consistiria numa maior exposição de resíduos hidrofóbicos do C-terminal ao solvente, permitindo o estabelecimento de interações eletrostáticas entre a membrana e lisinas do C-terminal, que auxiliariam na inserção deste através das membranas (Ambrosio *et al.*, 2005). Experimentos com peptídeos sintéticos correspondentes aos aminoácidos 115 ao 129 da região do C-terminal e experimentos de mutação sítio-dirigida também ressaltam a importância desta região, bem como sua composição (aminoácidos básicos e hidrofóbicos em posições específicas) para a atividade miotóxica destas proteínas (Ward, Alves *et al.*, 1998; Nunez *et al.*, 2001; Chioato *et al.*, 2002; Ward *et al.*, 2002; Lomonte, Angulo e Santamaria, 2003; Chioato *et al.*, 2007).

De maneira geral, os estudos que tentam explicar o modo de ação das Lys49-PLA₂s nas membranas biológicas são baseados na interação direta de seus C-terminais com a membrana. Porém, vale mencionar que em 1990 foi identificado um receptor em membranas de células musculares esqueléticas de coelhos com os quais as PLA₂s de veneno de serpentes interagem (Lambeau *et al.*, 1990). Além de serem expressos em células musculares, estes também são encontrados em outros tecidos, com pulmão, ovário e fígado (Lambeau *et al.*, 1991; Hseu *et al.*, 1997). Este receptor, conhecido como receptor do tipo M, embora apresente baixa identidade com receptores de manose de macrófagos (29%), possuem grande similaridade em termos de estrutura terciária com os mesmos (Ezekowitz *et al.*, 1990; Taylor *et al.*, 1990) e, assim como estes receptores, têm como função propiciar a internalização de proteínas que interagem com os mesmos (Pontow *et al.*, 1992).

Em contrapartida, estudos com peptídeos sintéticos na forma dextrógera (resíduos 115 ao 129) simulando a região C-terminal de Lys49-PLA₂s realizados por

Lomonte e colaboradores em 2003 demonstraram que estes peptídeos mantiveram igual capacidade de danificar músculos quando comparados com os mesmos aminoácidos na forma levógera (Lomonte, Angulo e Santamaria, 2003). Este achado sugere que a interação das Lys49-PLA₂s, pelo menos no que refere aos seus C-terminais, não se dá pela interação com aceptores / receptores da membrana muscular, mas sim de forma direta (Lomonte, Angulo e Santamaria, 2003).

1.4. Estrutura de Lys49-PLA₂s e a importância do seu arranjo quaternário

Um grande número de estruturas de PLA₂s de venenos de serpentes já foram resolvidas demonstrando que estas proteínas apresentam estrutura terciária bastante conservada. Apesar disso, diferentes atividades biológicas são exercidas por estas toxinas (neurotoxicidade, miotoxicidade, cardiotoxicidade, efeitos na agregação de plaquetas, ação anti-coagulante, efeitos convulsivos, atividade hipotensora, capacidade hemolítica e de indução de edema, dentre outros efeitos) (Chang e Lee, 1977; Bon *et al.*, 1979; Condrea *et al.*, 1981; Huang, 1984; Maraganore *et al.*, 1984; Kini e Evans, 1989; Gerrard *et al.*, 1993; Lloret e Moreno, 1993; Gutiérrez e Lomonte, 1997; Kini, 1997; Paramo *et al.*, 1998; Andriao-Escarso *et al.*, 2002; Beers *et al.*, 2002). Esta gama de possibilidades deve estar relacionada com as diferentes oligomerizações e arranjo quaternário assumido por estas PLA₂s, já que a formação de complexos muitas vezes elimina ligações não-específicas e potencializa a ligação da toxina a moléculas alvo (Doley e Kini, 2009). Desta forma, o conhecimento do arranjo tridimensional adotado por estas PLA₂s parece ser de fundamental importância para o entendimento de como elas são capazes de manifestar diferentes atividades biológicas (Murakami *et al.*, 2007; Marchi-Salvador *et al.*, 2008; Murakami *et al.*, 2008; Doley e Kini, 2009; Dos Santos, Soares *et al.*, 2009; Magro *et al.*, 2009; Dos Santos *et al.*, 2011).

Experimentos de eletroforese, análises espectroscópicas e experimentos de SAXS demonstraram que as Lys49-PLA₂s existem como dímeros em solução (Da Silva Giotto *et al.*, 1998; Arni *et al.*, 1999; Soares *et al.*, 2000; Murakami *et al.*, 2007). As primeiras estruturas cristalográficas destas proteínas foram resolvidas numa conformação quaternária em que os seus monômeros se relacionam por um eixo de ordem dois perpendicular às regiões das folhas-β, sendo estabilizados por interações entre os resíduos das folhas-β e das hélices N-terminais. Esta disposição entre os monômeros envolve resíduos estritamente conservados em Lys49-PLA₂s (Gln11,

Glu12, Trp77 e Lys80) e possibilita uma relativa flexibilidade entre eles (Ward, De Azevedo *et al.*, 1998; Magro *et al.*, 2003) (Figura 3). Em 2003, Lomonte e colaboradores (Lomonte, Angulo e Calderon, 2003) propuseram um mecanismo de ação para as Lys49-PLA₂s baseado nesta conformação dimérica (Lomonte, Angulo e Calderon, 2003). No entanto, em 2005, a estrutura cristalográfica da BaspTX-II complexada com suramina (um composto simétrico polisulfonado) foi resolvida numa conformação dimérica alternativa (Murakami *et al.*, 2005) para uma estrutura coerente e energeticamente favorável (Figura 3). Esta conformação dimérica alternativa adotada é estabilizada por contatos entre os *loops* de ligação do Ca²⁺ e a região C-terminal de ambos os monômeros, formando uma rota de comunicação entre os “sítios ativos” dos mesmos (Figura 3).

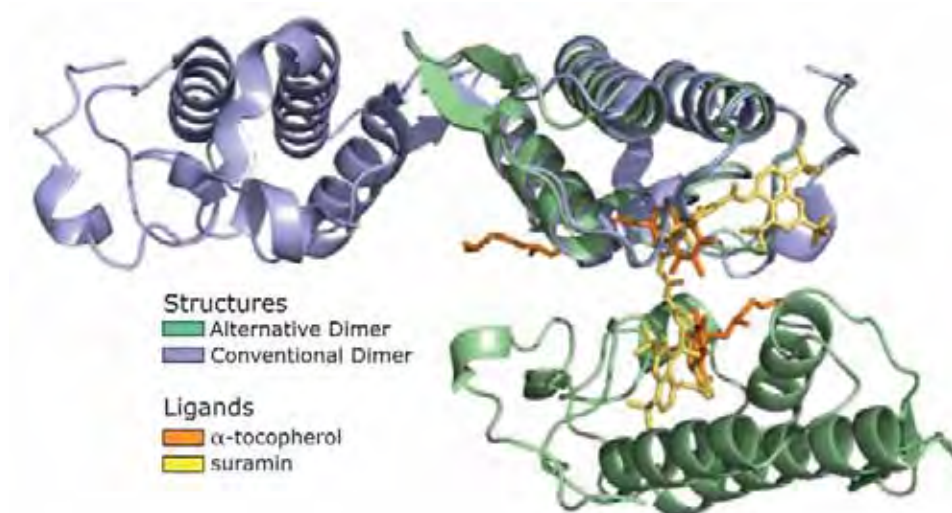


Figura 3. Conformações diméricas possíveis para as Lys49-PLA₂s. Em azul, o dímero convencional e, em verde, o dímero alternativo. A molécula de suramina (em amarelo) demonstra que o dímero alternativo é a conformação oligomérica ideal para a complexação com este inibidor. Figura extraída do artigo de dos Santos e colaboradores ((Dos Santos, Soares *et al.*, 2009).

Desde então, as estruturas de Lys49-PLA₂s passaram a ser discutidas já que o arranjo cristalino da qual as mesmas são inferidas não nos permite apontar a conformação dimérica representativa da unidade biológica destas proteínas. Um recente estudo, onde foram analisados os contatos na interface protéica para todas as

possibilidades de simetria cristalográfica e a interface com maior probabilidade de ocorrer em solução em todas as estruturas cristalográficas de Lys49-PLA₂s disponíveis no PDB, mostrou que o dímero alternativo apresenta a forma biológica com maior probabilidade de ocorrer em solução (Dos Santos, Soares *et al.*, 2009). Algumas outras evidências também favorecem o dímero alternativo como melhor representante da unidade biológica funcional: i) os sítios miotóxicos de ambos os monômeros se apresentam dispostos lado a lado nesta conformação dimérica, indicando assim uma possível colaboração entre eles para poder melhor ancorar a proteína (o dímero) na membrana (Figura 4a). Se considerarmos o dímero convencional, estes sítios ficariam de lados opostos, fazendo com que o modo de ação destas enzimas fosse menos eficaz ou mesmo inviável (Figura 4b) (Dos Santos, Soares *et al.*, 2009); ii) dados de espalhamento de raios X a baixo ângulo para a proteína BthTX-I nativa, que mostram que a conformação alternativa também é tida como a que melhor representa o envelope protéico teórico (Murakami *et al.*, 2007).

Assim, um novo modo de interação entre as Lys49-PLA₂s e membranas biológicas foi proposto recentemente (Dos Santos, Soares *et al.*, 2009) (Figura 5). Este novo modelo é baseado na conformação dimérica alternativa e leva em consideração a ideia de que íons como o fosfato podem simular a cabeça polar de fosfolipídios, indicando assim regiões protéicas que interagem diretamente com a membrana (Bahnsen, 2005). Neste modelo, é proposta a interação dos resíduos Lys20, Lys 115 e Arg118 com a cabeça polar de fosfolipídios de membrana, sendo este o primeiro evento que ocorre para a lesão de membranas (Figura 5 – passo 2). Logo após, outros eventos se sucedem, culminando com a desestabilização das membranas musculares (Figura 5 – passo 3).

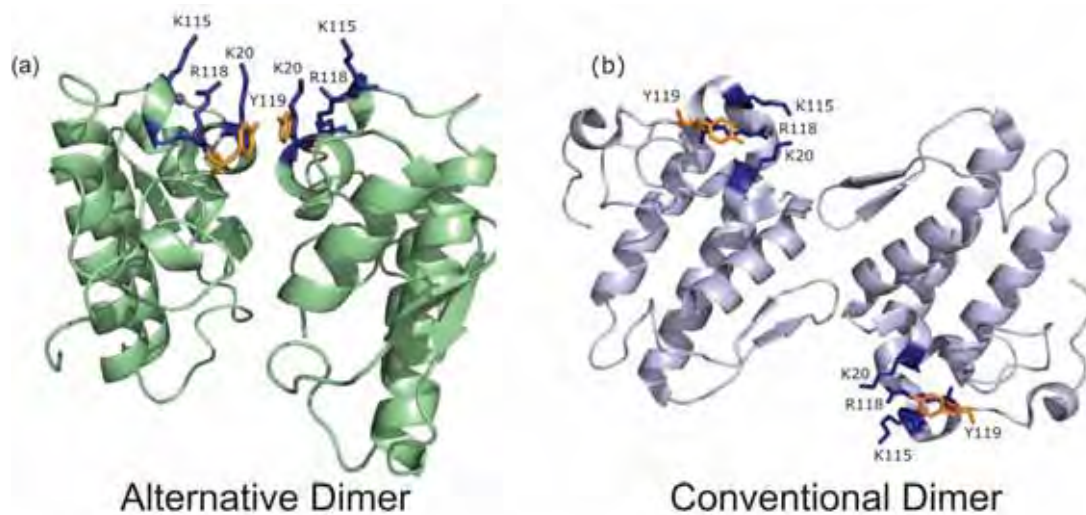


Figura 4. Localização do sítio miotóxico das Lys49-PLA₂s em ambas as conformações possíveis. **(a)** Dímero Alternativo com resíduos que constituem o sítio miotóxico (K20, K115 e R118) em azul e as tirosinas da posição 119 (Y119) de ambos os monômeros em alaranjado. **(b)** Dímero Convencional com os resíduos do sítio miotóxico e Y119 de ambos os monômeros nas mesmas cores que representados em (a). Figura extraída do artigo de dos Santos e colaboradores ((Dos Santos, Soares *et al.*, 2009).

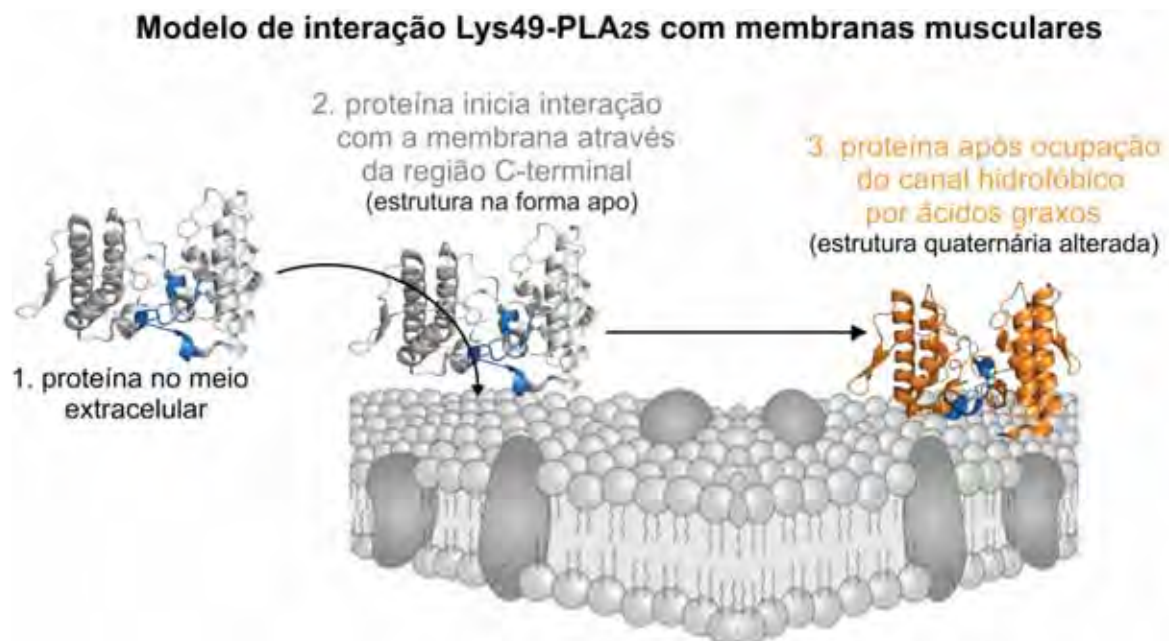


Figura 5. Modelo de interação entre Lys49-PLA₂s botrópicas e membranas musculares proposto por dos Santos e colaboradores, em 2009 (Dos Santos, Soares *et al.*, 2009). A proposta sugere um mecanismo de ação baseado em duas etapas: num primeiro momento, a toxina que se encontra no meio extracelular (passo 1) se aproxima da membrana muscular e estabelece interações com a mesma através da região C-terminal (representada em azul). Esta interação ocorre entre resíduos específicos (Lys20, Lys115 e Arg118) e a cabeça polar dos fosfolipídios da membrana (passo 2); posteriormente, ocorre um rearranjo na estrutura quaternária da toxina que favorece a entrada de porções hidrofóbicas dos fosfolipídios de membrana no canal hidrofóbico da proteína (passo 3).

1.5. Outras PLA₂s miotóxicas conhecidas

Além das Lys49-PLA₂s, outros quatro grupos de PLA₂s miotóxicas são encontradas no veneno de serpentes da subfamília Crotalinae (família Viperidae) (Gutierrez *et al.*, 1991; Kordis e Gubensek, 1997; Pan *et al.*, 1998; Pereira *et al.*, 1998; Toyama *et al.*, 1999; Bao *et al.*, 2005; Chijiwa *et al.*, 2006; Mebs *et al.*, 2006; Dos Santos *et al.*, 2011). Uma recente análise da evolução das PLA₂s de venenos de serpentes desta subfamília demonstra que elas se agrupam, de uma forma geral, em dois clados principais. Um deles é formado por PLA₂s básicas, miotóxicas e não-catalíticas (clado B da Figura 6) e o outro, por PLA₂s ácidas e que tem como principal atividade a catálise de fosfolipídios, embora a manifestação de outras atividades por parte destas proteínas seja observada (clado A da Figura 6) (Dos Santos *et al.*, 2011). Interessantemente, PLA₂s miotóxicas são encontradas nos dois clados, sendo que Asn49- e Gln49-PLA₂s estão representadas no ramo A e as Asp49-PLA₂s homólogas, Lys49-PLA₂s e Arg49-PLA₂s estão agrupadas no ramo B (Figura 6).

Apesar de as Lys49-PLA₂s serem bem caracterizadas na literatura tanto por experimentos funcionais quanto estruturais, os outros grupos de miotoxinas conhecidos (Asn49-, Gln49-, Arg49- e algumas Asp49-PLA₂s) são ainda pouco estudados, sendo que atualmente somente três estruturas cristalográficas de PLA₂s miotóxicas destes grupos são conhecidas. Uma destas estruturas é a da Arg49-PLA₂ do veneno de *Zhaoermia mangshanensis* (Murakami *et al.*, 2008), e as outras duas são das Asp49-PLA₂s miotóxicas PrTX-III, uma Asp49-PLA₂ miotóxica de *Bothrops pirajai* (Rigden *et al.*, 2003), e BthTX-II, uma Asp49-PLA₂ miotóxica de *Bothrops jararacussu* (Correa *et al.*, 2008). Embora estas proteínas tenham uma atividade em comum (miotoxicidade), a comparação de suas estruturas quaternárias mostra que as mesmas são representadas por diferentes arranjos diméricos, como observado para as estruturas cristalográficas de Lys49-PLA₂s, Arg49-PLA₂s e Asp49-PA₂s miotóxicas (Figura 6). Ainda, Lys49-PLA₂s são também encontradas sob a forma monomérica (Holland *et al.*, 1990; Arni *et al.*, 1999; Liu *et al.*, 2003; Murakami *et al.*, 2006) (Figura 6).

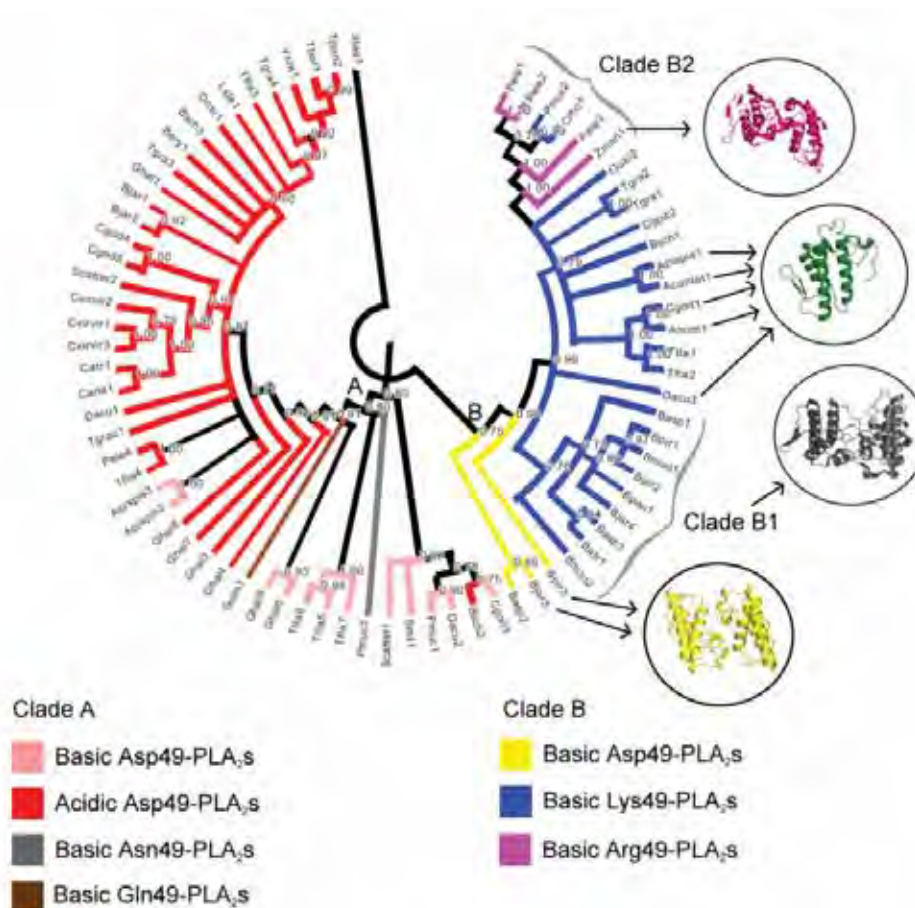


Figura 6. Árvore filogenética de fosfolipases A₂ de venenos de serpentes da família Viperidae, subfamília Crotalinae. A cor do ramo corresponde ao grupo a qual cada seqüência pertence. As configurações oligoméricas representadas correspondem às estruturas cristalográficas da BthTX-II (em amarelo; código de acesso no PDB: 2OQD), PrTX-I (em cinza; código de acesso no PDB: 2Q2J), Dacu3 (em verde ; código de acesso no PDB: 1MC2 ou 1MG6) e Zman1 (em magenta; código de acesso no PDB: 2PH4). A conformação biológica indicada pelo programa PISA foi utilizada na representação das estruturas da PrTX-I e BthTX-II. A configuração adotada pela BthTX-II e Zman 1 são equivalentes. Figura retirada do artigo de dos Santos e colaboradores (Dos Santos *et al.*, 2011).

A resolução da estrutura da BthTX-II mostrou que a mesma apresenta distorção na região do *loop* de ligação de cálcio para ambos os monômeros quando esta estrutura foi comparada à de outras Asp49-PLA₂s clássicas (PLA₂s cataliticamente ativas) (Correa *et al.*, 2008). Esta distorção foi associada à baixa atividade enzimática apresentada pela proteína, já que a literatura aponta que Asp49-PLA₂s miotóxicas são proteínas com reduzida atividade catalítica (Pereira *et al.*, 1998; Toyama *et al.*, 1999; Correa *et al.*, 2008). Esta distorção também foi observada na estrutura cristalográfica da PrTX-III (Rigden *et al.*, 2003), porém, quando se resolveu esta estrutura, tal distorção foi associada a um estado inativo da proteína devido à ausência de Ca²⁺ e, principalmente, substrato na condição de cristalização (Rigden *et al.*, 2003).

2. Objetivos

O presente trabalho foi desenvolvido com o intuito de melhor entender a relação estrutura / função de fosfolipases A2 (PLA₂s) miotóxicas. Para tanto, os seguintes estudos estruturais foram realizados:

- Lys49-PLA₂s complexadas com Mn²⁺ e ácido rosmarínico, dois compostos conhecidos como inibidores da atividade miotóxica destas proteínas, através da técnica de cristalografia de raios X;
- BthTX-II (uma Asp49-PLA₂ miotóxica homóloga) complexada com Ca²⁺, também através da técnica de cristalografia de raios X. Este estudo foi feito com o intuito de analisar a influência do íon cálcio na estrutura de Asp49-PLA₂s miotóxicas;
- estudos da oligomerização de Asp49-PLA₂s miotóxicas homólogas bem como comparação da estrutura quaternária destas proteínas com a de Lys49-PLA₂s no intuito de obter informações biologicamente relevantes a partir de suas estruturas tridimensionais.

3. Material e Métodos

A seguir são descritos os experimentos realizados durante o desenvolvimento deste trabalho bem como as amostras utilizadas nos mesmos. Uma breve introdução sobre as bases teóricas referente a estes experimentos pode ser encontrada no Apêndice I.

3.1. Amostras utilizadas nos experimentos de cristalização

As amostras protéicas utilizadas nos experimentos foram purificadas a partir do veneno bruto. As mesmas foram fornecidas por nosso colaborador (Prof. Dr. Andreimar Martins Soares) na forma liofilizada, não cabendo, portanto, a purificação das mesmas durante o desenvolvimento deste trabalho.

3.1.1. A Proteína PrTX-I

A PrTX-I é uma Lys49-PLA₂ miotóxica isolada do veneno de *Bothrops pirajai*. Esta proteína possui 121 aminoácidos na sua seqüência primária, pI de 8,3 e massa molecular aproximada de 13kDa (Mancuso *et al.*, 1995; Toyama *et al.*, 1998).

Esta toxina foi cristalizada na sua forma nativa e pertence ao grupo espacial P3₁21, apresentando duas moléculas na unidade assimétrica (Dos Santos, Soares *et al.*, 2009). Os dados foram coletados a 1,65 Å de resolução e a estrutura encontra-se depositada do banco de dados PDB, com código de acesso 2Q2J (Dos Santos, Soares *et al.*, 2009).

3.1.2. A Proteína BthTX-I

A BthTX-I é uma Lys49-PLA₂ homóloga miotóxica encontrada no veneno de *Bothrops jararacussu* (Homs-Brandeburgo *et al.*, 1988; Da Silva Giotto *et al.*, 1998). A purificação desta proteína é possível através da combinação de filtração em gel (Sephadex G-75) e cromatografia de troca iônica (SP-Sephadex C-25); sua massa molecular é de aproximadamente 13 kDa e seu pI é 8,2 (Homs-Brandeburgo *et al.*,

1988). Assim como a PrTX-I, esta proteína apresenta 121 aminoácidos em sua sequência primária, sendo que as mesmas diferem em somente 2 aminoácidos (na sequência da PrTX-I, encontramos uma asparagina na posição 67 e um ácido aspártico na posição 132, ao passo que na sequência da BthTX-I, são encontrados os resíduos ácido aspártico e prolina nestas posições).

Esta proteína já foi cristalizada na sua forma nativa em duas conformações diferentes: forma “aberta” e forma “fechada”. Os cristais pertencem ao grupo espacial $P3_221$ e $P3_121$, respectivamente (Da Silva Giotto *et al.*, 1998). Após a resolução destas estruturas, foram encontradas duas moléculas por unidade assimétrica (Da Silva Giotto *et al.*, 1998) (as estruturas descritas não estão disponíveis no banco de dados PDB). Recentemente, ela foi re-cristalizada em nosso laboratório, apresentando grupo espacial $P3_121$ e $C222_1$, respectivamente para as formas dimérica e monomérica (Fernandes *et al.*, 2011). As mencionadas estruturas foram depositadas no PDB sob código de acesso 3HZD (forma dimérica) e 3I3I (forma monomérica).

3.1.3. A Proteína BthTX-II

A BthTX-II é uma Asp49-PLA₂ miotóxica encontrada no veneno de *Bothrops jararacussu* (Gutierrez *et al.*, 1991; Pereira *et al.*, 1998). Esta proteína é composta por 122 aminoácidos, possui massa molecular de aproximadamente 14kDa (Pereira *et al.*, 1998) e já foi cristalizada na sua forma nativa, sendo que seus cristais pertencem ao grupo espacial C2 (Correa *et al.*, 2008). A estrutura cristalográfica revelou a existência de duas moléculas na unidade assimétrica (Correa *et al.*, 2008) (PDB ID 2OQD). Interessantemente, a conformação dimérica em que esta proteína foi resolvida é a mesma adotada pelo Dímero Convencional de Lys49-PLA₂s (Correa *et al.*, 2008).

3.1.4. Ácido rosmarínico

O ácido rosmarínico (AR) [3-(3,4-dihidroxifenil)-2-[(E)-3-(3, 4-dihidroxifenil)prop-2-enoil] ácido oxipropanóico] é um composto polifenólico encontrado em várias plantas das famílias Boraginaceae e Laminaceae que atua como molécula inibidora da atividade miotóxica de Lys49-PLA₂s (Ticli *et al.*, 2005). O

inibidor AR utilizado durante os experimentos foi adquirido da *Sigma-Aldrich* e apresenta pureza superior a 99%.

3.1.5. Íons manganês

Os experimentos de co-cristalização visando a incorporação de íons manganês à estrutura cristalográfica de Lys49-PLA₂s foram realizados utilizando-se os sais comerciais MnCl₂ e MnSO₄ (adquiridos da *Sigma-Aldrich*).

3.1.6. Íons cálcio

Os experimentos de co-cristalização visando a incorporação de íons cálcio à estrutura cristalográfica da Asp49-PLA₂ miotóxica BthTX-II foram realizados utilizando-se o sal comercial CaCl₂ (adquiridos da *Sigma-Aldrich*).

3.2. Estudos estruturais por cristalografia de raios X com o complexo PrTX-I/AR

A proteína PrTX-I na forma liofilizada foi dissolvida em água ultra-pura, na concentração de 12 mg/ml. Inicialmente, a busca da condição de cristalização foi realizada com quites de soluções prontas da Hampton Research (*Screen I* e *Screen II*). Para a montagem das placas foi utilizado 1,0µl de solução do poço, 0,7µl de solução protéica e 0,3µl de solução do inibidor ácido rosmarínico (AR), obedecendo -se a proporção molar de cinco moléculas de inibidor para cada molécula de proteína; o método utilizado em todos os experimentos foi o *sitting drop* e a temperatura foi de 18°C.

Os cristais foram submetidos à difração de raios X na linha MX-2 do LNLS, em Campinas / SP. Os dados foram processados com o software HKL2000 (Otwinowski e Minor, 1997) e a estrutura foi resolvida por substituição molecular com o programa Phaser (Mccoy, 2007), utilizando-se a proteína PrTX-I complexada com alfa-tocoferol (PDB ID 3CYL) (Dos Santos, Soares *et al.*, 2009) como modelo.

A estrutura do ligante AR (3-(3,4-dihidroxifenil)-2-[(E)-3-(3, 4-dihidroxifenil)prop-2-enoil] ácido oxipropanóico) foi construída utilizando-se o programa Avogadro (http://avogadro.openmolecules.net/wiki/Main_Page) (Avogadro: *an open-source molecular builder and visualization tool*) já que nenhum dado experimental correspondente à molécula em questão se encontrava disponível no momento da resolução da estrutura do complexo. A geometria do AR foi otimizada com o mesmo programa através de um processo de minimização de energia baseado no campo de força MMFF94 (Halgren e Nachbar, 1996), utilizando-se um algoritmo *steepest-descent* (500 passos foram realizados considerando 10^{-7} como critério de convergência).

O refinamento da estrutura foi realizado com o programa REFMAC (Murshudov *et al.*, 1997) e a modelagem manual com o programa Coot (Emsley e Cowtan, 2004). Para o reconhecimento da densidade eletrônica correspondente ao ácido rosmarínico, mapas-diferença ($F_o - |F_c|$) foram gerados. A análise estereoquímica das estruturas obtidas foi realizada no programa Procheck (Laskowski *et al.*, 1993).

3.3. Estudos estruturais por cristalografia de raios X com o complexo PrTX-I/Mn²⁺

As proteínas PrTX-I e BthTX-I na forma liofilizada foram dissolvidas em água ultra-pura, na concentração de 12 mg/ml. Como estas proteínas nas suas formas nativas já haviam sido cristalizadas por nosso grupo (Dos Santos *et al.*, 2007; Dos Santos, Soares *et al.*, 2009), utilizamos a condição de cristalização destas para os testes de cristalização do complexo formado entre as mesmas e íons manganês: 30% PEG 4000, 0,1M TrisHCl pH 7,8 e 0,2M sulfato de lítio. Para a montagem das placas foram utilizadas quantidades variáveis de solução do poço e μ l de solução protéica na gota; ainda, adicionamos quantidades variáveis de cloreto de manganês ou sulfato de manganês (0,1M) na gota, utilizando uma faixa de 5 a 30 íons de manganês para cada molécula protéica. O método utilizado foi o *hanging-drop* e os testes foram conduzidos à temperatura de 18°C. A formação de cristais foi observada seis semanas após a montagem dos experimentos. Os cristais foram submetidos à difração de raios X na linha MX-2 do LNLS, em Campinas/SP. Para estes experimentos, dados de espalhamento anômalo foram coletados no λ referente ao pico do elemento Mn tanto para o cristal com MnCl₂ quanto para o com MnSO₄ na condição de cristalização (λ de

1,89226 e 1,89220 Å, respectivamente). Ambos os cristais também serviram para coleta de dados no λ referente ao remoto (λ de 1,37757 e 1,45900 Å, respectivamente).

Os dados obtidos foram processados com o programa HKL2000 (Otwinowski e Minor, 1997) e as estruturas foram resolvidas por substituição molecular com o programa Phaser (McCoy, 2007). Para a substituição molecular, a estrutura cristalográfica das proteínas PrTX-I nativa (PDB ID 2Q2J) (Dos Santos, Soares *et al.*, 2009) e PrTX-I complexada com α -tocoferol (PDB ID 3CYL) (Dos Santos, Soares *et al.*, 2009) foram utilizadas como modelo para a resolução das estruturas obtidas referente ao cristais contendo $MnCl_2$ e $MnSO_4$ na condição de cristalização, respectivamente. O mapa de Patterson foi gerado para se checar as posições ocupadas pelos íons manganês na estrutura cristalográfica. Para manutenção dos íons na estrutura, os seguintes critérios foram estabelecidos: i) sinal de no mínimo 50% em relação à intensidade de sinal mais forte encontrado no mapa de Patterson (correspondente a um enxofre de uma das pontes dissulfeto encontradas na proteína) e ii) densidade eletrônica também presente no mapa diferença $|F_o| - |F_c|$. A possibilidade de íons sulfato também foi testada nos mesmos sítios de possível ocupação pelo Mn^{2+} , porém análises do fator temperatura e do mapa $|F_c| - |F_o|$ apontaram ser estes incompatíveis com o mapa de densidade eletrônica obtido.

O refinamento das estruturas foi realizado com o programa REFMAC (Murshudov *et al.*, 1997) e a modelagem manual, no programa Coot (Emsley e Cowtan, 2004). Para análises de ocupação do íon, as densidades eletrônicas nos mapas $|F_o| - |F_c|$ e $|F_c| - |F_o|$ foram consideradas. A análise estereoquímica dos modelos cristalográficos obtidos foi realizada no programa Procheck (Laskowski *et al.*, 1993).

3.4. Estudos estruturais por cristalografia de raios X com o complexo BthTX-II/ Ca^{2+}

A proteína BthTX-II na forma liofilizada foi dissolvida em água ultra-pura, na concentração de 12 mg/ml. Como esta proteína na sua forma nativa já havia sido cristalizada por nosso grupo (Correa *et al.*, 2006; Correa *et al.*, 2008), utilizamos a condição de cristalização desta para os testes de cristalização do complexo formado entre esta proteína e íons cálcio: 20% 2-propanol, 13% PEG4000 e 0,1M citrato de

sódio pH 5,6. Para a montagem das placas foram utilizadas quantidades variáveis de solução do poço e solução protéica na gota; cloreto de cálcio (0,1M) foi adicionado na gota como fonte de cálcio sempre considerando uma proporção de 30 moléculas de íons Ca^{2+} para cada molécula de BthTX-II. O método utilizado foi o *hanging-drop* e os testes foram conduzidos à temperatura de 18°C. Os cristais foram submetidos à difração de raios X na linha MX-2 do LNLS, em Campinas / SP.

Os dados foram processados com o programa HKL2000 (Otwinowski e Minor, 1997) e a estrutura foi resolvida por substituição molecular com o programa Phaser (McCoy, 2007), utilizando-se a proteína BthTX-II nativa (PDB ID 2OQD) (Correa *et al.*, 2008) como modelo. O refinamento das estruturas foi realizado com o programa REFMAC (Murshudov *et al.*, 1997) e a modelagem manual, com o programa Coot (Emsley e Cowtan, 2004). Para checar as regiões candidatas à presença de íons de cálcio, utilizou-se da inspeção manual da densidade eletrônica e da função *find ligands* do programa Coot (Emsley e Cowtan, 2004) usando o mapa diferença $|F_o| - |F_c|$ com corte mínimo de 3σ . Para manutenção do íon na região candidata, os seguintes critérios foram estabelecidos e verificados: ocupação maior ou igual a 0,7 após refinamento de ocupação no programa CNS (Brunger *et al.*, 1998), I/σ maior que 2,5 no mapa $2|F_o| - |F_c|$, preferência de interação com átomos de nitrogênio, enxofre e especialmente oxigênios, número de coordenação e formato do grupo de coordenação (incluindo presença de ligantes bidentados) (Fraústo Da Silva e Willians, 1991; Harding, 2000; 2001). Somente interações abaixo de 3,7 Å de distância foram consideradas (valor que inclui a primeira e segunda esfera de coordenação (Harding, 2001). A possibilidade de moléculas de água também foram testadas nos mesmos sítios de possível ocupação pelo íon cálcio, porém estas apresentaram valores de fator temperatura incompatíveis e foram então descartadas.

A análise estereoquímica das estruturas obtidas foi realizada no programa Procheck (Laskowski *et al.*, 1993).

3.5. Estudos estruturais comparativos entre as estruturas quaternárias de Asp49-PLA₂s miotóxicas e Lys49-PLA₂s

Estudos estruturais comparativos entre o arranjo quaternário das PLA₂s homólogas diméricas Asp49-PLA₂s miotóxicas e Lys49-PLA₂s foram realizados. Para checagem do arranjo quaternário, o programa PISA foi utilizado (Krissinel eHenrick, 2007). As proteínas BthTX-II (PDB ID 2OQD) (Correa *et al.*, 2008), PrTX-III (PDB ID 1GMZ) (Rigden *et al.*, 2003), BthTX-II/Ca²⁺ (estrutura descrita na seção 4.3.), DacuTX (uma Asp49-PLA₂ catalítica do veneno de *Deinagkistrodon acutus*; PDB ID 1IJL) (Gu *et al.*, 2002) e AhalTX (uma Asp49-PLA₂ catalítica do veneno de *Gloydius halys*, anteriormente denominada *Agkistrodon halys pallas*; PDB ID 1PSJ) (Wang *et al.*, 1996) foram analisadas. A área de interface e o ganho de energia livre quando o complexo se forma ($\Delta^{\ddagger}G$) foram os parâmetros considerados na análise (Krissinel eHenrick, 2007). Para sobreposição das estruturas, utilizou-se o programa Coot (Emsley eCowtan, 2004). Somente os C α foram considerados para sobreposição.

4. Resultados e Discussão

4.1. Estudos estruturais do complexo PrTX-I/AR por cristalografia de raios X

Os primeiros cristais do complexo formado entre a toxina PrTX-I e seu inibidor ácido rosmarínico (AR) (Figura 7a, b) foram obtidos dois meses após a montagem dos experimentos, numa condição de cristalização diferente da que é possível obter cristais da proteína PrTX-I na forma nativa. A otimização da condição nos levou aos melhores cristais quando utilizamos gotas de 1 μ l de solução protéica, 0,5 μ l de solução contendo AR (35mM) e 1 μ l de solução mãe (20% PEG4000, 0,1M citrato de sódio pH 5.6 e 20% 2-propanol). Os melhores cristais obtidos foram levados para coleta de dados na linha MX-2 da LNLS, em Campinas / SP e difrataram a 2,3 Å. Após o processamento dos dados, não foi possível identificar nenhuma densidade eletrônica que pudesse corresponder à molécula de AR durante a fase de refinamento. Três pontos foram então considerados: i) quantidade insuficiente do inibidor na solução de cristalização (inicialmente esta foi calculada em cinco moléculas de inibidor para cada molécula de proteína), ii) baixa resolução dos dados obtidos (considerando que o ligante pode ainda apresentar baixa ocupação), e iii) problemas de solubilidade do AR. Por esses motivos, tentativas de melhorar os cristais para aumentar a qualidade dos mesmos, bem como testes para melhorar a solubilidade do AR e aumentar a proporção do inibidor em relação à da proteína foram realizados. Uma nova busca inicial para obter uma possível diferente condição de cristalização também foi realizada, porém sem sucesso.

Nos novos experimentos realizados, a proporção de moléculas inibidor / proteína na gota foi aumentada e uma varredura por diferentes pHs em que os primeiros cristais do complexo foram obtidos foram testados. Após alguns meses, conseguimos cristais maiores (0,6 x 0,1 x 0,05 mm) (Figura 7c) e que difrataram à maior resolução (1,77 Å). As estatísticas da coleta de dados são apresentadas na Tabela I. Os cristais pertencem a grupo espacial $P2_12_12_1$, com parâmetros de cela unitária $a=49,4$, $b=67,0$ and $c=85,5$ Å. O conjunto de dados apresenta completeza de 95,1 % e R_{merge} de 6,8 %. Cálculos baseados no peso molecular da proteína indicaram a presença de duas moléculas na unidade assimétrica (Matthews, 1968).

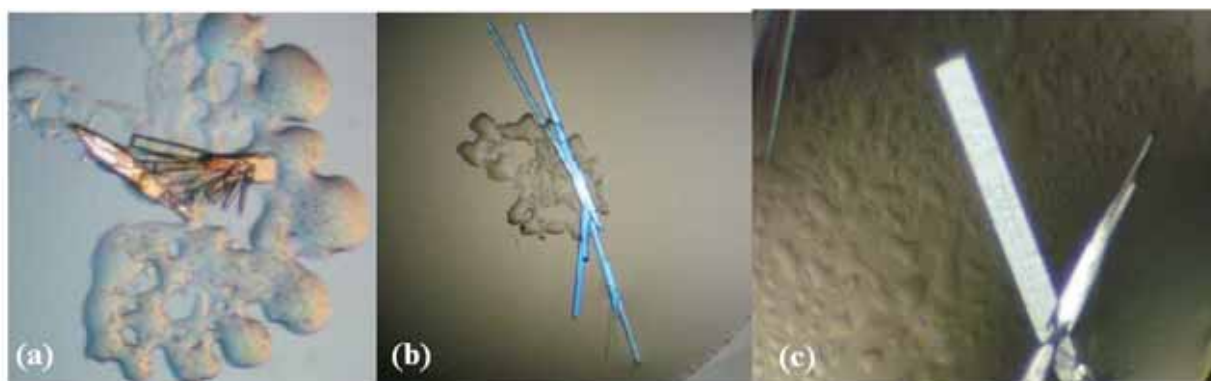


Figura 7. Cristais da proteína PrTX-I na presença do inibidor ácido rosmarínico (AR). (a) e (b) Policristais do complexo PrTX-I/AR. (c) Monocristal do complexo PrTX-I/AR obtido após otimização da condição de cristalização em que os cristais representados em (a) e (b) foram obtidos.

Após refinamento parcial da estrutura, observamos densidade eletrônica compatível com a do ligante em estudo na entrada de um dos canais hidrofóbicos da toxina (Figura 8). A inspeção da densidade eletrônica no mapa $2|F_{\text{obs}}| - |F_{\text{calc}}|$ também mostrou a presença de uma molécula de PEG4000 e oito moléculas de isopropanol (IOH) interagindo com a toxina.

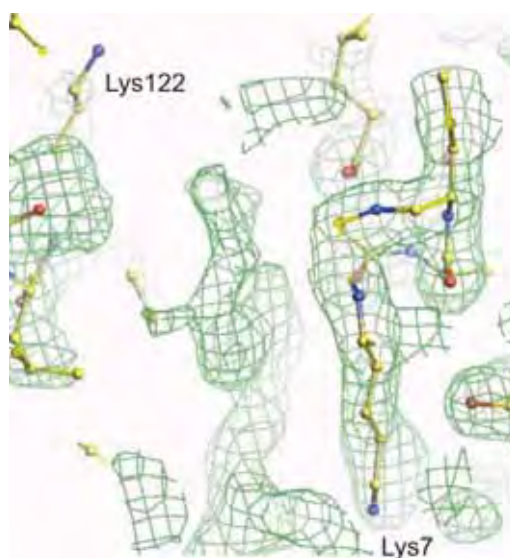


Figura 8. Mapa de densidade eletrônica $2|F_{\text{obs}}| - |F_{\text{c}}|$ (corte de 1σ) mostrando a região de entrada do canal hidrofóbico onde pode-se observar densidade eletrônica compatível com a de uma molécula de ácido rosmarínico nas proximidades dos aminoácidos Lys7 e Lys122. Figura retirada do artigo de dos Santos e colaboradores (Dos Santos *et al.*, 2010).

Tabela I. Estatísticas de coleta de dados de difração de raios X e de refinamento para a estrutura do complexo PrTX-I/AR.

	PrTX-I/AR
	a = 49,4
Cela unitária (Å)	b = 67,0
	c = 85,5
Grupo especial	P2 ₁ 2 ₁ 2 ₁
Resolução (Å)	40,0-1,77 (1,86-1,77) ^a
Reflexões únicas	26992 (3895) ^a
Dados completos a (%)	95,1 (97,5) ^a
Redundância	4,0 (3,3) ^a
R _{merge} ^b (%)	6,8 (41,2) ^a
Fonte de radiação	Síncrotron (linha MX2, LNLS)
Temperatura da coleta de dados (K)	100
I/σ(I)	16,5 (2,0) ^a
Coeficiente de Matthews V _M (Å ³ /Dalton)	2,62
Moléculas na unidade assimétrica	2
Conteúdo de solvente (%)	53,12
R _{crist} ^c (%)	16,0
R _{free} ^d (%)	21,7
B-factor médio (Å ²) ^e	
Total	37,2
Proteína	22,7
AR	44,2
Gráfico de Ramachandran ^e	
resíduos em regiões mais favoráveis (%)	89,9
resíduos em regiões adicionalmente permitidas (%)	9,1
resíduos em regiões generosamente permitidas (%)	1,0

^a Números em parênteses são para a faixa de mais alta resolução. ^b $R_{\text{merge}} = \frac{\sum_{\text{hkl}} (\sum_i (|I_{\text{hkl},i} - \langle I_{\text{hkl}} \rangle|))}{\sum_{\text{hkl},i} \langle I_{\text{hkl}} \rangle}$, onde $I_{\text{hkl},i}$ é a intensidade de uma medida individual de uma reflexão com índices de Miller h, k e l, e $\langle I_{\text{hkl}} \rangle$ é a intensidade média daquela reflexão. Calculado para $I > -3\sigma(I)$. ^c $R_{\text{crist}} = \frac{\sum_{\text{hkl}} (|F_{\text{obs}} - F_{\text{calc}}|)}{\sum_{\text{hkl}} F_{\text{obs}}}$, onde $|F_{\text{obs}}|$ e $|F_{\text{calc}}|$ são as amplitudes dos fatores de estrutura observados e calculados. ^d R_{free} é equivalente ao R_{crist} , porém calculado com 5% das reflexões omitidas no processo de refinamento. ^e Calculado com o programa Procheck (Laskowski *et al.*, 1993).

O modelo cristalográfico foi concluído e o mesmo apresentou $R = 16,0$ e $R_{\text{free}} = 21,7\%$ (Tabela I). Uma análise das interações estabelecidas pelo inibidor com a proteína mostra que o AR interage com a PrTX-I por meio de ligações de hidrogênio com os resíduos Phe3, Lys7, Leu10, Gln11 and Gly15 do monômero A (Figura 9) e com os resíduos Leu2, Arg72 e Trp77 deste mesmo monômero via molécula de água. Ainda, interações entre o AR e o resíduo Pro123 do monômero B são observadas (Figura 9), causando uma obstrução física da entrada do canal hidrofóbico do monômero A. Já o canal hidrofóbico do monômero B é ocupado por uma molécula de PEG4000, a qual estabelece contatos com a Phe3 e Lys7 do monômero B, sendo que a última ocorre também via uma molécula de água. Duas das oito moléculas de isopropanol (IOH) interagem com resíduos de His48 (átomos N δ 1) da estrutura dimérica através da molécula de água que faz parte do sítio ativo de PLA₂s catalíticas (Scott *et al.*, 1990). Ligações de hidrogênio também são observadas entre os resíduos Asn17:Tyr119 e Tyr119:Tyr119 dos monômeros que compõe a estrutura.

Os resíduos K36A, K78A, L116A e K129A no monômero A, e K70A, L116A e K127A no monômero B foram modelados como alaninas devido à falta de densidade eletrônica para as cadeias laterais dos resíduos em questão. Ainda, as cadeias laterais dos resíduos K38 e K69 do monômero A e E86, K93 e K122 do monômero B foram modeladas com configurações alternativas. A análise da qualidade do modelo demonstra que o mesmo apresenta uma boa estereoquímica, já que somente 1% dos resíduos se encontra em regiões menos favoráveis no gráfico de Ramachandran (Tabela I).

A comparação da estrutura do complexo PrTX-I/AR com a estrutura da proteína PrTX-I nativa (Dos Santos, Soares *et al.*, 2009) (PDB ID 2Q2J) mostrou um rearranjo entre seus monômeros induzido pela presença do ligante (Figura 10). Este rearranjo afetou principalmente o C-terminal de um de seus monômeros (r.m.s.d. geral de 1,04 and 0,59 Å para os monômeros A e B, respectivamente, e 2,65 e 0,58 Å para os respectivos C-terminais) (Figura 10). Este rearranjo pode ser caracterizado pelo estabelecimento da ligação de hidrogênio entre os resíduos de Tyr119 dos diferentes monômeros (Tyr 119-Tyr119) e é uma característica presente em todas as estruturas de Lys49-PLA₂s complexadas resolvidas até o presente momento (Dos Santos, Fernandes *et al.*, 2009; Dos Santos, Soares *et al.*, 2009; Marchi-Salvador *et al.*, 2009; Fernandes *et al.*, 2011).

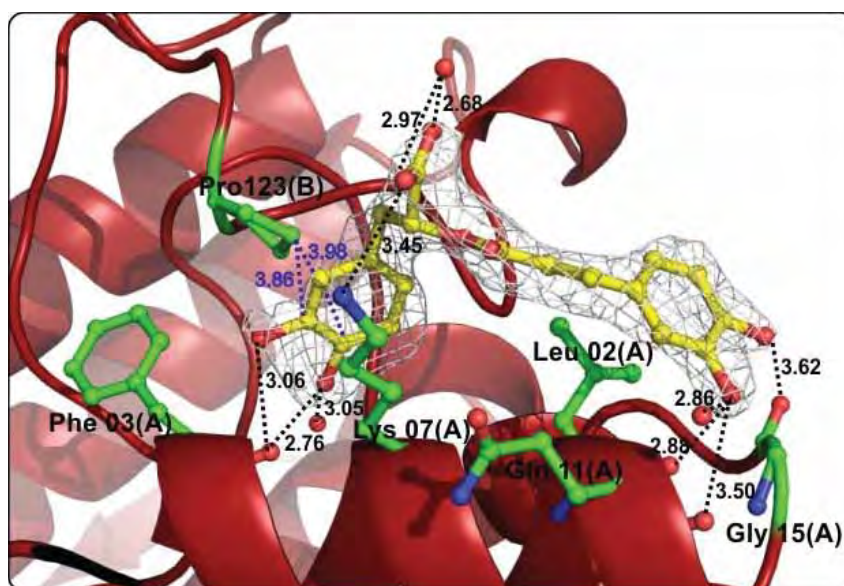


Figura 9. Interações entre a PrTX-I e seu inibidor ácido rosmarínico (AR). Resíduos cujos contatos se dão via moléculas de água não são demonstrados. Somente interações abaixo de 3,7Å são mostradas para interações ente o AR e o monômero A da proteína. Distâncias até 4,0 Å foram consideradas para interações entre o AR e o monômero B. O mapa de densidade eletrônica para a molécula de AR foi calculado com coeficientes $2|F_{\text{obs}}| - |F_{\text{calc}}|$ e contornados a 1.0σ . Figura gerada no programa *Pymol* (Delano, 2002).

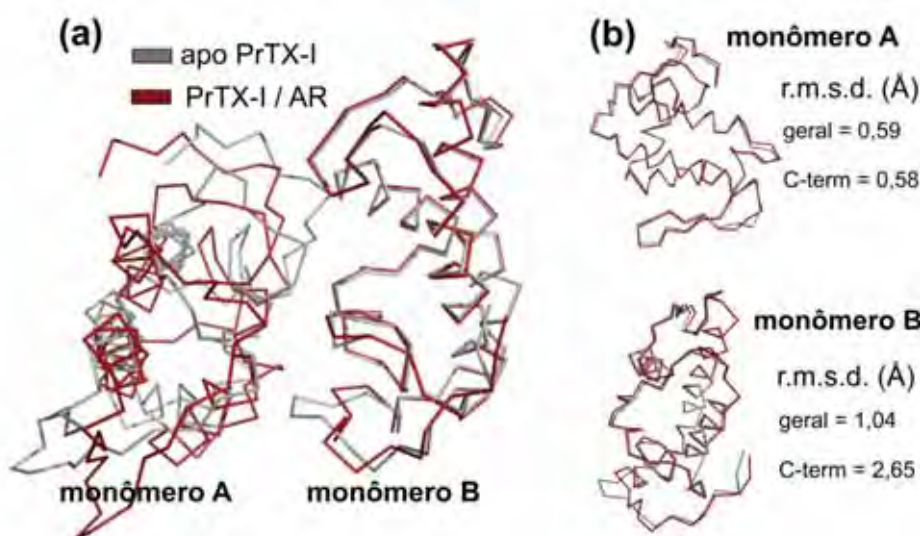


Figura 10. Sobreposição entre a PrTX-I nativa e PrTX-I/AR: (a) representação em forma de *ribbons* para os dímeros de ambas as estruturas; (b) sobreposição entre os monômeros correspondentes de ambas as estruturas. R.m.s.d. para o monômero todo e para o C-terminal (resíduos 115-129) é mostrado. O maior r.m.s.d. para o monômero B se deve a mudanças conformacionais induzidas na região C-terminal da PrTX-I após interação com o ligante AR. Figura gerada no programa *Pymol* (Delano, 2002).

Em 2009, uma revisão de todas as estruturas de Lys49-PLA₂s disponíveis no banco de dados PDB, tanto nas formas nativas quanto complexadas, serviu de base para a proposição do sítio miotóxico destas proteínas (resíduos responsáveis pela atividade desestabilizadora de membranas musculares) bem como seu mecanismo de ação (Dos Santos, Soares *et al.*, 2009). A proposta sugere um mecanismo de ação baseado em dois passos: num primeiro momento, ocorre a interação dos resíduos Lys20, Lys115 e Arg118 destas proteínas com a cabeça polar dos fosfolipídios de membrana e, posteriormente, ocorre um rearranjo na estrutura quaternária que possibilita a entrada de porções hidrofóbicas dos fosfolipídios no canal hidrofóbico da toxina (Dos Santos, Soares *et al.*, 2009). Desta forma, foi sugerido o envolvimento do canal hidrofóbico destas proteínas como parte do processo de miotoxicidade e a conservação dos resíduos que o compõe ficou então justificada (Dos Santos, Fernandes *et al.*, 2009; Dos Santos, Soares *et al.*, 2009).

A estrutura cristalográfica do complexo PrTX-I/AR evidencia que o inibidor interage com a toxina na entrada do seu canal hidrofóbico (Figura 11b). Considerando o recente e acima citado mecanismo de ação proposto para as Lys49-PLA₂s (Dos Santos, Soares *et al.*, 2009), sugere-se que o efeito inibitório do AR seja resultado de um impedimento estérico já que o mesmo bloqueia o acesso do substrato ao canal hidrofóbico da toxina, o qual é uma extensão do sítio miotóxico das Lys49-PLA₂s (Figura 12).

Interessantemente é possível observar que além do AR obstruir a entrada de um dos canais hidrofóbicos da PrTX-I, ele está diretamente relacionado com o C-terminal do outro monômero da toxina (Figura 11d). Esta observação demonstra como o arranjo quaternário (disposição dos monômeros entre si) das Lys49-PLA₂s botrópicas contribui para sua função (ex. porções hidrofóbicas dos fosfolipídios de membrana que se inserem no canal hidrofóbico de um monômero da toxina foram provavelmente “capturados / ancorados” pelo C-terminal do monômero oposto).

A comparação da estrutura do complexo PrTX-I/AR com duas outras estruturas de Lys49-PLA₂s complexadas com ácidos graxos (PDB ID 1QLL e 1XXS) (Lee *et al.*, 2001; Watanabe *et al.*, 2005) suporta a hipótese acima mencionada já que nesta

comparação fica evidente que o AR pode bloquear a entrada de ácidos graxos no canal hidrofóbico de Lys49-PLA₂s por obstruir fisicamente a entrada deste canal (Figura 11c).

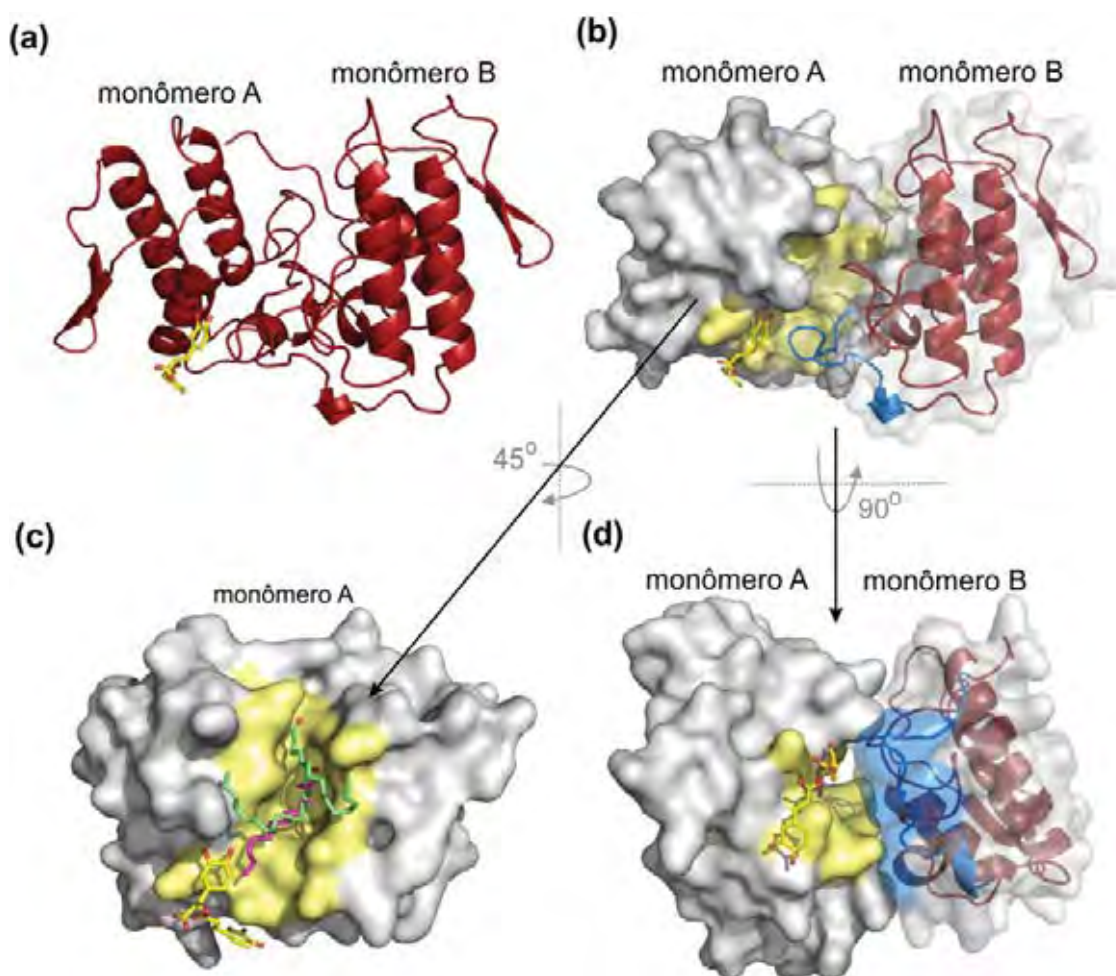


Figura 11. Estudos estruturais comparativos entre a PrTX-I/AR e duas outras estruturas de Lys49-PLA₂s complexadas com ácidos graxos. (a) Representação dimérica do complexo PrTX-I/AR em forma de *cartoon*; a molécula de AR é representada em *sticks*. (b) Representação dimérica do complexo PrTX-I/AR, onde os monômeros são representados na forma de superfície; o monômero B é representado com superfície semi-transparente e o AR, em *sticks*. (c) Sobreposição dos monômeros A dos complexos PrTX-I/AR, PrTX-II/ácido graxo (em azul) e MjTX-II/ácido graxo (em rosa), mostrando que os ácidos graxos ocupam o canal hidrofóbico da proteína, região cuja entrada é ocupada pelo AR. (d) Representação em superfície do complexo PrTX-I/AR onde fica evidente que o canal hidrofóbico do monômero A da estrutura está intimamente relacionado com a região C-terminal do monômero B. Para as representações em superfície, o canal hidrofóbico dos monômeros são mostrados em amarelo e os resíduos 119 a 125 do C-terminal do monômero B da proteína (resíduos 119-125) são mostrados em azul. Figura gerada no programa *Pymol* (Delano, 2002).

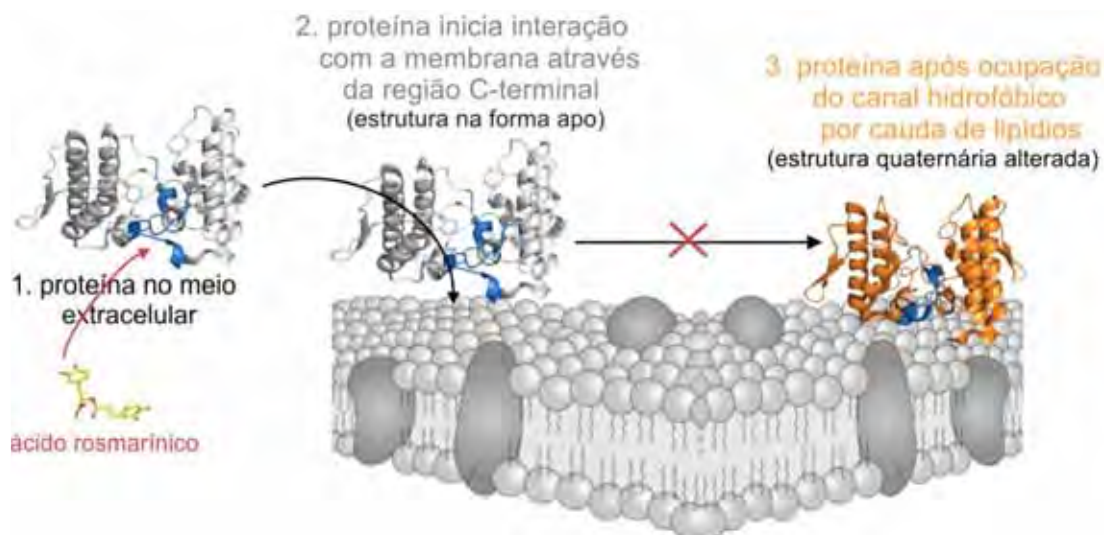


Figura 12. Modelo de inibição de Lys49-PLA₂s botrópicas pelo ácido rosmarínico (AR). O AR interage com resíduos específicos da toxina (Figura 9), ocupando a entrada do canal hidrofóbico de um de seus monômeros, conforme representado na Figura 11b. Nesta configuração, embora a toxina possa interagir com a membrana por meio da região C-terminal (em azul; passo 2), seu canal hidrofóbico não pode ser ocupado por porções hidrofóbicas de fosfolipídios da membrana já que o AR obstrui fisicamente sua entrada.

Durante o andamento deste trabalho, uma colaboração foi estabelecida com o Laboratório de Farmacologia da Junção Neuromuscular, chefiado pela profa. Dra. Márcia Gallacci, do Depto. de Farmacologia, da UNESP / Botucatu. O efeito *in vitro* do AR nas atividades de lesão muscular e de bloqueio neuromuscular causado pela PrTX-I foi avaliado em preparações nervo frênico - músculo diafragma neste laboratório durante o trabalho de mestrado do aluno Fábio Florença Cardoso. Os resultados obtidos demonstraram que o AR é capaz de prevenir aproximadamente 80% das lesões musculares e em torno de 90% o bloqueio neuromuscular causado pela toxina (artigo submetido; Anexo II). Desta forma, concluímos que a presença de inibidores que interagem com as Lys49-PLA₂s em locais diferentes do sítio miotóxico (região C-terminal) também são capazes de afetar a atividade destas toxinas. Assim, baseando-se no mecanismo de ação de Lys49-PLA₂s (Dos Santos, Soares *et al.*, 2009), é possível inferir maneiras diferentes e provavelmente simultâneas de inibir estas proteínas: i) por inibição da região C-terminal, diretamente do sítio miotóxico (ex. heparina) (Lomonte, Tarkowski *et al.*, 1994), e ii) por inibição física do canal hidrofóbico (ex. PEG400) (Murakami *et al.*, 2007) ou prevenção da sua ocupação (ex. AR). A combinação de todas estas possibilidades pode levar ao sucesso na inibição de Lys49-PLA₂s

botrópicas. Este conhecimento também pode servir como base para o desenho de compostos adjuvantes que complementem a soroterapia.

O artigo referente à cristalização deste complexo foi publicado no periódico **Acta Crystallographica – Section F**, em 2010: “*Crystallization and preliminary X-ray crystallographic studies of a Lys49-phospholipase A2 homologue from Bothrops pirajai venom complexed with rosmarinic acid*” (Anexo I). Recentemente, a redação do artigo referente à estrutura do complexo, juntamente com os dados funcionais obtidos no laboratório da profa. Márcia Gallacci, foi concluída e o mesmo está em fase de submissão (Anexo II).

4.1.1. Dificuldades encontradas para a obtenção da estrutura do complexo

Durante o trabalho com o complexo mencionado, alguns conjuntos de dados foram coletados e refinados. No entanto, em alguns deles não obtivemos sucesso na identificação de densidades eletrônicas para o AR, apesar da mudança de grupo espacial em relação à proteína nativa ($P2_12_12_1 \times P3_121$) estar sempre presente. A resolução do problema só foi possível quando o AR comercial foi dissolvido em solução contendo 50% de etanol.

4.2. Estudos estruturais com o Lys49-PLA₂s complexadas com Mn²⁺ por cristalografia de raios X

A seguir serão descritos os resultados e discussão relacionada aos estudos estruturais com a PrTX-I e BthTX-I complexadas com íons manganês. As etapas realizadas até a obtenção de resultados que permitiram afirmar a presença de Mn²⁺ na estrutura cristalográfica são relatadas. Os primeiros dados foram obtidos com a proteína PrTX-I, porém, devido à indisponibilidade da amostra em nosso laboratório, passamos a utilizar a proteína BthTX-I nos experimentos, já que esta apresenta 98% de identidade com a PrTX-I, conforme descrito na seção 3.1.2. Vale ressaltar aqui também que os trabalhos descritos a seguir também são parte do mestrado de Rafael Junqueira Borges, aluno de nosso laboratório.

4.2.1. Experimentos com $MnCl_2$ na condição de cristalização como fonte de íons manganês

Os primeiros cristais obtidos (Figura 13) foram submetidos à difração de raios X na linha MX-1 do LNLS, em Campinas / SP. Dois conjuntos de dados foram coletados (1,9Å e 2,1Å de resolução) e, após a elucidação das estruturas, observou-se que os cristais eram isomorfos ao da PrTX-I nativa (grupo espacial $P3_121$). As duas estruturas foram refinadas e as estatísticas para cada um dos conjuntos são apresentadas na Tabela II. Alguns possíveis locais de interação dos íons manganês com a proteína foram identificados após inspeção de densidades eletrônicas; no entanto, observou-se que tanto Li^+ , Cl^- e moléculas de água (também presentes na solução de cristalização) podiam ocupar estas posições. Assim, analisamos o fator temperatura dos três possíveis ligantes bem como as ocupações dos mesmos nas densidades correspondentes (com o programa CNS (Brunger *et al.*, 1998)). Como estas análises foram inconclusivas e descartou-se apenas a possibilidade das densidades serem correspondentes a íons lítio, optamos por tentar cristalizar o complexo na mesma condição de cristalização, porém utilizando $MnSO_4$ como fonte de Mn^{2+} ao invés de $MnCl_2$, já que os resultados obtidos nos levaria a descartar também os íons cloro. Outra tentativa de resolver este problema foi coletar dados em λ que gerassem dados anômalos para o manganês dos cristais do complexo em questão, já que a linha MX-2 do LNLS (Campinas / SP) oferece esta possibilidade.



Figura 13. Cristais do complexo PrTX-I / Mn^{2+} que difratam a 1,9 Å de resolução.

Tabela II. Estatísticas de coleta de dados de difração de raios X e refinamento para o complexo PrTX-I / Mn²⁺ a 2,1Å e 1,9Å

	Conjunto 2,1 Å	Conjunto 1,9 Å
Cela unitária (Å)	a = b = 56,78 c =130,36	a = b = 56,77 c =130,36
Grupo Espacial	P3 ₁ 21	P3 ₁ 21
Resolução (Å)	40,0-2,1 (2,18-2,10) ^a	40,0-1,90 (1,97-1,90) ^a
Reflexões únicas	13972 (1383) ^a	16872 (1647) ^a
Dados completo a (%)	96,5 (98,9) ^a	92,3 (91,8) ^a
R _{merge} ^b (%)	7,7 (59,6) ^a	10,1 (56,7) ^a
I/σ (I)	26,4 (1,8) ^a	13,8 (2,3) ^a
R _{crist} ^c (%)	22,17	19,71
R _{free} ^d (%)	26,72	23,04
Gráfico de Ramachandran ^e (%)		
- Resíduos em regiões favoráveis	86,7	87,2
- Resíduos em regiões adicionalmente permitidas	11,8	12,3
- Resíduos em regiões generosamente permitidas	1,0	0,5
- Resíduos em regiões não-permitidas	0,5	0

^a Números em parênteses são para a faixa de mais alta resolução. ^b $R_{merge} = \sum_{hkl} (\sum_i (|I_{hkl,i} - \langle I_{hkl} \rangle|)) / \sum_{hkl,i} \langle I_{hkl} \rangle$, onde $I_{hkl,i}$ é a intensidade de uma medida individual de uma reflexão com índices de Miller h, k e l, e $\langle I_{hkl} \rangle$ é a intensidade média daquela reflexão. Calculado para $I > -3\sigma(I)$. ^c $R_{crist} = R_{hkl} (| |F_{obs_{hkl}}| - |F_{calc_{hkl}}| |) / |F_{obs_{hkl}}|$, onde $|F_{obs_{hkl}}|$ e $|F_{calc_{hkl}}|$ são as amplitudes dos fatores de estrutura observados e calculados. ^d R_{free} é equivalente ao R_{crist} , porém calculado com 5% das reflexões omitidas no processo de refinamento. ^e Calculado com o programa Procheck (Laskowski *et al.*, 1993).

4.2.2. Experimentos com $MnSO_4$ na condição de cristalização como fonte de íons manganês

Os cristais obtidos na presença de $MnSO_4$ (Figura 14) difrataram à 1,54 Å na linha MX-2 do LNLS, Campinas/SP. O conjunto de dados obtido foi processado (Tabela III) e a substituição molecular foi realizada utilizando-se a proteína PrTX-I complexada com alfa-tocoferol como modelo (código de acesso no PDB 3CYL), já que esta apresenta o mesmo grupo espacial encontrado para o conjunto de dados em estudo. Após vários ciclos de refinamento, moléculas de PEG (polietilenoglicol), íons sulfato e água foram adicionados ao modelo. Cabe ressaltar aqui que densidades eletrônicas correspondentes a moléculas de PEG não foram encontradas nos outros dois conjuntos de dados obtidos (seção 4.2.1.). Curiosamente, o grupo espacial apresentado pelo cristal do complexo PrTX-I/ Mn^{2+} que cresceu em presença de $MnSO_4$ foi diferente do obtido pelo que cresceu em presença de $MnCl_2$ ($P2_1 \times P3_121$, respectivamente). Assim sendo, é provável que a maior concentração de SO_4^{2-} na gota tenha favorecido uma mudança no arranjo quaternário da toxina, já que havia igual concentração de PEG e outros compostos na solução de cristalização nos dois casos.

As estatísticas da coleta de dados e refinamento para o conjunto em questão são apresentadas na Tabela III.



Figura 14. Cristal de PrTX-I / Mn^{2+} crescido em presença de $MnSO_4$

Tabela III. Estatísticas de refinamento e dos dados de difração de raios X para o complexo PrTX-I / Mn²⁺ crescido em presença de MnSO₄

	a=39,45
Cela unitária (Å)	b=72,17
	c=44,90
Grupo Espacial	P2 ₁
Resolução (Å)	40,0-1,54 (1,60-1,54) ^a
Reflexões únicas	34200 (3403) ^a
Dados completos a (%)	93,7 (93,6) ^a
Redundância	2,7 (2,5) ^a
R _{merge} ^b (%)	5,9 (44,3) ^a
I/σ (I)	26,40 (1,97) ^a
R _{crist} ^{c, #} (%)	18,05
R _{free} ^{d, #} (%)	25,67
Gráfico de Ramachandran ^e (%)	
- Resíduos em regiões favoráveis	92,0
- Resíduos em regiões adicionalmente permitidas	8,0

^a Números em parênteses são para a faixa de mais alta resolução. ^b $R_{merge} = \sum_{hkl} (\sum_i (|I_{hkl,i} - \langle I_{hkl} \rangle|)) / \sum_{hkl,i} \langle I_{hkl} \rangle$, onde $I_{hkl,i}$ é a intensidade de uma medida individual de uma reflexão com índices de Miller h, k e l, e $\langle I_{hkl} \rangle$ é a intensidade média daquela reflexão. Calculado para $I > -3\sigma(I)$. ^c $R_{crist} = R_{hkl} (|\sum |F_{obs_{hkl}}| - |F_{calc_{hkl}}||) / \sum |F_{obs_{hkl}}|$, onde $|F_{obs_{hkl}}|$ e $|F_{calc_{hkl}}|$ são as amplitudes dos fatores de estrutura observados e calculados. ^d R_{free} é equivalente ao R_{crist} , porém calculado com 5% das reflexões omitidas no processo de refinamento. ^e Calculado com o programa Procheck (Laskowski *et al.*, 1993).

O refinamento do modelo foi realizado até as estatísticas de $R=18,0$ e $R_{free}=25,7\%$. Posteriormente, uma busca por regiões candidatas aos íons manganês observando-se a densidade eletrônica foi realizada. No entanto, não foi possível estabelecer uma metodologia que realmente assegurasse a presença dos íons em nenhuma das regiões candidatas, já que moléculas de água também poderiam ocupar estas posições, como descrito anteriormente (seção 4.2.1.). Ainda, devido à mudança do

grupo espacial, existia a possibilidade da interação de íons manganês em diferentes regiões (comparando-se este conjunto de dados com os outros dois em grupo espacial P3₁21 acima mencionados – seção 4.2.1.). Desta forma, concluímos que somente dados de espalhamento anômalo são capazes de diferenciar e provar a presença de Mn²⁺ interagindo com a PrTX-I.

4.2.3. Experimentos de espalhamento anômalo para o elemento manganês

Após insucesso nas tentativas de identificar Mn²⁺ nas estruturas cristalográficas do complexo PrTX-I/Mn²⁺ a partir de dados coletados em λ de 1,37757 Å (dados apresentados nas Tabelas II e III), alguns dos novos cristais obtidos (Figura 15) foram submetidos à varredura de fluorescência na linha MX-2 do LNLS, em Campinas/SP, para confirmação da presença de Mn²⁺ nos cristais bem como para estabelecer os comprimentos de onda em que os conjuntos de dados deveriam ser coletados (referente ao pico e remoto para o elemento em estudo). Este procedimento é realizado para maximizar o sinal do espalhamento anômalo para o átomo escolhido (no caso, o Mn²⁺).

Num primeiro momento, coletamos dois conjuntos de dados para o mesmo cristal (cuja fonte de Mn²⁺ era MnCl₂), porém em diferentes comprimentos de onda (Tabela IV).

Após elucidação da estrutura utilizando o conjunto de dados obtido no referente ao remoto (λ de 1,37757 Å; estatísticas de coleta na Tabela IV) e realização de refinamento automático (programa REFMAC) seguido de ajustes manuais (programa Coot), o modelo apresentou estatísticas de R=25% e R_{free}=31,2%. Neste momento, com o auxílio do programa FFT Map (disponível no pacote CCP4), um mapa de Patterson foi gerado utilizando-se o conjunto de reflexões referentes ao espalhamento anômalo para a identificação da(s) possível(-eis) posição(-ões) do manganês. Para esta finalidade, o conjunto de dados referente ao pico (λ =1,89226) foi utilizado já que neste λ maximiza-se a informação da diferença dos pares anômalos. Considerando um sinal de 5 σ , duas regiões candidatas foram observadas na densidade eletrônica (Figura 16).

Após a identificação das regiões correspondentes ao manganês, os íons foram inseridos em suas respectivas posições e o refinamento deste conjunto foi concluído. Após alguns ciclos de refinamento automático e ajustes manuais, adição de

moléculas de água, sulfato e de Tris, o modelo apresentou estatísticas de $R=18,5\%$ e $R_{\text{free}}=24,8\%$. A análise do modelo com o programa Procheck (Laskowski *et al.*, 1993) indicou uma ótima qualidade estereoquímica, já que nenhum resíduo foi encontrado fora da região permitida no gráfico de *Ramachandran* (Tabela IV). O fator temperatura dos íons de manganês neste momento era de 33,85 e 46,66 \AA^2 (Mn^{2+} com ocupação de 35% e 80%, respectivamente; fator temperatura médio do complexo = 36,2 \AA^2).

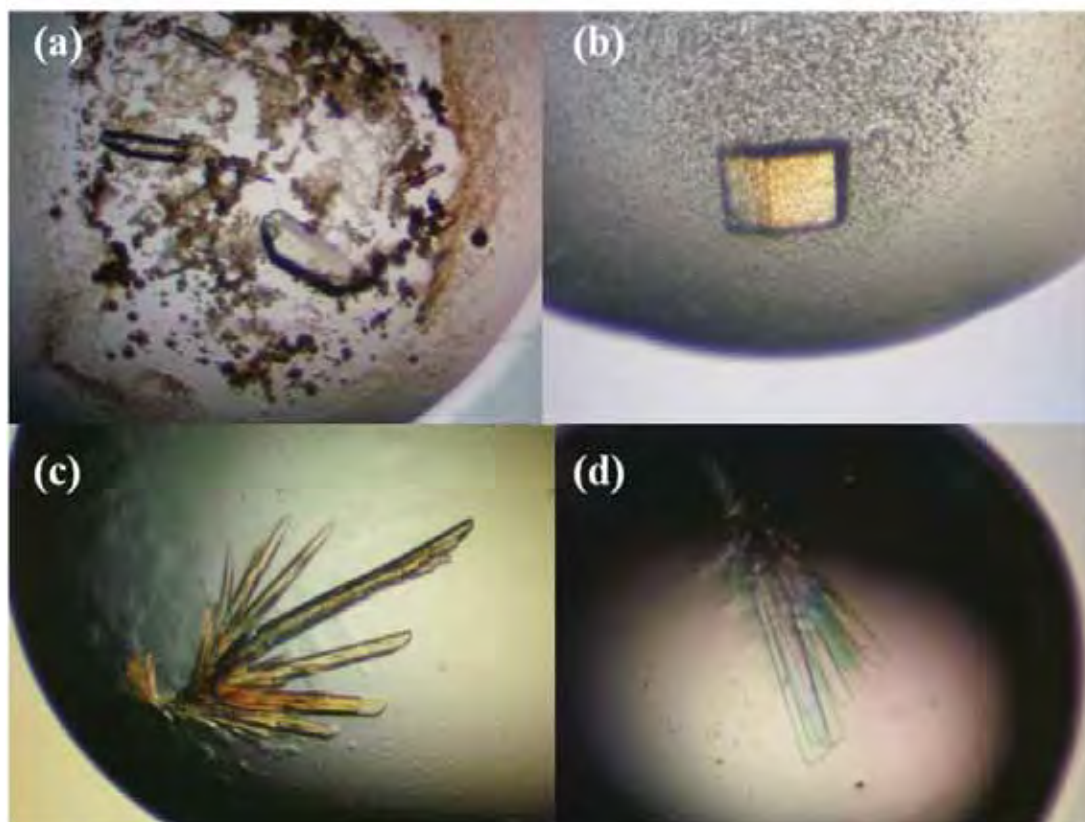


Figura 15. Cristais do complexo PrTX-I/ Mn^{2+} submetidos a testes de fluorescência. Dados foram coletados indicando que os mesmos pertencem ao grupo espacial $P3_121$ ((a) e (b)) e $P2_1$ ((c) e (d)). Os cristais que apresentam grupo espacial $P3_121$ apresentam-se únicos, em formato hexagonal, e tem um bom crescimento nas três dimensões ((a) e (b)); já os que apresentam grupo espacial $P2_1$ geralmente crescem em formato de feixes, e têm crescimento bem mais acentuado em duas de suas dimensões((c) e (d)).

Tabela IV. Estatísticas dos dados de difração de raios X e refinamento para o complexo PrTX-I/Mn²⁺ coletados nos comprimentos de onda referentes ao pico e remoto no grupo espacial P3₁21.

	Pico [#]	Remoto
Comprimento de onda (Å)	1,89226	1,37757
Energia da linha (eV)	6.552,2	9.000,2
	a = b = 57,08	a = b = 57,10
Cela unitária (Å)	c = 131,62	c = 131,64
Grupo espacial (Å)	P3 ₁ 21	P3 ₁ 21
Resolução (Å)	40,0-2,15 (2,24-2,15) ^a	40,0-1,85 (1,92-1,85) ^a
Reflexões únicas	14030 (1541) ^a	21134 (2239) ^a
% de dados coletados	98,9 (99,9) ^a	96,1 (94,6) ^a
Redundância	3,4 (3,3) ^a	3,3 (3,2) ^a
R _{merge} ^b (%)	6,0 (19,2) ^a	6,8 (38,9) ^a
I/σ (I)	17,59 (6,29) ^a	15,04 (3,11) ^a
R _{crist} ^c (%)	-	18,2
R _{free} ^d (%)	-	25,3
Gráfico de Ramachandran ^e (%)		
- resíduos em regiões favoráveis	-	89,4
- resíduos em regiões adicionalmente permitidas	-	9,6
- resíduos em regiões generosamente permitidas	-	1,0
- resíduos em regiões não-permitidas	-	0

^a Números em parênteses são para a faixa de mais alta resolução. ^b $R_{\text{merge}} = \sum_{\text{hkl}} (\sum_i (|I_{\text{hkl},i} - \langle I_{\text{hkl}} \rangle|)) / \sum_{\text{hkl},i} \langle I_{\text{hkl}} \rangle$, onde $I_{\text{hkl},i}$ é a intensidade de uma medida individual de uma reflexão com índices de Miller h, k e l, e $\langle I_{\text{hkl}} \rangle$ é a intensidade média daquela reflexão. Calculado para $I > -3\sigma(I)$. ^c $R_{\text{crist}} = R_{\text{hkl}} (| |F_{\text{obs}_{\text{hkl}}}| - |F_{\text{calc}_{\text{hkl}}}| |) / |F_{\text{obs}_{\text{hkl}}}|$, onde $|F_{\text{obs}_{\text{hkl}}}|$ e $|F_{\text{calc}_{\text{hkl}}}|$ são as amplitudes dos fatores de estrutura observados e calculados. ^d R_{free} é equivalente ao R_{crist} , porém calculado com 5% das reflexões omitidas no processo de refinamento. ^e Calculado com o programa Procheck (Laskowski *et al.*, 1993). [#] Conjunto de dados utilizado somente para gerar o mapa de Patterson.

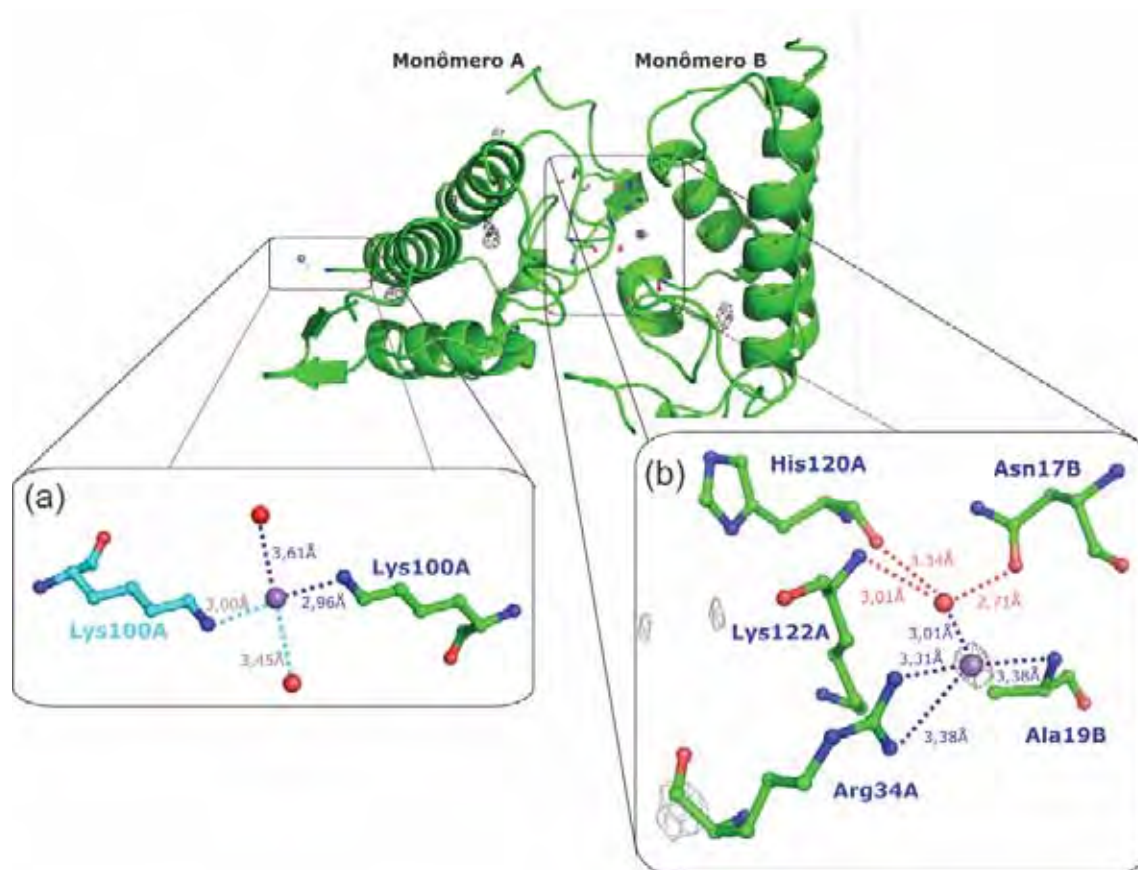


Figura 16. Regiões de coordenação do Mn^{2+} na estrutura da PrTX-I complexada com íons manganês obtida em grupo espacial $P3_121$. O modelo cristalográfico da estrutura da PrTX-I/ Mn^{2+} é representado em *cartoon* e os resíduos da proteína que participam da coordenação do Mn^{2+} são destacados em *sticks*. As esferas vermelhas e roxas correspondem a moléculas de água e íons Mn^{2+} , respectivamente. (a) Mn^{2+} sendo coordenado pela Lys100 do monômero A e uma molécula de água da estrutura cristalográfica e pelos mesmos átomos da simetria cristalográfica (ligações destacadas em azul claro). (b) Coordenação do íon manganês pelos resíduos Arg34 do monômero A, Ala19 do monômero B e uma água. A densidade eletrônica com sinal 5σ no mapa de Patterson para o átomo de manganês é mostrada na figura. Somente interações menores que 3,65 Å foram consideradas. Figura gerada no programa *Pymol* (Delano, 2002).

Para confirmar a presença do manganês na estrutura, um mapa de Patterson foi gerado novamente, porém agora utilizando o modelo de estrutura refinado contra o conjunto de dados de maior resolução (dados coletados para λ remoto; resolução de 1,85 Å), já que neste momento a estrutura apresentava melhores estatísticas, e conseqüentemente, uma melhor estimativa das fases. Então, os íons foram retirados do último modelo de 1,85 Å de resolução e foram realizados dez ciclos de refinamento anisotrópico. Após inspeção do mapa com sinal de espalhamento anômalo (mapa de Patterson), as regiões previamente estabelecidas foram confirmadas (Figura 16). Os íons foram então mantidos no modelo final e suas ocupações foram refinadas de acordo com

a análise do mapa diferença $F_c - |F_o|$, já que o uso de ocupação de 100% se mostrou incompatível com o mapa analisado para ambas as posições. A análise do modelo final indica que um destes íons manganês é encontrado nas proximidades da Lys100, em região de simetria cristalográfica, sendo coordenado pelo átomo N ζ de sua cadeia lateral e uma molécula de água (Figura 16a); já o outro íon manganês presente nesta estrutura é coordenado pela Arg34 do monômero A da toxina, pela Ala19 do monômero B e uma molécula de água (Figura 16b); ainda, o mesmo, juntamente com os resíduos His120 e Lys122 do monômero A e com a Asn17 do monômero B, faz parte da coordenação de uma molécula de água nesta estrutura cristalográfica (Figura 16b).

A coleta de dados referente ao cristal cuja fonte de Mn²⁺ era MnSO₄ também foi realizada no LNLS (Campinas, SP) sendo que dois conjuntos de dados, um referente ao pico e outro ao remoto (λ de 1,89200 e 1,45900 respectivamente), também foram coletados para este cristal (estatísticas de coleta na Tabela V). Interessantemente, após processamento destes dados foi possível observar que o cristal crescido na presença de MnSO₄ apresenta diferente empacotamento quando comparado ao crescido na presença de MnCl₂ (grupo espacial P2₁ X P3₁21, respectivamente). A estrutura foi resolvida por substituição molecular utilizando-se o conjunto de dados obtido no λ referente ao remoto. Após realização de refinamento automático (programa REFMAC) seguido de ajustes manuais (programa Coot), o modelo apresentou estatísticas de R=24,6% e R_{free}=26,8%. Neste momento, o mesmo procedimento adotado para o conjunto de dados P3₁21 foi empregado. Um mapa de Patterson foi gerado utilizando-se dados de espalhamento anômalo (coletado no λ 1,89220 Å; Tabela V) para a identificação das possíveis posições do manganês na estrutura cristalográfica. Considerando um sinal de 3 σ , duas regiões candidatas foram observadas na densidade eletrônica (Figura 17).

Após a identificação das regiões correspondentes ao manganês, os íons foram inseridos em suas respectivas posições e o refinamento deste conjunto foi concluído. Após alguns ciclos de refinamento automático e ajustes manuais, adição de moléculas de água e de sulfato, o modelo apresentou estatísticas de R=16,5% e R_{free}=22,0%. Os íons apresentaram ocupação de 50% e fator temperatura de 32,95 e 41,92 Å², respectivamente (fator temperatura médio da complexo = 27,3 Å²). A análise do modelo com o programa Procheck (Laskowski *et al.*, 1993) indicou uma ótima qualidade estereoquímica para o modelo, sendo que nenhum resíduo se apresenta fora da região permitida no gráfico de *Ramachandran* (Tabela V).

Tabela V. Estatísticas dos dados de difração de raios X e refinamento para o complexo BthTX-I/Mn²⁺ coletados nos comprimentos de onda referentes ao pico e remoto no grupo espacial P2₁.

	Pico [#]	Remoto
Comprimento de onda (Å)	1,89220	1,45900
Energia da linha (eV) [*]	6.553,1	8.497,8
Cela unitária (Å)	a = 39,4; b = 72,2; c = 44,78	a = 39,5; b = 72,4; c = 44,9
Grupo espacial (Å)	P2 ₁	P2 ₁
Resolução (Å)	40,0-2,05 (2,12-2,05) ^a	40,0-1,58 (1,66-1,58) ^a
Reflexões únicas	14361 (1385) ^a	32516 (4526) ^a
% de dados coletados	92,8 (90,4) ^a	96,1 (94,1) ^a
Redundância	3,1 (3,0) ^a	3,5 (3,4) ^a
R _{merge} ^b (%)	5,2 (9,2) ^a	6,2 (31,8) ^a
I/σ (I)	44,4 (26,4) ^a	17,5 (4,2) ^a
R _{críst} ^{c, #} (%)	-	16,5
R _{free} ^{d, #} (%)	-	22,0
Gráfico de Ramachandran ^{e, #} (%)		
- resíduos em regiões favoráveis	-	92,2
- resíduos em regiões adicionalmente permitidas	-	6,8
- resíduos em regiões generosamente permitidas	-	1,0
- resíduos em regiões não-permitidas	-	0

^a Números em parênteses são para a faixa de mais alta resolução. ^b $R_{\text{merge}} = \sum_{\text{hkl}} (\sum_i (|I_{\text{hkl},i} - \langle I_{\text{hkl}} \rangle|)) / \sum_{\text{hkl},i} \langle I_{\text{hkl}} \rangle$, onde $I_{\text{hkl},i}$ é a intensidade de uma medida individual de uma reflexão com índices de Miller h, k e l, e $\langle I_{\text{hkl}} \rangle$ é a intensidade média daquela reflexão. Calculado para $I > -3\sigma(I)$. ^c $R_{\text{críst}} = R_{\text{hkl}} (| |F_{\text{obs}}_{\text{hkl}}| - |F_{\text{calc}}_{\text{hkl}}| |) / |F_{\text{obs}}_{\text{hkl}}|$, onde $|F_{\text{obs}}_{\text{hkl}}|$ e $|F_{\text{calc}}_{\text{hkl}}|$ são as amplitudes dos fatores de estrutura observados e calculados. ^d R_{free} é equivalente ao $R_{\text{críst}}$, porém calculado com 5% das reflexões omitidas no processo de refinamento. ^e Calculado com o programa Procheck (Laskowski *et al.*, 1993). [#] Conjunto de dados utilizado somente para gerar o mapa de Patterson.

O modelo estrutural final da BthTX-I complexada com íons manganês obtido na presença de MnSO_4 (grupo espacial $P2_1$) evidencia a presença de PEG4000 em ambos os canais hidrofóbicos da proteína (Figura 17), fator este que provavelmente levou à mudança no grupo espacial (cristais crescidos na presença de MnCl_2 não possuem o polímero PEG4000 interagindo com o canal hidrofóbico da proteína, embora a concentração do mesmo na condição de cristalização seja idêntica em ambos os casos). Ainda, PEG4000 foi encontrado ao redor da lisina 7 de um dos monômeros, achado este que já foi observado em outras Lys49-PLA₂s crescidas em grupo espacial $P2_1$ ou $P2_12_12_1$ (Watanabe *et al.*, 2005; Dos Santos, Soares *et al.*, 2009; Fernandes *et al.*, 2011). Observam-se ainda neste modelo estrutural íons sulfato interagindo com a proteína, sendo que alguns deles estabelecem ligações de hidrogênio com os resíduos Lys20, Lys115 e Arg118, observações estas também já feitas em outras estruturas com semelhante empacotamento cristalino (Delatorre *et al.*; Dos Santos, Soares *et al.*, 2009).

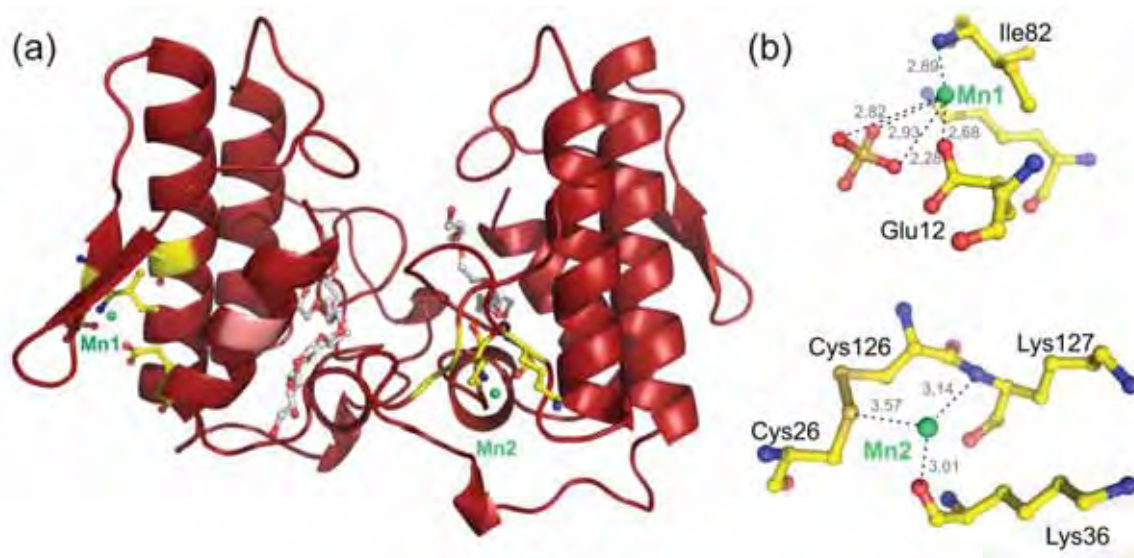


Figura 17. Estrutura da BthTX-I complexada com Mn^{2+} obtida no grupo espacial $P2_1$. (a) Modelo cristalográfico da estrutura da BthTX-I/ Mn^{2+} em *cartoon*. As moléculas do polímero PEG 4000 que interagem com a proteína são mostradas em *sticks*. Em verde, íons manganês. Os resíduos da proteína que fazem parte da coordenação dos íons Mn^{2+} também são destacados em *sticks*. (b) Coordenação dos íons manganês por alguns resíduos da BthTX-I e íon sulfato. Somente interações com distâncias inferiores a 3,7Å foram consideradas. Figura gerada no programa *Pymol* (Delano, 2002).

4.2.3.1. Dificuldades encontradas para o trabalho com dados anômalos

Durante o desenvolvimento deste trabalho, algumas tentativas de coleta de dados de espalhamento no LNLS foram dificultadas por problemas na linha MX-2. Desta forma, mesmo em posse de cristais que difratavam bem, dificilmente conseguíamos fazer o teste de fluorescência ou mesmo realizar a varredura para saber com exatidão o comprimento de onda relativo ao pico que deveríamos coletar novos dados. Esta precisão é importante visto que diferenciar o sinal de um espalhador anômalo dos demais átomos presentes na estrutura cristalográfica é difícil já que este sinal é bastante discreto; desta forma, dados coletados em λ errado poderiam inviabilizar a obtenção das informações necessárias para a confirmação das posições dos átomos de manganês na estrutura. Ainda, os íons manganês podem estar em baixa ocupação no cristal, sendo necessária então a coleta no λ mais preciso possível.

Em abril deste ano, durante a participação no curso RapiData (*A Practical Course in Macromolecular X-ray Diffraction Measurement*), houve disponibilização das linhas do NSLS (*National Synchrotron Light Source*) do BNL (*Brookhaven National Laboratory*) para os participantes do curso coletarem suas amostras. Assim, dois conjuntos de dados, um para cada grupo espacial, foram coletados. Para ambos os conjuntos, varreduras de fluorescência foram realizadas confirmando a presença de manganês nas amostras (Figura 18). A coleta de um conjunto de dados para cada grupo espacial foi realizada, porém somente no comprimento de onda relativo ao pico do elemento Mn^{2+} (λ de 1,72000 para o cristal com Mn^{2+} de grupo espacial $P3_121$ e λ de 1,8961 para o cristal com Mn^{2+} de grupo espacial $P2_1$; Energia de 7208,4 e 6.5389 eV, respectivamente).

Em seguida, os dados foram processados e, para ambos os casos (conjuntos de dados), nenhum pico demonstrando densidade eletrônica para o manganês foi detectado no mapa de Patterson, embora sinais de fluorescência tenham indicado a presença de manganês nas amostras (Figura 18). Somente densidades eletrônicas para o enxofre (correspondente às pontes dissulfeto e cadeias laterais de metioninas) foram observadas no mapa. Uma possível explicação para tal fato é que os cristais, antes de serem resfriados, eram “lavados” em solução-mãe livre de manganês e contendo 10% de solução de EDTA. Este procedimento, realizado na tentativa de extrair do cristal íons que não estivessem coordenados ou mesmo em canais da proteína, pode ter provocado o

deslocamento dos íons que estavam interagindo em posições consideradas importantes. Em vista disso, optamos por realizar novos experimentos de coleta dados sem prévia “lavagem” com EDTA para cristais crescidos em presença de MnSO_4 já que neste momento os dados dos cristais MnCl_2 já tinham sido coletados e as possíveis posições de interação do Mn^{2+} nesta estrutura, estabelecidas.

Vale ressaltar aqui também que em dois conjuntos de dados obtidos no grupo espacial $P2_1$ durante coletas na linha MX-2 do LNLS utilizando cristais lavados em solução de EDTA não observamos sinal para íons manganês quando geramos o mapa de Patterson, embora sinal de fluorescência tenha sido positivo para presença de manganês no cristal. Assim, suspeitávamos que o manganês não interagisse com a proteína quando havia mudança de grupo espacial, embora a possibilidade de baixa ocupação também não pudesse ser descartada. O sinal de manganês no mapa de Patterson para o cristal do complexo obtido no grupo espacial $P2_1$ só foi obtido recentemente quando utilizamos cristais sem prévia lavagem no EDTA para coleta (Tabela V; Figura 17). Ainda assim, o sinal de intensidade para os picos identificados no mapa de Patterson, quando comparado aos sinais de enxofre (correspondentes a pontes dissulfeto e metioninas), eram bastante fracos (entre 56% e 64% do sinal mais forte obtido, que correspondia a um átomo de S de uma das pontes dissulfeto da proteína). Somente a título de comparação, os sinais de Mn^{2+} no mapa de Patterson para o cristal crescido no grupo espacial $P3_121$ (dados apresentados na Tabela IV) e lavado em solução-mãe contendo 10% de EDTA antes da coleta apresentavam um sinal relativo de 87% e 84%.

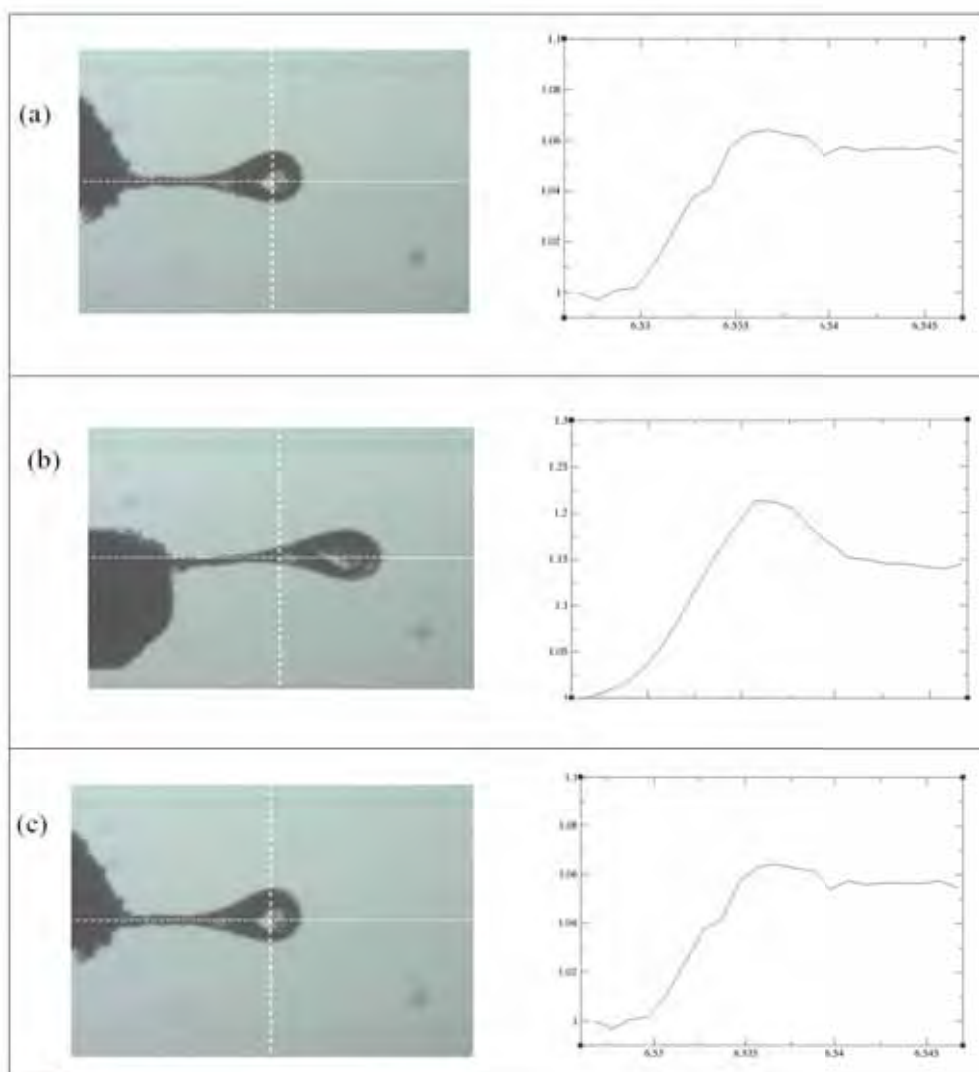


Figura 18. Testes de fluorescência realizados com feixe colimado (0,1 mm) em λ de 1,8961 ($E=6.5389$ eV) para os cristais coletados no NSLS. No gráfico, a Energia (eV) utilizada no experimento é representada no eixo das abcissas e a Intensidade Relativa, no eixo das ordenadas. Em (a) e (b) é mostrado o sinal de fluorescência para o cristal correspondente ao conjunto de dados que apresenta grupo espacial $P3_121$. Em (a) vemos a confirmação da presença de Mn^{2+} no cristal já que há sinal proveniente quando realiza-se varredura do cristal em λ específico para manganês. Em (b), o mesmo sinal, porém proveniente da solução-mãe. Em (c) é mostrado o sinal de fluorescência para o cristal correspondente ao conjunto de dados que apresenta grupo espacial $P2_1$, também evidenciando a presença de manganês na amostra.

4.2.4. Inibição de *Lys49-PLA_{2s}* por íons manganês

O desenvolvimento deste trabalho foi motivado pelo conhecimento de que íons manganês inibem a ação de *Lys49-PLA_{2s}* quando a toxina é pré-incubada com os mesmos e administrada em camundongos por via intra muscular (Soares *et al.*, 2002). Assim, de posse das estruturas cristalográficas acima descritas, procedemos com a

comparação entre estas e outras Lys49-PLA₂s nativas e complexadas na tentativa de conhecer as bases moleculares da inibição destas toxinas pelo Mn²⁺.

A comparação da estrutura da PrTX-I/Mn²⁺ obtida em grupo espacial P3₁21 (P3-PrTX-I/Mn²⁺) com outras Lys49-PLA₂s na forma nativa (que apresentam mesmo grupo espacial; Tabela VI) mostra, como única diferença estrutural entre esta estrutura e as demais comparadas, o deslocamento da cadeia lateral da Arg34 de um dos monômeros do complexo P3-PrTX-I/Mn²⁺ (Figura 19). Este deslocamento possui relação direta com a presença do íon manganês na estrutura, já que os átomos NH1 e NH2 da cadeia lateral da Arg34 fazem parte da coordenação do Mn²⁺ nesta estrutura (Figura 16b; Figura 19b). Já a comparação da estrutura BthTX-I/Mn²⁺ obtida no grupo espacial P2₁ (P2-BthTX-I/Mn²⁺) com outras Lys49-PLA₂s de grupo espacial P2₁ ou P2₁2₁2₁ (Tabela VI) mostrou não haver diferenças estruturais entre elas, em especial nas regiões onde há presença de manganês, demonstrando, desta forma, que o Mn²⁺ não induz nenhuma modificação estrutural na toxina de grupo espacial P2₁ com a qual interage (Figura 20). Vale ressaltar aqui também, que as regiões que estabelecem interações com Mn²⁺ identificadas na estrutura P2₁ são diferentes das regiões identificadas na estrutura P3₁21 (Figura 16 X Figura 17).

Tabela VI. Estruturas cristalográficas de Lys49-PLA₂s botrópicas utilizadas nas comparações dos complexos de manganês obtidos neste trabalho.

	Grupo espacial	Resolução (Å)	R (%)	R _{free} (%)	Código (PDB)*
BnSP-6	P3 ₁ 21	2,50	18,6	25,5	1PC9
BnSP-7	P3 ₁ 21	2,20	20,8	26,6	1PA0
BthTX-I	P3 ₁ 21	1,91	21,7	25,2	3HZD
BthTX-I / PEG400	P3 ₁ 21	1,90	22,8	27,7	2H8I
PrTX-I	P3 ₁ 21	1,65	21,4	25,8	2Q2J
BnIV / Ác. Mirístico	P2 ₁	2,21	20,7	25,3	3MLM
BthTX-I / α-tocoferol	P2 ₁	1,83	19,5	24,3	3CXI
BthTX-I / PEG 4000	P2 ₁	1,55	20,3	24,6	3IQ3
PrTX-I / α-tocoferol	P2 ₁	1,87	18,3	24,3	3CYL
PrTX-I / BPB	P2 ₁	2,34	22,3	25,2	2OK9
PrTX-II / Ác. graxo	P2 ₁	2,04	17,6	26,8	1QLL
BaspTX-II	P2 ₁ 2 ₁ 2 ₁	2,80	16,5	-	1CLP
BaspTX-II / suramina	P2 ₁ 2 ₁ 2 ₁	1,70	20,7	24,0	1Y4L
BthTX-I / BPB	P2 ₁ 2 ₁ 2 ₁	2,28	23,6	25,4	3HZW
MjTX-II / Ác. esteárico	P2 ₁ 2 ₁ 2 ₁	1,80	17,0	24,7	1XXS
PrTX-I / Ác. rosmarínico	P2 ₁ 2 ₁ 2 ₁	1,77	16,0	21,7	3QNL

*PDB: Protein Data Bank (www.pdb.org)

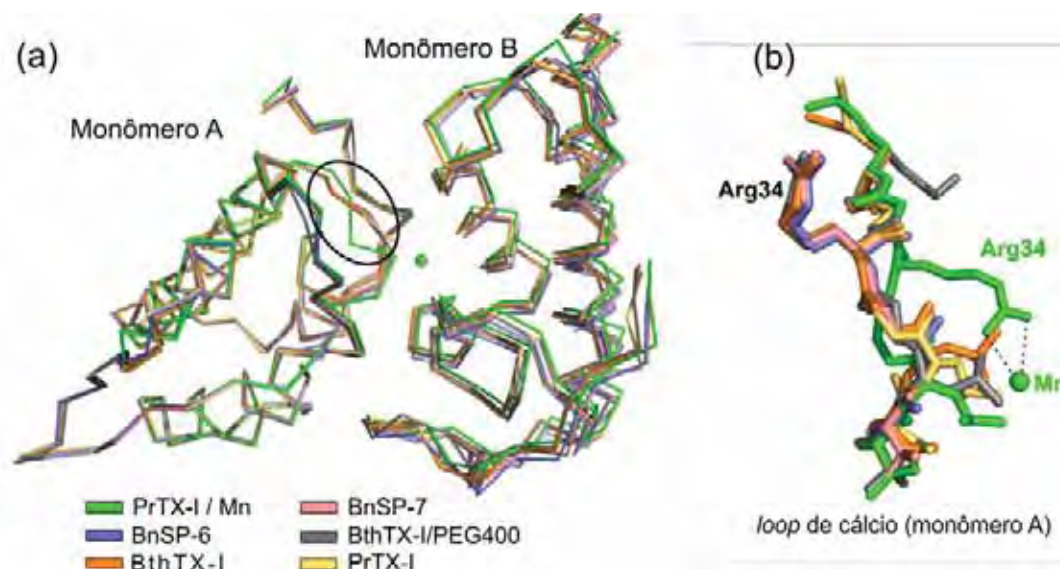


Figura 19. Sobreposição entre a estrutura *P3-PrTX-I/Mn²⁺* e outras Lys49-PLA₂s de grupo espacial P₃₁2₁. (a) Sobreposição dos monômeros A das Lys49-PLA₂s comparadas, com destaque para a região do *loop* de cálcio, onde é observada mudança conformacional da cadeia principal da proteína complexada com Mn²⁺ em relação a outras Lys49-PLA₂s de grupo espacial P₃₁2₁. (b) Sobreposição da cadeia principal para os resíduos 31 a 36 do *loop* de ligação de cálcio destacada em (a), onde diferente conformação da Arg34 causada pela presença do Mn²⁺ na região do *loop* de ligação de cálcio da estrutura *P3-PrTX-I/Mn²⁺* é observada. Para a comparação, as estruturas cristalográficas de grupo espacial P₃₁2₁ apresentadas na Tabela VI foram utilizadas e representadas na forma de *ribbons*. Figura gerada no programa *Pymol* (Delano, 2002).

Em 2009, em um trabalho realizado por nosso grupo onde foram avaliadas todas as estruturas de Lys49-PLA₂s disponíveis na literatura, foi levantada a hipótese de que o mecanismo de ação de Lys49-PLA₂s em membranas musculares ocorre em duas etapas (Dos Santos, Soares *et al.*, 2009). Num primeiro momento, o C-terminal destas toxinas (representadas pela forma apo da proteína, de grupo espacial P₃₁2₁) interage com a cabeça polar de fosfolipídios da membrana. Esta interação leva então a um rearranjo estrutural que permite a inserção de porções hidrofóbicas dos fosfolipídios da membrana no canal hidrofóbico da proteína, culminando com a desestabilização da membrana (Gallacci e Cavalcante, 2010). Este novo “estado” pode ser representado pela forma “ativada” da proteína, ou seja, por estruturas de grupo espacial P₂₁ ou P₂₁2₁2₁, dentre as quais podemos citar Lys49-PLA₂s com ligantes como ácidos graxos ou polímeros de alto peso molecular no canal hidrofóbico (estas estruturas são consideradas “ativadas” pois simulam a proteína em um estágio posterior à interação com membranas; os ligantes no canal hidrofóbico simulam porções hidrofóbicas dos fosfolipídios da membrana). Considerando este mecanismo de duas etapas na análise

dos dados obtidos para as duas formas do complexo de Mn^{2+} (dois grupos espaciais), importantes inferências podem ser feitas. Na estrutura obtida em grupo espacial $P3_121$ observou-se que o Mn^{2+} interage com duas regiões, sendo uma delas na simetria cristalográfica. Já para forma que apresenta PEG4000 no canal hidrofóbico (grupo espacial $P2_1$), duas regiões são apontadas, sendo que nenhuma delas é equivalente às regiões encontradas na estrutura $P3_121$. Ainda, considerando todas as posições que o manganês interage com a proteína, somente há mudança estrutural induzida pela presença do Mn^{2+} em um dos monômeros da estrutura $P3$ -PrTX-I/ Mn^{2+} (Figura 16b; Figura 19). Nesta posição, o Mn^{2+} leva à polarização da Arg34 de um dos monômeros da toxina (Figura 16b), provocando o deslocamento da região em que este aminoácido se contra (conhecida por *loop* de ligação de cálcio) (Figura 19).

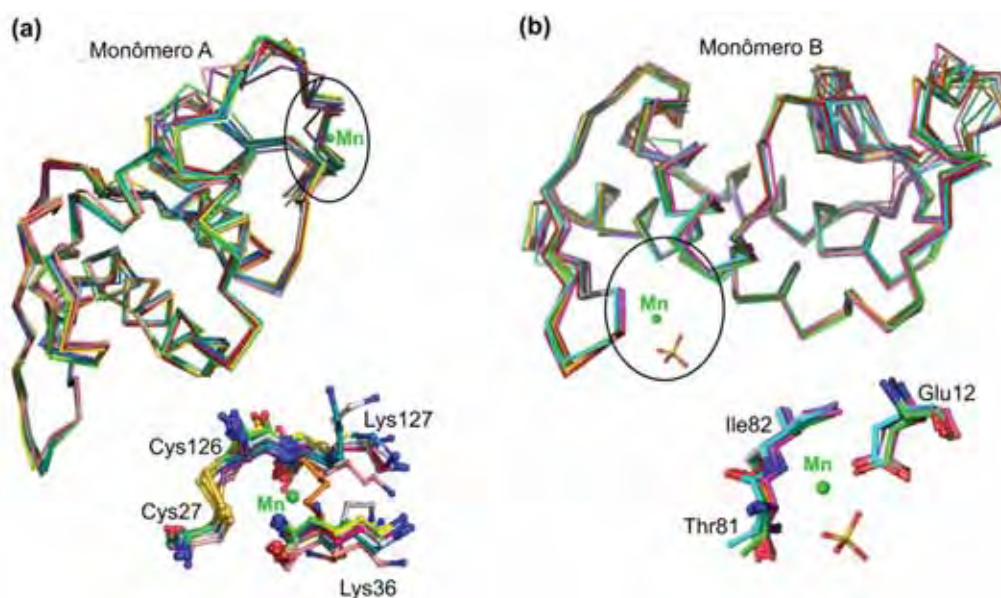


Figura 20. Comparação da estrutura BthTX-I complexada com manganês e outras estruturas cristalográficas de Lys49-PLA₂s de grupo espacial $P2_1$ e $P2_12_12_1$. Em (a), sobreposição do monômero A da estrutura BthTX-I/ Mn^{2+} com as demais estruturas comparadas. Em (b), sobreposição do monômero B da estrutura BthTX-I/ Mn^{2+} com as demais estruturas comparadas. A região destacada em cada um dos monômeros corresponde ao sítio de interação do Mn^{2+} e é mostrada em destaque (em *sticks*) para cada um dos monômeros logo abaixo da sobreposição dos monômeros. Para a comparação, as estruturas cristalográficas apresentadas na Tabela VI foram utilizadas e representadas na forma de *ribbons*. Figura gerada no programa *Pymol* (Delano, 2002).

A comparação entre estruturas de Lys49-PLA₂s nas suas formas apo (representadas pelo grupo espacial $P3_121$) e complexadas (representadas pelo grupo espacial $P2_1$ ou $P2_12_12_1$) evidencia que na presença de ligantes no canal hidrofóbico

ocorre um rearranjo quaternário, levando ao deslocamento entre os monômeros destas toxinas (Dos Santos, Soares *et al.*, 2009) (Figura 21). Ainda, a região do *loop* de ligação de cálcio de um dos monômeros da Lys49-PLA₂ sofre deslocamento (Figura 21), demonstrando que esta região sofre influência direta do ligante presente no canal hidrofóbico (Figura 21). Diante do exposto, fica estabelecida a relação entre ligantes no canal hidrofóbico e alterações no *loop* de cálcio destas toxinas. No caso da estrutura do complexo P3-PrTX-I/Mn²⁺, observa-se que o Mn²⁺ responsável pela polarização da Arg34 se encontra no canal hidrofóbico da proteína, sendo coordenado por resíduos de ambos os monômeros, conforme apresentado na seção 4.2.3. (Figura 16b). Ainda, quando a cadeia lateral da Arg34 é polarizada, esta passa também a ocupar parte do canal hidrofóbico (Figura 22). Desta forma, fica demonstrado como o manganês leva à inibição de Lys49-PLA₂s, já que este, juntamente com a Arg34, passa a ocupar a região que seria ocupada por ácidos graxos da membrana numa etapa posterior à interação do C-terminal de Lys49-PLA₂s com a cabeça polar de fosfolipídios (Figura 22; Figura 23).

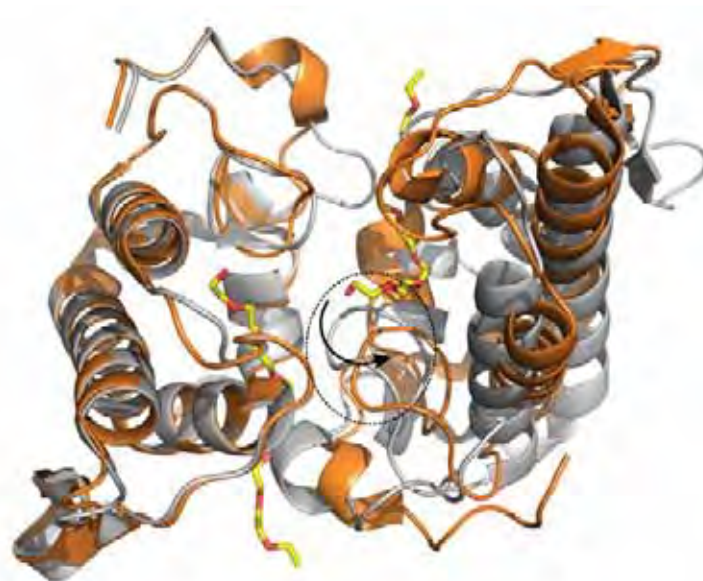


Figura 21. Rearranjo quaternário observado em Lys49-PLA₂s botrópicas após interação com ligantes. A estrutura cristalográfica da BthTX-I mostrada em cinza nesta figura corresponde à forma apo da proteína e é representativa de todas as estruturas cristalográficas de Lys49-PLA₂s nativas obtidas em grupo espacial P3₁21 mostradas na Tabela VI. A estrutura cristalográfica da BthTX-I complexada com PEG 4000 mostrada em alaranjado nesta figura é representativa de todas as estruturas cristalográficas de Lys49-PLA₂s complexadas obtidas em grupo espacial P2₁ ou P2₁2₁2₁ mostradas na Tabela VI. Em destaque, observa-se o *loop* de ligação de cálcio de um dos monômeros da toxina que sofre deslocamento (representado pela seta) quando ligantes, como por exemplo, o PEG4000 (em amarelo, representado em *sticks*), estão presentes no canal hidrofóbico da proteína. Figura gerada no programa *Pymol* (Delano, 2002).

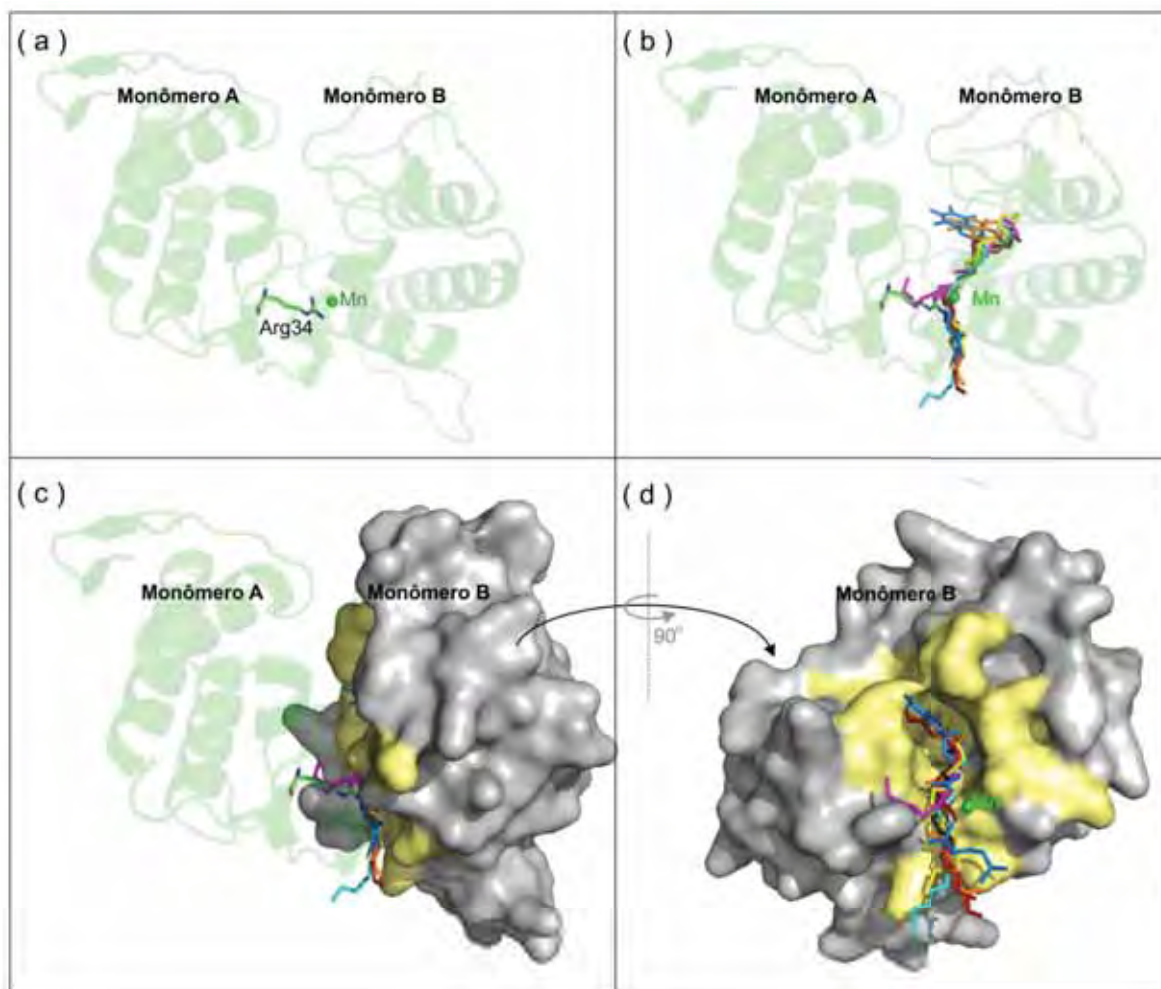


Figura 22. Comparação da estrutura $P3$ -PrTX-I/ Mn^{2+} (grupo espacial $P3_121$) e Lys49-PLA₂s botrópicas de grupo espacial $P2_1$ e $P2_12_12_1$ com ligantes presentes no canal hidrofóbico. Em (a), a estrutura da $P3$ -PrTX-I/ Mn^{2+} é representada em *cartoon* com destaque para a Arg34 do monômero A (representada em *sticks*). Em (b), os ligantes presentes no canal hidrofóbico do monômero B de todas as estruturas comparadas são representados em *sticks*: em azul escuro e alaranjado, molécula de α -tocoferol (α T) encontradas nos complexos BthTX-I/ α T e PrTX-I/ α T, respectivamente; em azul claro e vermelho, moléculas de PEG4000 encontradas no complexo BthTX-I/PEG4000 e $P2$ -BthTX-I/ Mn^{2+} (grupo espacial $P2_1$); em amarelo, molécula de PEG3350 encontrada no complexo BaspTX-II/suramina; em preto, rosa e cinza claro, moléculas de ácidos graxos dos complexos PrTX-II/ácido graxo, MjTX-II/ácido esteárico e BnIV/ácido mirístico, respectivamente. Em (c), a mesma configuração adotada em (b) é mostrada, porém o monômero B é mostrado na forma de superfície (em cinza), com destaque para seu canal hidrofóbico, em amarelo. Em (d), é destacado o monômero B representado em superfície em (c), porém com rotação de 90° para melhor visualização dos ligantes presentes no canal hidrofóbico. Figura gerada no programa *Pymol* (Delano, 2002).

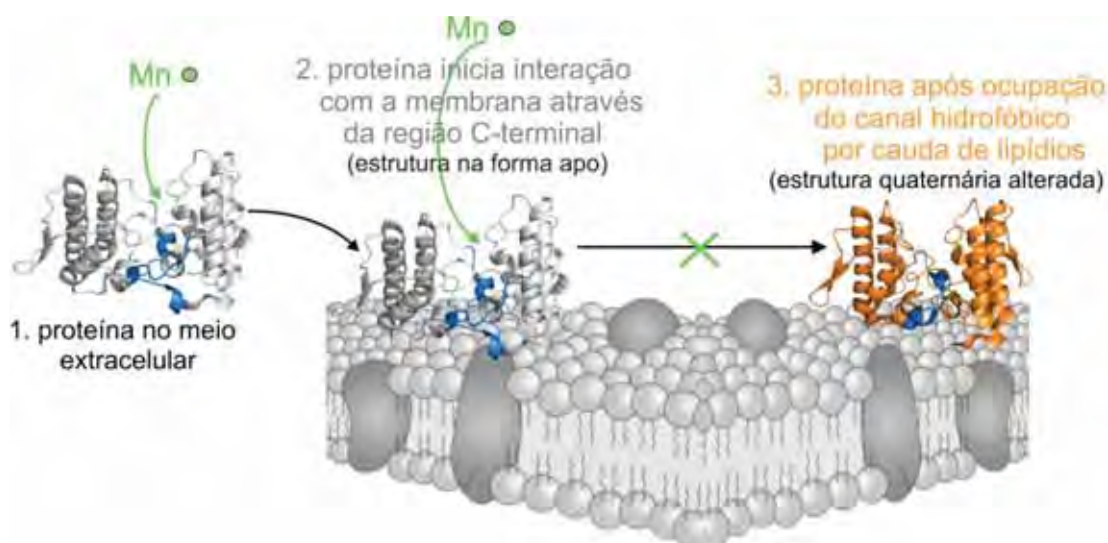


Figura 23. Modelo de inibição de Lys49-PLA₂s botrópicas por íons manganês. O íon manganês interage com resíduos específicos da toxina (Figura 16b), ocupando o canal hidrofóbico de um de seus monômeros (passos 1 e 2), conforme representado na Figura 22. Nesta configuração, embora a toxina possa interagir com a membrana por meio da região C-terminal (em azul; passo 2), seu canal hidrofóbico não pode ser ocupado por porções hidrofóbicas de fosfolipídios da membrana já que o Mn²⁺ é coordenado nesta região.

Interessantemente, como pode ser observado na Figura 22, a modificação estrutural induzida pelo Mn²⁺ em um dos monômeros da toxina dimérica leva ao bloqueio do canal hidrofóbico do monômero oposto, demonstrando uma provável “colaboração” entre ambos os monômeros da toxina durante sua atuação. Esta possível colaboração entre os monômeros de Lys49-PLA₂s foi proposta também quando da análise da estrutura da PrTX-I complexada com ácido rosmarínico (seção 4.1.).

Os dados obtidos com as estruturas cristalográficas dos complexos de Mn²⁺ aqui apresentados, considerando-se a hipótese de ação de Lys49-PLA₂s em duas etapas levantada por nosso grupo em 2009 (Dos Santos, Soares *et al.*, 2009), mostram que tanto a forma “inativa” quanto “ativada” da toxina são representadas (estruturas P3-PrTX-I/Mn²⁺ e P2-BthTX-I/Mn²⁺, respectivamente), sendo as mesmas provavelmente representativas das conformações de Lys49-PLA₂s antes e após interação com membranas musculares, conforme há pouco descrito. Por conseguinte, a observação de que somente a estrutura P3₁21 do complexo sofre alterações estruturais na presença de manganês corrobora a hipótese de nosso grupo, pois esta representa a forma “inativa” da proteína, conformação adotada antes da interação com a membrana. Já a forma P2₁,

correspondente à forma ativada das Lys49-PLA₂s, não é passível de alteração estrutural pela presença de Mn²⁺ já que representa um estado protéico onde a interação com a membrana já ocorreu, permitindo a inserção de ácidos graxos no seu canal hidrofóbico, não tendo, portanto, como ser inibida nesta fase.

4.3. Estudos estruturais por cristalografia de raios X com o complexo BthTX-II/Ca²⁺

Os estudos estruturais da BthTX-II complexada com íons cálcio foram iniciados em 2008, durante a Iniciação Científica do aluno Rafael Junqueira Borges, atual mestrando do laboratório, que na época estava sob minha co-orientação. Os cristais do complexo foram obtidos utilizando-se a condição de cristalização da proteína nativa (Correa *et al.*, 2006), acrescentando-se solução de CaCl₂ 0,1M na gota como fonte de Ca²⁺. Os dados de difração de raios X foram processados com o programa HKL2000 (Otwinowski e Minor, 1997), mostrando que os cristais do complexo são isomorfos aos da proteína nativa, e pertencem ao grupo espacial C2 (Tabela VII).

O cálculo do coeficiente de Matthews (Matthews, 1968) indicou a presença de um dímero na unidade assimétrica. A análise do empacotamento cristalino demonstrou duas configurações diméricas possíveis para a elucidação da estrutura, conforme já descrito quando da resolução da estrutura da BthTX-II nativa (Correa *et al.*, 2008) e da estrutura PrTX-III nativa (Rigden *et al.*, 2003). Tanto para a estrutura da BthTX-II nativa quanto para a da BthTX-II/Ca²⁺, o arranjo quaternário escolhido mostra que seus monômeros se relacionam por um eixo aproximado de ordem dois perpendicular às suas folhas β (Figura 24). Vale ressaltar que esta configuração dimérica é semelhante à adotada pelo chamado “dímero convencional” das Lys49-PLA₂s (Dos Santos, Fernandes *et al.*, 2009; Dos Santos, Soares *et al.*, 2009).

Tabela VII. Estatísticas da coleta de dados de difração de raios X e refinamento do complexo BthTX-II/Ca²⁺

Cela unitária (Å)	a=59,23 b=100,88 c=47,16
Grupo espacial	C2
Resolução (Å)	50,44 – 2,05 (2,15 – 2,05) ^a
Reflexões únicas	14060 (1377) ^a
Dados completos a	97,9 (98,5) ^a
R _{merge} ^b (%)	9,0 (62,5) ^a
Fonte de radiação	Síncrotron (MX2 - LNLS)
Temperatura da coleta de dados (K)	100
I/σ (I)	11,53 (2,34) ^a
Redundância	3,6 (3,3) ^a
Moléculas nas unidade assimétrica	2
R _{crist} ^c (%)	22,0
R _{free} ^d (%)	26,8
B-factor médio(Å ²)	
geral	42,2
proteína	42,6
íons cálcio	61,0
moléculas de água	56,5
Ocupação média – íons cálcio	0,90
Gráfico de Ramachandran ^e	
Resíduos na região mais favorável (%)	88,2
Resíduos em regiões adicionalmente permitidas (%)	11,8

^a Números em parênteses são para a faixa de mais alta resolução. ^b $R_{merge} = \sum_{hkl} (\sum_i (|I_{hkl,i} - \langle I_{hkl} \rangle|)) / \sum_{hkl,i} \langle I_{hkl} \rangle$, onde $I_{hkl,i}$ é a intensidade de uma medida individual de uma reflexão com índices de Miller h, k e l, e $\langle I_{hkl} \rangle$ é a intensidade média daquela reflexão. Calculado para $I > -3\sigma(I)$. ^c $R_{crist} = R_{hkl} (|F_{obs_{hkl}}| - |F_{calc_{hkl}}|) / |F_{obs_{hkl}}|$, onde $|F_{obs_{hkl}}|$ e $|F_{calc_{hkl}}|$ são as amplitudes dos fatores de estrutura observados e calculados. ^d R_{free} é equivalente ao R_{crist} , porém calculado com 5% das reflexões omitidas no processo de refinamento. ^e Calculado com o programa Procheck (Laskowski *et al.*, 1993).

O refinamento do modelo foi realizado por ciclos de refinamento automático com o programa REFMAC (Murshudov *et al.*, 1997) alternados com alguns ciclos de ajustes manuais no programa Coot (Emsley eCowtan, 2004), até as estatísticas $R=22,0\%$ e $R_{\text{free}}=26,8\%$. Mesmo na presença de grande quantidade de íons cálcio nos experimentos de cristalização, a inspeção da densidade eletrônica na região do *loop* de cálcio evidencia a inexistência de qualquer ligante nesta região. No entanto, observou-se a presença destes íons interagindo com os monômeros da BthTX-II em duas regiões equivalentes (Figura 25). Os locais de interação dos íons foram identificados segundo critérios pré-estabelecidos (seção 3.4.).

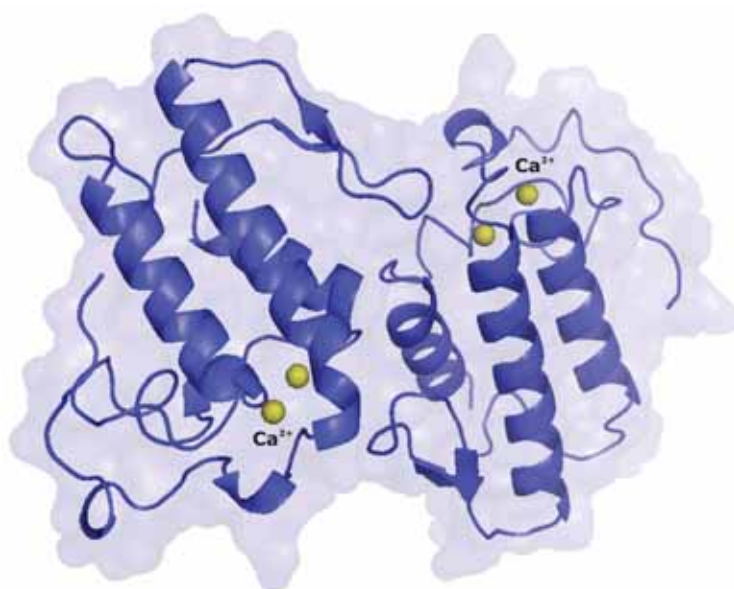


Figura 24. Estrutura cristalográfica do complexo BthTX-II/Ca²⁺. Íons cálcio coordenados pela proteína são mostrados em amarelo. Figura extraída do artigo de dos Santos e colaboradores (Dos Santos *et al.*, 2011).

Uma boa qualidade estereoquímica foi observada para o modelo final, mostrando que todos os resíduos se encontram nas regiões favoráveis no gráfico de Ramachandran (Tabela VII). Além disso, o modelo apresentou melhor qualidade estereoquímica do que o esperado para estruturas de mesma resolução. A estrutura foi depositada no banco de dados PDB (código de acesso 3JR8).

Assim como outras PLA₂s de classe II, observou-se a presença de sete pontes dissulfeto em cada um dos monômeros da estrutura e a conservação dos resíduos da rede catalítica (His48, Tyr52, Tyr73 and Asp99) (Scott *et al.*, 1990; Arni eWard, 1996) e dos envolvidos na coordenação do cálcio (Tyr28, Gly30, Gly32 and Asp49) (Scott *et al.*, 1990; Arni eWard, 1996).

A estrutura do complexo BthTX-II/Ca²⁺ aqui apresentada foi refinada pelo mestrando Rafael Junqueira Borges. Este trabalho teve início durante a iniciação científica deste, e desde então temos trabalhos em colaboração já que co-orientei o aluno durante seu período de iniciação científica.

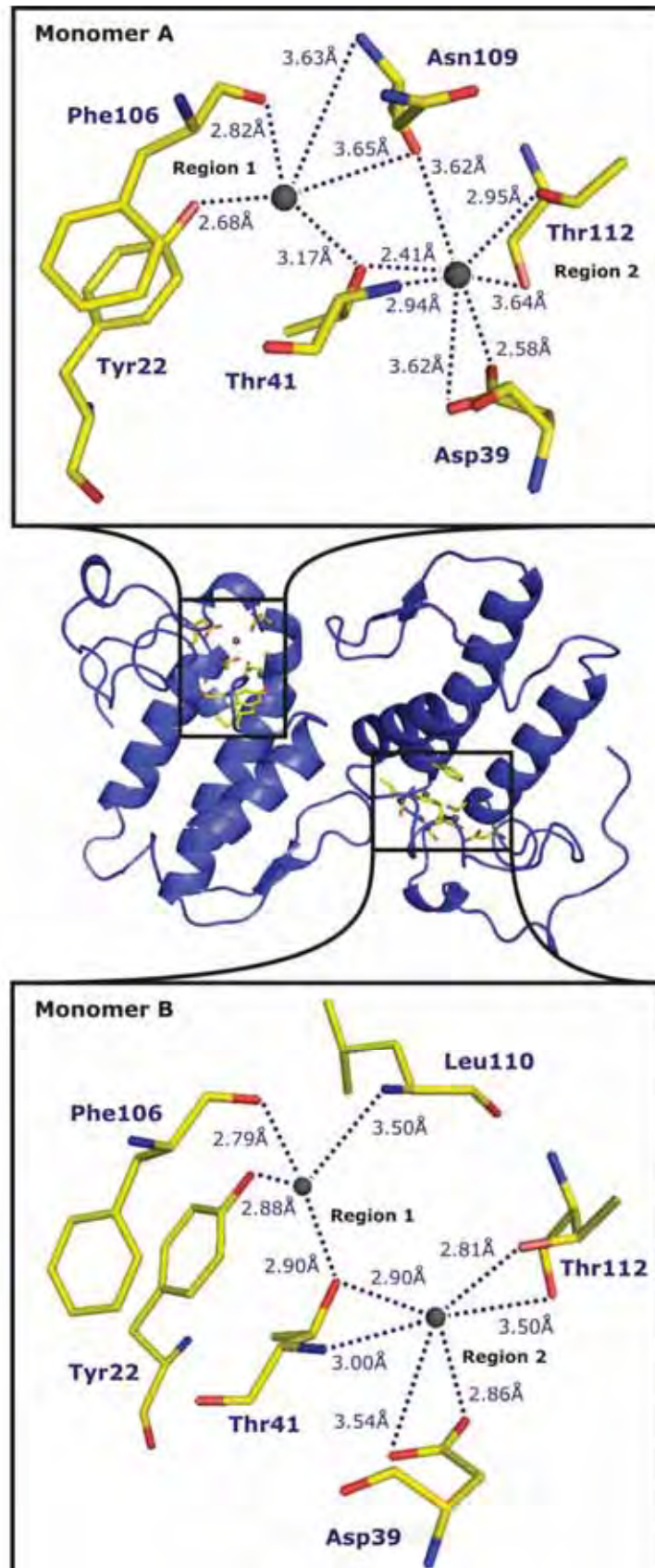


Figura 25. Sítios de coordenação dos íons cálcio no complexo BthTX-II/ Ca^{2+} . Os íons são coordenados em regiões equivalentes dos monômeros. Apenas distâncias abaixo de $3,7\text{\AA}$ foram consideradas. Figura extraída do artigo de dos Santos e colaboradores (Dos Santos *et al.*, 2011).

4.3.1. Dificuldades encontradas durante a resolução da estrutura do complexo

A dificuldade no trabalho com este conjunto de dados se deveu à presença de anisotropia cristalina. Durante a indexação das primeiras imagens coletadas, havia indicação de simetria maior que a observada no conjunto nativo e no qual o complexo foi resolvido. Porém, durante a integração das imagens, muitas reflexões passavam a ser descartadas, indicando problemas com sistema cristalino escolhido (C222). Desta forma, optamos por resolver a estrutura numa simetria menor (grupo espacial C2), já que desta forma o conjunto de dados pôde ser resolvido e obtivemos completeza adequada.

4.3.2. Comparação entre a BthX-II/Ca²⁺ e sua forma nativa

A sobreposição entre a BthX-II complexada com cálcio e a forma nativa da proteína resultou em r.m.s.d. de 0,39 Å e 0,55 Å para os monômeros A e B, respectivamente (somente Ca foram considerados). A comparação das duas formas da proteína indicou que o *loop* de ligação de cálcio da BthTX-II/Ca²⁺ é mantido distorcido, seguindo a mesma orientação observada na forma nativa da proteína (Figura 26). Ainda, observou-se a presença de algumas cadeias laterais com disposição diferente, porém sem relação aparente entre este achado e a presença de cálcio em algumas regiões.

A região compreendida entre os resíduos 77 a 81 do monômero B da BthTX-II/Ca²⁺ apresenta o maior r.m.s.d. quando comparado com a mesma região da proteína nativa (circulado na Figura 26). No entanto, considerando-se a distância de 10,5 Å entre o íon cálcio e o átomo mais próximo da região citada (oxigênio da cadeia principal do resíduo Glu78), é improvável que o íon tenha provocado tal distorção. Nenhuma outra diferença significativa foi observada entre as estruturas comparadas (Figura 26), sugerindo que o cálcio não induziu nenhuma alteração na estrutura terciária ou quaternária da proteína em estudo.

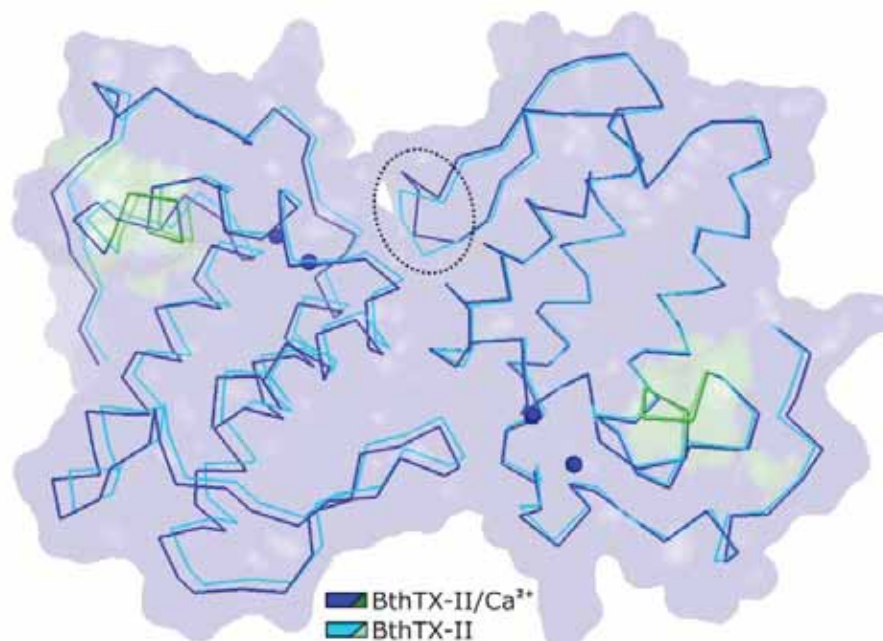


Figura 26. Sobreposição entre as estruturas cristalográficas BthTX-II nativa e BthTX-II/Ca²⁺. Regiões em verde indicam o *loop* de ligação de cálcio e a área circulada corresponde à região com maior r.m.s.d. entre as duas estruturas. Esferas em azul representam os íons cálcio coordenados na estrutura da BthTX-II. Figura extraída do artigo de dos Santos e colaboradores (Dos Santos *et al.*, 2011).

4.4. Arranjo quaternário da BthTX-II/Ca²⁺ e outras Asp49-PLA₂s miotóxicas

4.4.1. Estrutura quaternária mais provável de ocorrência em solução para Asp49-PLAs miotóxicas

As Asp49-PLA₂s miotóxicas, assim como as Lys49-PLA₂s, são proteínas díméricas (Da Silva Giotto *et al.*, 1998; Soares *et al.*, 2000; Rigden *et al.*, 2003; Murakami *et al.*, 2007; Correa *et al.*, 2008). Atualmente, três estruturas cristalográficas de Asp49-PLA₂s miotóxicas são conhecidas: a da BthTX-II nativa (Correa *et al.*, 2008), a da BthTX-II complexada com cálcio (descrita nesta seção 4.3.) e a da PrTX-III (Rigden *et al.*, 2003). As três estruturas foram resolvidas no grupo espacial C2 e a observação dos contatos cristalinos demonstra haver duas possíveis configurações para o arranjo dímérico das mesmas (Figura 27). Ao analisar o arranjo quaternário destas proteínas com o programa PISA (Krissinel e Henrick, 2007), nota-se que há um arranjo quaternário em comum para as três estruturas analisadas (Figura 27) e que este arranjo é o mais provável de ocorrer em solução (Tabela VIII). Ainda, neste arranjo sugerido pelo PISA, a disposição entre seus monômeros é diferente daquela adotada para a resolução

das estruturas BthTX-II nativa e BthTX-II/Ca²⁺ (Figura 27; Tabela VIII). Visto que o mecanismo de atuação destas PLA₂s homólogas é ainda desconhecido, estas novas informações podem ser bastante importantes para a extração de informações biológicas baseadas em suas estruturas.

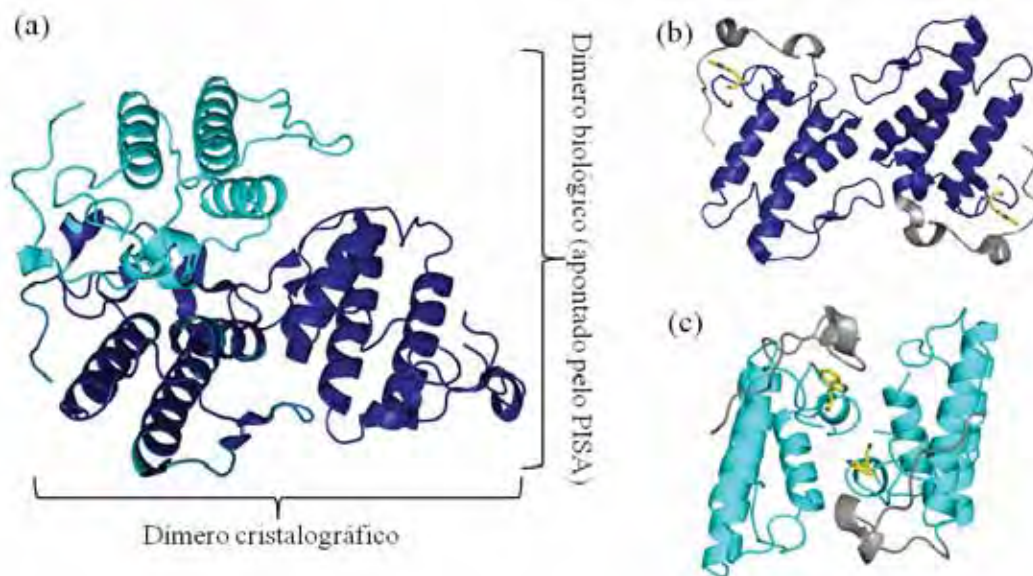


Figura 27. Possíveis conformações diméricas para a resolução das estruturas de Asp49-PLA₂s miotóxicas quando observam-se seus contatos na rede cristalina. Em (a) são demonstradas as duas possibilidades, sendo que a representada em azul escuro corresponde à estrutura cristalográfica da BthTX-II e, em azul claro, à conformação apontada pelo PISA (Krissinel e Henrick, 2007) como sendo a forma mais provável de ocorrer em solução (Tabela VIII). Em (b), as posições dos C-terminais (em cinza) e dos Trp31 (em amarelo) no Dímero Cristalográfico são evidenciados. Em (c), os mesmos detalhes apresentados em (b) são mostrados, porém na estrutura do Dímero Biológico (azul claro). Figura gerada no programa *Pymol* (Delano, 2002).

Tabela VIII. Valores de área de interface e energia livre de solvatação segundo análises do programa *online* PISA (Krissinel e Henrick, 2007) disponível no servidor do *European Bioinformatics Institute server* (<http://www.ebi.ac.uk>).

Proteínas / Dímero	Área interface (Å²)	Δ¹G (kcal/mol)^a
BthTX-II (2OQD)		
Dímero cristalográfico	456,5	-2,7
Dímero biológico	669,5	-13,5
BthTX-II/Ca²⁺ (3JR8)		
Dímero cristalográfico	422,5	-1,5
Dímero biológico	631,9	-14,6
PrTX-III (1GMZ)		
Dímero cristalográfico	522,3	0,3
Dímero biológico	639,9	-10,4

Δ¹G indica o ganho de energia livre quando o complexo se forma, em kcal/M. O valor é calculado como a diferença entre a energia de solvatação para as estruturas isoladas e quando há complexação. Valores negativos de Δ¹G correspondem a interfaces hidrofóbicas, ou afinida protéica positiva. Este valor não inclui o efeito de ligações de hidrogênio e pontes salinas da interface. A **Área de Interface**, em Å², é calculada como a diferença entre as áreas de superfície totais expostas ao solvente para as estruturas isoladas e quando há formação do complexo dividido por dois.

4.4.2. Expressão da miotoxicidade e ausência de atividade catalítica das Asp49-PLA₂s miotóxicas do ponto de vista estrutural

A literatura aponta que a BthTX-II e a PrTX-III são proteínas miotóxicas (Gutierrez *et al.*, 1991; Pereira *et al.*, 1998; Toyama *et al.*, 1999) e, até recentemente, acreditava-se que estas apresentavam reduzida atividade catalítica se comparadas a outras Asp49-PLA₂s catalíticas não-miotóxicas (Pereira *et al.*, 1998; Toyama *et al.*, 1999). Estas proteínas conservam tanto os resíduos da rede catalítica His48, Tyr52, Tyr73 e Asp99 quanto os resíduos Tyr28, Gly30, Gly32 e Asp49, que estão envolvidos na coordenação do co-fator cálcio em Asp49-PLA₂s catalíticas (Scott *et al.*, 1990; Arni e Ward, 1996; Ward, De Azevedo *et al.*, 1998).

A elucidação das estruturas cristalográficas da BthTX-II e PrTX-III evidenciou a presença de uma distorção no *loop* de ligação de cálcio destas proteínas (Rigden *et al.*, 2003; Correa *et al.*, 2008), cuja ocorrência foi associada a uma possível inatividade

catalítica por parte das mesmas (Correa *et al.*, 2008). Ao elucidar a estrutura da BthTX-II/ Ca^{2+} , percebemos que tal distorção se mantém (seção 4.3.2.; Figura 26; Figura 28) e que a coordenação de cálcio por resíduos presentes neste *loop* (Tyr28, Gly30 e Gly32) não ocorre mesmo havendo excesso de cálcio nos experimentos de co-cristalização (seção 3.4.).

Côrrea e colaboradores propuseram que a não-coordenação de cálcio nestas proteínas deve-se ao fato de elas apresentarem o resíduo triptofano na posição 31 de suas seqüências primárias (Correa *et al.*, 2008), pois a presença deste resíduo de cadeia lateral longa poderia ter provocado a distorção do *loop* em questão. Porém, uma revisão da literatura mostra que há outras Asp49-PLA₂s catalíticas e não miotóxicas com este mesmo resíduo na posição 31 (resultados não mostrados). Ainda, as estruturas cristalográficas da DacuTX (uma Asp49-PLA₂ de *Deinagkistrodon acutus*) (Gu *et al.*, 2002) e da AhalTX (uma Asp49-PLA₂ de *Gloydius halys*, anteriormente denominada *Agkistrodon halys pallas* (Wang *et al.*, 1996), proteínas que apresentam atividade enzimática dependente de cálcio e cuja seqüências primárias mostram um triptofano na posição 31, evidencia que ambas são capazes de coordenar íons cálcio (Figura 28a, b) e que seus *loops* de cálcio não se apresentam “distorcidos” como os das Asp49-PLA₂s miotóxicas (Figura 28a).

Interessantemente, os aminoácidos compreendidos entre os resíduos 25 e 35 da seqüência primária da BthTX-II são idênticos aos da AhalTX para a mencionada região, evidenciando que a distorção do *loop* de cálcio nas Asp49-PLA₂s miotóxicas e sua conseqüente incapacidade de coordenar íons cálcio não pode ser atribuída à presença de aminoácidos específicos na seqüência primária do *loop* de cálcio das Asp49-PLA₂s miotóxicas.

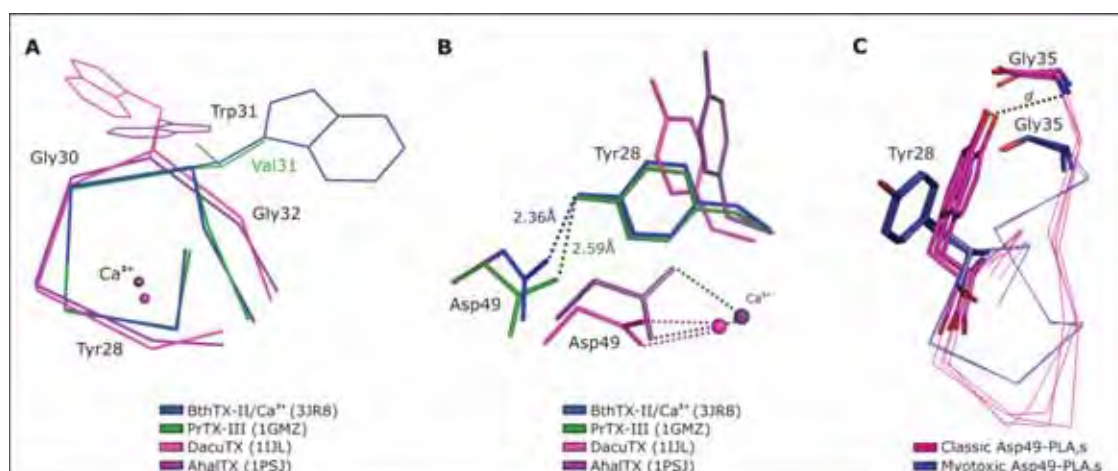


Figura 28. Conformação adotada pelo *loop* de ligação de cálcio de algumas estruturas cristalográficas de PLA₂s de serpentes da família Viperidae. Em azul, a BthTX-II, uma Asp49-PLA₂ básica e miotóxica do veneno de *Bothrops asper* (PDB ID 3JR8); em verde, a PrTX-III, uma Asp49-PLA₂ miotóxica do veneno de *Bothrops pirajai* (PDB ID 1GMZ), em cor-de-rosa, a DacuTX, uma Asp49-PLA₂ não-miotóxica do veneno de *Deinagkistrodon acutus* (PDB ID 1IJL) e, em roxo, a AhalTX, uma Asp49-PLA₂ não-miotóxica do veneno de *Gloydius halys* (PDB ID 1PSJ). (A) Sobreposição do *loop* de cálcio através do Ca das estruturas cristalográficas citadas com destaque para a cadeia lateral do aminoácido Trp31. (B) Conformação adotada pelos resíduos Asp49 (parte do sítio catalítico) e Tyr28 (*loop* de cálcio) nas estruturas citadas mostrando que a coordenação de Ca²⁺ não é impedida nas estruturas de AhalTX e DacuTX, embora estas proteínas apresentem triptofano na posição 31 de suas seqüências primárias. As estruturas de Asp49-PLA₂s miotóxicas apresentam uma distorção no *loop* de cálcio que permite que o átomo O δ do resíduo Asp49 interaja com o O η da Tyr28, inviabilizando, conseqüentemente, a coordenação de Ca²⁺ pelos O δ do resíduo Asp49. (C) Conformação adotada pelo O η da cadeia lateral da Tyr28 e pelo grupamento amino da Gly35 em estruturas de Asp49 PLA₂s clássicas (cor-de-rosa) e Asp49-PLA₂s miotóxicas (azul). A distância *d* entre os átomos citados é mostrada (3,1 Å < *d* < 3,5 Å). As Asp49-PLA₂s clássicas são representadas pela AhalTX e DacuTX, e as Asp49-PLA₂s miotóxicas, pela BthTX-II e PrTX-III. Figura extraída do artigo de dos Santos e colaboradores (Dos Santos *et al.*, 2011).

Diante da impossibilidade de inferir o motivo da distorção observada no *loop* de cálcio das Asp49-PLA₂s miotóxicas pela comparação de suas seqüências primárias com a de outras PLA₂s, resolvemos analisar a estrutura quaternária destas toxinas, visto que a distorção observada pode ser conseqüência da oligomerização adotada por estas proteínas (Doley e Kini, 2009). Na estrutura quaternária das Asp49-PLA₂s miotóxicas sugerida pelo PISA (Figura 27; Figura 31), o *loop* de cálcio e, mais especificamente, o resíduo Trp31, faz parte da interface do dímero (Figura 29). Ainda, nestas miotoxinas o Trp31 está voltado para a região C-terminal das mesmas (Figura 27; Figura 29).

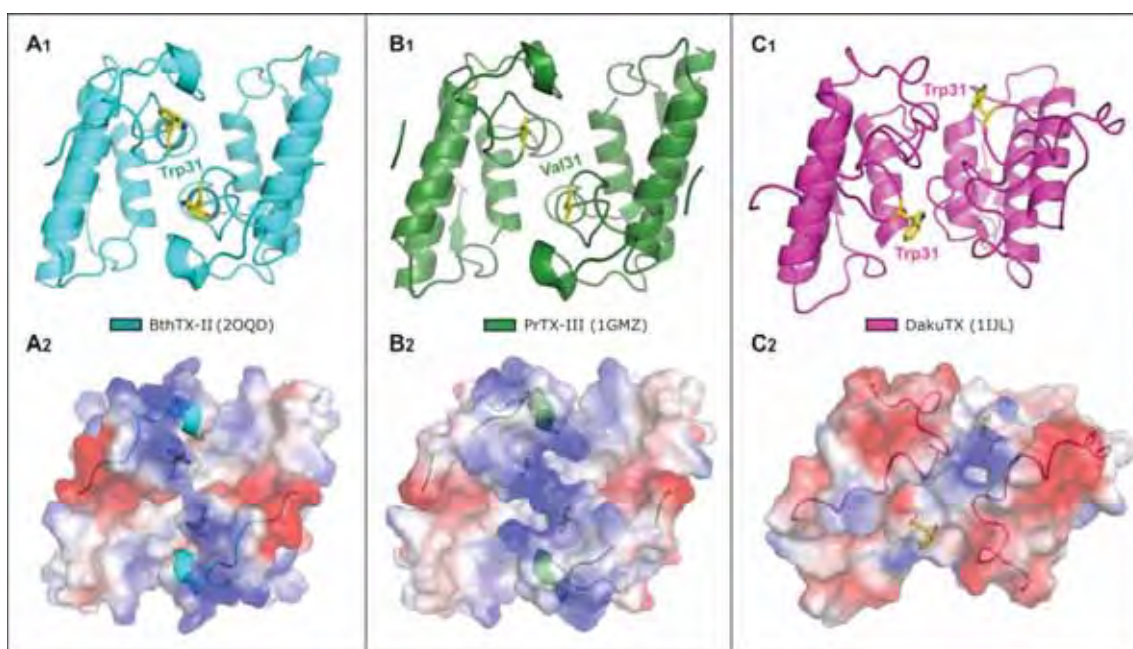


Figura 29. Conformação quaternária mais provável de ocorrer em solução para as estruturas BthTX-II (A₁), PrTX-III (B₁) e DacuTX (C₁). A₁ também representa a estrutura do complexo BthTX-II/Ca²⁺, conforme indicado por análises no programa PISA (Tabela VIII). Nas Asp49-PLA₂s miotóxicas, observa-se que os resíduos Trp31 estão dispostos lado a lado bem como voltados para a região C-terminal de seus respectivos monômeros (A₂ e B₂), o que permite o estabelecimento de uma rota de comunicação entre o *loop* de ligação de cálcio e os C-terminais destas miotoxinas. Em A₂, B₂ e C₂ está representada a distribuição de cargas para a superfície das proteínas em análise. Uma região básica (em azul) é observada ao longo da região C-terminal das proteínas BthTX-II e PrTX-III A₂ e B₂, respectivamente. Os C-terminais (resíduos 111 ao 133) da BthTX-II, PrTX-III e DacuTX estão representados em forma de *cartoon* em A₂, B₂ e C₂, respectivamente. Figura extraída do artigo de dos Santos e colaboradores (Dos Santos *et al.*, 2011).

Estudos com peptídeos sintéticos e de mutação sítio-dirigida baseados na sequência primária de Lys49-PLA₂s demonstraram ser o C-terminal a região responsável pela expressão da miotoxicidade nestas PLA₂s homólogas (Lomonte, Moreno *et al.*, 1994; Ward, Alves *et al.*, 1998; Nunez *et al.*, 2001; Chioato *et al.*, 2002; Ward *et al.*, 2002; Lomonte, Angulo e Santamaria, 2003; Chioato *et al.*, 2007). A composição do C-terminal também foi demonstrada como importante para manifestação da miotoxicidade em Lys49-PLA₂s. Segundo dados da literatura, a grande proporção de resíduos básicos e aromáticos nesta região é importante para a atividade destas PLA₂s homólogas (Lomonte, Moreno *et al.*, 1994; Lomonte, Tarkowski *et al.*, 1994; Nunez *et al.*, 2001; Chioato *et al.*, 2002; Lomonte, Angulo e Santamaria, 2003; Ambrosio *et al.*, 2005; Chioato *et al.*, 2007). Com base nesta informação, comparamos os C-terminais de Asp49-PLA₂s miotóxicas com os de algumas Lys49-PLA₂s e Asp49-PLA₂s catalíticas (Tabela IX e X). As análises apontam que Asp49-PLA₂s miotóxicas, assim como as

Lys49-PLA₂s, apresentam uma maior proporção de resíduos básicos nesta região em comparação com Asp49-PLA₂s catalíticas (Tabela IX; Figura 29), corroborando com a hipótese de que o C-terminal das Asp49-PLA₂s miotóxicas também é o responsável pela expressão da miotoxicidade. No entanto, a análise da distribuição de resíduos aromáticos nesta mesma região não mostrou haver diferenças significativas quando as PLA₂s dos diferentes grupos foram comparadas (Tabela X).

Considerando a grande identidade e similaridade dos C-terminais de Lys49-PLA₂s e Asp49-PLA₂s miotóxicas com conseqüente conservação das propriedades dos resíduos que constituem o C-terminal dos mesmos (Tabelas IX e X), a proximidade evolutiva destas PLA₂s homólogas (seção 4.5.) (Dos Santos *et al.*, 2011) e sabendo-se que ambas manifestam o mesmo tipo de atividade (são miotoxinas desprovidas de atividade catalítica), sugerimos que a distorção do *loop* de cálcio observada nas Asp49-PLA₂s miotóxicas ocorre para favorecer o mecanismo de ação destas toxinas já que esta distorção permite a formação do dímero, sendo o Trp31 parte da interface (Figura 29). Ainda, no arranjo quaternário adotado, o Trp31 está voltado para o C-terminal, provavelmente conferindo suporte mecânico a esta região (Figura 29). Esta disposição entre os monômeros de Asp49-PLA₂s miotóxicas deve estar associada à melhor ancoragem da proteína na membrana, conforme proposto / demonstrado para as Lys49-PLA₂s (Dos Santos, Soares *et al.*, 2009). Ainda, nesta configuração quaternária, os C-terminais das Asp49-PLA₂s miotóxicas se encontram lado a lado, fato que também auxilia na melhor ancoragem da proteína na membrana (Figura 29).

Tabela IX. Distribuição de resíduos carregados positivamente (arginina, lisina e histidina) na região C-terminal* de PLA₂s de venenos de serpentes da subfamília Crotalinae (família Viperidae)

	Cgod2	Tgra1	Tfla1	Ooki2	MjTX-I	BthTX-I	Basp1	BthTX-II	PrTX-III
PLA₂s Miotóxicas #	6	7	5	6	6	7	6	7	8
	Tfla5	Bsch2	Ooki1	BthA-1	Catr1	Bery1	Apispis2	Cgod3	Pmuc1
PLA₂s Catalíticas#	3	3	3	3	3	2	5	5	5

* Resíduos numerados de 111 a 133 em Lys49-PLA₂s e os correspondentes a esta região em Asp49-PLA₂s foram avaliados.

Códigos utilizados encontram correspondência na Figura 33 (seção 4.5.)

Tabela X. Distribuição de resíduos aromáticos (fenilalanina, triptofano, tirosina e histidina) na região C-terminal* de PLA₂s de venenos de serpentes da subfamília Crotalinae (família Viperidae)

		Cgod2	Tgra1	Tfla1	Ooki2	MjTX-I	BthTX-I	Basp1	BthTX-II	PrTX-III
PLA₂s Miotóxicas[#]	Phe/Trp	1	1	1	2	1	1	0	0	0
	Tyr	3	1	3	2	2	3	4	3	3
	Hist	1	0	0	0	0	1	0	0	1
		Tfla5	Bsch2	Ooki1	BthA-1	Catr1	Bery1	Apispis2	Cgod3	Pmuc1
PLA₂s Catalíticas[#]	Phe/Trp	2	2	2	2	2	3	1	2	2
	Tyr	2	3	2	3	2	2	3	3	3
	Hist	0	0	0	0	0	0	0	0	0

*Resíduos numerados de 111 a 133 em Lys49-PLA₂s e os correspondentes a esta região em Asp49-PLA₂s foram avaliados.

[#] Códigos utilizados encontram correspondência na Figura 33 (seção 4.5.)

Ao apresentar estes dados num congresso, tivemos a oportunidade de conhecer a o trabalho da doutoranda Mariana Cintra-Francischinelli, que no momento apresentava dados da avaliação da atividade de Lys49-PLA₂s em cultura celular de miotubos, demonstrando a não influência do cálcio nos resultados por ela obtidos. Desta forma, estabelecemos uma colaboração para avaliar o efeito da BthTX-II em cultura celular de miotubos e avaliar a influência de íons cálcio nestes experimentos. Neste estudo, foi demonstrado que a BthTX-II, embora seja miotóxica, não necessita de Ca²⁺ para exercer tal atividade. Ainda, nestes mesmos experimentos, ficou comprovada que a presença de Ca²⁺ no meio extracelular não leva a proteína a manifestar um aumento na atividade miotóxica ou mesmo a exercer atividade catalítica (Dos Santos *et al.*, 2011). Conseqüentemente, foi demonstrado que a BthTX-II não apresenta atividade fosfolipásica como era de se esperar para qualquer Asp49-PLA₂, corroborando então os dados estruturais e a hipótese do nosso grupo sobre a não atividade catalítica das Asp49-PLA₂s miotóxicas (Correa *et al.*, 2008).

Diante destas evidências, os dados da literatura que caracterizaram a BthTX-II e a PrTX-III como proteínas catalíticas (Pereira *et al.*, 1998; Toyama *et al.*, 1999) foram refutados. A dificuldade de purificação e separação destas PLA₂s (Schaloske e Dennis,

2006) pode ter sido o motivo da observação de baixa atividade catalítica nos referidos experimentos, visto que traços de PLA₂s catalíticas poderiam estar presentes nos mesmos.

Desta forma, as particularidades estruturais das Asp49-PLA₂s miotóxicas foram justificadas: i) dada a inatividade enzimática destas proteínas, não há motivo para que a arquitetura da região de coordenação do cálcio seja preservada; ii) o arranjo quaternário que estas proteínas assumem favorece a manifestação da sua atividade (miotoxicidade) e justifica a distorção do *loop* de cálcio já que o resíduo Trp31 passa a fazer parte da interface protéica e ao mesmo tempo confere suporte mecânico ao C-terminal da proteína, região esta responsável pela expressão da miotoxicidade.

Apesar da comparação das sequências primárias e estruturas terciárias de Asp49-PLA₂s miotóxicas com outras Asp49-PLA₂s catalíticas não ter fornecido indícios sobre o motivo da distorção do *loop* de ligação de cálcio nas Asp49-PLA₂s miotóxicas, duas interessantes observações foram feitas durante estas análises: i) uma ligação de hidrogênio se estabelece entre o O δ do resíduo Asp49 e o O η da Tyr28 na BthTX-II e PrTX-III enquanto ambos os O δ são responsáveis pela coordenação do Ca²⁺ nas PLA₂s clássicas (Figura 28c); ii) uma interação com distância conservada (3,1 Å < d < 3,5 Å) entre o O η da Tyr28 e o grupamento amino da Gly35 das Asp49-PLA₂s clássicas (Figura 28c; Tabela XI). Estes “padrões” observados, que permitem a diferenciação entre Asp49-PLA₂s clássicas e Asp49-PLA₂s miotóxicas, se devem às diferentes orientações assumidas pelos resíduos Asp49 e os presentes na região do *loop* de ligação de cálcio (Figura 28b, 28c).

A interação observada entre Tyr28 e Gly35 nas PLA₂s clássicas deve prover estabilidade estrutural para o *loop* de ligação de cálcio já que resíduos considerados essenciais para a coordenação do co-fator são mantidos em orientações favoráveis quando esta interação está presente. Por outro lado, quando se observa distorção no *loop* de ligação de Ca²⁺, a distância *d* não é preservada e há impossibilidade de coordenação do íon. As observações feitas estão de acordo com a proposição feita por Zhou e colaboradores em 2008 (Zhou *et al.*, 2008), de que a ausência da interação Tyr28-Gly35 é a responsável pela distorção do *loop* de ligação de cálcio em uma Ser49-PLA₂ presente no veneno de *Echis carinatus sochureki* (Zhou *et al.*, 2008).

Tabela XI. Distância (d) entre o átomo O_{η} da Tyr28 e o grupamento amino do resíduo Gly35 em estruturas de Asp49-PLA₂s.

	Proteína (código do PDB)	d (Å)
Asp49-PLA ₂ s clássicas	BthA-I-PLA ₂ (1U73)	3,07
	PLA ₂ ácida de <i>G. halys</i> * (1PSJ)	3,50
	PLA ₂ ácida de <i>D. acutus</i> (1IJL)	3,49
	DPLA ₂ (1FB2)	3,51
	β2-Bungarotoxina (1BUN)	3,51
	PLA ₂ de pâncreas bovino (1G4I)	3,28
Asp49-PLA ₂ s miotóxicas	PrTX-III (1GMZ)	7,87
	BthTX-II (2OQD)	7,64

* anteriormente descrita como *Agkistrodon halys pallas*

Durante a execução deste trabalho, um estudo evolutivo com todas as Asp49-PLA₂s da família Viperidae foi realizado por meio de uma colaboração com o Dr. Antônio Sérgio Kimuz Braz (professor da Universidade Federal do ABC e colaborador de nosso laboratório) e com o doutorando Carlos Alexandre Henriques Fernandes. Os dados resultantes deste estudo, juntamente com os aqui apresentados foram reunidos num artigo recentemente publicado no periódico *Proteins: Structure, Function and Bioinformatics* (“Structural, functional and bioinformatics studies reveal a new snake venom homologue phospholipase A₂ class”; Anexo III) (Dos Santos *et al.*, 2011).

4.5. Arranjo quaternário das PLA₂s homólogas Asp49 e Lys49: estudo comparativo e implicações funcionais

Estudos estruturais comparativos entre Asp49-PLA₂s miotóxicas e Lys49-PLA₂s botrópicas foram propostos no projeto inicial. A intenção do estudo era avaliar semelhanças estruturais entre estas PLA₂s homólogas diméricas já que, embora a

literatura mostre a existência de diferentes conformações quaternárias para estas toxinas (Arni *et al.*, 1995; Arni e Ward, 1996; Magro *et al.*, 2003; Rigden *et al.*, 2003; Murakami *et al.*, 2007; Correa *et al.*, 2008; Dos Santos, Soares *et al.*, 2009), elas apresentam o mesmo tipo de atividade.

Diversas estruturas cristalográficas de Lys49-PLA₂s nativas e/ou complexadas se encontram disponíveis no banco de dados de domínio público PDB, porém não há uniformidade quanto ao arranjo quaternário das mesmas. As primeiras estruturas de Lys49-PLA₂s foram resolvidas numa conformação quaternária em que os seus monômeros se relacionam por um eixo de ordem dois perpendicular às regiões das folhas-β, sendo estabilizados por interações entre os resíduos das folhas-β e das hélices N-terminais (Figura 30). Porém, em 2005, a estrutura do complexo BaspTX-II/suramina foi resolvida numa conformação dimérica alternativa (Murakami *et al.*, 2005) e, a partir de então, este arranjo quaternário passou a ser adotado na resolução das novas estruturas (Figura 30).

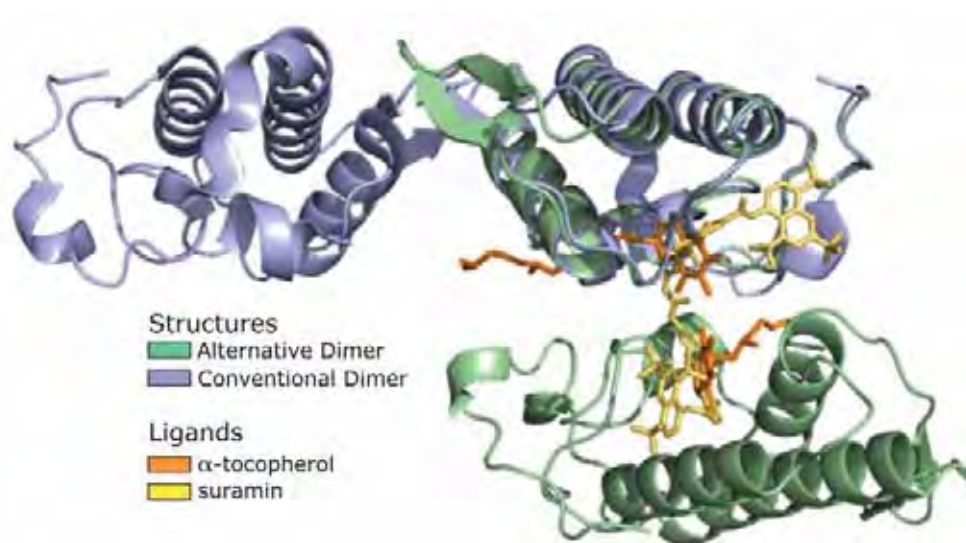


Figura 30. Conformações diméricas possíveis para as Lys49-PLA₂s. Em azul, o dímero convencional e, em verde, o dímero alternativo. A molécula de suramina (em amarelo) demonstra que o dímero alternativo é a conformação oligomérica ideal para a complexação com este inibidor. Figura extraída do artigo de dos Santos e colaboradores ((Dos Santos, Soares *et al.*, 2009).

Recentemente, nosso grupo avaliou as estruturas cristalográficas destas proteínas com o auxílio do programa PISA (Dos Santos, 2007; Dos Santos, Soares *et al.*, 2009) e o dímero alternativo foi apontado como sendo comum a todas elas. A análise da energia livre de solvatação e a área de interface para cada uma das estruturas de Lys49-PLA₂s conhecidas demonstrou que este arranjo proposto parece corresponder à conformação biológica da proteína encontrada em solução (Dos Santos, 2007; Dos Santos, Soares *et al.*, 2009). Ainda, outras evidências a favor deste arranjo quaternário são apontadas no trabalho que revisou estas estruturas. Uma delas se baseia na orientação assumida pelos sítios miotóxicos que, na conformação dimérica alternativa proposta estão dispostos lado a lado, mostrando assim uma possível colaboração entre eles para melhor ancorar a proteína (o dímero) na membrana (Figura 31). Outra evidência provém de dados de espalhamento de raios X a baixo ângulo para a proteína BthTX-I nativa, que mostram que a conformação alternativa também é tida como a que melhor representa o envelope protéico teórico (Murakami *et al.*, 2007).

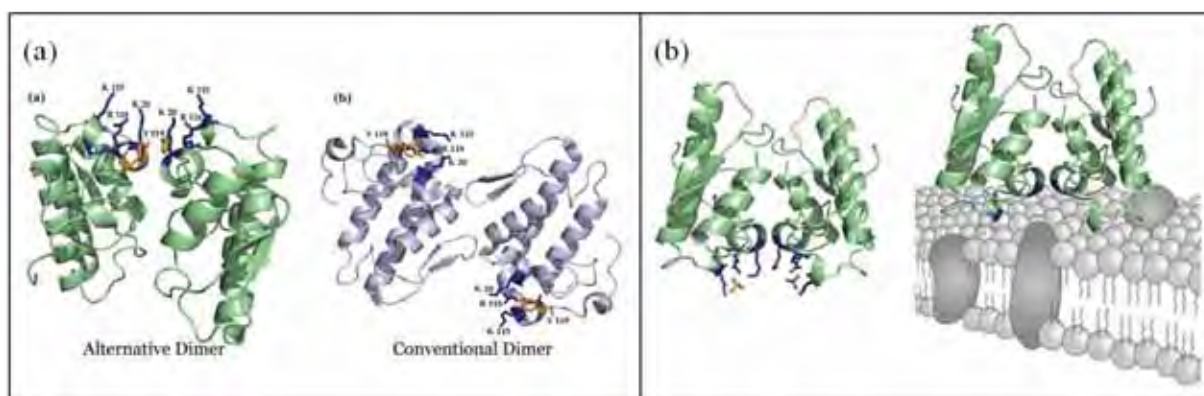


Figura 31. Sítio miotóxico de Lys49-PLA₂s e interação com membranas. Em (a), localização do sítio miotóxico (resíduos K20, K115 e R118) das Lys49-PLA₂s no Dímero Alternativo (em verde) e no Dímero Convencional (em azul). Em (b), modelo de interação de Lys49-PLA₂s em membranas musculares baseado no Dímero Alternativo. Figuras extraídas do artigo de dos Santos e colaboradores (Dos Santos, Soares *et al.*, 2009).

Na seção anterior (seção 4.4.1.), demonstramos que existe duas possíveis conformações diméricas para a resolução das estruturas de Asp49-PLA₂s miotóxicas quando observam-se seus contatos na rede cristalina (Figura 27). Uma destas possibilidades, semelhante ao dímero convencional das Lys49-PLA₂s, foi adotada para a resolução das estruturas BthTX-II nativa e complexada com íons cálcio (Correa *et al.*,

2008; Dos Santos *et al.*, 2011) (seção 4.3.). No entanto, análises destas proteínas no programa PISA apontam para um arranjo quaternário em comum para estas PLA₂s miotóxicas, diferente da escolhida na resolução das estruturas cristalográficas, que deve corresponder à conformação destas proteínas em solução (Tabela VIII – seção 4.4.1. ; Figura 27c; Figura 32). Embora esta conformação seja diferente da sugerida para as Lys49-PLA₂s (Figura 32), nela os C-terminais das Asp49-PLA₂s miotóxicas também se encontram num mesmo plano (lado a lado), característica também observada no Dímero Alternativo de Lys49-PLA₂s (Dos Santos, Soares *et al.*, 2009) (Figura 32).

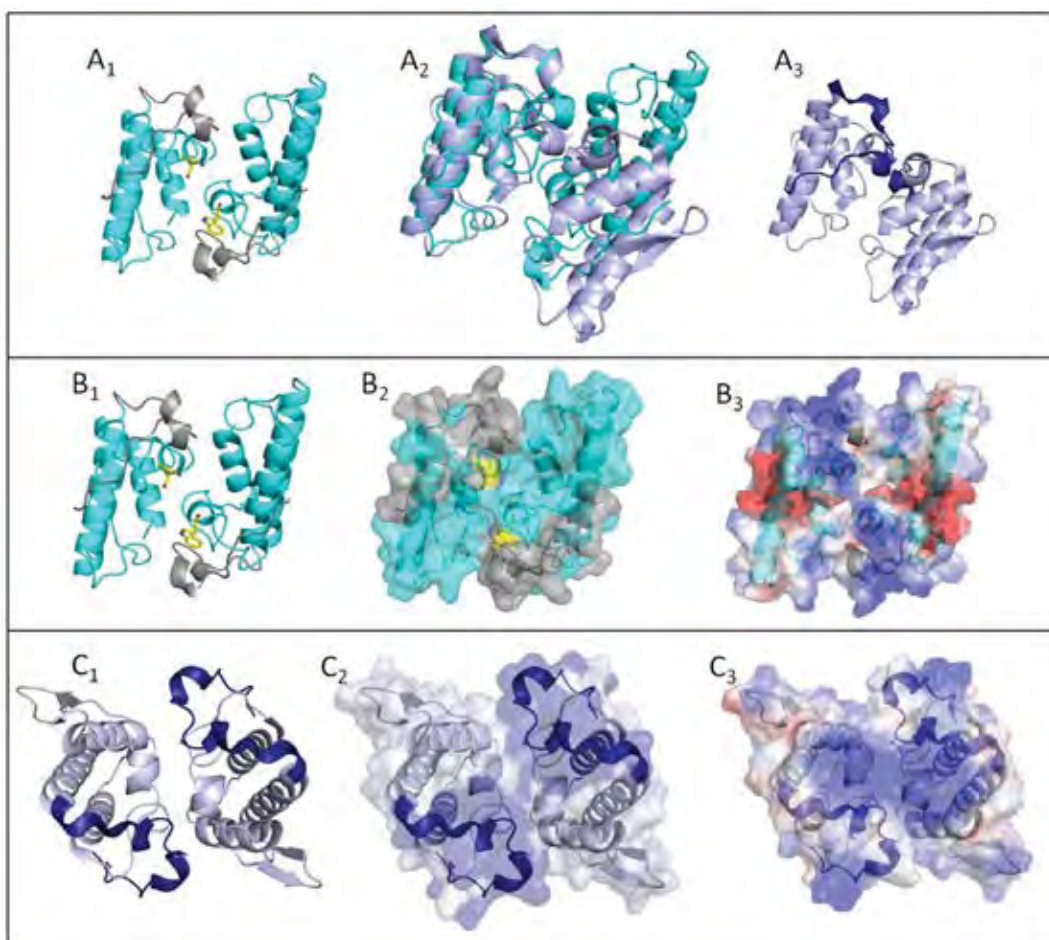


Figura 32. Diferenças estruturais entre o arranjo quaternário sugerido pelo PISA para Asp49-PLA₂s miotóxicas e Lys49-PLA₂s. Em A₂, a estrutura quaternária da Asp49-PLA₂ miotóxica BthTX-II (A₁, em azul claro) é sobreposta com a estrutura quaternária da Lys49-PLA₂ PrTX-I nativa (A₃, em roxo). No painel B, destaque para algumas características da proteína BthTX-II (B₁), como a proximidade dos resíduos Trp31 (em amarelo) que estão na interface do dímero e a disposição dos C-terminais (em cinza) na superfície da proteína (B₂). Em B₃ é mostrada a distribuição de cargas na superfície da BthTX-II, evidenciando o caráter básico da região mostrada. No painel C, destaque para os C-terminais da proteína PrTX-I (C₁), que estão lado a lado na superfície da proteína (C₂). Em C₃ é mostrada a distribuição de cargas na superfície da PrTX-I, evidenciando o caráter básico da região mostrada. Figura gerada no programa *Pymol* (Delano, 2002).

Para adquirir mais informações sobre possíveis semelhanças entre estes dois grupos de miotoxinas, após conversas com o Dr. Antônio Sérgio Kimuz Braz (professor da Universidade Federal do ABC e colaborador de nosso laboratório) e com o doutorando Carlos Alexandre Henriques Fernandes, resolvemos avaliar a proximidade evolutiva entre estas toxinas. Para tanto, uma árvore filogenética com todas as PLA₂s de venenos de serpentes da subfamília Crotalinae (família Viperidae) disponível no banco de dados de domínio público NCBI (<http://www.ncbi.nlm.nih.gov/>) foi construída (Figura 33). Este estudo comprovou a proximidade evolutiva entre estas Asp49-PLA₂s miotóxicas e Lys49-PLA₂s já que elas são seqüências mais primitivas dentro do ramo B (Figura 33) (Dos Santos *et al.*, 2011). Ainda, importantes informações foram fornecidas por este estudo: i) o ancestral destas fosfolipases era básico e sua seqüência primária apresentava um aspartato na posição 49; ii) um ancestral básico deu origem a dois grupos estatisticamente consistentes, sendo um deles miotóxico (Figura 33 – ramo B) e outro não-miotóxico (Figura 33 – ramo A), divergindo dos resultados até então apresentados na literatura que apontavam as Asp49-PLA₂s miotóxicas e as Lys49-PLA₂s como seqüências mais derivadas dentro das Asp49-PLA₂s de caráter ácido; iii) a análise da árvore filogenética mostrou que as Lys49-PLA₂s do gênero *Bothrops* formam um consistente ramo monofilético (Figura 33 – clado B1), corroborando com a recente hipótese levantada por dos Santos e colaboradores de que há um sítio miotóxico exclusivo para as Lys49-PLA₂s do gênero *Bothrops* (dos Santos, Soares, 2009); iv) dentro do ramo miotóxico, observaram-se alguns ramos monofiléticos que são representados por diferentes configurações oligoméricas, como o formado pelas Asp49-PLA₂s miotóxicas (Figura 33 – em amarelo) e os que podem ser representados por Arg49-PLA₂s e algumas Lys49-PLA₂s (Figura 33 – clado B2), dando suporte à hipótese de que dentro do grupo miotóxico há diferentes sítios para a expressão da miotoxicidade, embora tal atividade deva ser inerente da região C-terminal destas toxinas; v) a BthTX-II, embora seja uma Asp49-PLA₂, agrupa com PLA₂s miotóxicas no ramo não-catalítico (ramo B da Figura 33), sugerindo que a mesma não necessita de Ca²⁺ para exercer tal atividade. Esta hipótese é corroborada por experimentos em cultura celular (Dos Santos *et al.*, 2011), demonstrando que a mesma não apresenta atividade fosfolipásica como era de se esperar para qualquer Asp49-PLA₂, já que estas conservam todos os resíduos considerados importantes para a atividade catalítica.

A reunião destes dados com os provenientes da comparação dos C-terminais de Lys49-PLA₂s e Asp49-PLA₂s apresentados na seção 4.4.1. (Tabela IX e X) e presentes na árvore filogenética representada na Figura 33 demonstram que a expressão da miotoxicidade nas PLA₂s homólogas do clado B deve ser proveniente do C-terminal, embora diferentes sítios para a expressão da miotoxicidade possam existir nestas proteínas (diferentes aminoácidos e de diferentes posições na sequência protéica). Estes sítios podem ser resultado das diferentes oligomerizações assumidas por proteínas deste clado (monômeros ou dímeros) e / ou também dos diferentes arranjos quaternários assumidos pelas miotoxinas que fazem fazer dele (Figura 33). Como exemplo deste último caso, podemos citar as diferentes configurações entre os monômeros das miotoxinas botrópicas Asp49-PLA₂s homólogas e Lys49-PLA₂s: embora com arranjos diferentes, os monômeros destas proteínas estão dispostos de forma a propiciar que seus C-terminais fiquem dispostos lado a lado, fato este sugerido como importante para a potencialização do efeito miotóxico nas Lys49-PLA₂s (Dos Santos, 2007; Dos Santos, Soares *et al.*, 2009).

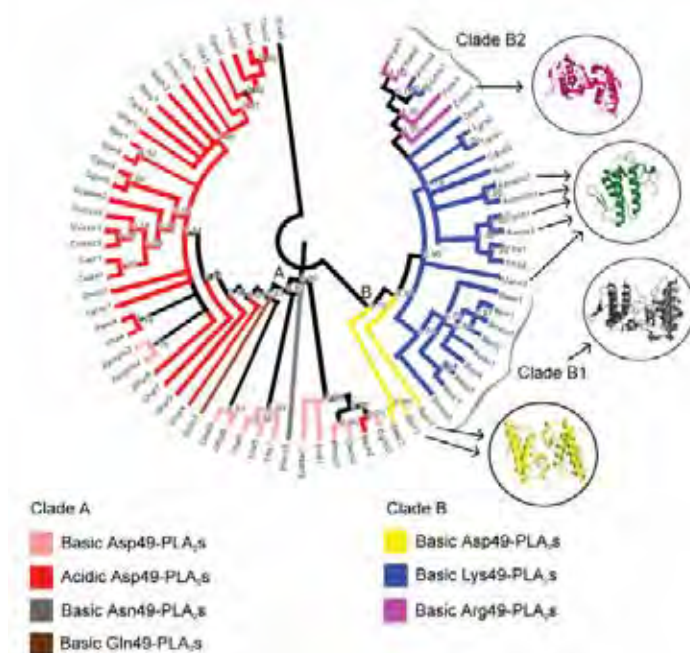


Figura 33. Árvore filogenética de fosfolipases A₂ de venenos de serpentes da família Viperidae, subfamília Crotalinae. A cor do ramo corresponde ao grupo a qual cada seqüência pertence. As configurações oligoméricas representadas correspondem às estruturas cristalográficas da BthTX-II (em amarelo; código de acesso no PDB: 2OQD), PrTX-I (em cinza; código de acesso no PDB: 2Q2J), Dacu3 (em verde ; código de acesso no PDB: 1MC2 ou 1MG6) e Zman1 (em magenta; código de acesso no PDB: 2PH4). A conformação biológica indicada pelo programa PISA foi utilizada na representação das estruturas da PrTX-I e BthTX-II. A configuração adotada pela BthTX-II e Zman 1 são equivalentes. Figura extraída do artigo de dos Santos e colaboradores (Dos Santos *et al.*, 2011).

Os dados cristalográficos da BthTX-II/Ca²⁺ e as análises estruturais realizadas com Asp49-PLA₂s miotóxicas (seções 4.3. a 4.5.), juntamente com o abrangente estudo evolutivo de PLA₂s de veneno de serpentes da família Viperidae e estudos *in vitro* realizados pela Dra. Mariana Cintra-Francischinelli (seção 4.4.2.) foram reunidos no artigo “*Structural, functional and bioinformatics studies reveal a new snake venom homologue phospholipase A₂ class*”, publicado no periódico ***Proteins: Structure, Function, and Bioinformatics***, em 2011 (Dos Santos *et al.*, 2011) (Anexo III).

5. Considerações Finais

Os estudos cristalográficos aqui apresentados possibilitaram uma melhor compreensão do mecanismo de atuação das miotoxinas Lys49-PLA₂s e Asp49-PLA₂s. O estudo dos complexos formado entre Lys49-PLA₂s e os inibidores ácido rosmarínico e manganês não só evidenciaram o sítio de interação destes inibidores nestas proteínas como também possibilitaram um avanço no que se refere ao conhecimento do modo de atuação destas toxinas e maneiras de inibi-las. Estes estudos corroboraram uma recém hipótese de nosso grupo, auxiliando na comprovação de que o canal hidrofóbico destas proteínas é uma extensão de seus sítios miotóxicos (Dos Santos, 2007; Dos Santos, Soares *et al.*, 2009). No caso do complexo PrTX-I/AR, foi demonstrado que o inibidor interage com a toxina na entrada do seu canal hidrofóbico (Figura 11), impedindo que ácidos graxos da membrana tenham acesso a essa região; conseqüentemente, o mecanismo de atuação da proteína fica prejudicado já que, embora seus C-terminais estejam livres para interagir com a membrana, as porções hidrofóbicas dos ácidos graxos desta não conseguem se inserir no canal hidrofóbico da toxina porque o mesmo se encontra fisicamente obstruído. Já no complexo formado entre Lys49-PLA₂s e íons manganês, o Mn²⁺ interage com a toxina em diferentes regiões (Figuras 16 e 17), porém em somente uma delas observa-se mudança na estrutura terciária da proteína (Figura 16b). Nesta posição, o Mn²⁺ se encontra no canal hidrofóbico, sendo coordenado tanto por resíduos do monômero A quanto do monômero B da toxina (Figura 16b). A coordenação do íon nesta região leva à inibição da proteína provavelmente por dois motivos: i) por impedir que os monômeros da toxina se afastem para abrigar ácidos graxos da membrana, e também ii) por estar ocupando fisicamente o espaço que seria ocupado por porções hidrofóbicas dos ácidos graxos da membrana, ou seja, assim como o AR, por obstruir fisicamente o canal hidrofóbico. Desta forma, os dados obtidos contribuíram para um avanço no conhecimento do modo de atuação das Lys49-PLA₂s de uma forma geral, demonstrando que o canal hidrofóbico destas proteínas pode ser também o alvo de inibidores.

O estudo estrutural do complexo BthTX-II/Ca²⁺ e estudos comparativos entre Asp49-PLA₂s miotóxicas e não-miotóxicas também trouxeram importantes conclusões. Primeiramente, ficou demonstrado que Asp49-PLA₂s miotóxicas apresentam *loop* de ligação de cálcio distorcido e que esta observação não corresponde a um estado inativo destas proteínas pela ausência do co-fator Ca²⁺, sendo sim uma característica intrínseca

das mesmas. Ainda, a avaliação desta distorção do ponto de vista funcional permitiu importantes conclusões: i) devido à comprovada inatividade catalítica destas proteínas (Dos Santos *et al.*, 2011), as mesmas não precisam preservar a arquitetura desta região; ii) o arranjo quaternário que estas proteínas assumem favorece a manifestação da sua atividade (miotoxicidade) e justifica a distorção do *loop* de cálcio já que o resíduo Trp31(do *loop* de ligação de cálcio) passa a fazer parte da interface protéica e ao mesmo tempo confere suporte mecânico ao C-terminal da proteína, região esta responsável pela expressão da miotoxicidade; iii) os C-terminais das Asp49-PLA₂s miotóxicas se encontram lado a lado na configuração de maior probabilidade de ocorrência em solução para estas miotoxinas (Tabela VIII; Figura 27, 29 e 32), fato que também deve auxiliar para uma melhor ancoragem destas proteínas na membrana.

6. Referências Bibliográficas

Ambrosio, A. L. B., Nonato, M. C., De Araujo, H. S. S., Arni, R., Ward, R. J., Ownby, C. L., De Souza, D. H. F. e Garratt, R. C. A molecular mechanism for Lys(49)-phospholipase A(2) activity based on ligand-induced conformational change. **Journal of Biological Chemistry**, v.280, n.8, p.7326-7335. 2005.

Andriao-Escarso, S. H., Soares, A. M., Fontes, M. R., Fuly, A. L., Correa, F. M., Rosa, J. C., Greene, L. J. e Giglio, J. R. Structural and functional characterization of an acidic platelet aggregation inhibitor and hypotensive phospholipase A(2) from Bothrops jararacussu snake venom. **Biochem Pharmacol**, v.64, n.4, Aug 15, p.723-32. 2002.

Arni, R. K., Fontes, M. R., Barberato, C., Gutierrez, J. M., Diaz, C. e Ward, R. J. Crystal structure of myotoxin II, a monomeric Lys49-phospholipase A2 homologue isolated from the venom of Cerrophidion (Bothrops) godmani. **Arch Biochem Biophys**, v.366, n.2, Jun 15, p.177-82. 1999.

Arni, R. K. e Ward, R. J. Phospholipase A2 - a structural review. **Toxicon**, v.34, n.8, Aug, p.827-41. 1996.

Arni, R. K., Ward, R. J., Gutierrez, J. M. e Tulinsky, A. Structure of a calcium-independent phospholipase-like myotoxic protein from Bothrops asper venom. **Acta Crystallographica Section D-Biological Crystallography**, v.51, p.311-317. 1995.

Bahnson, B. J. Structure, function and interfacial allostereism in phospholipase A2: insight from the anion-assisted dimer. **Arch Biochem Biophys**, v.433, n.1, Jan 1, p.96-106. 2005.

Bao, Y., Bu, P., Jin, L., Hongxia, W., Yang, Q. e An, L. Purification, characterization and gene cloning of a novel phospholipase A2 from the venom of Agkistrodon blomhoffii ussurensis. **Int J Biochem Cell Biol**, v.37, n.3, Mar, p.558-65. 2005.

Beers, S. A., Buckland, A. G., Koduri, R. S., Cho, W., Gelb, M. H. e Wilton, D. C. The antibacterial properties of secreted phospholipases A2: a major physiological role for the group IIA enzyme that depends on the very high pI of the enzyme to allow penetration of the bacterial cell wall. **J Biol Chem**, v.277, n.3, Jan 18, p.1788-93. 2002.

Bon, C., Changeux, J. P., Jeng, T. W. e Fraenkel-Conrat, H. Postsynaptic effects of crotoxin and of its isolated subunits. **Eur J Biochem**, v.99, n.3, Sep, p.471-81. 1979.

Brunger, A. T., Adams, P. D., Clore, G. M., Delano, W. L., Gros, P., Grosse-Kunstleve, R. W., Jiang, J. S., Kuszewski, J., Nilges, M., Pannu, N. S., Read, R. J., Rice, L. M., Simonson, T. e Warren, G. L. Crystallography & NMR system: A new software suite for macromolecular structure determination. **Acta Crystallographica Section D-Biological Crystallography**, v.54, Sep 1, p.905-921. 1998.

Brunie, S., Bolin, J., Gewirth, D. e Sigler, P. B. The refined crystal structure of dimeric phospholipase A2 at 2.5 Å. Access to a shielded catalytic center. **J Biol Chem**, v.260, n.17, Aug 15, p.9742-9. 1985.

Cardoso, J. L., Fan, H. W., Franca, F. O., Jorge, M. T., Leite, R. P., Nishioka, S. A., Avila, A., Sano-Martins, I. S., Tomy, S. C., Santoro, M. L. e Et Al. Randomized comparative trial of three antivenoms in the treatment of envenoming by lance-headed vipers (*Bothrops jararaca*) in Sao Paulo, Brazil. **Q J Med**, v.86, n.5, May, p.315-25. 1993.

Cavalcante, W. L. G., Campos, T. O., Dal Pai-Silva, M., Pereira, P. S., Oliveira, C. Z., Soares, A. M. e Gallacci, M. Neutralization of snake venom phospholipase A(2) toxins by aqueous extract of *Casearia sylvestris* (Flacourtiaceae) in mouse neuromuscular preparation. **Journal of Ethnopharmacology**, v.112, n.3, p.490-497. 2007.

Chang, C. C. e Lee, J. D. Crotoxin, the neurotoxin of South American rattlesnake venom, is a presynaptic toxin acting like beta-bungarotoxin. **Naunyn Schmiedebergs Arch Pharmacol**, v.296, n.2, Jan, p.159-68. 1977.

Chijiwa, T., Tokunaga, E., Ikeda, R., Terada, K., Ogawa, T., Oda-Ueda, N., Hattori, S., Nozaki, M. e Ohno, M. Discovery of novel [Arg49]phospholipase A2 isozymes from *Protobothrops elegans* venom and regional evolution of Crotalinae snake venom phospholipase A2 isozymes in the southwestern islands of Japan and Taiwan. **Toxicon**, v.48, n.6, Nov, p.672-82. 2006.

Chioato, L., Aragao, E. A., Ferreira, T. L., De Medeiros, A. I., Faccioli, L. H. e Ward, R. J. Mapping of the structural determinants of artificial and biological membrane damaging activities of a Lys49 phospholipase A(2) by scanning alanine mutagenesis. **Biochimica Et Biophysica Acta-Biomembranes**, v.1768, n.5, p.1247-1257. 2007.

Chioato, L., De Oliveira, A. H. C., Ruller, R., Sa, J. M. e Ward, R. J. Distinct sites for myotoxic and membrane-damaging activities in the C-terminal region of a Lys(49)-phospholipase A(2). **Biochemical Journal**, v.366, p.971-976. 2002.

Condrea, E., Yang, C. C. e Rosenberg, P. Lack of correlation between anticoagulant activity and phospholipid hydrolysis by snake venom phospholipases A2. **Thromb Haemost**, v.45, n.1, Feb 23, p.82-5. 1981.

Correa, L. C., Marchi-Salvador, D. P., Cintra, A. C., Sampaio, S. V., Soares, A. M. e Fontes, M. R. Crystal structure of a myotoxic Asp49-phospholipase A2 with low catalytic activity: Insights into Ca²⁺-independent catalytic mechanism. **Biochim Biophys Acta**, v.1784, n.4, Apr, p.591-9. 2008.

Correa, L. C., Marchi-Salvador, D. P., Cintra, A. C., Soares, A. M. e Fontes, M. R. Preliminary X-ray crystallographic studies of BthTX-II, a myotoxic Asp49-phospholipase A2 with low catalytic activity from Bothrops jararacussu venom. **Acta Crystallogr Sect F Struct Biol Cryst Commun**, v.62, n.Pt 8, Aug 1, p.765-7. 2006.

Da Silva Giotto, M. T., Garratt, R. C., Oliva, G., Mascarenhas, Y. P., Giglio, J. R., Cintra, A. C., De Azevedo, W. F., Jr., Arni, R. K. e Ward, R. J. Crystallographic and spectroscopic characterization of a molecular hinge: conformational changes in bothropstoxin I, a dimeric Lys49-phospholipase A2 homologue. **Proteins**, v.30, n.4, Mar 1, p.442-54. 1998.

Da Silva, J. O., Fernandes, R. S., Ticli, F. K., Oliveira, C. Z., Mazzi, M. V., Franco, J. J., Giuliatti, S., Pereira, P. S., Soares, A. M. e Sampaio, S. V. Triterpenoid saponins, new metalloprotease snake venom inhibitors isolated from *Pentaclethra macroloba*. **Toxicon**, v.50, n.2, Aug, p.283-91. 2007.

De Oliveira, R. C. W., F.H.; Sifuentes, D.N. Epidemiologia dos Acidentes por Animais Peçonhentos. In: **Animais peçonhentos do Brasil: biologia, clínica e terapêutica dos envenenamentos**, (Ed.). São Paulo: Sarvier, 2009.

Delano, W. L. **The PyMOL Molecular Graphics System**. San Carlos, CA: DeLano Scientific LLC. 2002

Delatorre, P., Rocha, B. A., Santi-Gadelha, T., Gadelha, C. A., Toyama, M. H. e Cavada, B. S. Crystal structure of Bn IV in complex with myristic acid: a Lys49 myotoxic phospholipase A from *Bothrops neuwiedi* venom. **Biochimie**, v.93, n.3, Mar, p.513-8.

Doley, R. e Kini, R. M. Protein complexes in snake venom. **Cell Mol Life Sci**, v.66, n.17, Sep, p.2851-71. 2009.

Dos Santos, J. I. **Estudos estruturais com fosfolipases A2 homólogas do veneno de serpentes do gênero *Bothrops*: proposição de um novo sítio miotóxico**. 2007. 93 p.(Dissertação de Mestrado). UNESP, Botucatu.

Dos Santos, J. I., Cintra-Francischinelli, M., Borges, R. J., Fernandes, C. A., Pizzo, P., Cintra, A. C., Braz, A. S., Soares, A. M. e Fontes, M. R. Structural, functional, and bioinformatics studies reveal a new snake venom homologue phospholipase A class. **Proteins**, v.79, n.1, Jan, p.61-78. 2011.

Dos Santos, J. I., Fernandes, C. A., Magro, A. J. e Fontes, M. R. The intriguing phospholipases A2 homologues: relevant structural features on myotoxicity and catalytic inactivity. **Protein Pept Lett**, v.16, n.8, p.887-93. 2009.

Dos Santos, J. I., Marchi-Salvador, D. P., Fernandes, C. A., Silveira, L. B., Soares, A. M. e Fontes, M. R. Preliminary X-ray crystallographic studies of a Lys49-phospholipase A2 homologue from *Bothrops pirajai* venom complexed with p-bromo-phenacyl bromide and alpha-tocopherol inhibitors. **Protein Pept Lett**, v.14, n.7, p.698-701. 2007.

Dos Santos, J. I., Santos-Filho, N. A., Soares, A. M. e Fontes, M. R. Crystallization and preliminary X-ray crystallographic studies of a Lys49-phospholipase A2 homologue from *Bothrops pirajai* venom complexed with rosmarinic acid. **Acta Crystallogr Sect F Struct Biol Cryst Commun**, v.66, n.Pt 6, Jun 1, p.699-701. 2010.

Dos Santos, J. I., Soares, A. M. e Fontes, M. R. Comparative structural studies on Lys49-phospholipases A(2) from *Bothrops* genus reveal their myotoxic site. **J Struct Biol**, v.167, n.2, Aug, p.106-16. 2009.

Emsley, P. e Cowtan, K. Coot: model-building tools for molecular graphics. **Acta Crystallogr D Biol Crystallogr**, v.60, n.Pt 12 Pt 1, Dec, p.2126-32. 2004.

Esmeraldino, L. E., Souza, A. M. e Sampaio, S. V. Evaluation of the effect of aqueous extract of *Croton urucurana* Baillon (Euphorbiaceae) on the hemorrhagic activity induced by the venom of *Bothrops jararaca*, using new techniques to quantify hemorrhagic activity in rat skin. **Phytomedicine**, v.12, n.8, Aug, p.570-6. 2005.

Ezekowitz, R. A., Sastry, K., Bailly, P. e Warner, A. Molecular characterization of the human macrophage mannose receptor: demonstration of multiple carbohydrate recognition-like domains and phagocytosis of yeasts in Cos-1 cells. **J Exp Med**, v.172, n.6, Dec 1, p.1785-94. 1990.

Fan, H. W. e Cardoso, J. L. Clinical toxicology os snake bites in South America. In: **Handbook of clinical toxicology of animal venoms and poisons**, J. Meier, White, J. (Ed.). Boca Raton (Florida): CRC Press, 1995. p.667-688.

Fernandes, C. A., Marchi-Salvador, D. P., Salvador, G. M., Silva, M. C., Costa, T. R., Soares, A. M. e Fontes, M. R. Comparison between apo and complexed structures of bothropstoxin-I reveals the role of Lys122 and Ca(2+)-binding loop region for the catalytically inactive Lys49-PLA(2)s. **J Struct Biol**, Apr 4. 2011.

Francis, B., Gutierrez, J. M., Lomonte, B. e Kaiser, Ii. Myotoxin II from *Bothrops asper* (Terciopelo) venom is a lysine-49 phospholipase A2. **Arch Biochem Biophys**, v.284, n.2, Feb 1, p.352-9. 1991.

Fraústo Da Silva, J. J. R. e Willians, R. J. P. **The Biological Chemistry of the Elements - The Inorganic Chemistry of Life**: Oxford University Press: Oxford. 1991. 561 p.

Fremont, D. H., Anderson, D. H., Wilson, I. A., Dennis, E. A. e Xuong, N. H. Crystal structure of phospholipase A2 from Indian cobra reveals a trimeric association. **Proc Natl Acad Sci U S A**, v.90, n.1, Jan 1, p.342-6. 1993.

Gallacci, M. e Cavalcante, W. L. Understanding the in vitro neuromuscular activity of snake venom Lys49 phospholipase A2 homologues. **Toxicon**, v.55, n.1, Jan, p.1-11. 2010.

Gerrard, J. M., Robinson, P., Narvey, M. e Mcnicol, A. Increased phosphatidic acid and decreased lysophosphatidic acid in response to thrombin is associated with inhibition of platelet aggregation. **Biochem Cell Biol**, v.71, n.9-10, Sep-Oct, p.432-9. 1993.

Gomes, A., Das, R., Sarkhel, S., Mishra, R., Mukherjee, S. e Bhattacharya, S. Herbs and herbal constituents active against snake bite. **Indian J Exp Biol**, v.48, n.9, Sep, p.865-78.

Gu, L., Zhang, H., Song, S., Zhou, Y. e Lin, Z. Structure of an acidic phospholipase A2 from the venom of *Deinagkistrodon acutus*. **Acta Crystallogr D Biol Crystallogr**, v.58, n.Pt 1, Jan, p.104-10. 2002.

Gutierrez, J. M. Understanding snake venoms: 50 years of research in Latin America. **Rev Biol Trop**, v.50, n.2, Jun, p.377-94. 2002.

Gutierrez, J. M., Leon, G. e Lomonte, B. Pharmacokinetic-pharmacodynamic relationships of immunoglobulin therapy for envenomation. **Clin Pharmacokinet**, v.42, n.8, p.721-41. 2003.

Gutierrez, J. M., Leon, G., Rojas, G., Lomonte, B., Rucavado, A. e Chaves, F. Neutralization of local tissue damage induced by *Bothrops asper* (terciopelo) snake venom. **Toxicon**, v.36, n.11, Nov, p.1529-38. 1998.

Gutierrez, J. M. e Lomonte, B. Phospholipase A2 myotoxins from Bothrops snake venoms. **Toxicon**, v.33, n.11, Nov, p.1405-24. 1995.

Gutierrez, J. M., Lomonte, B., Leon, G., Alape-Giron, A., Flores-Diaz, M., Sanz, L., Angulo, Y. e Calvete, J. J. Snake venomics and antivenomics: Proteomic tools in the design and control of antivenoms for the treatment of snakebite envenoming. **J Proteomics**, v.72, n.2, Mar 6, p.165-82. 2009.

Gutierrez, J. M., Nunez, J., Diaz, C., Cintra, A. C., Homs-Brandeburgo, M. I. e Giglio, J. R. Skeletal muscle degeneration and regeneration after injection of bothropstoxin-II, a phospholipase A2 isolated from the venom of the snake Bothrops jararacussu. **Exp Mol Pathol**, v.55, n.3, Dec, p.217-29. 1991.

Gutierrez, J. M. e Ownby, C. L. Skeletal muscle degeneration induced by venom phospholipases A2: insights into the mechanisms of local and systemic myotoxicity. **Toxicon**, v.42, n.8, Dec 15, p.915-31. 2003.

Gutierrez, J. M., Ponce-Soto, L. A., Marangoni, S. e Lomonte, B. Systemic and local myotoxicity induced by snake venom group II phospholipases A2: comparison between crotoxin, crotoxin B and a Lys49 PLA2 homologue. **Toxicon**, v.51, n.1, Jan, p.80-92. 2008.

Gutierrez, J. M., Rucavado, A., Escalante, T. e Diaz, C. Hemorrhage induced by snake venom metalloproteinases: biochemical and biophysical mechanisms involved in microvessel damage. **Toxicon**, v.45, n.8, Jun 15, p.997-1011. 2005.

Gutierrez, J. M., Sanz, L., Flores-Diaz, M., Figueroa, L., Madrigal, M., Herrera, M., Villalta, M., Leon, G., Estrada, R., Borges, A., Alape-Giron, A. e Calvete, J. J. Impact of regional variation in Bothrops asper snake venom on the design of antivenoms: integrating antivenomics and neutralization approaches. **J Proteome Res**, v.9, n.1, Jan, p.564-77. 2010.

Gutierrez, J. M., Theakston, R. D. e Warrell, D. A. Confronting the neglected problem of snake bite envenoming: the need for a global partnership. **PLoS Med**, v.3, n.6, Jun, p.e150. 2006.

Halgren, T. A. e Nachbar, R. B. Merck molecular force field. IV. conformational energies and geometries for MMFF94. **Journal of Computational Chemistry**, v.17, n.5-6, p.587-615. 1996.

Harding, M. M. The geometry of metal-ligand interactions relevant to proteins. II. Angles at the metal atom, additional weak metal-donor interactions. **Acta Crystallogr D Biol Crystallogr**, v.56, n.Pt 7, Jul, p.857-67. 2000.

Harding, M. M. Geometry of metal-ligand interactions in proteins. **Acta Crystallogr D Biol Crystallogr**, v.57, n.Pt 3, Mar, p.401-11. 2001.

Harris, J. B. e Cullen, M. J. Muscle necrosis caused by snake venoms and toxins. **Electron Microsc Rev**, v.3, n.2, p.183-211. 1990.

Holland, D. R., Clancy, L. L., Muchmore, S. W., Ryde, T. J., Einspahr, H. M., Finzel, B. C., Henrikson, R. L. e Watenpugh, K. D. The crystal structure of a lysine 49 phospholipase A2 from the venom of the cottonmouth snake at 2.0-Å resolution. **J Biol Chem**, v.265, n.29, Oct 15, p.17649-56. 1990.

Homsí-Brandeburgo, M. I., Queiroz, L. S., Santo-Neto, H., Rodrigues-Simioni, L. e Giglio, J. R. Fractionation of *Bothrops jararacussu* snake venom: partial chemical characterization and biological activity of bothropstoxin. **Toxicon**, v.26, n.7, p.615-27. 1988.

Hseu, M. J., Yen, C. Y., Tseng, C. C. e Tzeng, M. C. Purification and partial amino acid sequence of a novel protein of the reticulocalbin family. **Biochem Biophys Res Commun**, v.239, n.1, Oct 9, p.18-22. 1997.

Huang, H. C. Release of slow reacting substance from the guinea-pig lung by phospholipases A2 of *Vipera russelli* snake venom. **Toxicon**, v.22, n.3, p.359-72. 1984.

Izidoro, L. F., Rodrigues, V. M., Rodrigues, R. S., Ferro, E. V., Hamaguchi, A., Giglio, J. R. e Homs-Brandeburgo, M. I. Neutralization of some hematological and hemostatic alterations induced by neuwiedase, a metalloproteinase isolated from *Bothrops neuwiedi pauloensis* snake venom, by the aqueous extract from *Casearia mariquitensis* (Flacourtiaceae). **Biochimie**, v.85, n.7, Jul, p.669-75. 2003.

Januario, A. H., Santos, S. L., Marcussi, S., Mazzi, M. V., Pietro, R. C., Sato, D. N., Ellena, J., Sampaio, S. V., Franca, S. C. e Soares, A. M. Neo-clerodane diterpenoid, a new metalloprotease snake venom inhibitor from *Baccharis trimera* (Asteraceae): anti-proteolytic and anti-hemorrhagic properties. **Chem Biol Interact**, v.150, n.3, Dec 7, p.243-51. 2004.

Kasturiratne, A., Wickremasinghe, A. R., De Silva, N., Gunawardena, N. K., Pathmeswaran, A., Premaratna, R., Savioli, L., Lalloo, D. G. e De Silva, H. J. The global burden of snakebite: a literature analysis and modelling based on regional estimates of envenoming and deaths. **PLoS Med**, v.5, n.11, Nov 4, p.e218. 2008.

Kini, R. M. Phospholipase A₂ - A complex multifunctional protein puzzle. In: **Venom Phospholipase A₂ Enzymes: Structure, Function and Mechanism**, (Ed.), 1997. p.1-28.

Kini, R. M. e Chan, Y. M. Accelerated evolution and molecular surface of venom phospholipase A₂ enzymes. **J Mol Evol**, v.48, n.2, Feb, p.125-32. 1999.

Kini, R. M. e Evans, H. J. A model to explain the pharmacological effects of snake venom phospholipases A₂. **Toxicon**, v.27, n.6, p.613-35. 1989.

Kordis, D. e Gubensek, F. Bov-B long interspersed repeated DNA (LINE) sequences are present in *Vipera ammodytes* phospholipase A₂ genes and in genomes of Viperidae snakes. **Eur J Biochem**, v.246, n.3, Jun 15, p.772-9. 1997.

Krissinel, E. e Henrick, K. Inference of macromolecular assemblies from crystalline state. **Journal of Molecular Biology**, v.372, n.3, Sep 21, p.774-797. 2007.

Laloo, D. G. e Theakston, R. D. Snake antivenoms. **J Toxicol Clin Toxicol**, v.41, n.3, p.277-90; 317-27. 2003.

Lambeau, G., Lazdunski, M. e Barhanin, J. Properties of receptors for neurotoxic phospholipases A2 in different tissues. **Neurochem Res**, v.16, n.6, Jun, p.651-8. 1991.

Lambeau, G., Schmid-Alliana, A., Lazdunski, M. e Barhanin, J. Identification and purification of a very high affinity binding protein for toxic phospholipases A2 in skeletal muscle. **J Biol Chem**, v.265, n.16, Jun 5, p.9526-32. 1990.

Laskowski, R. A., Macarthur, M. W., Moss, D. S. e Thornton, J. M. Procheck - a Program to Check the Stereochemical Quality of Protein Structures. **Journal of Applied Crystallography**, v.26, Apr 1, p.283-291. 1993.

Lee, W. H., Da Silva Giotto, M. T., Marangoni, S., Toyama, M. H., Polikarpov, I. e Garratt, R. C. Structural basis for low catalytic activity in Lys49 phospholipases A2--a hypothesis: the crystal structure of piratoxin II complexed to fatty acid. **Biochemistry**, v.40, n.1, Jan 9, p.28-36. 2001.

Liu, Q., Huang, Q., Teng, M., Weeks, C. M., Jelsch, C., Zhang, R. e Niu, L. The crystal structure of a novel, inactive, lysine 49 PLA2 from Agkistrodon acutus venom: an ultrahigh resolution, AB initio structure determination. **J Biol Chem**, v.278, n.42, Oct 17, p.41400-8. 2003.

Liu, S. Y., Yoshizumi, K., Oda, N., Ohno, M., Tokunaga, F., Iwanaga, S. e Kihara, H. Purification and amino acid sequence of basic protein II, a lysine-49-phospholipase A2 with low activity, from Trimeresurus flavoviridis venom. **J Biochem**, v.107, n.3, Mar, p.400-8. 1990.

Lloret, S. e Moreno, J. J. Oedema formation and degranulation of mast cells by phospholipase A2 purified from porcine pancreas and snake venoms. **Toxicon**, v.31, n.8, Aug, p.949-56. 1993.

Lomonte, B., Angulo, Y. e Calderon, L. An overview of lysine-49 phospholipase A2 myotoxins from crotalid snake venoms and their structural determinants of myotoxic action. **Toxicon**, v.42, n.8, Dec 15, p.885-901. 2003.

Lomonte, B., Angulo, Y. e Santamaria, C. Comparative study of synthetic peptides corresponding to region 115-129 in Lys49 myotoxic phospholipases A2 from snake venoms. **Toxicon**, v.42, n.3, Sep, p.307-12. 2003.

Lomonte, B., Gutierrez, J. M., Carmona, E. e Rovira, M. E. Equine antibodies to *Bothrops asper* myotoxin II: isolation from polyvalent antivenom and neutralizing ability. **Toxicon**, v.28, n.4, p.379-84. 1990.

Lomonte, B., Gutierrez, J. M., Moreno, E. e Cerdas, L. Antibody neutralization of a myotoxin from the venom of *Bothrops asper* (terciopelo). **Toxicon**, v.25, n.4, p.443-9. 1987.

Lomonte, B., Gutierrez, J. M., Ramirez, M. e Diaz, C. Neutralization of myotoxic phospholipases A2 from the venom of the snake *Bothrops asper* by monoclonal antibodies. **Toxicon**, v.30, n.3, Mar, p.239-45. 1992.

Lomonte, B., Moreno, E., Tarkowski, A., Hanson, L. A. e Maccarana, M. Neutralizing interaction between heparins and myotoxin II, a lysine 49 phospholipase A2 from *Bothrops asper* snake venom. Identification of a heparin-binding and cytolytic toxin region by the use of synthetic peptides and molecular modeling. **J Biol Chem**, v.269, n.47, Nov 25, p.29867-73. 1994.

Lomonte, B., Tarkowski, A., Bagge, U. e Hanson, L. A. Neutralization of the cytolytic and myotoxic activities of phospholipases A2 from *Bothrops asper* snake venom by glycosaminoglycans of the heparin/heparan sulfate family. **Biochem Pharmacol**, v.47, n.9, Apr 29, p.1509-18. 1994.

Magro, A. J., Fernandes, C. A., Dos Santos, J. I. e Fontes, M. R. Influence of quaternary conformation on the biological activities of the Asp49-phospholipases A2s from snake venoms. **Protein Pept Lett**, v.16, n.8, p.852-9. 2009.

Magro, A. J., Soares, A. M., Giglio, J. R. e Fontes, M. R. Crystal structures of BnSP-7 and BnSP-6, two Lys49-phospholipases A(2): quaternary structure and inhibition mechanism insights. **Biochem Biophys Res Commun**, v.311, n.3, Nov 21, p.713-20. 2003.

Mancuso, L. C., Correa, M. M., Vieira, C. A., Cunha, O. A., Lachat, J. J., De Araujo, H. S., Ownby, C. L. e Giglio, J. R. Fractionation of Bothrops pirajai snake venom: isolation and characterization of piratoxin-I, a new myotoxic protein. **Toxicon**, v.33, n.5, May, p.615-26. 1995.

Maraganore, J. M., Merutka, G., Cho, W., Welches, W., Kezdy, F. J. e Heinrikson, R. L. A new class of phospholipases A2 with lysine in place of aspartate 49. Functional consequences for calcium and substrate binding. **J Biol Chem**, v.259, n.22, Nov 25, p.13839-43. 1984.

Marchi-Salvador, D. P., Correa, L. C., Magro, A. J., Oliveira, C. Z., Soares, A. M. e Fontes, M. R. Insights into the role of oligomeric state on the biological activities of crotoxin: crystal structure of a tetrameric phospholipase A2 formed by two isoforms of crotoxin B from *Crotalus durissus terrificus* venom. **Proteins**, v.72, n.3, Aug 15, p.883-91. 2008.

Marchi-Salvador, D. P., Fernandes, C. A., Silveira, L. B., Soares, A. M. e Fontes, M. R. Crystal structure of a phospholipase A(2) homolog complexed with p-bromophenacyl bromide reveals important structural changes associated with the inhibition of myotoxic activity. **Biochim Biophys Acta**, v.1794, n.11, Nov, p.1583-90. 2009.

Marcussi, S., Sant'ana, C. D., Oliveira, C. Z., Rueda, A. Q., Menaldo, D. L., Belebani, R. O., Stabeli, R. G., Giglio, J. R., Fontes, M. R. e Soares, A. M. Snake venom phospholipase A2 inhibitors: medicinal chemistry and therapeutic potential. **Curr Top Med Chem**, v.7, n.8, p.743-56. 2007.

Martz, W. Plants with a reputation against snakebite. **Toxicon**, v.30, n.10, Oct, p.1131-42. 1992.

Matthews, B. W. Solvent content of protein crystals. **J Mol Biol**, v.33, n.2, Apr 28, p.491-7. 1968.

Mccooy, A. J. Solving structures of protein complexes by molecular replacement with Phaser. **Acta Crystallogr D Biol Crystallogr**, v.63, n.Pt 1, Jan, p.32-41. 2007.

Mebs, D., Kuch, U., Coronas, F. I. V., Batista, C. V. F., Gumprecht, A. e Possani, L. D. Biochemical and biological activities of the venom of the Chinese pitviper *Zhafermia mangshanensis*, with the complete amino acid sequence and phylogenetic analysis of a novel Arg49 phospholipase A(2) myotoxin. **Toxicon**, v.47, n.7, Jun 1, p.797-811. 2006.

Melo, P. A. e Ownby, C. L. Ability of wedelolactone, heparin, and para-bromophenacyl bromide to antagonize the myotoxic effects of two crotaline venoms and their PLA2 myotoxins. **Toxicon**, v.37, n.1, Jan, p.199-215. 1999.

Ministério Da Saúde. **Manual de Diagnóstico e Tratamento de Acidentes por Animais Peçonhentos**. 2a. ed., 2001. 120 p.

Ministério Da Saúde. **Doenças Infecciosas e Parasitárias, Guia de Bolso**. 8a. edição, 2010. p.

Mora, J., Mora, R., Lomonte, B. e Gutierrez, J. M. Effects of *Bothrops asper* snake venom on lymphatic vessels: insights into a hidden aspect of envenomation. **PLoS Negl Trop Dis**, v.2, n.10, p.e318. 2008.

Mors, W. B., Nascimento, M. C., Pereira, B. M. e Pereira, N. A. Plant natural products active against snake bite--the molecular approach. **Phytochemistry**, v.55, n.6, Nov, p.627-42. 2000.

Moura-Da-Silva, A. M., Cardoso, D. F., Tanizaki, M. M. e Mota, I. Neutralization of myotoxic activity of *Bothrops* venoms by antisera to purified myotoxins and to crude venoms. **Toxicon**, v.29, n.12, p.1471-80. 1991.

Murakami, M. T., Arruda, E. Z., Melo, P. A., Martinez, A. B., Calil-Elias, S., Tomaz, M. A., Lomonte, B., Gutierrez, J. M. e Arni, R. K. Inhibition of myotoxic activity of

Bothrops asper myotoxin II by the anti-trypanosomal drug suramin. **Journal of Molecular Biology**, v.350, n.3, Jul 15, p.416-426. 2005.

Murakami, M. T., Kuch, U., Betzel, C., Mebs, D. e Arni, R. K. Crystal structure of a novel myotoxic Arg49 phospholipase A(2) homolog (zhaoermiatoxin) from Zhaoermia mangshanensis snake venom: Insights into Arg49 coordination and the role of Lys122 in the polarization of the C-terminus. **Toxicon**, v.51, n.5, p.723-735. 2008.

Murakami, M. T., Melo, C. C., Angulo, Y., Lomonte, B. e Arni, R. K. Structure of myotoxin II, a catalytically inactive Lys49 phospholipase A(2) homologue from Atropoides nummifer venom. **Acta Crystallographica Section F-Structural Biology and Crystallization Communications**, v.62, p.423-426. 2006.

Murakami, M. T., Vicoti, M. M., Abrego, J. R., Lourenzoni, M. R., Cintra, A. C., Arruda, E. Z., Tomaz, M. A., Melo, P. A. e Arni, R. K. Interfacial surface charge and free accessibility to the PLA2-active site-like region are essential requirements for the activity of Lys49 PLA2 homologues. **Toxicon**, v.49, n.3, Mar 1, p.378-87. 2007.

Murshudov, G. N., Vagin, A. A. e Dodson, E. J. Refinement of macromolecular structures by the maximum-likelihood method. **Acta Crystallogr D Biol Crystallogr**, v.53, n.Pt 3, May 1, p.240-55. 1997.

Nakashima, K., Nobuhisa, I., Deshimaru, M., Nakai, M., Ogawa, T., Shimohigashi, Y., Fukumaki, Y., Hattori, M., Sakaki, Y., Hattori, S. e Et Al. Accelerated evolution in the protein-coding regions is universal in crotalinae snake venom gland phospholipase A2 isozyme genes. **Proc Natl Acad Sci U S A**, v.92, n.12, Jun 6, p.5605-9. 1995.

Nakashima, K., Ogawa, T., Oda, N., Hattori, M., Sakaki, Y., Kihara, H. e Ohno, M. Accelerated evolution of Trimeresurus flavoviridis venom gland phospholipase A2 isozymes. **Proc Natl Acad Sci U S A**, v.90, n.13, Jul 1, p.5964-8. 1993.

Nishioka Sde, A. e Silveira, P. V. A clinical and epidemiologic study of 292 cases of lance-headed viper bite in a Brazilian teaching hospital. **Am J Trop Med Hyg**, v.47, n.6, Dec, p.805-10. 1992.

Nunez, C. E., Angulo, Y. e Lomonte, B. Identification of the myotoxic site of the Lys49 phospholipase A(2) from *Agkistrodon piscivorus piscivorus* snake venom: synthetic C-terminal peptides from Lys49, but not from Asp49 myotoxins, exert membrane-damaging activities. **Toxicon**, v.39, n.10, Oct, p.1587-94. 2001.

Nunez, V., Castro, V., Murillo, R., Ponce-Soto, L. A., Merfort, I. e Lomonte, B. Inhibitory effects of *Piper umbellatum* and *Piper peltatum* extracts towards myotoxic phospholipases A2 from *Bothrops* snake venoms: isolation of 4-nerolidylcatechol as active principle. **Phytochemistry**, v.66, n.9, May, p.1017-25. 2005.

Ogawa, T., Oda, N., Nakashima, K., Sasaki, H., Hattori, M., Sakaki, Y., Kihara, H. e Ohno, M. Unusually high conservation of untranslated sequences in cDNAs for *Trimeresurus flavoviridis* phospholipase A2 isozymes. **Proc Natl Acad Sci U S A**, v.89, n.18, Sep 15, p.8557-61. 1992.

Oliveira, A. K., Paes Leme, A. F., Asega, A. F., Camargo, A. C., Fox, J. W. e Serrano, S. M. New insights into the structural elements involved in the skin haemorrhage induced by snake venom metalloproteinases. **Thromb Haemost**, v.104, n.3, Sep, p.485-97.

Otero, R., Fonnegra, R., Jimenez, S. L., Nunez, V., Evans, N., Alzate, S. P., Garcia, M. E., Saldarriaga, M., Del Valle, G., Osorio, R. G., Diaz, A., Valderrama, R., Duque, A. e Velez, H. N. Snakebites and ethnobotany in the northwest region of Colombia: Part I: traditional use of plants. **J Ethnopharmacol**, v.71, n.3, Aug, p.493-504. 2000.

Otero, R., Gutierrez, J., Beatriz Mesa, M., Duque, E., Rodriguez, O., Luis Arango, J., Gomez, F., Toro, A., Cano, F., Maria Rodriguez, L., Caro, E., Martinez, J., Cornejo, W., Mariano Gomez, L., Luis Uribe, F., Cardenas, S., Nunez, V. e Diaz, A. Complications of *Bothrops*, *Porthidium*, and *Bothriechis* snakebites in Colombia. A clinical and epidemiological study of 39 cases attended in a university hospital. **Toxicon**, v.40, n.8, Aug, p.1107-114. 2002.

Otero, R., Leon, G., Gutierrez, J. M., Rojas, G., Toro, M. F., Barona, J., Rodriguez, V., Diaz, A., Nunez, V., Quintana, J. C., Ayala, S., Mosquera, D., Conrado, L. L., Fernandez, D., Arroyo, Y., Paniagua, C. A., Lopez, M., Ospina, C. E., Alzate, C., Fernandez, J., Meza, J. J., Silva, J. F., Ramirez, P., Fabra, P. E., Ramirez, E., Cordoba, E., Arrieta, A. B., Warrell, D. A. e Theakston, R. D. Efficacy and safety of two whole IgG polyvalent antivenoms, refined by caprylic acid fractionation with or without beta-

propiolactone, in the treatment of *Bothrops asper* bites in Colombia. **Trans R Soc Trop Med Hyg**, v.100, n.12, Dec, p.1173-82. 2006.

Otwinowski, Z. e Minor, W. Processing of X-ray diffraction data collected in oscillation mode. **Macromolecular Crystallography, Pt A**, v.276, p.307-326. 1997.

Pan, H., Liu, X. L., Ou-Yang, L. L., Yang, G. Z., Zhou, Y. C., Li, Z. P. e Wu, X. F. Diversity of cDNAs encoding phospholipase A2 from *Agkistrodon halys pallas* venom, and its expression in *E. coli*. **Toxicon**, v.36, n.8, Aug, p.1155-63. 1998.

Paramo, L., Lomonte, B., Pizarro-Cerda, J., Bengoechea, J. A., Gorvel, J. P. e Moreno, E. Bactericidal activity of Lys49 and Asp49 myotoxic phospholipases A2 from *Bothrops asper* snake venom--synthetic Lys49 myotoxin II-(115-129)-peptide identifies its bactericidal region. **Eur J Biochem**, v.253, n.2, Apr 15, p.452-61. 1998.

Pereira, M. F., Novello, J. C., Cintra, A. C., Giglio, J. R., Landucci, E. T., Oliveira, B. e Marangoni, S. The amino acid sequence of bothropstoxin-II, an Asp-49 myotoxin from *Bothrops jararacussu* (*Jararacucu*) venom with low phospholipase A2 activity. **J Protein Chem**, v.17, n.4, May, p.381-6. 1998.

Pontow, S. E., Kery, V. e Stahl, P. D. Mannose receptor. **Int Rev Cytol**, v.137B, p.221-44. 1992.

Ramos, O. H. e Selistre-De-Araujo, H. S. Snake venom metalloproteases--structure and function of catalytic and disintegrin domains. **Comp Biochem Physiol C Toxicol Pharmacol**, v.142, n.3-4, Mar-Apr, p.328-46. 2006.

Renetseder, R., Brunie, S., Dijkstra, B. W., Drenth, J. e Sigler, P. B. A comparison of the crystal structures of phospholipase A2 from bovine pancreas and *Crotalus atrox* venom. **J Biol Chem**, v.260, n.21, Sep 25, p.11627-34. 1985.

Rigden, D. J., Hwa, L. W., Marangoni, S., Toyama, M. H. e Polikarpov, I. The structure of the D49 phospholipase A2 piratoxin III from *Bothrops pirajai* reveals unprecedented structural displacement of the calcium-binding loop: possible relationship to cooperative

substrate binding. **Acta Crystallogr D Biol Crystallogr**, v.59, n.Pt 2, Feb, p.255-62. 2003.

Rodrigues-Simioni, L., Prado-Franceschi, J., Cintra, A. C., Giglio, J. R., Jiang, M. S. e Fletcher, J. E. No role for enzymatic activity or dantrolene-sensitive Ca²⁺ stores in the muscular effects of bothropstoxin, a Lys49 phospholipase A2 myotoxin. **Toxicon**, v.33, n.11, Nov, p.1479-89. 1995.

Schaloske, R. H. e Dennis, E. A. The phospholipase A2 superfamily and its group numbering system. **Biochim Biophys Acta**, v.1761, n.11, Nov, p.1246-59. 2006.

Scott, D. L., Achari, A., Vidal, J. C. e Sigler, P. B. Crystallographic and biochemical studies of the (inactive) Lys-49 phospholipase A2 from the venom of *Agkistridon piscivorus piscivorus*. **J Biol Chem**, v.267, n.31, Nov 5, p.22645-57. 1992.

Scott, D. L., White, S. P., Otwinowski, Z., Yuan, W., Gelb, M. H. e Sigler, P. B. Interfacial catalysis: the mechanism of phospholipase A2. **Science**, v.250, n.4987, Dec 14, p.1541-6. 1990.

Shimohigashi, Y., Tani, A., Matsumoto, H., Nakashima, K. e Yamaguchi, Y. Lysine-49-phospholipases A2 from *Trimeresurus flavoviridis* venom are membrane-acting enzymes. **J Biochem**, v.118, n.5, Nov, p.1037-44. 1995.

Soares, A. M., Fontes, M. R. M. e Giglio, J. R. Phospholipase A(2) myotoxins from Bothrops snake venoms: Structure-function relationship. **Current Organic Chemistry**, v.8, n.17, p.1677-1690. 2004.

Soares, A. M., Guerra-Sa, R., Borja-Oliveira, C. R., Rodrigues, V. M., Rodrigues-Simioni, L., Rodrigues, V., Fontes, M. R., Lomonte, B., Gutierrez, J. M. e Giglio, J. R. Structural and functional characterization of BnSP-7, a Lys49 myotoxic phospholipase A(2) homologue from *Bothrops neuwiedi pauloensis* venom. **Arch Biochem Biophys**, v.378, n.2, Jun 15, p.201-9. 2000.

Soares, A. M., Oshima-Franco, Y., Vieira, C. A., Leite, G. B., Fletcher, J. E., Jiang, M. S., Cintra, A. C., Giglio, J. R. e Rodrigues-Simioni, L. Mn(2+) ions reduce the enzymatic and pharmacological activities of bothropstoxin-I, a myotoxic Lys49 phospholipase A(2) homologue from Bothrops jararacussu snake venom. **Int J Biochem Cell Biol**, v.34, n.6, Jun, p.668-77. 2002.

Soares, A. M., Ticli, F. K., Marcussi, S., Lourenco, M. V., Januario, A. H., Sampaio, S. V., Giglio, J. R., Lomonte, B. e Pereira, P. S. Medicinal plants with inhibitory properties against snake venoms. **Curr Med Chem**, v.12, n.22, p.2625-41. 2005.

Taylor, M. E., Conary, J. T., Lennartz, M. R., Stahl, P. D. e Drickamer, K. Primary structure of the mannose receptor contains multiple motifs resembling carbohydrate-recognition domains. **J Biol Chem**, v.265, n.21, Jul 25, p.12156-62. 1990.

Theakston, R. D. e Warrell, D. A. Crisis in snake antivenom supply for Africa. **Lancet**, v.356, n.9247, Dec 16, p.2104. 2000.

Theakston, R. D., Warrell, D. A. e Griffiths, E. Report of a WHO workshop on the standardization and control of antivenoms. **Toxicon**, v.41, n.5, Apr, p.541-57. 2003.

Ticli, F. K., Hage, L. I., Cambraia, R. S., Pereira, P. S., Magro, A. J., Fontes, M. R., Stabeli, R. G., Giglio, J. R., Franca, S. C., Soares, A. M. e Sampaio, S. V. Rosmarinic acid, a new snake venom phospholipase A2 inhibitor from *Cordia verbenacea* (Boraginaceae): antiserum action potentiation and molecular interaction. **Toxicon**, v.46, n.3, Sep 1, p.318-27. 2005.

Toyama, M. H., Costa, P. D., Novello, J. C., De Oliveira, B., Giglio, J. R., Da Cruz-Hofling, M. A. e Marangoni, S. Purification and amino acid sequence of MP-III 4R D49 phospholipase A2 from *Bothrops pirajai* snake venom, a toxin with moderate PLA2 and anticoagulant activities and high myotoxic activity. **J Protein Chem**, v.18, n.3, Apr, p.371-8. 1999.

Toyama, M. H., Soares, A. M., Vieira, C. A., Novello, J. C., Oliveira, B., Giglio, J. R. e Marangoni, S. Amino acid sequence of piratoxin-I, a myotoxin from *Bothrops pirajai* snake venom, and its biological activity after alkylation with p-bromophenacyl bromide. **Journal of Protein Chemistry**, v.17, n.7, Oct, p.713-718. 1998.

Trento, E. P., Garcia, O. S., Rucavado, A., Franca, S. C., Batalini, C., Arantes, E. C., Giglio, J. R. e Soares, A. M. Inhibitory properties of the anti-bothropic complex from *Didelphis albiventris* serum on toxic and pharmacological actions of metalloproteases and myotoxins from *Bothrops asper* venom. **Biochem Pharmacol**, v.62, n.11, Dec 1, p.1521-9. 2001.

Vale, L. H., Mendes, M. M., Hamaguchi, A., Soares, A. M., Rodrigues, V. M. e Homs-Brandeburgo, M. I. Neutralization of pharmacological and toxic activities of bothrops snake venoms by *Schizolobium parahyba* (Fabaceae) aqueous extract and its fractions. **Basic Clin Pharmacol Toxicol**, v.103, n.1, Jul, p.104-7. 2008.

Van Deenen, L. L. M. e De Haas, G. H. The Substrate Specificity of Phospholipase A2. **Biochim Biophys Acta**, v.70, Oct 22, p.538-53. 1963.

Veronese, E. L., Esmeraldino, L. E., Trombone, A. P., Santana, A. E., Bechara, G. H., Kettelhut, I., Cintra, A. C., Giglio, J. R. e Sampaio, S. V. Inhibition of the myotoxic activity of *Bothrops jararacussu* venom and its two major myotoxins, BthTX-I and BthTX-II, by the aqueous extract of *Tabernaemontana catharinensis* A. DC. (Apocynaceae). **Phytomedicine**, v.12, n.1-2, Jan, p.123-30. 2005.

Wallnoefer, H. G., Lingott, T., Gutierrez, J. M., Merfort, I. e Liedl, K. R. Backbone flexibility controls the activity and specificity of a protein-protein interface: specificity in snake venom metalloproteases. **J Am Chem Soc**, v.132, n.30, Aug 4, p.10330-7.

Wang, X. Q., Yang, J., Gui, L. L., Lin, Z. J., Chen, Y. C. e Zhou, Y. C. Crystal structure of an acidic phospholipase A2 from the venom of *Agkistrodon halys pallas* at 2.0 Å resolution. **J Mol Biol**, v.255, n.5, Feb 9, p.669-76. 1996.

Ward, R. J., Alves, A. R., Ruggiero Neto, J., Arni, R. K. e Casari, G. A SequenceSpace analysis of Lys49 phospholipases A2: clues towards identification of residues involved in a novel mechanism of membrane damage and in myotoxicity. **Protein Eng**, v.11, n.4, Apr, p.285-94. 1998.

Ward, R. J., Chioato, L., De Oliveira, A. H., Ruller, R. e Sa, J. M. Active-site mutagenesis of a Lys49-phospholipase A2: biological and membrane-disrupting activities in the absence of catalysis. **Biochem J**, v.362, n.Pt 1, Feb 15, p.89-96. 2002.

Ward, R. J., De Azevedo, W. F., Jr. e Arni, R. K. At the interface: crystal structures of phospholipases A2. **Toxicon**, v.36, n.11, Nov, p.1623-33. 1998.

Ward, R. J., Monesi, N., Arni, R. K., Larson, R. E. e Paco-Larson, M. L. Sequence of a cDNA encoding bothropstoxin I, a myotoxin from the venom of *Bothrops jararacussu*. **Gene**, v.156, n.2, Apr 24, p.305-6. 1995.

Warrell, D. A. The global problem of snake bite: Its prevention and treatment. In: **Recent advances in toxinology research.**, P. Gopalakrishnakone e C. K. Tan (Ed.). Singapore: National University of Singapore, 1992. p.121-153.

Warrell, D. A. Clinical features of envenoming from snake bites. In: **Envenomings and their treatments**, C. Bon e M. Goyffon (Ed.). Lyon: Fondation Marcel Mérieux 1996. p.63-76.

Watanabe, L., Soares, A. M., Ward, R. J., Fontes, M. R. e Arni, R. K. Structural insights for fatty acid binding in a Lys49-phospholipase A2: crystal structure of myotoxin II from *Bothrops moojeni* complexed with stearic acid. **Biochimie**, v.87, n.2, Feb, p.161-7. 2005.

Yamaguchi, Y., Shimohigashi, Y., Chiwata, T., Tani, A., Chijiwa, T., Lomonte, B. e Ohno, M. Lys-49-phospholipases A2 as active enzyme for beta-arachidonoyl phospholipid bilayer membranes. **Biochem Mol Biol Int**, v.43, n.1, Sep, p.19-26. 1997.

Yoshizumi, K., Liu, S. Y., Miyata, T., Saita, S., Ohno, M., Iwanaga, S. e Kihara, H. Purification and amino acid sequence of basic protein I, a lysine-49-phospholipase A2 with low activity, from the venom of *Trimeresurus flavoviridis* (Habu snake). **Toxicon**, v.28, n.1, p.43-54. 1990.

Yu, B. Z., Berg, O. G. e Jain, M. K. The divalent cation is obligatory for the binding of ligands to the catalytic site of secreted phospholipase A2. **Biochemistry**, v.32, n.25, Jun 29, p.6485-92. 1993.

Zhou, X., Tan, T. C., Valiyaveetil, S., Go, M. L., Kini, R. M., Velazquez-Campoy, A. e Sivaraman, J. Structural characterization of myotoxic ecarpholin S from *Echis carinatus* venom. **Biophys J**, v.95, n.7, Oct, p.3366-80. 2008.

APÊNDICE

1. Cristalografia de raios X

O estudo cristalográfico de proteínas nas suas formas nativas e complexadas pode ser bastante interessante pois permite conhecer a estrutura tridimensional destas, as mudanças conformacionais que elas podem assumir dependendo do estado em que se encontram (nativas *X* na presença de ligantes, por exemplo) e analisar regiões/aminoácidos específicos, bem como suas possíveis interações com seus ligantes (inibidores, por exemplo). Isso traz a possibilidade de realização de estudos comparativos entre as diversas proteínas, podendo, até mesmo, esclarecer as bases moleculares de seus mecanismos de ação.

As estruturas de diversas PLA₂s de venenos de serpentes já foram elucidadas e muitas delas se encontram disponíveis no banco de dados de domínio público PDB (*Protein Data Bank*: <http://www.pdb.org/pdb/home/home.do>), tanto na sua forma nativa quanto complexadas com inibidores (Arni *et al.*, 1995; Da Silva Giotto *et al.*, 1998; Lee *et al.*, 2001; Magro *et al.*, 2003; Ambrosio *et al.*, 2005; Murakami *et al.*, 2005; Watanabe *et al.*, 2005; Murakami *et al.*, 2006; Murakami *et al.*, 2007; Dos Santos *et al.*, 2009; Marchi-Salvador *et al.*, 2009; Fernandes *et al.*, 2011).

O fluxograma da Figura 1 mostra, de maneira simplificada, as etapas para resolução de uma estrutura protéica por cristalografia de difração de raios X.

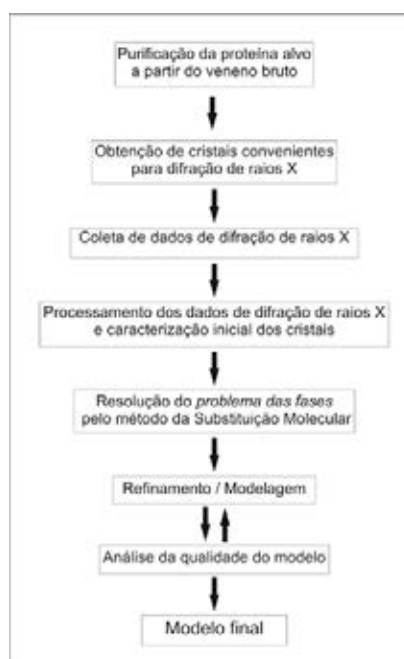


Figura 1. Etapas para resolução de uma estrutura protéica por difração de raios X através de Substituição Molecular.

A seguir, descrevemos alguns dos passos citados na Figura 1 que foram importantes para o desenvolvimento do presente trabalho.

1.1. Purificação da proteína alvo a partir do veneno

No caso das PLA₂s de veneno de serpentes, a purificação é geralmente conduzida a temperatura ambiente, sem perda de sua atividade, em duas etapas: (a) Filtração em Sephadex ou HPLC de fase reversa seguido de (b) uma coluna de troca iônica (Gutierrez e Lomonte, 1995). Outra possibilidade é a utilização de cromatografia de afinidade, explorando o princípio pelo qual as miotoxinas básicas interagem com a heparina (Soares *et al.*, 2000). Para tanto, pode-se utilizar uma coluna de afinidade em heparina-agarose.

1.2. Cristalização e co-cristalização

Para a cristalização / co-cristalização dos complexos de Lys49-PLA₂s com ácido rosmarínico, manganês e cálcio foi utilizado o processo de *salting-out*, que consiste na preparação de uma solução de um agente precipitante (sal, polietilenoglicol – PEG, ou solvente orgânico) e proteína (ou proteína-ligante), com posterior aumento gradativo da concentração do agente precipitante até se alcançar o ponto de supersaturação da proteína ou do complexo proteína-ligante, ocorrendo, então, precipitação ou cristalização; é importante lembrar que, em termos termodinâmicos, o estado de menor energia para o complexo é a forma cristalina.

Um método bastante eficiente para o aumento gradativo da concentração do agente precipitante é a difusão de vapor (McPherson, 2003). Neste método, em um recipiente fechado, são colocadas duas soluções que podem realizar trocas apenas pela fase gasosa. Uma das soluções é formada por um agente precipitante com alta concentração e a outra, pelo mesmo agente mais a proteína (e o ligante, quando houver). Como o volume do agente precipitante depositado no poço (sistema fechado) é muito maior que o volume do mesmo na gota, após algum tempo, a concentração final da gota onde está a proteína será igual à concentração da solução de dentro do poço (isso ocorrerá devido à

difusão de vapor provocada pelas diferentes concentrações iniciais entre a gota e a solução do poço).

Para a obtenção de cristais de qualquer proteína as moléculas desta devem ser levadas à supersaturação, estado termodinamicamente instável, podendo resultar em uma fase cristalina ou amorfa, quando as mesmas retornam ao equilíbrio (Figura 2). É importante lembrar que o cristal apresenta ordem em sua estrutura interna e que esse arranjo é periódico. Em condições de supersaturação, o sistema caminha para o estado de equilíbrio, no qual a proteína se encontra entre uma fase sólida e uma fase solúvel. Nestas condições, ligações químicas novas e estáveis são energeticamente favoráveis. A proteína então cristaliza porque sua energia livre diminui com o aumento das interações favoráveis (Mcpherson, 2003).

A supersaturação pode ser obtida pela evaporação lenta do solvente ou pela variação de alguns parâmetros, como pH, força iônica, tipo de íon, temperatura e concentração do solvente orgânico, que podem ser usados para diminuir a solubilidade da proteína, tornando a solução saturada ou supersaturada (Blundell e Johnson, 1976). A solução supersaturada eventualmente dá origem aos núcleos, alguns dos quais crescerão e se tornarão cristais maiores. O processo pode ser dividido em três estágios: nucleação, crescimento e cessação de crescimento (Kobe *et al.*, 1999). A nucleação, onde ocorre formação dos primeiros agregados ordenados, é o processo inicial na obtenção de cristais, os quais representam a fase sólida de uma proteína. Quando o núcleo atinge um tamanho crítico, começa a fase de crescimento. Um cristal pequeno pode crescer pela incorporação de átomos (moléculas) nas suas faces planas em duas ou três dimensões, ou sobre defeitos na superfície do cristal, incorporando moléculas via interações tridimensionais. O mecanismo dependerá da energia das interações entre os constituintes do cristal nas direções consideradas. A morfologia do cristal corresponde diretamente à taxa de crescimento de cada face: faces crescidas lentamente serão maiores e bem desenvolvidas, enquanto as que crescem mais rapidamente tendem a ser menores. A taxa de crescimento é, geralmente, diretamente proporcional à supersaturação da solução e à solubilidade da molécula num dado solvente, sendo também fortemente influenciada pela presença de impurezas, já que a nucleação pode ocorrer sobre as mesmas. O crescimento de um cristal cessa provavelmente quando há acúmulo de defeitos dentro da rede cristalina, impedindo desta forma a continuação do crescimento de suas faces (Mcpherson, 2003).

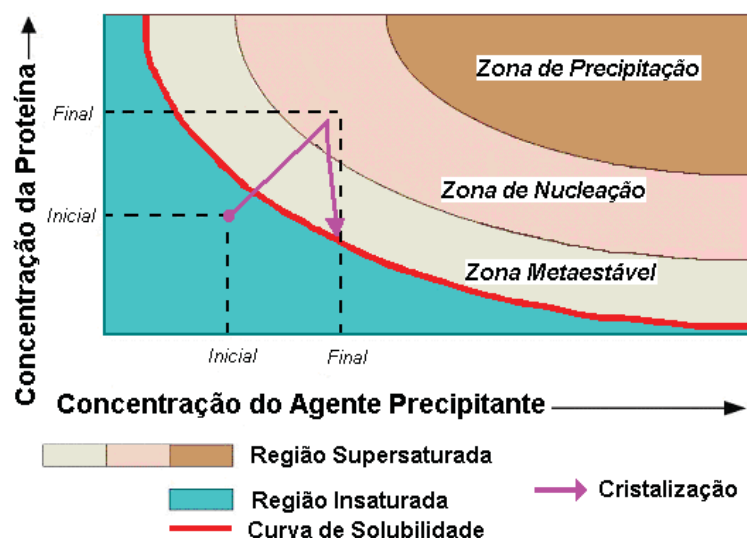


Figura 2. Curva de Solubilidade para proteínas.

Para cristalizar uma proteína, deve-se fazer uma procura das melhores condições de crescimento dos cristais. Isto é feito utilizando-se várias combinações dos fatores já descritos (pH, tampão, concentração / tipo do agente precipitante, temperatura de cristalização, força iônica da solução). Normalmente, o processo é feito sob temperatura constante (geralmente 4°C ou 18°C), variando-se a concentração, tipos de agentes precipitantes e pHs. Para tanto pode-se utilizar o método da matriz esparsa (Jancarik e Kim, 1991) ou alguma variação desta metodologia, no qual é coberto um grande número de condições de cristalização (utilizando-se diferentes sais, precipitantes e pHs) em menos de uma centena de soluções.

Para os testes de co-cristalização dos complexos em estudo foi utilizada a técnica de *hanging drop* e *sitting drop*. O procedimento para utilização da técnica de *sitting drop* se dá da seguinte forma: a solução preparada, contendo o agente precipitante, é inserida em um dos poços da placa utilizada na cristalização (Figura 3a). A solução contendo os ligantes de interesse (no caso o ácido rosmarínico, íons manganês e íons cálcio) é adicionada sobre a gota de solução protéica que já estão depositadas na *microbridge* (Figura 3b); em seguida, um determinado volume da solução do poço é colocado sobre a solução contendo proteína + ligante. A *microbridge* é então inserida no poço, o qual é tampado com uma lamínula de vidro, vedando-se o sistema com uma graxa especial para que as trocas que ocorrerão a partir de então se dêem somente entre os componentes do sistema – com isso elimina-se a interferência do ambiente (Figura 3c).

Para o *hanging drop*, ao invés de colocar a gota e seus componentes sobre a *microbridge*, estes são depositados diretamente na lamínula de vidro. Uma opção durante a montagem do experimento é deixar a solução de proteína mais o ligante durante certo tempo sobre a *microbridge* ou lamínula de vidro, à temperatura controlada, antes da adição de solução do poço para que ocorra uma maior interação entre eles (isso aumenta a chance de interação entre proteína e ligante).

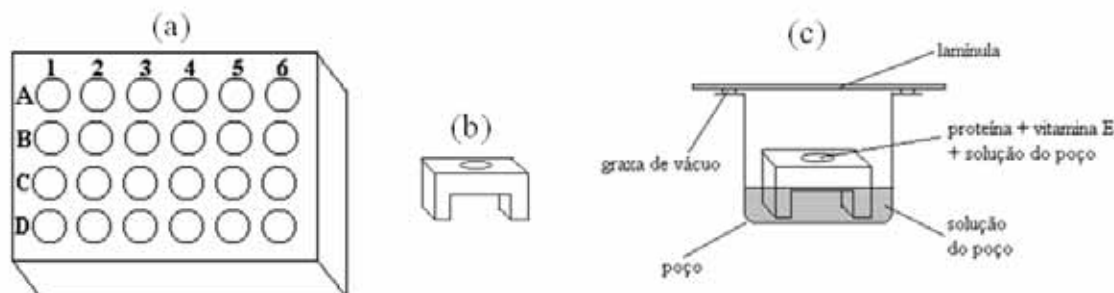


Figura 3. Placa (a) e *microbridge* (b) utilizadas para a montagem dos experimentos de cristalização. Em (c) está representado um dos poços da placa (a), onde o experimento já está montado. É possível observar que a solução contendo proteína realiza trocas somente com a solução-mãe (solução de cristalização) contida no poço, já que o sistema está isolado.

1.3. Coleta de dados de difração de raios X

A coleta de dados de difração de raios X é muito importante, pois constitui a única fonte de dados através da qual podemos obter a estrutura cristalográfica (Blundell e Johnson, 1976). Os dados são obtidos quando um feixe de raios X, após incidir sobre um material cristalino, sofre difração. Estes dados podem ser obtidos através da utilização de uma fonte de raios X convencional, com um ânodo rotatório, ou raios X de um síncrotron (como o existente no Laboratório Nacional de Luz Síncrotron, em Campinas / SP). Nestes equipamentos, o cristal de proteína é colocado em um *loop* cujo diâmetro seja adequado para abrigar o cristal. No *loop* também é necessária a presença da solução-mãe (solução que proporcionou a nucleação e crescimento do cristal), ou uma solução similar, e normalmente é necessária a adição de um crioprotetor (como, por exemplo, o glicerol) para impedir a formação de cristais de gelo ao redor do cristal em estudo, ou para que este não sofra danos irreversíveis e seja perdido. O cristal é,

então, exposto ao feixe de raios X e também a um fluxo de nitrogênio gasoso, à temperatura controlada (normalmente 100 K). Isto permite um aumento no tempo de coleta, pois promove aumento no tempo útil do cristal comparado com coletas sem o resfriamento do mesmo (cristal montado em capilar). Para que seja possível a obtenção de um conjunto de dados adequado, os cristais devem apresentar um tamanho que pode variar entre 0,1 e 1,0 mm. Atualmente, utilizando-se feixes altamente colimados com grande fluxo, já é possível utilizar cristais com dimensões menores que esta. Vale ressaltar que o cristal, no interior do *loop* de nylon, é alinhado ao feixe de raios X de tal maneira que o mesmo fique exposto à radiação de maneira homogênea durante os movimentos oscilatórios a que este será submetido durante a coleta (McCree, 1993). Um determinado número de imagens é coletado e, em posse destas imagens, os dados obtidos podem ser processados utilizando-se programas específicos, como o DENZO/SCALEPACK, que é largamente utilizado pela comunidade cristalográfica (Otwinowski e Minor, 1997). Informações iniciais como grupo espacial, parâmetros de rede do cristal, número de monômeros da proteína na unidade assimétrica cristalina e uma estimativa da porcentagem de solvente no cristal podem ser obtidas a partir do processamento do conjunto de dados.

1.4. Elucidação de estruturas tridimensionais

A determinação da estrutura tridimensional de uma proteína requer vários passos, conforme já demonstrado na Figura 1. Após a coleta de dados de difração de raios X, os dados coletados são processados e então utilizados para dar início à determinação do modelo estrutural. Os programas Mosflm (Leslie, 1992) e HKL2000 (Otwinowski e Minor, 1997) são os mais utilizados atualmente para o processamento dos dados obtidos.

A elucidação da estrutura de uma proteína pode ser feita através do método de Substituição Molecular, utilizando-se programas como o AMoRe (Navaza, 1994), MolRep (Vagin e Teplyakov, 2010) ou Phaser (McCoy, 2007). Porém, uma restrição para o uso deste método é a necessidade de uma alta similaridade seqüencial entre a proteína em estudo e a proteína que servirá de modelo, cuja estrutura deve ser conhecida. O procedimento baseia-se no fato de proteínas com seqüências semelhantes de aminoácidos possuírem enovelamentos similares (McCree, 1993).

Após o processamento dos dados provenientes da coleta de dados de difração de raios X, é gerado um mapa de densidade eletrônica e inicia-se o refinamento da estrutura. O modelo gerado pela substituição molecular é então refinado até a máxima concordância entre dados experimentais e a estereoquímica da molécula, o que pode ser feito utilizando-se programas como o CNS (Brunger *et al.*, 1998), o REFMAC (Murshudov *et al.*, 1997) e o Phenix (Adams *et al.*). Durante as etapas de refinamento, ajustes manuais do modelo à densidade eletrônica são feitos utilizando-se, por exemplo, o programa gráfico Coot (Emsley e Cowtan, 2004). A qualidade estereoquímica do modelo obtido pode ser checada pelo programa Procheck (Laskowski *et al.*, 1993) ou MolProbity (<http://molprobity.biochem.duke.edu/>) (Davis *et al.*, 2007), através de vários parâmetros como o *G-factor* geral e o Gráfico de Ramachandran.

1.5. Espalhamento anômalo e cristalografia de proteínas

Para a reconstrução da imagem molecular (obtenção da densidade eletrônica proteica) a partir dos dados de cristalografia de raios X, a intensidade e a fase de cada uma das reflexões medidas durante a coleta de dados deve ser conhecida. A intensidade das reflexões pode ser obtida através do padrão de difração de raios X, e suas respectivas fases podem ser obtidas de diferentes maneiras. Quando há alguma proteína homóloga cuja estrutura tridimensional seja conhecida e esta apresente elevado grau de identidade e similaridade com a proteína que se deseja obter a estrutura, utiliza-se a Substituição Isomorfa (Mcree, 1993). Nesta operação, as fases da proteína utilizada como modelo são usadas como estimativas das “fases iniciais” da proteína cuja estrutura se deseja conhecer. Porém, na inexistência de um molde, podemos utilizar a idéia de incorporar elementos que funcionem como espalhadores anômalos à estrutura protéica.

A utilização de espalhadores anômalos na estrutura cristalina é baseado no conhecimento de que todos os elementos são capazes de absorver energia de comprimentos de onda específicos (Rhodes, 2006). Desta forma, quando se dispõe de linhas de luz cujos comprimentos de onda podem ser alterados (escolhidos dentro de uma faixa, como é o caso da maioria dos síncrotrons), as mesmas podem ser utilizadas levando-se em consideração as bordas de absorção dos diferentes átomos

(http://skuld.bmsc.washington.edu/scatter/AS_periodic.html). Assim, os conjuntos de dados podem ser coletados em condições que maximizam o espalhamento anômalo por um átomo de interesse. Esta propriedade é bastante utilizada, por exemplo, para resolver estruturas de proteínas recombinantes onde suas metioninas são mudadas para selênio-metioninas (Rhodes, 2006), já que é possível selecionar λ específicos para maximizar as informações sobre os átomos de selênio incorporados na estrutura.

A utilização da propriedade acima citada pode ser importante tanto na resolução de estruturas inéditas de macromoléculas quanto para a localização de um determinado átomo que interage com a estrutura protéica. Assim, o uso de espalhamento anômalo para o elemento manganês foi importante para determinar a(s) posição (posições) destes no complexo formado entre a PrTX-I e íons manganês. Embora a estrutura nativa da PrTX-I já seja conhecida, a diferenciação de íons manganês em relação a moléculas de água ou outros íons presentes na condição de cristalização não foi possível somente pela inspeção da densidade eletrônica dos dados coletados no λ geralmente utilizado na linha de luz (no caso da MX-2, em Campinas/SP, o λ aproximado utilizado na linha geralmente de 1,45 Å, correspondente a uma energia aproximada de 8500 eV). Desta forma, a coleta de dados no λ relativo à borda de absorção do manganês (λ utilizado de 1,89226, correspondente a uma energia de aproximadamente 6.539 eV) permitiu o reconhecimento do local ocupado pelo íon em questão na estrutura cristalográfica.

2. Estudo da estrutura quaternária de macromoléculas com a utilização do programa PISA

A determinação da estrutura quaternária que seja representativa da unidade funcional de uma determinada proteína é de fundamental importância. Esta informação nos ajuda a entender, por exemplo, o mecanismo de ação de proteínas, como elas interagem com outras proteínas, receptores ou aceptores (sítios de interação), e também podem servir de base para o desenho racional de fármacos. Assim, se o arranjo oligomérico de uma proteína ou de um complexo for determinado de forma incorreta, isto poderá ter importantes implicações e até mesmo invalidar os estudos que utilizam estas estruturas como base.

Ao se resolver a estrutura de uma proteína por cristalografia de raios X, pode-se observar mais de uma possibilidade para o arranjo entre os diferentes monômeros que compõem sua estrutura quaternária. Desta forma, uma possibilidade para se checar qual o arranjo quaternário com maior probabilidade de ocorrer em solução pode ser feito com o programa PISA (*Protein Interfaces, Surfaces and Assemblies*: http://www.ebi.ac.uk/msd-srv/prot_int/pistart.html) (Krissinel e Henrick, 2007). Este programa faz análises que sugerem a oligomerização e as interfaces de macromoléculas com maior probabilidade de ocorrer em solução. Para tanto, parâmetros físico-químicos subjacentes à formação de complexos macromoleculares e também abordagens teóricas disponíveis para o cálculo da afinidade macromolecular e entropia de complexação são considerados. Assim, este método pode ser usado para detecção automática de arranjos macromoleculares depositados no banco de dados PDB (*Protein Data Bank*) que são resultados de experimentos de cristalografia de raios X na tentativa de recuperar interfaces que apresentam relevância biológica, já que algumas interfaces encontradas nas estruturas cristalográficas são efeito de empacotamento cristalino (e desta forma, biologicamente insignificantes). As estatísticas demonstram que as unidades biológicas são recuperadas a uma taxa de sucesso que vai de 80 a 90% (Krissinel e Henrick, 2007).

3. Referências Bibliográficas

Adams, P. D., Afonine, P. V., Bunkoczi, G., Chen, V. B., Davis, I. W., Echols, N., Headd, J. J., Hung, L. W., Kapral, G. J., Grosse-Kunstleve, R. W., McCoy, A. J., Moriarty, N. W., Oeffner, R., Read, R. J., Richardson, D. C., Richardson, J. S., Terwilliger, T. C. e Zwart, P. H. PHENIX: a comprehensive Python-based system for macromolecular structure solution. **Acta Crystallogr D Biol Crystallogr**, v.66, n.Pt 2, Feb, p.213-21.

Ambrosio, A. L. B., Nonato, M. C., De Araujo, H. S. S., Arni, R., Ward, R. J., Ownby, C. L., De Souza, D. H. F. e Garratt, R. C. A molecular mechanism for Lys(49)-phospholipase A(2) activity based on ligand-induced conformational change. **Journal of Biological Chemistry**, v.280, n.8, p.7326-7335. 2005.

Arni, R. K., Ward, R. J., Gutierrez, J. M. e Tulinsky, A. Structure of a calcium-independent phospholipase-like myotoxic protein from Bothrops asper venom. **Acta Crystallographica Section D-Biological Crystallography**, v.51, p.311-317. 1995.

Blundell, T. L. e Johnson, L. N. **Protein Crystallography**. London: Academic Press: Academic Press. 1976 (Protein Crystallography)

Brunger, A. T., Adams, P. D., Clore, G. M., Delano, W. L., Gros, P., Grosse-Kunstleve, R. W., Jiang, J. S., Kuszewski, J., Nilges, M., Pannu, N. S., Read, R. J., Rice, L. M., Simonson, T. e Warren, G. L. Crystallography & NMR system: A new software suite for macromolecular structure determination. **Acta Crystallographica Section D-Biological Crystallography**, v.54, Sep 1, p.905-921. 1998.

Da Silva Giotto, M. T., Garratt, R. C., Oliva, G., Mascarenhas, Y. P., Giglio, J. R., Cintra, A. C., De Azevedo, W. F., Jr., Arni, R. K. e Ward, R. J. Crystallographic and spectroscopic characterization of a molecular hinge: conformational changes in bothropstoxin I, a dimeric Lys49-phospholipase A2 homologue. **Proteins**, v.30, n.4, Mar 1, p.442-54. 1998.

Davis, I. W., Leaver-Fay, A., Chen, V. B., Block, J. N., Kapral, G. J., Wang, X., Murray, L. W., Arendall, W. B., 3rd, Snoeyink, J., Richardson, J. S. e Richardson, D. C. MolProbity: all-atom contacts and structure validation for proteins and nucleic acids. **Nucleic Acids Res**, v.35, n.Web Server issue, Jul, p.W375-83. 2007.

Dos Santos, J. I., Soares, A. M. e Fontes, M. R. Comparative structural studies on Lys49-phospholipases A(2) from Bothrops genus reveal their myotoxic site. **J Struct Biol**, v.167, n.2, Aug, p.106-16. 2009.

Emsley, P. e Cowtan, K. Coot: model-building tools for molecular graphics. **Acta Crystallogr D Biol Crystallogr**, v.60, n.Pt 12 Pt 1, Dec, p.2126-32. 2004.

Fernandes, C. A., Marchi-Salvador, D. P., Salvador, G. M., Silva, M. C., Costa, T. R., Soares, A. M. e Fontes, M. R. Comparison between apo and complexed structures of bothropstoxin-I reveals the role of Lys122 and Ca(2+)-binding loop region for the catalytically inactive Lys49-PLA(2)s. **J Struct Biol**, Apr 4. 2011.

Gutierrez, J. M. e Lomonte, B. Phospholipase A2 myotoxins from Bothrops snake venoms. **Toxicon**, v.33, n.11, Nov, p.1405-24. 1995.

Jancarik, J. e Kim, S. H. Sparse-Matrix Sampling - a Screening Method for Crystallization of Proteins. **Journal of Applied Crystallography**, v.24, Aug 1, p.409-411. 1991.

Kobe, B., Gleichmann, T., Teh, T., Heierhorst, J. e Kemp, B. E. Crystallization of protein kinases and phosphatases. In: **Protein phosphorylation: a practical approach**, D. G. Hardie (Ed.): Oxford University Press, 1999. p.127-151.

Krissinel, E. e Henrick, K. Inference of macromolecular assemblies from crystalline state. **Journal of Molecular Biology**, v.372, n.3, Sep 21, p.774-797. 2007.

Laskowski, R. A., MacArthur, M. W., Moss, D. S. e Thornton, J. M. Procheck - a Program to Check the Stereochemical Quality of Protein Structures. **Journal of Applied Crystallography**, v.26, Apr 1, p.283-291. 1993.

Lee, W. H., Da Silva Giotto, M. T., Marangoni, S., Toyama, M. H., Polikarpov, I. e Garratt, R. C. Structural basis for low catalytic activity in Lys49 phospholipases A2--a hypothesis: the crystal structure of piratoxin II complexed to fatty acid. **Biochemistry**, v.40, n.1, Jan 9, p.28-36. 2001.

Leslie, A. G. W. Recent changes to the MOSFLM package for processing film and image plate data. **Protein Crystallography**, v.26, n.Joint CCP4 + ESF-EAMCB Newsletter on Protein Crystallography, p.27-33. 1992.

Magro, A. J., Soares, A. M., Giglio, J. R. e Fontes, M. R. Crystal structures of BnSP-7 and BnSP-6, two Lys49-phospholipases A(2): quaternary structure and inhibition mechanism insights. **Biochem Biophys Res Commun**, v.311, n.3, Nov 21, p.713-20. 2003.

Marchi-Salvador, D. P., Fernandes, C. A., Silveira, L. B., Soares, A. M. e Fontes, M. R. Crystal structure of a phospholipase A(2) homolog complexed with p-bromophenacyl bromide reveals important structural changes associated with the inhibition of myotoxic activity. **Biochim Biophys Acta**, v.1794, n.11, Nov, p.1583-90. 2009.

Mccoy, A. J. Solving structures of protein complexes by molecular replacement with Phaser. **Acta Crystallogr D Biol Crystallogr**, v.63, n.Pt 1, Jan, p.32-41. 2007.

Mcperson, A. **Introduction to Macromolecular Cristallography**. Hoboken: Wiley-Liss. 2003. 237 p.

Mcree, D. E. **Practical Protein Crystallography**: Academic Press (San Diego). 1993. 477 p.

Murakami, M. T., Arruda, E. Z., Melo, P. A., Martinez, A. B., Calil-Elias, S., Tomaz, M. A., Lomonte, B., Gutierrez, J. M. e Arni, R. K. Inhibition of myotoxic activity of Bothrops asper myotoxin II by the anti-trypanosomal drug suramin. **Journal of Molecular Biology**, v.350, n.3, Jul 15, p.416-426. 2005.

Murakami, M. T., Melo, C. C., Angulo, Y., Lomonte, B. e Arni, R. K. Structure of myotoxin II, a catalytically inactive Lys49 phospholipase A(2) homologue from *Atropoides nummifer* venom. **Acta Crystallographica Section F-Structural Biology and Crystallization Communications**, v.62, p.423-426. 2006.

Murakami, M. T., Vicoti, M. M., Abrego, J. R., Lourenzoni, M. R., Cintra, A. C., Arruda, E. Z., Tomaz, M. A., Melo, P. A. e Arni, R. K. Interfacial surface charge and free accessibility to the PLA2-active site-like region are essential requirements for the activity of Lys49 PLA2 homologues. **Toxicon**, v.49, n.3, Mar 1, p.378-87. 2007.

Murshudov, G. N., Vagin, A. A. e Dodson, E. J. Refinement of macromolecular structures by the maximum-likelihood method. **Acta Crystallogr D Biol Crystallogr**, v.53, n.Pt 3, May 1, p.240-55. 1997.

Navaza, J. Amore - an Automated Package for Molecular Replacement. **Acta Crystallographica Section A**, v.50, Mar 1, p.157-163. 1994.

Otwinowski, Z. e Minor, W. Processing of X-ray diffraction data collected in oscillation mode. **Macromolecular Crystallography, Pt A**, v.276, p.307-326. 1997.

Rhodes, G. **Crystallography Made Crystal Clear**: Elsevier Science Publisher CO. 2006. 352 p. (A guide for users of macromolecular models)

Soares, A. M., Guerra-Sa, R., Borja-Oliveira, C. R., Rodrigues, V. M., Rodrigues-Simioni, L., Rodrigues, V., Fontes, M. R., Lomonte, B., Gutierrez, J. M. e Giglio, J. R. Structural and functional characterization of BnSP-7, a Lys49 myotoxic phospholipase A(2) homologue from *Bothrops neuwiedi pauloensis* venom. **Arch Biochem Biophys**, v.378, n.2, Jun 15, p.201-9. 2000.

Vagin, A. e Teplyakov, A. Molecular replacement with MOLREP. **Acta Crystallogr D Biol Crystallogr**, v.66, n.Pt 1, Jan, p.22-25. 2010.

Watanabe, L., Soares, A. M., Ward, R. J., Fontes, M. R. e Arni, R. K. Structural insights for fatty acid binding in a Lys49-phospholipase A2: crystal structure of myotoxin II from *Bothrops moojeni* complexed with stearic acid. **Biochimie**, v.87, n.2, Feb, p.161-7. 2005.

ANEXO I

Acta Crystallographica Section F

**Structural Biology
and Crystallization
Communications**

ISSN 1744-3091

Editors: **H. M. Einspahr** and **M. S. Weiss**

Crystallization and preliminary X-ray crystallographic studies of a Lys49-phospholipase A₂ homologue from *Bothrops pirajai* venom complexed with rosmarinic acid

Juliana I. dos Santos, Norival A. Santos-Filho, Andreimar M. Soares and Marcos R. M. Fontes

Acta Cryst. (2010). **F66**, 699–701

Copyright © International Union of Crystallography

Author(s) of this paper may load this reprint on their own web site or institutional repository provided that this cover page is retained. Republication of this article or its storage in electronic databases other than as specified above is not permitted without prior permission in writing from the IUCr.

For further information see <http://journals.iucr.org/services/authorrights.html>



Acta Crystallographica Section F: Structural Biology and Crystallization Communications is a rapid all-electronic journal, which provides a home for short communications on the crystallization and structure of biological macromolecules. It includes four categories of publication: protein structure communications; nucleic acid structure communications; structural genomics communications; and crystallization communications. Structures determined through structural genomics initiatives or from iterative studies such as those used in the pharmaceutical industry are particularly welcomed. *Section F* is essential for all those interested in structural biology including molecular biologists, biochemists, crystallization specialists, structural biologists, biophysicists, pharmacologists and other life scientists.

Crystallography Journals **Online** is available from journals.iucr.org

Juliana I. dos Santos,^{a,b}
Norival A. Santos-Filho,^{b,c}
Andreimar M. Soares^{b,c} and
Marcos R. M. Fontes^{a,b*}

^aDepartamento de Física e Biofísica, Instituto de Biociências, UNESP – Universidade Estadual Paulista, Botucatu-SP, Brazil, ^bInstituto Nacional de Ciência e Tecnologia em Toxinas, CNPq, Brazil, and ^cDepartamento de Análises Clínicas, Toxicológicas e Bromatológicas, FCFRP, USP, Ribeirão Preto-SP, Brazil

Correspondence e-mail: fontes@ibb.unesp.br

Received 4 March 2010

Accepted 13 April 2010

Crystallization and preliminary X-ray crystallographic studies of a Lys49-phospholipase A₂ homologue from *Bothrops pirajai* venom complexed with rosmarinic acid

PrTX-I, a noncatalytic and myotoxic Lys49-phospholipase A₂ from *Bothrops pirajai* venom, was crystallized in the presence of the inhibitor rosmarinic acid (RA). This is the active compound in the methanolic extract of *Cordia verbenacea*, a plant that is largely used in Brazilian folk medicine. The crystals diffracted X-rays to 1.8 Å resolution and the structure was solved by molecular-replacement techniques, showing electron density that corresponds to RA molecules at the entrance to the hydrophobic channel. The crystals belong to space group $P2_12_12_1$, indicating conformational changes in the structure after ligand binding: the crystals of all apo Lys49-phospholipase A₂ structures belong to space group $P3_121$, while the crystals of complexed structures belong to space groups $P2_1$ or $P2_12_12_1$.

1. Introduction

Envenomation by snakes belonging to the *Bothrops* genus is economically and socially important in Latin America as it is responsible for more than 85% of all ophidian accidents reported in the area (Ferreira *et al.*, 1992; Ribeiro *et al.*, 1998; de Oliveira, 2009). These envenomations are characterized by prominent local tissue damage arising from myonecrosis, haemorrhage and oedema (Rosenberg, 1990). These drastic local effects are not efficiently neutralized by serum therapy and may cause permanent tissue loss and amputation of the affected limb (Gutierrez & Lomonte, 1995).

Phospholipases A₂ (PLA₂s) are the main components of these venoms and in addition to their catalytic role show a broad spectrum of pharmacological activities such as neurotoxicity, myotoxicity and cardiotoxicity. Some of these activities are correlated with the enzymatic activity, while others are completely independent (Kini & Evans, 1989; Soares & Giglio, 2003). PLA₂s also affect the coagulation cascade, platelet aggregation and the inflammatory response (Kini, 1997; Andriao-Escarso *et al.*, 2002).

PLA₂ homologues with skeletal muscle-damaging activity (myotoxicity) are widely distributed in venomous snakes, with Lys49-PLA₂s being the most studied and best characterized subgroup. The loss of catalytic activity in PLA₂ homologues was initially attributed to the natural substitution D49K, as a lysine in this position impairs Ca²⁺ coordination (Maraganore *et al.*, 1984; Arni & Ward, 1996; Ward *et al.*, 1998), but other peculiarities have subsequently also been demonstrated to be involved in this phenomenon (Ward *et al.*, 2002; Lee *et al.*, 2001; dos Santos, Fernandes *et al.*, 2009). Synthetic peptides and site-directed mutagenesis studies have strongly suggested that the C-terminal region of these proteins contains the sequence that is responsible for the expression of this activity in Lys49-PLA₂s (Chioato *et al.*, 2002, 2007; Lomonte, Angulo & Calderon, 2003; Lomonte, Angulo & Santamaria, 2003; Nunez *et al.*, 2001; Ward *et al.*, 1998, 2002; Cintra-Francischinelli *et al.*, 2010).

In recent years, great efforts have been made with the aim of understanding the mechanism of action of snake-venom myotoxins in order to find efficient inhibitors of these proteins. One of these attempts has focused on the scientific study of plant species that are of general use in folk medicine (Mors *et al.*, 2000; Borges *et al.*, 2000, 2001; Biondo *et al.*, 2003, 2004; Januario *et al.*, 2004; Veronese *et al.*, 2005; Esmeraldino *et al.*, 2005; Oliveira *et al.*, 2005). Tieli and



© 2010 International Union of Crystallography
All rights reserved

coworkers studied a methanolic extract of *Cordia verbenacea* and demonstrated that this extract was able to neutralize paw oedema induced by *B. jararacussu* snake venom and by its main basic Lys49-PLA₂s (Ticli *et al.*, 2005). After the isolation of rosmarinic acid (RA) as the active component of the abovementioned extract, it was shown that RA is able to significantly inhibit the myotoxic effect induced by two basic bothropic PLA₂s (BthTX-I and BthTX-II; Ticli *et al.*, 2005). Electrophoretic analysis showed that the basis of such inhibition could not be attributed to proteolytic degradation of the myotoxic PLA₂s (Ticli *et al.*, 2005), while circular-dichroism studies showed that no significant secondary-structural changes were observed on ligand binding (Ticli *et al.*, 2005).

In this work, we report the crystallization and X-ray diffraction data collection of PrTX-I, a basic myotoxic Lys49-PLA₂ isolated from *B. pirajai* snake venom, complexed with RA. The final crystallographic model of the complex may provide insight into the mechanism(s) that lead to inhibition of the myotoxicity of snake-venom PLA₂s.

2. Materials and methods

2.1. Protein purification and crystallization

PrTX-I was isolated from *B. pirajai* snake venom as described previously (Mancuso *et al.*, 1995), while RA was purchased from Sigma–Aldrich. The lyophilized sample of PrTX-I was dissolved to a concentration of 12 mg ml⁻¹ in Tris–HCl pH 7.5 buffer. The same buffer was used to dissolve the commercial RA to a 10:1 molar ratio of inhibitor:protein. The sparse-matrix method (Jancarik & Kim, 1991) was used to perform initial screening of the crystallization conditions (Crystal Screens I and II, Hampton Research). Crystals were obtained by the sitting-drop vapour-diffusion method (McPherson, 1982), combining 1 µl protein solution, 0.5 µl RA solution and 1 µl reservoir solution, and were equilibrated against 0.5 ml of the same precipitant solution (Fig. 1). After the optimization process, the best crystals were obtained at 291 K in a reservoir solution containing 20% PEG 4000, sodium citrate pH 5.6 and 20% propanol. These crystals measured approximately 0.6 × 0.1 × 0.05 mm after one month.

2.2. X-ray data collection and processing

X-ray diffraction data were collected at a wavelength of 1.427 Å (at 100 K) using a synchrotron-radiation source [the MX2 station at Laboratório Nacional de Luz Síncrotron (LNLS), Campinas, Brazil]

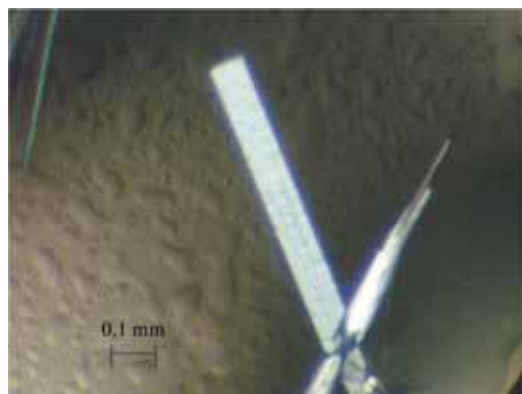


Figure 1
Crystal of PrTX-I complexed with rosmarinic acid.

Table 1

X-ray diffraction data-collection and processing statistics.

Values in parentheses are for the highest resolution shell. Data were processed using the *HKL* suite (Otwinowski & Minor, 1997).

Unit-cell parameters (Å)	$a = 49.4, b = 67.0, c = 85.5$
Space group	$P2_12_12_1$
Resolution (Å)	40.0–1.80 (1.89–1.80)
Unique reflections	25698 (3766)
Completeness (%)	95.0 (98.8)
R_{merge}^\dagger (%)	6.9 (37.3)
Radiation source	Synchrotron (MX2 station, LNLS)
Data-collection temperature (K)	100
Average $I/\sigma(I)$	18.7 (2.6)
Redundancy	4.0 (3.7)
Matthews coefficient V_M (Å ³ Da ⁻¹)	2.6
Molecules in the asymmetric unit	2
Solvent content (%)	53.1

$^\dagger R_{\text{merge}} = \sum_{hkl} \sum_i |I_i(hkl) - \langle I(hkl) \rangle| / \sum_{hkl} \sum_i I_i(hkl)$, where $I_i(hkl)$ is the intensity of an individual measurement of the reflection with Miller indices hkl and $\langle I(hkl) \rangle$ is the mean intensity of that reflection. Calculated for $I > -3\sigma(I)$.

using a MAR CCD imaging-plate detector (MAR Research). A crystal was mounted in a nylon loop and flash-cooled in a stream of nitrogen at 100 K without using any cryoprotectant. The data were processed using the *HKL* program package (Otwinowski & Minor, 1997).

3. Results and discussion

The data-collection statistics are given in Table 1. The crystals belong to the orthorhombic system and the data set was 95.0% complete at 1.8 Å resolution, with an R_{merge} of 6.9%.

Calculations based on the molecular weight of the protein indicated the presence of two molecules in the asymmetric unit. This corresponds to a Matthews coefficient (V_M ; Matthews, 1968) of

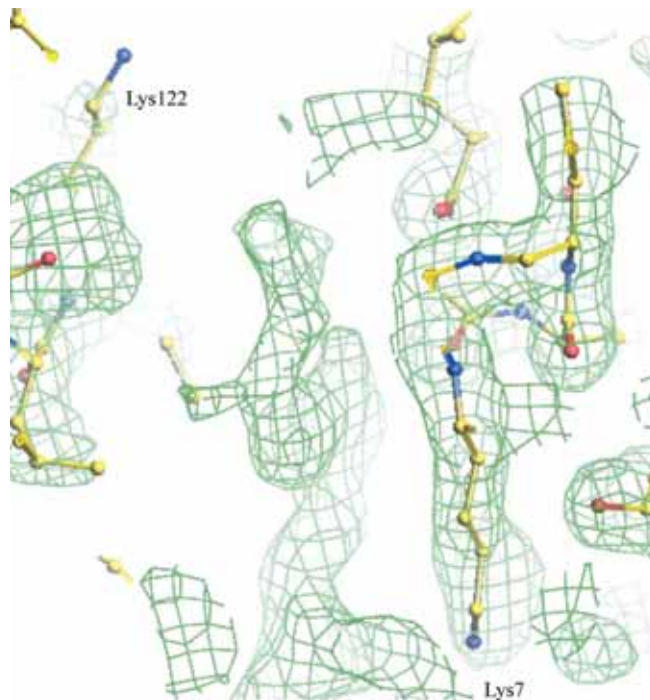


Figure 2
 $2|F_{\text{obs}}| - |F_{\text{calc}}|$ electron-density map contoured at 1.0 standard deviation at the entrance to the hydrophobic channel, where electron density that corresponds to rosmarinic acid was found.

$2.6 \text{ \AA}^3 \text{ Da}^{-1}$ and a calculated solvent content of the crystals of 53.1%. These values are within the expected range for typical protein crystals, assuming a value of $0.74 \text{ cm}^3 \text{ g}^{-1}$ for the partial specific volume of the protein.

The crystal structure was solved by the molecular-replacement technique as implemented in the program *AMoRe* (Navaza, 1994) using the coordinates of native PrTX-I (dos Santos, Soares *et al.*, 2009) as a model and confirmed the presence of a dimer in the asymmetric unit. Electron-density maps that unambiguously correspond to RA molecules were observed at the entrance to the hydrophobic channels (Fig. 2).

A recent review of Lys49-PLA₂ crystallographic structures indicated that the apo structures belong to space group $P3_121$, while the complexed forms belong to space groups $P2_1$ and $P2_12_12_1$ (dos Santos, Soares *et al.*, 2009). The space-group change is a consequence of conformational changes that occur when a ligand is bound to Lys49-PLA₂s (dos Santos, Soares *et al.*, 2009). Since space group $P2_12_12_1$ was observed for the PrTX-I-RA complex, it is possible to suggest that inhibitor binding has led to changes in the quaternary structure of PrTX-I. After refinement of the structure, we will be able to confirm the presence of the inhibitor and the interactions that are established between RA and PrTX-I.

It has been demonstrated that RA is able to potentiate the ability of commercial equine polyvalent antivenom to neutralize the lethal and myotoxic effects of crude *B. jararacussu* venom (Ticli *et al.*, 2005). RA was also capable of neutralizing two isolated Lys49-PLA₂s from *B. jararacussu* snake venom in experimental models (Ticli *et al.*, 2005). Therefore, detailed structural studies of the PrTX-I-RA complex may provide new and important insights into how structural changes in the quaternary structure of Lys49-PLA₂s after ligand binding can lead to toxin inhibition.

The authors gratefully acknowledge financial support from Fundação de Amparo à Pesquisa do Estado de São Paulo (FAPESP), Conselho Nacional de Desenvolvimento Científico e Tecnológico (CNPq) and Laboratório Nacional de Luz Síncrotron (LNLS, Campinas-SP).

References

- Andriao-Escarso, S. H., Soares, A. M., Fontes, M. R., Fuly, A. L., Correa, F. M., Rosa, J. C., Greene, L. J. & Giglio, J. R. (2002). *Biochem. Pharmacol.* **64**, 723–732.
- Arni, R. K. & Ward, R. J. (1996). *Toxicon*, **34**, 827–841.
- Biondo, R., Pereira, A. M. S., Marcussi, S., Pereira, P. S., Franca, S. C. & Soares, A. M. (2003). *Biochimie*, **85**, 1017–1025.
- Biondo, R., Soares, A. M., Bertoni, B. W., Franca, S. C. & Pereira, A. M. S. (2004). *Plant Cell Rep.* **22**, 549–552.
- Borges, M. H., Soares, A. M., Rodrigues, V. M., Andriao-Escarso, S. H., Diniz, H., Hamaguchi, A., Quintero, A., Lizano, S., Gutierrez, J. M., Giglio, J. R. & Homs-Brandeburgo, M. I. (2000). *Comp. Biochem. Physiol. B Biochem. Mol. Biol.* **127**, 21–30.
- Borges, M. H., Soares, A. M., Rodrigues, V. M., Oliveira, F., Fransheschi, A. M., Rucavado, A., Giglio, J. R. & Homs-Brandeburgo, M. I. (2001). *Toxicon*, **39**, 1863–1869.
- Chioato, L., Aragao, E. A., Ferreira, T. L., de Medeiros, A. I., Faccioli, L. H. & Ward, R. J. (2007). *Biochim. Biophys. Acta*, **1768**, 1247–1257.
- Chioato, L., De Oliveira, A. H., Ruller, R., Sa, J. M. & Ward, R. J. (2002). *Biochem. J.* **366**, 971–976.
- Cintra-Francischinelli, M., Pizzo, P., Angulo, Y., Gutierrez, J. M., Montecucco, C. & Lomonte, B. (2010). *Toxicon*, **55**, 590–596.
- dos Santos, J. I., Fernandes, C. A., Magro, A. J. & Fontes, M. R. (2009). *Protein Pept. Lett.* **16**, 887–893.
- dos Santos, J. I., Soares, A. M. & Fontes, M. R. (2009). *J. Struct. Biol.* **167**, 106–116.
- Esmeraldino, L. E., Souza, A. M. & Sampaio, S. V. (2005). *Phytomedicine*, **12**, 570–576.
- Ferreira, M. L., Moura-da-Silva, A. M., Franca, F. O., Cardoso, J. L. & Mota, I. (1992). *Toxicon*, **30**, 1603–1608.
- Gutierrez, J. M. & Lomonte, B. (1995). *Toxicon*, **33**, 1405–1424.
- Jancarik, J. & Kim, S.-H. (1991). *J. Appl. Cryst.* **24**, 409–411.
- Januario, A. H., Santos, S. L., Marcussi, S., Mazzi, M. V., Pietro, R. C., Sato, D. N., Ellena, J., Sampaio, S. V., Franca, S. C. & Soares, A. M. (2004). *Chem. Biol. Interact.* **150**, 243–251.
- Kini, R. M. (1997). *Venom Phospholipase A₂ Enzymes: Structure, Function and Mechanism*, pp. 1–28. Chichester: Wiley.
- Kini, R. M. & Evans, H. J. (1989). *Toxicon*, **27**, 613–635.
- Lee, W. H., da Silva Giotto, M. T., Marangoni, S., Toyama, M. H., Polikarpov, I. & Garratt, R. C. (2001). *Biochemistry*, **40**, 28–36.
- Lomonte, B., Angulo, Y. & Calderon, L. (2003). *Toxicon*, **42**, 885–901.
- Lomonte, B., Angulo, Y. & Santamaria, C. (2003). *Toxicon*, **42**, 307–312.
- Mancuso, L. C., Correa, M. M., Vieira, C. A., Cunha, O. A., Lachat, J. J., de Araujo, H. S., Ownby, C. L. & Giglio, J. R. (1995). *Toxicon*, **33**, 615–626.
- Maraganore, J. M., Merutka, G., Cho, W., Welches, W., Kezdy, F. J. & Heinrichson, R. L. (1984). *J. Biol. Chem.* **259**, 13839–13843.
- Matthews, B. W. (1968). *J. Mol. Biol.* **33**, 491–497.
- McPherson, A. (1982). *Preparation and Analysis of Protein Crystals*. New York: Wiley.
- Mors, W. B., Nascimento, M. C., Pereira, B. M. & Pereira, N. A. (2000). *Phytochemistry*, **55**, 627–642.
- Navaza, J. (1994). *Acta Cryst.* **A50**, 157–163.
- Nunez, C. E., Angulo, Y. & Lomonte, B. (2001). *Toxicon*, **39**, 1587–1594.
- Oliveira, C. Z., Maiorano, V. A., Marcussi, S., Sant'ana, C. D., Januario, A. H., Lourenco, M. V., Sampaio, S. V., Franca, S. C., Pereira, P. S. & Soares, A. M. (2005). *J. Ethnopharmacol.* **98**, 213–216.
- Oliveira, R. C. W. de (2009). *Animais Peçonhentos do Brasil: Biologia, Clínica e Terapêutica dos Envenenamentos*. São Paulo: Sarvier.
- Otwinowski, Z. & Minor, W. (1997). *Methods Enzymol.* **276**, 307–326.
- Ribeiro, L. A., Albuquerque, M. J., de Campos, V. A., Katz, G., Takaoka, N. Y., Lebrao, M. L. & Jorge, M. T. (1998). *Rev. Assoc. Med. Bras.* **44**, 312–318.
- Rosenberg, P. (1990). *Handbook of Toxinology*, edited by W. T. Shyer & D. Mebs, pp. 68–223. New York: Dekker.
- Soares, A. M. & Giglio, J. R. (2003). *Toxicon*, **42**, 855–868.
- Ticli, F. K., Hage, L. I., Cambraia, R. S., Pereira, P. S., Magro, A. J., Fontes, M. R., Stabeli, R. G., Giglio, J. R., Franca, S. C., Soares, A. M. & Sampaio, S. V. (2005). *Toxicon*, **46**, 318–327.
- Veronese, E. L., Esmeraldino, L. E., Trombone, A. P., Santana, A. E., Bechara, G. H., Kettelhut, I., Cintra, A. C., Giglio, J. R. & Sampaio, S. V. (2005). *Phytomedicine*, **12**, 123–130.
- Ward, R. J., Alves, A. R., Ruggiero Neto, J., Arni, R. K. & Casari, G. (1998). *Protein Eng.* **11**, 285–294.
- Ward, R. J., Chioato, L., de Oliveira, A. H., Ruller, R. & Sa, J. M. (2002). *Biochem. J.* **362**, 89–96.

ANEXO II

**Structural and functional studies of a bothropic myotoxin complexed
to rosmarinic acid: new insights into Lys49-PLA₂s' inhibition
mechanisms**

**Juliana I. dos Santos^{1,2}, Fábio F. Cardoso³, Andreimar M. Soares⁴, Maeli dal Pai
Silva⁵, Márcia Gallacci^{3#}, Marcos R. M. Fontes^{1,2,*}**

¹Departamento de Física e Biofísica, Instituto de Biociências, UNESP – Univ Estadual Paulista,
Botucatu/SP – Brazil; ²Instituto Nacional de Ciência e Tecnologia em Toxinas, CNPq – Brazil;

³Departamento de Farmacologia, Instituto de Biociências, UNESP – Univ Estadual Paulista,
Botucatu/SP – Brazil; ⁴Al Sukkar Biotecnologia Industrial, Ribeirão Preto/SP - Brazil;

⁵Departamento de Morfologia, Instituto de Biociências, UNESP – Univ Estadual Paulista,
Botucatu/SP – Brazil.

#Address correspondence to this author at the Departamento de Farmacologia, Instituto de
Biociências, UNESP, C. P. 510, CEP 18618-000, Botucatu-SP, Brazil; Tel: +55.14.38116253;
Fax: +55.14.38153744; E-mail: gallacci@ibb.unesp.br

*Address correspondence to this author at the Departamento de Física e Biofísica, Instituto de
Biociências, UNESP, C. P. 510, CEP 18618-000, Botucatu-SP, Brazil; Tel: +55.14.38156254;
Fax: +55.14.38153744; E-mail: fontes@ibb.unesp.br

Abstract

Envenoming resulting from snakebites is an important public health problem in many tropical and subtropical countries, and has been considered a neglected tropical disease by the World Health Organization. Most severe cases of snakebite envenoming are inflicted by species of the families Elapidae and Viperidae, and lead to a number of systemic and local alterations in the victim. One of the main problems regarding viperidic accidents is prominent local tissue damage whose pathogenesis is complex and involves the combined actions of a variety of venom components. Phospholipases A₂ (PLA₂s) are the most abundant muscle-damaging components of these venoms and are classified into different groups and subgroups. Herein, we report functional and structural studies of PrTX-I, a Lys49-PLA₂ from *Bothrops pirajai* snake venom, and the influence of rosmarinic acid (RA) upon this toxin's activities. RA is a known active component of some plant extracts and has been reported as presenting anti-myotoxic and other properties related to bothropic envenomation. The myotoxic activity of PrTX-I and other Lys49-PLA₂s is well established in the literature and although no *in vivo* neurotoxicity has been observed among these toxins, *in vitro* neuromuscular blockade has been reported for some of these proteins. Our *in-vitro* studies on mice neuromuscular preparations show RA is able to drastically reduce both the muscle damage and the neuromuscular blockade exerted by PrTX-I on these preparations (~80% and ~90%, respectively). These results support the hypothesis that the two effects are closely related and led us to suggest that they are consequences of the Lys49-PLA₂s' muscle membrane-destabilizing activity. Although the C-terminal region of these proteins has been reported in the literature as containing their myotoxic site, we demonstrate by X-ray crystallographic studies that RA interacts with PrTX-I in a different region away from this site. Consequently, a new mode of inhibiting Lys49-PLA₂s is proposed. Comparison of our results with others available in the literature led us to suggest possible ways to inhibit these bothropic snake venom myotoxins in order to improve future serum therapy.

INTRODUCTION

Envenoming resulting from snakebites is an important public health problem in many tropical and subtropical countries [1,2]. Although scarce data on this topic are available worldwide, a recent study estimates that at least 421,000 envenomations and 20,000 deaths due to snakebites occur each year [2]. This problem is particularly important in the rural tropics because the populations of these areas usually have poor access to health systems and, in some cases, antivenom is scarce [1,3]. A large number of victims survive with permanent physical and also psychological sequelae. Young agricultural workers, especially males, are the most affected group, making snakebite envenoming a truly occupational disease [1] now considered a neglected tropical disease by the World Health Organization (WHO) (http://www.who.int/neglected_diseases/diseases/snakebites/en/index.html).

Even though the majority of deaths due to snakebite envenoming occur in South and Southeast Asia and sub-Saharan Africa [2], these accidents are also an important health problem in Latin America [4] where snakebites from the *Bothrops* genus (Viperidae family) are responsible for more than 85% of all reported ophidian accidents[5,6]. One of the main problems regarding these accidents is prominent local tissue damage characterized by swelling, blistering, hemorrhaging and necrosis of the skeletal muscle, and which develops rapidly after the snakebite [1]. Consequently, a delay in access to health facilities frequently results in drastic tissue damage and permanent disability [1,7,8,9,10,11].

The pathogenesis of myonecrosis is complex and involves the combined actions of a variety of venom components, such as myotoxins and metalloproteinases [12,13,14,15,16,17,18]. Nowadays, parenteral administration of animal-derived antivenoms that consist of whole IgG molecules (~150kDa), F(ab')₂ or Fab fragments [19,20,21,22] constitutes the only specific treatment available against snakebite envenoming. But despite the success of this therapy in neutralizing toxins responsible for the systemic effects of snakebite envenomation, this antivenom presents a limited effectiveness in protecting against myonecrosis establishment [23]. Therefore, an advance in the treatment of this local pathology may be achieved by elucidating the snake venom components involved in its genesis and the molecular bases of their mechanism of action.

Phospholipases A₂ (PLA₂s) are the most abundant proteins found in Viperidae snake venoms [24] and, in addition to their well-established ability to hydrolyze lysophospholipids by a calcium-dependent mechanism [25], these proteins can display toxic effects by different mechanisms[26]. A recent phylogenetic study shows that these snake venom PLA₂s can be classified into two groups according to their evolutionary pathway: i) the calcium-dependent catalytically active enzymes, such as Asp49-, Asn49- and Gln49-PLA₂s and ii) the catalytically inactive homologue PLA₂s that exert their effects through a still unsolved calcium-independent

mechanism (Lys49- Arg49-and some Asp49-PLA₂s) [27]. The former group usually includes acidic PLA₂s that act as monomeric toxins whereas the latter includes basic PLA₂s whose action requires a dimeric conformation to produce muscle damage [27].

Despite their lack of enzymatic activity, Lys49-PLA₂ myotoxins play a key role in myonecrosis, given that when they are selectively neutralized, most of the muscle-damaging effect of whole venoms is prevented [28,29,30,31,32]. In addition, several other biological activities have been described for these toxins both *in vivo* and *in vitro* [15]. Although myotoxic Lys49-PLA₂s are devoid of significant neurotoxicity *in vivo* [15], some of them are able to induce an inhibitory neuromuscular activity *in vitro* [33,34,35,36,37,38]. Recently, a review of the all the experimental evidence available on this topic has suggested that both the *in vitro* neuromuscular blockade and the muscle damage induced by Lys49-PLA₂s are consequences of their general muscle membrane-destabilizing activity [38].

Studies involving the interaction of myotoxic Lys49-PLA₂s with potential neutralizing molecules have been one of the main methodologies employed to elucidate the action mechanism and structural determinants of the biological activities of these toxins [35,39,40,41,42]. Furthermore, PLA₂ inhibitors may provide therapeutic molecular models with antiophidian properties and may be applicable as a supplement to the conventional serum therapy [42]. Thus, medicinal plants constitute an important source of bioactive compounds able to antagonize the activity of various crude venoms and purified toxins [40,42,43,44,45,46,47,48,49,50,51,52,53]. In 2005, Ticli and colleagues showed that rosmarinic acid (RA) isolated from *Cordia verbenacea* significantly inhibits the myotoxic effect induced by two main basic Lys49-PLA₂s (BthTX-I and BthTX-II) from *Bothrops jararacussu* snake venom [40]. The authors also demonstrated that RA enhances the effect of commercial equine polyvalent antivenom against isolated myotoxins or the crude venom [40].

In this work we report structural and functional studies concerning the mechanism through which RA neutralizes the *in vitro* inhibitory neuromuscular effect and muscle damage caused by PrTX-I, a Lys49-PLA₂ from *Bothrops pirajai* snake venom [54]. The data obtained show that RA is able to drastically reduce both the muscle damage and the neuromuscular blockade caused by the toxin, supporting the hypothesis that these two effects are mainly consequences of the muscle membrane-destabilizing activity of Lys49-PLA₂s. X-ray crystallographic studies demonstrates that RA interacts with PrTX-I at the entrance of its hydrophobic channel and not in its C-terminus, a region indicated as responsible for the myotoxic effects of Lys49-PLA₂s [15,55,56,57,58,59]. Comparison of our results with others available in the literature led us to suggest possible ways to inhibit bothropic snake venom myotoxins so as to achieve future improvement in serum therapy.

METHODS

Protein purification and Inhibitor Source

PrTX-I was isolated from *Bothrops pirajai* snake venom as previously described [54] and rosmarinic acid (RA) was purchased from Sigma-Aldrich.

Functional Studies

Animals

Adult male mice weighing 25-30g were maintained under a 12h light-dark cycle (lights on at 07:00 AM) in a temperature-controlled environment ($22 \pm 2^\circ\text{C}$) for at least 10 days prior to the experiments. Food and water were freely available. Animal procedures were in accordance with the guidelines prepared by the Committee on Care and Use of Laboratory Animal Resources, National Research Council, USA.

Neuromuscular-blocking activity

Mice were killed by exsanguination after ether anesthesia. Phrenic-diaphragm preparation was removed and mounted vertically in a conventional isolated organ-bath chamber containing 15mL of physiological solution of the following composition (mmol/L): NaCl, 135; KCl, 5; MgCl₂, 1; CaCl₂, 2; NaHCO₃, 15; Na₂HPO₄, 1; glucose, 11. This solution was bubbled with carbogen (95% O₂ and 5% CO₂). The preparation was attached to an isometric force transducer (Grass, FT03) to record the twitch tension. The transducer signal output was amplified and recorded on a computer via a transducer signal conditioner (Gould, 13-6615-50) with an AcquireLab Data Acquisition System (Gould). The resting tension was 5g. Indirect contractions were evoked by supramaximal pulses (0.2Hz, 0.5ms) delivered from an electronic stimulator (Grass-S88K) and applied to the phrenic nerve by means of a suction electrode.

The preparation was stabilized for 45 minutes before the addition of a single concentration of toxin. For inhibition experiments, a fixed amount of PrTX-I dissolved in physiological saline solution (PSS 0.9% NaCl) was mixed with the same quantity of RA, in order to obtain a 1:1 (w/w) toxin/RA ratio. Mixtures were incubated for 30 minutes at $35 \pm 2^\circ\text{C}$. Control experiments were performed in the absence of toxin or in the presence of RA alone. The degree of protection offered by RA after 90 minutes of contact with the preparation was expressed as a percentage of neuromuscular blockade observed in the presence of the mixture of toxin plus RA relative to the blockade seen in the presence of toxin alone.

Muscle-damaging activity

At the end of the functional study, phrenic-diaphragm muscle was removed from the bath and immersed in Bouin's fixative, processed, and embedded in Histo-resin (Kit Histo-resin Leica). Histological transverse sections (5 μ m thick) were cut out in a microtome and stained with hematoxylin and eosin (HE) prior to examination by light microscopy [60]. Muscle samples were also fixed in Karnovsky's fixative for 4h and washed in 1% osmium tetroxide. The tissue was dehydrated in ascending concentrations of acetone and embedded in Epon resin. Sections (1.5 μ m) were stained with uranyl acetate and lead citrate, and examined by electron microscope.

Morphological damage was quantified in HE-stained preparations, using an Imaging Analysis System (Leica, Qwin). The number of fibers with lesions was expressed as a percentage of the total number of cells (muscle damage index), in three non-overlapping non-adjacent areas of each muscle, observed at the same magnification. The degree of neutralization offered by RA was expressed as a percentage of the myonecrosis index in the presence of toxin plus RA relative to that index in the presence of the toxin alone.

Statistical analysis

Results are expressed as mean \pm S.E. Data were analyzed by ANOVA complemented by the Tukey-Kramer test. Values of $P < 0.05$ were considered significant.

Structural Studies

Crystallographic studies

Co-crystallization experiments were performed with PrTX-I at a concentration of 12 mg/mL [61]. Crystals of the complex were obtained by the sitting drop method [62] after thirty minutes of protein/ligand pre-incubation. The best crystals were produced by combining 1 μ l of protein solution, 0.5 μ l of RA solution (35mM) and 1 μ l of reservoir solution and equilibrated against 0.5 ml of the same precipitant solution - 20% PEG4000, sodium citrate pH 5.6 and 20% 2-propanol [61].

X-ray data collection and processing

X-ray diffraction data were collected at a wavelength of 1.427 \AA (at 100 K) using a synchrotron radiation source (MX2 station - Laboratório Nacional de Luz Síncrotron, LNLS, Campinas, Brazil) and a MAR CCD imaging-plate detector (MAR Research). A crystal was mounted in a nylon loop and flash-cooled in a stream of nitrogen at 100 K using no cryoprotectant [61]. Data were processed using the HKL program package [63].

Structure determination and refinement

The crystal structures were solved by the Molecular Replacement Method using the program Phaser [64] and the coordinates of PrTX-I complexed with α -tocopherol [65] as a model. The model was improved, as judged by the free R-factor [66], through rounds of crystallographic refinement using the REFMAC program [67]. Manual rebuilding was performed with the COOT program [68]. The quality of the model was checked by the program Procheck [69].

Ligand design

The program Avogadro v.1.0.0 [70] (<http://avogadro.openmolecules.net/>) was used to design the RA molecule (3-(3,4-dihydroxyphenyl)-2-[(E)-3-(3,4-dihydroxyphenyl)prop-2-enyl]oxypropanoic acid) and improve its overall structure by an energy minimization process based on the MMFF94 force field [71]. Geometric optimization was performed with a steepest-descent algorithm (500 steps with a 10^{-7} convergence criteria).

RESULTS

Neuromuscular blocking activity

PrTX-I (1 μ M) induced a time-dependent blockade of indirectly evoked twitches in phrenic-diaphragm preparations. After 90 minutes, the twitch amplitudes were reduced to 4.5% \pm 2.9% (Figure 1). The mean time required to reduce the twitch amplitudes by 50% ($t_{1/2}$) was 31.9 \pm 3.2 minutes. The neuromuscular blockade induced by PrTX-I was not reversed when preparations were washed for 30 minutes with toxin-free physiological solution (data not shown). RA significantly prevented the neuromuscular blockade induced by PrTX-I when both were pre-incubated, but alone the RA did not affect the twitches (Figure 1).

Muscle-damaging activity

Light microscopy showed that a majority of both control (Figure 2a) and RA-exposed (Figure 2b) diaphragm muscle fibers presented normal appearance. Fibers were clearly delimited by a thin layer of connective tissue (the endomysium) and presented a polygonal shape, acidophilic sarcoplasm and peripheral nuclei (Figure 2a, b). Few fibers from the control (0.6 \pm 0.1%) and RA-treated muscles (0.9 \pm 0.1%) were injured (Figure 3).

After 90 minutes of contact with PrTX-I, diaphragm muscle presented fibers with different degrees of damage. The most common features were round fibers and edema in endomysium connective tissue that was characterized by larger spaces between fibers. Many fibers presented cytoplasm areas devoid of myofibrils, some with a central nucleus (Figure 2c). The muscle damage index was $35.1 \pm 0.7\%$ (Figure 3). Ultra-structural analysis revealed muscle fibers with the loss of myofilaments, leaving sarcoplasmic spaces apparently devoid of myofibrils. Mitochondria showed swelling with reduced or ruptured cristae (Figure 4d).

On the other hand, preparations exposed to PrTX-I pre-incubated with RA showed most fibers with normal aspects (Figures 2d, 4e and 4f); the muscle damage index was $7.9 \pm 0.9\%$ (Figure 3).

Crystallographic studies

Crystals of the complex PrTX-I/RA diffracted X-rays at 1.77 Å resolution [61]. Data collection statistics are shown in Table I. The crystals belong to orthorhombic space group $P2_12_12_1$, with unit-cell parameters $a=49.4$, $b=67.0$ and $c=85.5$ Å. The data set is 95.1 % complete with an $R_{\text{merge}}=6.8$ %. Calculations based on the protein molecular weight [72] indicate the presence of two molecules in the asymmetric unit [61] (Figure 5a).

After molecular replacement and some cycles of manual and automated refinement, an electron density that corresponds to an RA molecule was observed at the entrance of one of the hydrophobic channels of the complex (Figure 5b) [61]. Inspection of the $2|F_{\text{obs}}|-|F_{\text{calc}}|$ electronic density map also showed that one PEG4000 and eight molecules of isopropanol (IOH) interact with the toxin. RA establishes hydrogen bonds with the residues Phe3, Lys7, Leu10, Gln11 and Gly15 of monomer A (Figure 6) and interacts with the residues Leu2, Arg72 and Trp77 of the same monomer through water molecules. The hydrophobic channel of the other monomer is occupied by one PEG4000 molecule. This PEG molecule establishes contacts with Phe3 and Lys7 of monomer B, with the latter being established via a water molecule. Two of the eight isopropanol (IOH) molecules interact with both His48 residues (Nδ1 atoms) of the dimeric structure through the well-known “active-site” water molecule [73]. Asn17:Tyr119 and Tyr119:Tyr119 hydrogen bonds are observed between the protein monomers.

Due to the lack of electron density, side chains of the following residues were mutated to alanine: K36A, K78A, L116A and K129A of monomer A, and K70A, L116A and K127A of monomer B. The side chains of some amino acids were modeled as presenting alternative configurations.

Comparison of the complex PrTX-I/RA with the apo PrTX-I structure [65] (PDB ID 2Q2J) showed that a rearrangement of the monomers induced by the presence of RA occurred

and affected mainly one of their C-termini (overall r.m.s.d. of 1.04 and 0.59 Å for monomers A and B, respectively, and 2.65 and 0.58 Å for their C-termini monomers A and B, respectively) (Figure 7). This rearrangement can be characterized by the establishment of the Tyr119-Tyr119 interchain hydrogen bond and is a feature present in all complexed Lys49-PLA₂s solved up to this date [65,74,75,76].

DISCUSSION

Myonecrosis is an important consequence of envenomation following *Bothrops* snakebites because it is poorly neutralized by conventional serum therapy and, in severe cases, may lead to amputation and disability of the victim [1,2,4,7,9,77]. Therefore, there has been a growing interest in the study of venom components involved in the genesis of myonecrosis, their mode of action and the structural bases underlying their biological activities. Several of these investigations have been focused on the myotoxic Lys49-PLA₂ homologues that are widely found in Viperidae snake venoms [15,78,79]. One of the possible experimental strategies used for the study of these myotoxins is based on the evaluation of the functional and structural consequences of their interaction with potential neutralizing agents. Therefore, in this work we investigated the ability of rosmarinic acid (RA) to neutralize the muscle-damaging and the neuromuscular-blocking activities of PrTX-I, a Lys49-PLA₂ from *Bothrops pirajai* snake venom. Additionally, the complex PrTX-I/RA was co-crystallized in order to clarify the structural sites involved in the toxic effects presented by this Lys49-PLA₂.

The present data show that RA significantly reduces (up to 90%) the blockade of indirectly evoked contractions induced by PrTX-I and inhibits, by about 80%, the muscle damage caused by this toxin in isolated phrenic-diaphragm preparations. The ability of PrTX-I and several other Lys49-PLA₂s to block neuromuscular transmission in isolated preparations has been previously described [33,34,35,36,37,38]. However, interpreting this finding has been a challenging task since these myotoxins are devoid of significant neurotoxicity *in vivo* [15]. Nevertheless, a recent review of all the available experimental evidence led to the hypothesis that both the *in vitro* inhibitory neuromuscular effect and the muscle damage promoted by Lys49-PLA₂s result from their ability to destabilize muscle cell membranes [38]. The first consequence of the muscle membrane destabilization is the collapse of the ionic gradient which leads to cell depolarization, probably due to the re-equilibration of Na⁺ and K⁺ ions [80]. In fact, initial contractures and reduction of the resting membrane potential, which indicate membrane cell depolarization, are characteristics of the *in vitro* neuromuscular blockade induced by Lys49-PLA₂s in frog, chick or mouse preparations [33,80,81]. Thus, it has been suggested that the persistent cell depolarization induced by Lys49-PLA₂s creates areas of membrane inexcitability

due to inactivation of voltage-dependent Na⁺-channels, thus impairing the generation of the action potential along the muscle fibers [80]. The neuromuscular transmission is highly susceptible to this depolarizing blockade because it depends on the electrical excitability of a restricted membrane area surrounding the endplate region, known as perijunctional zone [38]. Moreover, the disruption of the muscle fiber membranes induced by Lys49-PLA₂ homologues also promotes an increase in the concentration of the cytosolic calcium that initiates a complex series of degenerative effects on muscle fibers [38,82]. The fact that RA considerably reduces both the paralysis and the muscle damage caused by PrTX-I confirms the hypothesis that these effects are closely related.

Rosmarinic acid is a polyphenolic compound found in various plants of the *Boraginaceae* and *Laminaceae* families [83]. Several biological properties have been described for this compound including its ability to neutralize inflammatory, myotoxic and hemorrhagic activities of both crude snake venoms and their isolated toxins [40,84]. In addition, it has been shown that RA inhibits some enzymes including acetylcholinesterase [85,86]. However, this anticholinesterasic activity occurs within a concentration range that is one to two orders of magnitude higher than that used in our experiments [85,86] and probably does not explain the ability of RA to neutralize PrTX-I-induced neuromuscular blockade. Additionally, the observation that RA alone does not significantly affect the indirectly evoked contractions supports this idea. Electrophoresis and circular dichroism studies exclude the proteolytic degradation of the toxin as a potential mechanism involved in inhibiting of myotoxic and inflammatory activities of Lys49-PLA₂s from *Bothrops jararacussu* venom by RA [40]. In view of the abovementioned characteristics, RA is an apt tool for investigating the structural basis underlying the toxic activities of Lys49-PLA₂s and may even become a potential effective molecule to complement serum therapy.

The muscle membrane-destabilizing activity exerted by Lys49-PLA₂s has long been attributed to the presence of some basic and aromatic residues situated at specific positions of the C-terminal region of these toxins [15,55,56,57,59,87,88,89] (residues 115-129 according to the numbering system adopted by Renetseder and colleagues [90]). Experiments with glycosaminoglycans show that heparins bind to the C-termini of these myotoxins, thus demonstrating a protective effect against muscle damage [91,92]. On the other hand, ligands that bind to other sites of Lys49-PLA₂s have also been described in the literature and are also known by their ability to diminish the myotoxic effects induced by Lys49-PLA₂s [39,93,94,95].

A 2009 review of all apo and complexed structures of Lys49-PLA₂s available in the Protein Data Bank (PDB: <http://www.pdb.org/pdb/home/home.do>) served as the basis for a proposal addressing the residues involved in the muscle membrane-destabilizing activity of these proteins (denominated a “myotoxic site”) and their two-step action mechanism [65].

According to the proposal, the first step of the mechanism is the interaction of the Lys20, Lys115 and Arg118 of these proteins with the phospholipid headgroup region [65]. Afterwards, a quaternary rearrangement takes place that allows long-chain hydrophobic portions of membrane phospholipids to be inserted into the hydrophobic channel of the toxin [65]. Therefore, the hydrophobic channel was demonstrated to be involved in one of the steps required for the action mechanism of Lys49-PLA₂s, thereby justifying its conservancy among proteins that do not present catalytic activity [65,74].

The crystal structure of PrTX-I complexed to RA shows that the inhibitor interacts with the toxin at the entrance of its hydrophobic channel (Figure 5), thus describing for the first time a ligand that interacts with this region of a Lys49-PLA₂. Considering the action mechanism proposed by dos Santos and colleagues [65], this finding demonstrates that the inhibitory effect of RA seems to be the result of a steric hindrance that blocks the access of substrates to the hydrophobic channel, which is an extension of the toxin's "myotoxic site". Interestingly, we can observe in Figure 8 that RA not only occludes the entrance of PrTX-I hydrophobic channel but is also directly connected with the C-terminus of the other monomer of the toxin. This observation suggests that the C-terminal region of one monomer is closely related to the hydrophobic channel of the other and, taken together with the recent action mechanism proposed for the Lys49-PLA₂s [65], shows how the quaternary arrangement of these toxins' monomers contributes to their function (e.g. long-chain hydrophobic portions of membrane phospholipids that get inserted into the hydrophobic channel of one monomer of the toxin were "captured" by the C-termini of the other monomer). Supporting this hypothesis, comparison of PrTX-I/RA with structures of two Lys49-PLA₂s complexed to fatty acids [96,97] (PDB ID 1QLL and 1XXS) demonstrates that RA really seems to impair the binding of fatty acids to the toxin hydrophobic channel by physically blocking its entrance (Figure 8).

The presence of only one RA molecule interacting with the dimeric structure of PrTX-I can be justified by the presence of one PEG4000 molecule in the other hydrophobic channel of the dimeric structure. This fact can be explained by the great number of PEG molecules in the crystallization condition and by the high affinity of the hydrophobic channel of these toxins for hydrophobic molecules.

In conclusion, it was demonstrated that RA interacts with PrTX-I at the entrance of its hydrophobic channel, consequently affecting its membrane destabilizing activity. Nevertheless, the presence of ligands bound outside the well-characterized "myotoxic site" of a Lys49-PLA₂ (e.g. the C-termini) is demonstrated to also affect the toxin's ability to destabilize muscle membranes. Therefore, considering the two-step mechanism by which Lys49-PLA₂s act [65], it is possible to infer different and probably simultaneous ways to inhibit these myotoxins: i) by

inhibition of the “myotoxic site” / the C-terminal region (e.g. heparin [91]), ii) by physical inhibition of the hydrophobic channel (e.g. PEG400 [39]) or by preventing its occupancy (e.g. RA). The combination of all these possibilities may lead to a successful inhibition of bothropic Lys49-PLA₂s myotoxins and may therefore serve as a guide to select compounds for an adjuvant to complement serum therapy.

Atomic coordinates

The RA coordinates were deposited in the Protein Data Bank with identification code 3QNL.

Acknowledgements

This work was supported by FAPESP, INCTTOX, CNPq, and LNLS.

REFERENCES

1. Gutierrez JM, Theakston RD, Warrell DA (2006) Confronting the neglected problem of snake bite envenoming: the need for a global partnership. *PLoS Med* 3: e150.
2. Kasturiratne A, Wickremasinghe AR, de Silva N, Gunawardena NK, Pathmeswaran A, et al. (2008) The global burden of snakebite: a literature analysis and modelling based on regional estimates of envenoming and deaths. *PLoS Med* 5: e218.
3. Theakston RD, Warrell DA (2000) Crisis in snake antivenom supply for Africa. *Lancet* 356: 2104.
4. Gutierrez JM, Lomonte B (1995) Phospholipase A2 myotoxins from Bothrops snake venoms. *Toxicon* 33: 1405-1424.
5. de Oliveira RCW, F.H.; Sifuentes, D.N. (2009) *Epidemiologia dos Acidentes por Animais Peçonhentos. Animais peçonhentos do Brasil: biologia, clínica e terapêutica dos envenenamentos.* São Paulo: Sarvier.
6. Ministério da Saúde (2001) *Manual de Diagnóstico e Tratamento de Acidentes por Animais Peçonhentos.* In: Saúde FNd, editor. 2a. ed. ed: Ministério da Saúde. pp. 120.
7. Nishioka Sde A, Silveira PV (1992) A clinical and epidemiologic study of 292 cases of lance-headed viper bite in a Brazilian teaching hospital. *Am J Trop Med Hyg* 47: 805-810.
8. Cardoso JL, Fan HW, Franca FO, Jorge MT, Leite RP, et al. (1993) Randomized comparative trial of three antivenoms in the treatment of envenoming by lance-headed vipers (*Bothrops jararaca*) in Sao Paulo, Brazil. *Q J Med* 86: 315-325.
9. Otero R, Gutierrez J, Beatriz Mesa M, Duque E, Rodriguez O, et al. (2002) Complications of Bothrops, Porthidium, and Bothriechis snakebites in Colombia. A clinical and epidemiological study of 39 cases attended in a university hospital. *Toxicon* 40: 1107-1114.
10. Fan HW, Cardoso JL (1995) Clinical toxicology os snake bites in South America. In: Meier J, White, J., editor. *Handbook of clinical toxicology of animal venoms and poisons.* Boca Raton (Florida): CRC Press. pp. 667-688.
11. Warrell DA (1996) Clinical features of envenoming from snake bites. In: Bon C, Goyffon M, editors. *Envenomings and their treatments.* Lyon: Fondation Marcel Mérieux pp. 63-76.
12. Rosenberg P (1990) *Handbook of toxinology.* In: Shyer WT, Mebs D, editors. New York: Dekker.
13. Gutierrez JM (2002) Understanding snake venoms: 50 years of research in Latin America. *Rev Biol Trop* 50: 377-394.
14. Soares AM, Fontes MRM, Giglio JR (2004) Phospholipase A(2) myotoxins from Bothrops snake venoms: Structure-function relationship. *Current Organic Chemistry* 8: 1677-1690.
15. Lomonte B, Angulo Y, Calderon L (2003) An overview of lysine-49 phospholipase A2 myotoxins from crotalid snake venoms and their structural determinants of myotoxic action. *Toxicon* 42: 885-901.
16. Moura-da-Silva AM, Laing GD, Paine MJ, Dennison JM, Politi V, et al. (1996) Processing of pro-tumor necrosis factor-alpha by venom metalloproteinases: a hypothesis explaining local tissue damage following snake bite. *Eur J Immunol* 26: 2000-2005.
17. Ramos OH, Selistre-de-Araujo HS (2006) Snake venom metalloproteases--structure and function of catalytic and disintegrin domains. *Comp Biochem Physiol C Toxicol Pharmacol* 142: 328-346.
18. Gutierrez JM, Rucavado A, Escalante T, Diaz C (2005) Hemorrhage induced by snake venom metalloproteinases: biochemical and biophysical mechanisms involved in microvessel damage. *Toxicon* 45: 997-1011.
19. Lalloo DG, Theakston RD (2003) Snake antivenoms. *J Toxicol Clin Toxicol* 41: 277-290; 317-227.
20. Theakston RD, Warrell DA, Griffiths E (2003) Report of a WHO workshop on the standardization and control of antivenoms. *Toxicon* 41: 541-557.
21. Gutierrez JM, Sanz L, Flores-Diaz M, Figueroa L, Madrigal M, et al. Impact of regional variation in *Bothrops asper* snake venom on the design of antivenoms: integrating antivenomics and neutralization approaches. *J Proteome Res* 9: 564-577.
22. Gutierrez JM, Lomonte B, Leon G, Alape-Giron A, Flores-Diaz M, et al. (2009) Snake venomomics and antivenomics: Proteomic tools in the design and control of antivenoms for the treatment of snakebite envenoming. *J Proteomics* 72: 165-182.
23. Warrell DA (1992) The global problem of snake bite: Its prevention and treatment. In: Gopalakrishnakone P, Tan CK, editors. *Recent advances in toxinology research.* Singapore: National University of Singapore. pp. 121-153.

24. Kini RM (2003) Excitement ahead: structure, function and mechanism of snake venom phospholipase A(2) enzymes. *Toxicon* 42: 827-840.
25. Van Deenen LLM, De Haas GH (1963) The Substrate Specificity of Phospholipase A2. *Biochim Biophys Acta* 70: 538-553.
26. Doley R, Kini RM (2009) Protein complexes in snake venom. *Cell Mol Life Sci* 66: 2851-2871.
27. dos Santos JI, Cintra-Francischinelli M, Borges RJ, Fernandes CA, Pizzo P, et al. (2010) Structural, functional, and bioinformatics studies reveal a new snake venom homologue phospholipase A2 class. *Proteins* 79: 61-78.
28. Lomonte B, Gutierrez JM, Moreno E, Cerdas L (1987) Antibody neutralization of a myotoxin from the venom of *Bothrops asper* (terciopelo). *Toxicon* 25: 443-449.
29. Lomonte B, Gutierrez JM, Ramirez M, Diaz C (1992) Neutralization of myotoxic phospholipases A2 from the venom of the snake *Bothrops asper* by monoclonal antibodies. *Toxicon* 30: 239-245.
30. Moura-da-Silva AM, Cardoso DF, Tanizaki MM, Mota I (1991) Neutralization of myotoxic activity of *Bothrops* venoms by antisera to purified myotoxins and to crude venoms. *Toxicon* 29: 1471-1480.
31. Melo PA, Ownby CL (1999) Ability of wedelolactone, heparin, and para-bromophenacyl bromide to antagonize the myotoxic effects of two crotaline venoms and their PLA2 myotoxins. *Toxicon* 37: 199-215.
32. Trento EP, Garcia OS, Rucavado A, Franca SC, Batalini C, et al. (2001) Inhibitory properties of the anti-bothropic complex from *Didelphis albiventris* serum on toxic and pharmacological actions of metalloproteases and myotoxins from *Bothrops asper* venom. *Biochem Pharmacol* 62: 1521-1529.
33. Heluany NF, Homs-Brandeburgo MI, Giglio JR, Prado-Franceschi J, Rodrigues-Simioni L (1992) Effects induced by bothropstoxin, a component from *Bothrops jararacussu* snake venom, on mouse and chick muscle preparations. *Toxicon* 30: 1203-1210.
34. Rodrigues-Simioni L, Prado-Franceschi J, Cintra AC, Giglio JR, Jiang MS, et al. (1995) No role for enzymatic activity or dantrolene-sensitive Ca²⁺ stores in the muscular effects of bothropstoxin, a Lys49 phospholipase A2 myotoxin. *Toxicon* 33: 1479-1489.
35. de Oliveira M, Cavalcante WL, Arruda EZ, Melo PA, Dal-Pai Silva M, et al. (2003) Antagonism of myotoxic and paralyzing activities of bothropstoxin-I by suramin. *Toxicon* 42: 373-379.
36. Cavalcante WL, Silva MD, Gallacci M (2005) Influence of temperature upon paralyzing and myotoxic effects of bothropstoxin-I on mouse neuromuscular preparations. *Chem Biol Interact* 151: 95-100.
37. Cavalcante WLG, Campos TO, Dal Pai-Silva M, Pereira PS, Oliveira CZ, et al. (2007) Neutralization of snake venom phospholipase A(2) toxins by aqueous extract of *Casearia sylvestris* (Flacourtiaceae) in mouse neuromuscular preparation. *Journal of Ethnopharmacology* 112: 490-497.
38. Gallacci M, Cavalcante WL (2010) Understanding the in vitro neuromuscular activity of snake venom Lys49 phospholipase A2 homologues. *Toxicon* 55: 1-11.
39. Murakami MT, Vicoti MM, Abrego JR, Lourenzoni MR, Cintra AC, et al. (2007) Interfacial surface charge and free accessibility to the PLA2-active site-like region are essential requirements for the activity of Lys49 PLA2 homologues. *Toxicon* 49: 378-387.
40. Ticli FK, Hage LI, Cambraia RS, Pereira PS, Magro AJ, et al. (2005) Rosmarinic acid, a new snake venom phospholipase A2 inhibitor from *Cordia verbenacea* (Boraginaceae): antiserum action potentiation and molecular interaction. *Toxicon* 46: 318-327.
41. Lomonte B, Leon G, Angulo Y, Rucavado A, Nunez V (2009) Neutralization of *Bothrops asper* venom by antibodies, natural products and synthetic drugs: contributions to understanding snakebite envenomings and their treatment. *Toxicon* 54: 1012-1028.
42. Marcussi S, Sant'Ana CD, Oliveira CZ, Rueda AQ, Menaldo DL, et al. (2007) Snake venom phospholipase A2 inhibitors: medicinal chemistry and therapeutic potential. *Curr Top Med Chem* 7: 743-756.
43. Otero R, Nunez V, Jimenez SL, Fonnegra R, Osorio RG, et al. (2000) Snakebites and ethnobotany in the northwest region of Colombia: Part II: neutralization of lethal and enzymatic effects of *Bothrops atrox* venom. *J Ethnopharmacol* 71: 505-511.
44. Otero R, Nunez V, Barona J, Fonnegra R, Jimenez SL, et al. (2000) Snakebites and ethnobotany in the northwest region of Colombia. Part III: neutralization of the haemorrhagic effect of *Bothrops atrox* venom. *J Ethnopharmacol* 73: 233-241.
45. Borges MH, Soares AM, Rodrigues VM, Andriao-Escarso SH, Diniz H, et al. (2000) Effects of aqueous extract of *Casearia sylvestris* (Flacourtiaceae) on actions of snake and bee venoms and

- on activity of phospholipases A(2). *Comparative Biochemistry and Physiology B-Biochemistry & Molecular Biology* 127: 21-30.
46. Borges MH, Soares AM, Rodrigues VM, Oliveira F, Fransheschi AM, et al. (2001) Neutralization of proteases from Bothrops snake venoms by the aqueous extract from *Casearia sylvestris* (Flacourtiaceae). *Toxicon* 39: 1863-1869.
 47. Biondo R, Pereira AM, Marcussi S, Pereira PS, Franca SC, et al. (2003) Inhibition of enzymatic and pharmacological activities of some snake venoms and toxins by *Mandevilla velutina* (Apocynaceae) aqueous extract. *Biochimie* 85: 1017-1025.
 48. Biondo R, Soares AM, Bertoni BW, Franca SC, Pereira AM (2004) Direct organogenesis of *Mandevilla illustris* (Vell) Woodson and effects of its aqueous extract on the enzymatic and toxic activities of *Crotalus durissus terrificus* snake venom. *Plant Cell Rep* 22: 549-552.
 49. Januario AH, Santos SL, Marcussi S, Mazzi MV, Pietro RC, et al. (2004) Neo-clerodane diterpenoid, a new metalloprotease snake venom inhibitor from *Baccharis trimera* (Asteraceae): anti-proteolytic and anti-hemorrhagic properties. *Chem Biol Interact* 150: 243-251.
 50. Maiorano VA, Marcussi S, Daher MA, Oliveira CZ, Couto LB, et al. (2005) Antiophidian properties of the aqueous extract of *Mikania glomerata*. *J Ethnopharmacol* 102: 364-370.
 51. Oliveira CZ, Maiorano VA, Marcussi S, Sant'ana CD, Januario AH, et al. (2005) Anticoagulant and antifibrinolytic properties of the aqueous extract from *Bauhinia forficata* against snake venoms. *J Ethnopharmacol* 98: 213-216.
 52. da Silva JO, Coppede JS, Fernandes VC, Sant'ana CD, Ticli FK, et al. (2005) Antihemorrhagic, antinucleolytic and other antiophidian properties of the aqueous extract from *Pentaclethra macroloba*. *J Ethnopharmacol* 100: 145-152.
 53. Soares AM, Ticli FK, Marcussi S, Lourenco MV, Januario AH, et al. (2005) Medicinal plants with inhibitory properties against snake venoms. *Curr Med Chem* 12: 2625-2641.
 54. Mancuso LC, Correa MM, Vieira CA, Cunha OA, Lachat JJ, et al. (1995) Fractionation of *Bothrops pirajai* snake venom: isolation and characterization of piratoxin-I, a new myotoxic protein. *Toxicon* 33: 615-626.
 55. Lomonte B, Angulo Y, Santamaria C (2003) Comparative study of synthetic peptides corresponding to region 115-129 in Lys49 myotoxic phospholipases A2 from snake venoms. *Toxicon* 42: 307-312.
 56. Ward RJ, Alves AR, Ruggiero Neto J, Arni RK, Casari G (1998) A SequenceSpace analysis of Lys49 phospholipases A2: clues towards identification of residues involved in a novel mechanism of membrane damage and in myotoxicity. *Protein Eng* 11: 285-294.
 57. Ward RJ, Chioato L, de Oliveira AH, Ruller R, Sa JM (2002) Active-site mutagenesis of a Lys49-phospholipase A2: biological and membrane-disrupting activities in the absence of catalysis. *Biochem J* 362: 89-96.
 58. Chioato L, Aragao EA, Ferreira TL, de Medeiros AI, Faccioli LH, et al. (2007) Mapping of the structural determinants of artificial and biological membrane damaging activities of a Lys49 phospholipase A(2) by scanning alanine mutagenesis. *Biochimica Et Biophysica Acta-Biomembranes* 1768: 1247-1257.
 59. Ambrosio ALB, Nonato MC, de Araujo HSS, Arni R, Ward RJ, et al. (2005) A molecular mechanism for Lys(49)-phospholipase A(2) activity based on ligand-induced conformational change. *Journal of Biological Chemistry* 280: 7326-7335.
 60. Bancroft JD, Stevens A (1990) *Theory and practice of histological techniques*. Edinburgh: Churchill Livingstone.
 61. dos Santos JI, Santos-Filho NA, Soares AM, Fontes MR (2010) Crystallization and preliminary X-ray crystallographic studies of a Lys49-phospholipase A2 homologue from *Bothrops pirajai* venom complexed with rosmarinic acid. *Acta Crystallogr Sect F Struct Biol Cryst Commun* 66: 699-701.
 62. McPherson A (1999) *Crystallization of Biological Macromolecules*. New York: Cold Spring Harbor Laboratory Press.
 63. Otwinowski Z, Minor W (1997) Processing of X-ray diffraction data collected in oscillation mode. *Macromolecular Crystallography, Pt A* 276: 307-326.
 64. McCoy AJ (2007) Solving structures of protein complexes by molecular replacement with Phaser. *Acta Crystallogr D Biol Crystallogr* 63: 32-41.
 65. dos Santos JI, Soares AM, Fontes MR (2009) Comparative structural studies on Lys49-phospholipases A(2) from *Bothrops* genus reveal their myotoxic site. *J Struct Biol* 167: 106-116.
 66. Brunger AT, Adams PD, Clore GM, DeLano WL, Gros P, et al. (1998) Crystallography & NMR system: A new software suite for macromolecular structure determination. *Acta Crystallographica Section D-Biological Crystallography* 54: 905-921.

67. Murshudov GN, Vagin AA, Dodson EJ (1997) Refinement of macromolecular structures by the maximum-likelihood method. *Acta Crystallogr D Biol Crystallogr* 53: 240-255.
68. Emsley P, Cowtan K (2004) Coot: model-building tools for molecular graphics. *Acta Crystallogr D Biol Crystallogr* 60: 2126-2132.
69. Laskowski RA, MacArthur MW, Moss DS, Thornton JM (1993) Procheck - a Program to Check the Stereochemical Quality of Protein Structures. *Journal of Applied Crystallography* 26: 283-291.
70. Avogadro: an open-sourcemoлекуlar builder and visualization tool. 1.XX. ed.
71. Halgren TA, Nachbar RB (1996) Merck molecular force field. IV. conformational energies and geometries for MMFF94. *Journal of Computational Chemistry* 17: 587-615.
72. Kantardjieff KA, Rupp B (2003) Matthews coefficient probabilities: Improved estimates for unit cell contents of proteins, DNA, and protein-nucleic acid complex crystals. *Protein Sci* 12: 1865-1871.
73. Scott DL, White SP, Otwinowski Z, Yuan W, Gelb MH, et al. (1990) Interfacial catalysis: the mechanism of phospholipase A2. *Science* 250: 1541-1546.
74. dos Santos JI, Fernandes CA, Magro AJ, Fontes MR (2009) The intriguing phospholipases A2 homologues: relevant structural features on myotoxicity and catalytic inactivity. *Protein Pept Lett* 16: 887-893.
75. Marchi-Salvador DP, Fernandes CA, Silveira LB, Soares AM, Fontes MR (2009) Crystal structure of a phospholipase A(2) homolog complexed with p-bromophenacyl bromide reveals important structural changes associated with the inhibition of myotoxic activity. *Biochim Biophys Acta* 1794: 1583-1590.
76. Fernandes CA, Marchi-Salvador DP, Salvador GM, Silva MC, Costa TR, et al. Comparison between apo and complexed structures of bothropstoxin-I reveals the role of Lys122 and Ca(2+)-binding loop region for the catalytically inactive Lys49-PLA(2)s. *J Struct Biol*.
77. Gutierrez JM, Ponce-Soto LA, Marangoni S, Lomonte B (2008) Systemic and local myotoxicity induced by snake venom group II phospholipases A2: comparison between crotoxin, crotoxin B and a Lys49 PLA2 homologue. *Toxicon* 51: 80-92.
78. Lomonte B, Angulo Y, Sasa M, Gutierrez JM (2009) The phospholipase A2 homologues of snake venoms: biological activities and their possible adaptive roles. *Protein Pept Lett* 16: 860-876.
79. Arni RK, Ward RJ, Gutierrez JM, Tulinsky A (1995) Structure of a calcium-independent phospholipase-like myotoxic protein from *Bothrops asper* venom. *Acta Crystallographica Section D-Biological Crystallography* 51: 311-317.
80. Rodrigues-Simioni L, Borgese N, Ceccarelli B (1983) The effects of *Bothrops jararacussu* venom and its components on frog nerve-muscle preparation. *Neuroscience* 10: 475-489.
81. Aragao EA, Randazzo-Moura P, Rostelato-Ferreira S, Rodrigues-Simioni L, Ward RJ (2009) Shared structural determinants for the calcium-independent liposome membrane permeabilization and sarcolemma depolarization in *Bothropstoxin-I*, a LYS49-PLA(2) from the venom of *Bothrops jararacussu*. *Int J Biochem Cell Biol* 41: 2588-2593.
82. Gutierrez JM, Ownby CL (2003) Skeletal muscle degeneration induced by venom phospholipases A2: insights into the mechanisms of local and systemic myotoxicity. *Toxicon* 42: 915-931.
83. Petersen M, Simmonds MS (2003) Rosmarinic acid. *Phytochemistry* 62: 121-125.
84. Aung HT, Furukawa T, Nikai T, Niwa M, Takaya Y (2011) Contribution of cinnamic acid analogues in rosmarinic acid to inhibition of snake venom induced hemorrhage. *Bioorg Med Chem* 19: 2392-2396.
85. Falé PL, Borges C, Amorim Madeira PJ, Ascensão L, Araújo MEM, et al. (2009) Rosmarinic acid, scutellarein 4'-methyl ether 7-O-glucuronide and (16S)-coleon E are the main compounds responsible for the antiacetylcholinesterase and antioxidant activity in herbal tea of *Plectranthus barbatus* ("falso boldo"). *Food Chemistry* 114: 798-805.
86. Orhan I, Aslant S, Kartal M, Sener B, Baser KHC (2008) Inhibitory effect of Turkish *Rosmarinus officinalis* L. on acetylcholinesterase and butyrylcholinesterase enzymes. *Food Chemistry* 108: 663-668.
87. Chioato L, de Oliveira AHC, Ruller R, Sa JM, Ward RJ (2002) Distinct sites for myotoxic and membrane-damaging activities in the C-terminal region of a Lys(49)-phospholipase A(2). *Biochemical Journal* 366: 971-976.
88. Chioato L, Aragao EA, Lopes Ferreira T, Medeiros AI, Faccioli LH, et al. (2007) Mapping of the structural determinants of artificial and biological membrane damaging activities of a Lys49 phospholipase A2 by scanning alanine mutagenesis. *Biochim Biophys Acta* 1768: 1247-1257.
89. Nunez CE, Angulo Y, Lomonte B (2001) Identification of the myotoxic site of the Lys49 phospholipase A(2) from *Agkistrodon piscivorus piscivorus* snake venom: synthetic C-terminal

peptides from Lys49, but not from Asp49 myotoxins, exert membrane-damaging activities. *Toxicon* 39: 1587-1594.

90. Renetseder R, Dijkstra BW, Huizinga K, Kalk KH, Drenth J (1988) Crystal-Structure of Bovine Pancreatic Phospholipase-A2 Covalently Inhibited by Para-Bromo-Phenacyl-Bromide. *Journal of Molecular Biology* 200: 181-188.
91. Lomonte B, Moreno E, Tarkowski A, Hanson LA, Maccarana M (1994) Neutralizing interaction between heparins and myotoxin II, a lysine 49 phospholipase A2 from *Bothrops asper* snake venom. Identification of a heparin-binding and cytolytic toxin region by the use of synthetic peptides and molecular modeling. *J Biol Chem* 269: 29867-29873.
92. Lomonte B, Tarkowski A, Bagge U, Hanson LA (1994) Neutralization of the cytolytic and myotoxic activities of phospholipases A2 from *Bothrops asper* snake venom by glycosaminoglycans of the heparin/heparan sulfate family. *Biochem Pharmacol* 47: 1509-1518.
93. Diaz-Oreiro C, Gutierrez JM (1997) Chemical modification of histidine and lysine residues of myotoxic phospholipases A2 isolated from *Bothrops asper* and *Bothrops godmani* snake venoms: effects on enzymatic and pharmacological properties. *Toxicon* 35: 241-252.
94. Murakami MT, Arruda EZ, Melo PA, Martinez AB, Calil-Elias S, et al. (2005) Inhibition of myotoxic activity of *Bothrops asper* myotoxin II by the anti-trypanosomal drug suramin. *Journal of Molecular Biology* 350: 416-426.
95. Diaz C, Gutierrez JM, Lomonte B, Nunez J (1993) p-Bromophenacyl bromide modification of *Bothrops asper* myotoxin II, a lysine-49 phospholipase A2, affects its pharmacological activities. *Toxicon* 31: 1202-1206.
96. Lee WH, da Silva Giotto MT, Marangoni S, Toyama MH, Polikarpov I, et al. (2001) Structural basis for low catalytic activity in Lys49 phospholipases A2--a hypothesis: the crystal structure of piratoxin II complexed to fatty acid. *Biochemistry* 40: 28-36.
97. Watanabe L, Soares AM, Ward RJ, Fontes MR, Arni RK (2005) Structural insights for fatty acid binding in a Lys49-phospholipase A2: crystal structure of myotoxin II from *Bothrops moojeni* complexed with stearic acid. *Biochimie* 87: 161-167.

Figure Legends

Figure 1. Effects of PrTX-I alone and pre-incubated with RA on indirectly evoked twitches in mouse phrenic-diaphragm preparations

Effects of PrTX-I alone and pre-incubated with RA on indirectly evoked twitches in mouse phrenic-diaphragm preparations. The ordinate represents the % amplitude of twitches relative to the initial amplitude. The abscissa indicates the time after the addition of toxin to the organ bath. The points are the mean \pm S.E. * indicates the point at which differences between PrTX-I and the control become significant.

Figure 2. Light micrographs of mouse diaphragm muscles submitted to hematoxilin and eosin staining

Light micrographs of mouse diaphragm muscles submitted to hematoxilin and eosin staining: Control muscle (a) and muscle exposed to RA (b) show fibers with normal appearance. Observe the polygonal aspect of fibers (F) and endomysium (EN). (c) Muscle exposed to PrTX-I: edema (ED), round fibers (RF) some of which present loss of myofibrils (LM). (d) Muscle exposed to PrTX-I pre-incubated with RA: most fibers are presenting normal appearance.

Figure 3. Effect of RA upon the muscle damage index induced by PrTX-I in mouse diaphragm preparations

Effect of RA upon the muscle damage index induced by PrTX-I in mouse diaphragm preparations: the ordinate represents the % of damaged fibers relative to normal fibers and the abscissa indicates the experimental groups. The bars are expressed as mean \pm S.E.

Figure.4. Electron micrographs of mouse diaphragm muscle

Electron micrographs of mouse diaphragm muscle. Control muscle (a, b) show normal morphology with plasma membrane (PM), myofibrils (M) and mitochondria (MI). Muscle exposed to PrTX-I (c, d) presents fibers with myofibril disorganization (MD), cytoplasm areas devoid of myofibrils (DM) and mitochondrial swelling with reduced or ruptured cristae (MS). Muscle exposed to PrTX-I pre-incubated with RA (e, f) show normal aspect of fibers. Note myofibrils (M) and mitochondria (MI).

Figure 5. Crystallographic model for the complex PrTX-I/RA

Crystallographic model for the complex PrTX-I/RA: (a) dimeric conformation of PrTX-I/RA; (b) surface charge distribution for the PrTX-I/RA crystallographic model shows RA occluding the entrance of PrTX-I hydrophobic channel.

Figure 6. Interactions between RA and PrTX-I atoms

Interactions between RA and PrTX-I atoms. Residues whose contacts are established through water molecules are not shown. Only interactions below 3.7Å are represented. Electron density map for RA molecule was calculated with coefficients $2|F_{\text{obs}}| - |F_{\text{calc}}|$ and contoured at 1.0 standard deviation.

Figure 7. Superposition between the apo form of PrTX-I and PrTX-I/RA

Superposition between the apo form of PrTX-I and PrTX-I/RA: (a) dimeric ribbons represent both dimeric structures; (b) superposition between corresponding monomers of each structure. R.m.s.d. for the whole superposition of the monomers and for the C-terminal region is shown. The higher r.m.s.d. for monomer B is due to changes induced by the ligand in the C-terminal region. Residues 115 to 129 were considered for the C-termini superposition.

Figure 8. Comparative structural studies among PrTX-I/RA complex and two other Lys49-PLA₂s complexed to fatty acids

Comparative structural studies among PrTX-I/RA complex and two other Lys49-PLA₂s complexed to fatty acids: for surface representation, the hydrophobic channel of PrTX-I monomer A is shown in yellow while residues 119-125 of the C-terminus of monomer B are shown in blue. RA is represented by sticks. (a) Dimeric representation of the PrTX-I/RA complex shows RA occluding the entrance of the monomer A hydrophobic channel. Surface representation is used for monomer A and cartoon representation is employed for monomer B. (b) Superposition of PrTX-I/RA complex with the PrTX-II/fatty acid (in light blue) and MjTX-II/stearic acid (in light green) complexes (only monomers A of the dimeric toxins are represented). (c) Surface view of the PrTX-I/RA complex shows that the hydrophobic channel of monomer A is closely related to the C-terminal region of monomer B.

Table

Table I. X-ray data collection and refinement statistics for PrTX-I/RA

	PrTX-I/RA
	a = 49.4
Unit cell (Å)	b = 67.0
	c = 85.5
Space group	P2 ₁ 2 ₁ 2 ₁
Resolution (Å)	40-1.77 (1.86-1.77) ^a
Unique reflections	26992 (3895) ^a
Completeness (%)	95.1 (97.5) ^a
R _{merge} ^b (%)	6.8 (41.2) ^a
Radiation source	Synchrotron (MX2 station, LNLS)
Data collection temperature (K)	100
I/σ(I)	16.5 (2.0) ^a
Matthews coefficient V _M (Å ³ /Dalton)	2.62
Molecules in asymmetric unit	2
Solvent content (%)	53.12
R _{cryst} ^c (%)	16.0
R _{free} ^d (%)	21.7
Mean B-factor (Å ²) ^e	
Overall	37.2
Protein	22.7
RA molecule	44.2
R.m.s. deviations from ideal values ^e	
bond lengths (Å)	0.022
bond angles (°)	2.0

Ramachandran plot^f

residues in most favorable region (%)	89.9
residues in additionally allowed regions (%)	9.1
residues in generously / not allowed regions (%)	1.0/0

Coordinate error (Å)

SIGMAA (cross-validated SIGMAA) ^e	0.07 (0.08)
--	-------------

^a Numbers in parenthesis are for the highest resolution shell.

^b $R_{\text{merge}} = \sum_{hkl} (\sum_i (|I_{hkl,i} - \langle I_{hkl} \rangle|)) / \sum_{hkl,i} \langle I_{hkl} \rangle$, where $I_{hkl,i}$ is the intensity of an individual measurement of the reflection with Miller indices h, k and l, and $\langle I_{hkl} \rangle$ is the mean intensity of that reflection. Calculated for $I > 3\sigma(I)$.

^c $R_{\text{cryst}} = \sum_{hkl} (||\text{Fobs}_{hkl}| - |\text{Fcalc}_{hkl}||) / |\text{Fobs}_{hkl}|$, where $|\text{Fobs}_{hkl}|$ and $|\text{Fcalc}_{hkl}|$ are the observed and calculated structure factor amplitudes.

^d R_{free} is equivalent to R_{cryst} but calculated with reflections (5 %) omitted from the refinement process.

^e Calculated with the program REFMAC [67].

^f Calculated with the program PROCHECK [69].

ANEXO III

Structural, functional, and bioinformatics studies reveal a new snake venom homologue phospholipase A₂ class

Juliana I. dos Santos,^{1#} Mariana Cintra-Francischinelli,^{2#} Rafael J. Borges,¹ Carlos A. H. Fernandes,¹ Paola Pizzo,² Adélia C. O. Cintra,³ Antonio S. K. Braz,¹ Andreimar M. Soares,³ and Marcos R. M. Fontes^{1*}

¹ Departamento de Física e Biofísica, Instituto de Biociências, UNESP – Univ Estadual Paulista, Botucatu-SP and Instituto Nacional de Ciência e Tecnologia em Toxinas, CNPq, Brazil

² Dipartimento di Scienze Biomediche, Università di Padova, Padova, Italy

³ Departamento de Análises Clínicas, Toxicológicas e Bromatológicas, FCFRP, USP, Ribeirão Preto-SP, Brazil

ABSTRACT

Phospholipases A₂ (PLA₂s) are enzymes responsible for membrane disruption through Ca²⁺-dependent hydrolysis of phospholipids. Lys49-PLA₂s are well-characterized homologue PLA₂s that do not show catalytic activity but can exert a pronounced local myotoxic effect. These homologue PLA₂s were first believed to present residual catalytic activity but experiments with a recombinant toxin show they are incapable of catalysis. Herein, we present a new homologue Asp49-PLA₂ (BthTX-II) that is also able to exert muscle damage. This toxin was isolated in 1992 and characterized as presenting very low catalytic activity. Interestingly, this myotoxic homologue Asp49-PLA₂ conserves all the residues responsible for Ca²⁺ coordination and of the catalytic network, features thought to be fundamental for PLA₂ enzymatic activity. Previous crystallographic studies of apo BthTX-II suggested this toxin could be catalytically inactive since a distortion in the calcium binding loop was observed. In this article, we show BthTX-II is not catalytic based on an *in vitro* cell viability assay and time-lapse experiments on C2C12 myotube cell cultures, X-ray crystallography and phylogenetic studies. Cell culture experiments show that BthTX-II is devoid of catalytic activity, as already observed for Lys49-PLA₂s. Crystallographic studies of the complex BthTX-II/Ca²⁺ show that the distortion of the calcium binding loop is still present and impairs ion coordination even though Ca²⁺ are found interacting with other regions of the protein. Phylogenetic studies demonstrate that BthTX-II is more phylogenetically related to Lys49-PLA₂s than to other Asp49-PLA₂s, thus allowing Crotalinae subfamily PLA₂s to be classified into two main branches: a catalytic and a myotoxic one.

Proteins 2011; 79:61–78.
© 2010 Wiley-Liss, Inc.

Key words: phospholipase A₂; myotoxin; X-ray crystallography; phylogenetic analysis; myotube cell culture; calcium imaging.

INTRODUCTION

Phospholipases A₂ (PLA₂s) are small (~14kDa), stable, calcium-dependent, disulfide-rich enzymes that cleave membrane phospholipids at the *sn*-2 position, producing lysophospholipids and free fatty acids.¹ The released fatty acids can function as energy stores, second messengers^{2,3} and precursors of eicosanoids, which are potent mediators of inflammation.^{4,5} On the other hand, lysophospholipids are involved in cell signaling and phospholipid remodeling and are associated with membrane perturbation.^{6,7} PLA₂s are structurally characterized by the conserved residues His48, Asp49, Tyr52, Tyr73, and Asp99 that constitute their catalytic network⁸ (numbering system according to Renetseder *et al.*⁹). As a rule for typical PLA₂s (E.C. 3.1.1.4.), Ca²⁺ is considered an essential cofactor for their enzymatic activity,^{10–12} in which Tyr28, Gly30, Gly32, and Asp49 are the residues usually involved in the ion coordination.^{8,13,14}

These proteins are currently categorized into 15 classes¹⁵ and are abundant and widespread in snake venoms.^{16,17} Additionally, proteins that exhibit a natural amino acid mutation in position 49 and adopt a PLA₂ folding (e.g. Lys49-PLA₂s, Arg49-PLA₂s, Ser49-PLA₂s, Gln49-PLA₂s, and Asn49-PLA₂s) are also found in these venoms and are responsible for additional or other pharmacological properties such as neurotoxic, myotoxic, anticoagulant, bactericidal, hypotensive, and edema-inducing activities.^{18–37}

Additional Supporting Information may be found in the online version of this article.

*The authors Juliana I. dos Santos and Mariana Cintra-Francischinelli contributed equally to this work.

A.S.K.B.'s current address is Univ Federal do ABC, CCNH, Santo André-SP, Brazil

*Correspondence to: M.R.M. Fontes, Departamento de Física e Biofísica, Instituto de Biociências, UNESP – Univ Estadual Paulista, Botucatu-SP and Instituto Nacional de Ciência e Tecnologia em Toxinas, CNPq, Brazil. E-mail: fontes@ibb.unesp.br

Received 18 May 2010; Revised 22 July 2010; Accepted 13 August 2010

Published online 23 August 2010 in Wiley Online Library (wileyonlinelibrary.com).

DOI: 10.1002/prot.22858

Their ability to exhibit such a diverse spectrum of activities is intriguing since PLA₂s share significant sequential and structural similarity and since these activities emerge from a single structural scaffold.⁸

The action mechanism(s) of myotoxins, which include the natural mutants Lys49-PLA₂s, Arg49-PLA₂s, Gln49-PLA₂s, Asn49-PLA₂s, Ser49-PLA₂s, and some Asp49-PLA₂s, are of great scientific interest since they are able to rapidly damage muscle fibers after snake bites and, like other proteins and peptides (e.g. metalloproteases), can provoke permanent tissue loss and disability.^{38–42} Trials to efficiently neutralize these toxins have not yet achieved definitive results up to these days although many studies have been performed in recent years.⁴³

Homologue Lys49-PLA₂s, the largest studied and best characterized subgroup among these proteins, are known to be myotoxic despite their lack of enzymatic activity.^{34,44} This fact was first attributed to the natural amino acid substitution D49K presented by these PLA₂s⁴⁵ but later other peculiarities were also demonstrated to be involved in their loss of the catalytic activity.^{44,46} Synthetic peptides and site-directed mutagenesis studies strongly suggest the C-terminal region of these proteins as being the domain responsible for this activity in Lys49-PLA₂s.^{34,44,47–55} Replacement of Arg and Lys residues by Ala in the region 117–122 of BthTX-I resulted in a significant reduction of myotoxic activity.⁴⁷ Based on these and other studies, Lomonte and colleagues proposed that Lys49-PLA₂ action arises from the interaction of the C-terminal positive residues with membrane anionic phospholipids. Recently, after a review of many crystallographic structures of Lys49-PLA₂s, dos Santos *et al.* concluded that the residues Lys20, Lys115, and Arg118 probably constitute the myotoxic site of bothropic Lys49-PLA₂s.⁵⁶

Other myotoxins, beyond this well-characterized subgroup, require deeper functional and structural studies. One of these subgroups includes the myotoxic Asp49-PLA₂s BthTX-II and PrTX-III, proteins that are able to induce muscle damage but present very low catalytic activity.^{57–60} These toxins seem to be an exception among the classic Asp49-PLA₂s since they present reduced catalytic potency¹⁸ even though they conserve the residues of the catalytic network.^{59–62} BthTX-II, a basic Asp49-PLA₂ toxin from *B. jararacussu*, is also known for its edematogenic and hemolytic effects^{57,58,63} and for its ability to induce platelet aggregation and secretion through multiple signal transduction pathways.⁶⁴ The residues between Thr112 and Pro121 from BthTX-II primary sequence are assumed to be responsible for its myotoxic activity.^{30,59}

The maintenance of the calcium-binding-loop architecture is essential for the catalytic activity of snake venom PLA₂s. Residues Tyr28, Gly30, and Gly32 from this region, together with Asp49, are responsible for Ca²⁺ coordination.^{8,13,14} Recent structural studies on BthTX-

II showed that the calcium binding loop of this protein is distorted when compared to classic Asp49-PLA₂s.⁶¹ Rigden *et al.* had also observed this distortion when the PrTX-III crystallographic structure was solved.⁶² Therefore, it was suggested that these toxins could be catalytically inactive.⁶¹

In this work we demonstrate that BthTX-II presents myotoxic activity but is not catalytic. This finding was achieved by experiments with C2C12 myotube cell culture and is supported by X-ray crystallography and phylogenetic studies. The Viperidae family evolution and the possible relationships between snake venom PLA₂s and some of their members that adopt a PLA₂ folding but do not present enzymatic activity are also discussed.

MATERIAL AND METHODS

BthTX-II purification and PLA₂ activity assay

BthTX-II was isolated from *Bothrops jararacussu* snake venom by gel filtration and ion-exchange chromatography as previously described.⁵⁷ Purity of the toxin was assessed in reduced conditions by polyacrylamide gel electrophoresis in the presence of sodium dodecyl sulphate (SDS-PAGE) with Coomassie Blue staining. PLA₂ activity was measured with a sPLA₂ assay kit (Cayman Chemicals, Ann Arbor, MI), using the 1,2-dithio diheptanoyl phosphatidylcholine analog, which serves as a substrate for most PLA₂s with exception of cytosolic PLA₂s. Upon hydrolysis of the thio-ester bond at the sn-2 position by PLA₂, free thiols were detected using DTNB (5,5-dithio-bis-(2-nitrobenzoic acid)).

Cellular studies

Cell culture

The murine skeletal muscle C2C12 cell line obtained from the American Type Culture Collection (CRL-1772, ATCC) was used as the toxin target. C2C12 cells were maintained at subconfluent levels in growth medium consisting of Dulbecco's modified Eagle medium (DMEM) (Gibco) supplemented with 10% foetal bovine serum (EuroClone). To induce differentiation (5–6 days), cells were grown to 80% confluence and then the medium was replaced with DMEM supplemented with 2% horse serum (Gibco) and changed every 24–48 h. For microscopy, cells were plated on coverslips (24 mm diameter) (10–20 × 10⁴ cells/well) coated overnight with poly-L-lysine (Sigma) and then treated for 2 h with collagen (BD Biosciences).

Calcium measurements

Cells were loaded with fura-2 by incubation with 3 μM fura-2/AM at 37°C for about 30 min in modified

Krebs–Ringer Buffer (see below) containing 0.04% pluronic (Molecular Probes, Eugene, OR). To prevent fura-2 leakage and sequestration, 250 μ M sulfinpyrazone was present throughout the loading procedure and $[\text{Ca}^{2+}]_i$ measurements. The coverslips were washed with a modified Krebs–Ringer Buffer (mKRB, 140mM NaCl, 2.8mM KCl, 2mM MgCl_2 , 1mM CaCl_2 , 10mM HEPES, 11mM glucose pH 7.4), mounted on a thermostated chamber (Medical System, NY) at 37°C, placed on the stage of an inverted microscope (Zeiss, Axiovert 100 TV) equipped for single cell fluorescence measurements and imaging analysis (TILL Photonics, Martinsried, Germany). Where indicated, a Ca^{2+} -free EGTA (200 μ M)-containing medium was used. The sample was alternatively illuminated ($t = 200$ ms) by monochromatic light (at 340 and 380 nm wave lengths), every second for 10 min after toxin exposure, through a 40 \times oil immersion objective (NA = 1.30; Zeiss). The emitted fluorescence was passed through a dichroic beamsplitter (455DRPL), filtered at 505–530 nm (Omega Optical and Chroma Technologies, Brattleboro, VT) and captured by a cooled CCD camera (Imago, TILL Photonics). For presentation, the ratios (F340/F380) of different cells were off-line normalized to the resting value measured within the first minute of the experiment.

Cytotoxicity assay

Differentiated myotubes were grown in 96-well plates and then exposed to toxin for ten or thirty minutes; their viability was then measured with the MTS (3-(4,5-dimethylthiazol-2-yl-5-)-3-carboxymethoxyphenyl-2-(4-sulfonophenyl)-2H-tetrazolium, inner salt) assay. The CellTiter 96 AQueous One Solution Cell Proliferation Assay (Promega) was used and instructions from the manufacturer were followed. Each cytotoxicity test was repeated 3–6 times. The percentage of cell death was expressed as the mean \pm SEM. Student's t -test was used for statistical comparison of the data. A value of $P < 0.05$ was considered to indicate significance.

Crystallographic studies

Crystallization of BthTX-II in the presence of Ca^{2+}

Cocrystallization experiments were performed with lyophilized samples of BthTX-II⁶¹ in the presence of calcium. The protein was dissolved in ultrapure water at a concentration of 12 mg mL⁻¹. A ratio of 30 ions for each protein molecule was considered for cocrystallization experiments. Crystals were obtained by the hanging drop vapor diffusion method⁶⁵ in the same crystallization condition under which the apo BthTX-II was crystallized: 20% (v/v) 2-propanol, 13% (w/v) polyethylene glycol 4000, and 0.05M sodium citrate pH 5.6.⁶¹ Calcium chloride 0.01M was added in the crystallization drop as calcium ions source.

X-ray data collection, processing, structure determination, and refinement

X-ray diffraction data were collected using a wavelength of 1.427 Å at a synchrotron-radiation source (MX2 station - LNLS, Campinas, Brazil). Crystals were mounted in a nylon loop and flash-cooled in a nitrogen stream at 100 K without cryoprotectant. Data were processed using the HKL program package.⁶⁶

The crystals were highly isomorphous with the crystals of apo BthTX-II⁶¹; therefore this structure (PDB code 2OQD) was used as starting model for crystallographic refinement. The model was improved, as judged by the free R-factor,⁶⁷ through rounds of crystallographic refinement using the REFMAC program,⁶⁸ and manual rebuilding was performed with the “Coot” program.⁶⁹ During the refinement 111 water molecules were added to the BthTX-II/ Ca^{2+} model. Due to the lack of electron density, side chains of the following residues were excluded: Arg43, Lys54, Lys69, Glu78, Ile82, Glu86, Lys114, Lys115, Asp122, Lys128, and Lys132 of monomer A; and Arg111 and Lys115 of monomer B.

The insertion of calcium ions in the crystallographic model was carefully analyzed and refined. The candidate regions for calcium placement were found by electron density inspection and using the function “find ligands” of the software Coot⁶⁹ using the difference map ($F_{\text{obs}} - F_{\text{calc}}$) with a signal of at least 3σ . The following prerequisites were used for their maintenance in the structure: (i) occupancy values higher than 0.7 after refinement (CNS program⁷⁰); (ii) I/σ higher than 2.5 in the $2F_{\text{obs}} - F_{\text{calc}}$ map; (iii) preference for donor atoms of nitrogen, sulphur, and specially oxygen; (iv) coordination number and shape of coordination group (including presence of bidentate ligands).^{71–73} Only interactions below 3.6 Å were considered, a value that includes primary and secondary coordination spheres.⁷¹ Additionally, the possibility of water molecules in the same position was also investigated and discarded.

The refinement statistics for the final model are shown in Table I. The quality of the model was checked by the Procheck program.⁷⁴

Comparative structural studies

Molecular comparison between the crystallographic structure of apo BthTX-II⁶¹ (PDB id code 2OQD) and BthTX-II/ Ca^{2+} was performed using the “O” program.⁷⁵ The same program was used to perform comparative analyses between BthTX-II and other Asp-PLA₂s and Lys49-PLA₂s which have X-ray crystallographic structures available in the Protein Data Bank (PDB—<http://www.pdb.org>). For all these purposes, only C α coordinates were considered.

Analyses of the quaternary assemblies and interfacial contacts of the crystallographic models were performed using PISA program⁷⁶ available at the European Bioinformatics Institute server (http://www.ebi.ac.uk/msd-srv/prot_int/pistart.html). All the figures corresponding to

Table 1
X-ray Data Collection and Refinement Statistics for BthTX-II/Ca²⁺

Unit cell (Å)	a = 59.24 b = 100.88 c = 47.17
Space group	C2
Resolution (Å)	50.44–2.10 (2.20–2.10) ^a
Unique reflections	12718 (1625) ^a
Completeness	97.4 (99.4) ^a
R _{merge} ^b (%)	10.4 (51.00) ^a
Radiation source	Synchrotron (LNLS—MX2)
Data collection temperature (K)	100
//σ (I)	10.79 (2.55) ^a
Redundancy	3.7 (3.5) ^a
Molecules in asymmetric unit	2
R _{cryst} ^c (%)	21.7
R _{free} ^d (%)	24.9
Mean B-factor (Å ²) ^e	
Overall	39.7
Protein	40.1
Calcium ions	59.6
Water molecules	55.1
Mean Occupancy—calcium ions	0.90
R.m.s. deviations from ideal values ^e	
Bond lengths (Å)	0.019
Bond angles (°)	1.68
Ramachandran plot ^f	
Residues in most favorable region (%)	89.2
Residues in additionally allowed regions (%)	10.8
Residues in generously/not allowed regions (%)	0

^aNumbers in parenthesis are for the highest resolution shell.

^bR_{merge} = $\sum_{hkl}(\sum_i(|I_{hkl,i}| - \langle I_{hkl} \rangle)) / \sum_{hkl,i}(|I_{hkl,i}|)$, where $I_{hkl,i}$ is the intensity of an individual measurement of the reflection with Miller indices h , k , and l , and $\langle I_{hkl} \rangle$ is the mean intensity of that reflection. Calculated for $I > -3\sigma(I)$.

^cR_{cryst} = $R_{hkl}(|F_{obs,hkl}| - |F_{calc,hkl}|) / |F_{obs,hkl}|$, where $|F_{obs,hkl}|$ and $|F_{calc,hkl}|$ are the observed and calculated structure factor amplitudes.

^dR_{free} is equivalent to R_{cryst} but calculated with reflections (5%) omitted from the refinement process.

^eCalculated with the program CNS¹.

^fCalculated with the program PROCHECK².

oligomeric analyses were generated using the Pymol program.⁷⁷

Dynamic light scattering

The dynamic light scattering (DLS) measurements were performed with lyophilized BthTX-II at 283 K, at a concentration of 3.5 mg mL⁻¹ using the instrument DynaPro TITAN (Wyatt Technology). The protein was prepared with the same buffer used in the crystallization condition (100 mM sodium citrate pH 5.6). Data were measured one hundred times and results were analyzed with Dynamics v.6.10 software.

Phylogenetic studies

Identification of homologous sequences

Homologous sequences were obtained from the NCBI database (<http://www.ncbi.nlm.nih.gov>) using the BLASTP algorithm and the Bothropstoxin I sequence (GI: 265051) from *Bothrops jararacussu* as the query. The

BLOSUM62 matrix was used for scoring alignments, with other algorithm parameters set as default. The minimum e -value presented by the selected sequences was 3.10^{-44} . The selected homologous proteins and their respective database identification codes are shown in Table V.

Sequence alignment and phylogenetic analysis

Alignment of the selected sequences was performed by AMAP program v. 2.0.⁷⁸ The final alignment was used to construct a phylogenetic tree by Bayesian inference utilizing MrBayes v. 3.1.1 software.⁷⁹ Two concurrent MCMC runs of 3,000,000 generations were used using four progressively heated chains, a temperature value of 0.2, tree sampling every 100 generations and a burn-in of 2500 trees. The phylogenetic tree was visualized using the Mesquite program version 2.72.⁸⁰ All the protein sequences used in the phylogenetic analysis and their respective identification codes are shown in Table V.

RESULTS AND DISCUSSION

Characterization of BthTX-II and its effects on C2C12 myotubes

BthTX-II is able to form a dimer in solution as observed in SDS-PAGE and dynamic light scattering experiments. DLS experiments performed with BthTX-II indicated a mean hydrodynamic radius (R_H) of 2.5 nm and a polydispersity of 10.7%. This R_H value corresponds to a molecular weight of ~27 kDa and is, thus, equivalent to a dimer. This finding is in agreement with previous studies^{59,61} and demonstrates the natural tendency of *Bothrops* myotoxins to oligomerize.^{30,61,62,81–88}

Measurement of BthTX-II ability to cleave phospholipids revealed that its activity was 0.097 ± 0.017 μmol/min/mg. This value is much lower than those presented by other Asp49-PLA₂s (e.g. 282.0 ± 24.6 μmol/min/mg for Mt-I, a myotoxic Asp49-PLA₂ from *B. asper*⁸⁹ but comparable with those produced by Lys49-PLA₂s⁸⁹ (0.028 ± 0.003 and 0.62 ± 0.42 μmol/min/mg, respectively, for Mt-II and BthTX-I⁸⁹). This curious finding gives rise to an interesting question: is extracellular calcium necessary to enable BthTX-II toxin to exert its action?

To answer this question calcium imaging experiments, cell viability assay and time-lapse experiments were performed on C2C12 myotubes bathed in medium with or without extracellular calcium. BthTX-II caused a progressive degeneration of myotubes as can be observed by loss of their morphology, accumulation of aggregates in their cytosol, fragmentation and eventually disappearance of their sarcolemma (Fig. 1). BthTX-II was able to cause cellular damage also in the absence of extracellular calcium (Fig. 2), while control cells maintained their normal morphology (data not shown).

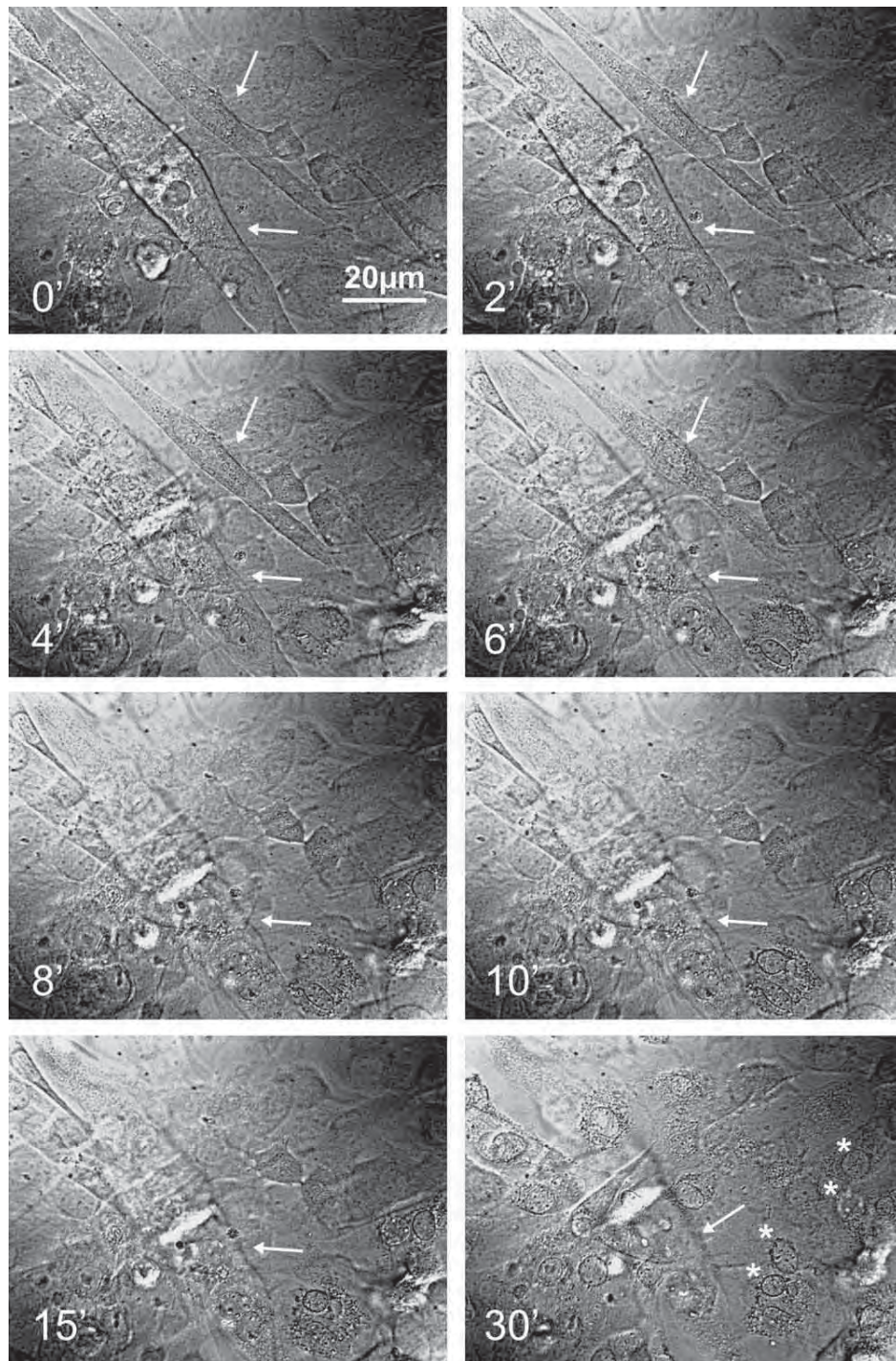


Figure 1

Time-lapse images show morphological changes induced by BthTX-II in C2C12 cells. Myotubes were treated with BthTX-II (50 µg/mL) for 30 min in Ca²⁺-containing buffer and were observed in bright field. Arrows indicate myotubes, differentiated C2C12 cells. After 6 minutes it is possible to observe disruption of plasma membranes with loss of myotubes' morphology and at 30 minutes some damaged cells are observed as nuclei (asterisks).

Cytosolic calcium concentration, [Ca²⁺]_c, measurements in differentiated C2C12 myotubes showed that BthTX-II caused a rapid increase in [Ca²⁺]_c followed by

a second irregular rise characterized by slow waves [Fig. 3(A)]. In Ca²⁺-free medium supplemented with EGTA, the first Ca²⁺ peak was still observed but the second

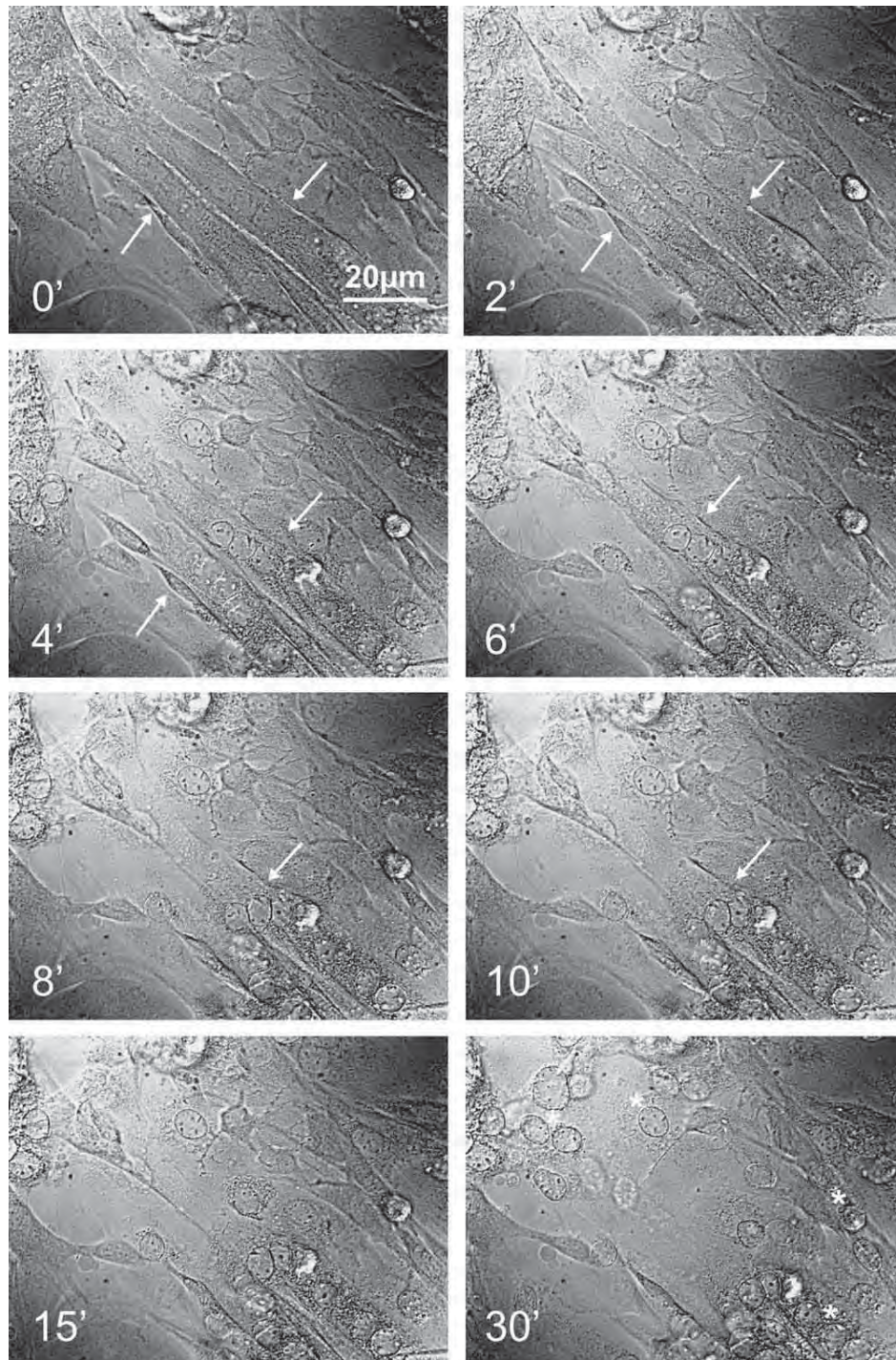


Figure 2

Time-lapse images show morphological changes induced by BthTX-II in C2C12 cells. Myotubes were treated with BthTX-II (50 µg/mL) for 30 min in Ca^{2+} -free medium supplemented with EGTA and observed in bright field. Arrows indicate myotubes, differentiated C2C12 cells. After 6 minutes it is possible to observe disruption of plasma membranes with loss of myotubess' morphology and at 30 minutes some damaged cells are observed as nuclei (asterisks).

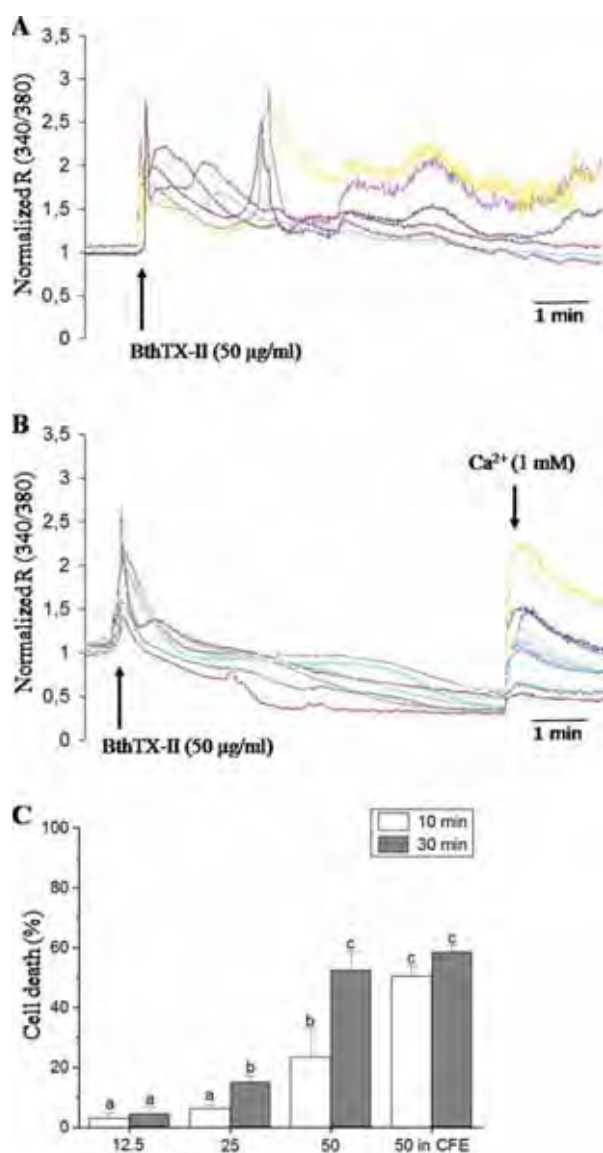


Figure 3

Effects of BthTX-II on $[Ca^{2+}]_c$ and viability of C2C12 myotubes. Panels A and B show intracellular calcium profiles in myotubes. The $[Ca^{2+}]_c$ was tracked as a change in the fura-2 fluorescence ratio (340/380 nm) in different cells after addition of BthTX-II (50 µg/mL) in Ca^{2+} -containing buffer (Panel A), or in Ca^{2+} -free EGTA-containing medium (Panel B). Owing to the elongated shape of myotubes, the individual traces refer to different cells or to different regions of the same cell. For presentation, the ratios were normalized to the resting value. Panel C shows percentages of cell death after treatment with different doses of BthTX-II for 10 (empty bars) or 30 minutes (gray bars). Bars represent mean values \pm SEM estimated in three or more experiments performed in duplicates. Student's *t*-test was used for statistical comparison of the data. A value of $P < 0.05$ was considered to indicate significance. [Color figure can be viewed in the online issue, which is available at www.interscience.wiley.com.]

irregular $[Ca^{2+}]_c$ rise was completely abolished [Fig. 3(B)], indicating the extracellular Ca^{2+} source of this second event, as also observed with other Lys49-PLA₂ and

Asp49-PLA₂ toxins.⁸⁹ However, even under this condition, BthTX-II was able to alter the myotube plasma membrane permeability, since the addition of calcium to the cells [1 mM; arrow in Fig. 3(B)] caused a clear $[Ca^{2+}]_c$ rise, indicating a Ca^{2+} influx through the plasma membrane, differently from the controls where no $[Ca^{2+}]_c$ increase was observed (data not shown). In agreement with these findings, cell death of myotubes exposed to BthTX-II increased significantly in a time- and dose-dependent manner [Fig. 3(C)]. Using the same toxin concentration (50 µg/mL), the cytotoxic effect of BthTX-II was also observed in the absence of extracellular calcium and was actually moderately stronger than under physiological conditions at 10 min [Fig. 3(C)].

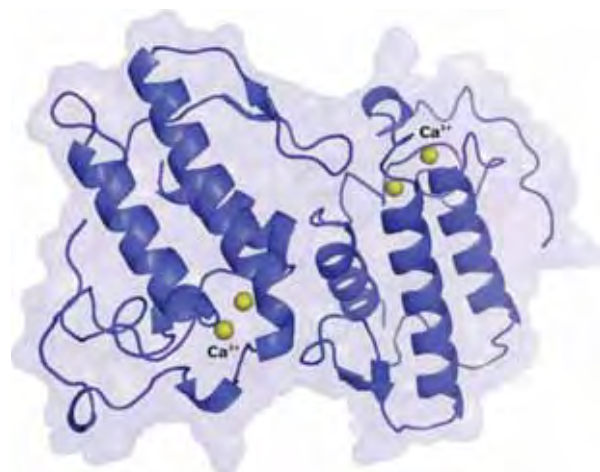
These results clearly show that BthTX-II is able to exert its function even in the absence of extracellular calcium, which is contrary to the notion that all Asp49-PLA₂s are enzymatically active and Ca^{2+} -dependent proteins.

Crystallographic structure of BthTX-II grown in the presence of calcium

Crystals of BthTX-II/ Ca^{2+} were obtained under the same crystallization conditions in which the apo protein was crystallized⁶¹ and diffracted X-rays to 2.10 Å resolution. Data-processing and refinement statistics are presented in Table I. The final model presents a final *R* value of 21.7% (*R*_{free} of 24.9%).

A dimer was found in the asymmetric unit of the crystal as indicated by the Matthews coefficient,⁹⁰ and in agreement with DLS and electrophoresis experiments. BthTX-II/ Ca^{2+} crystal structure is isomorphous to the apo form of the protein and belongs to the C2 space group⁶¹ (Table I). Examination of unit-cell packing showed two possible dimeric configurations for this structure, as already described by Côrrea *et al.*⁶¹ The quaternary assembly chosen for apo BthTX-II in which the monomers are related by an approximated two-fold axis perpendicular to its β -wings was also used for BthTX-II/ Ca^{2+} (Fig. 4). This dimeric configuration resembles the “conventional dimer” configuration adopted by Lys49-PLA₂s^{46,56,91} and had already been observed by Rigden *et al.* when they solved the PrTX-III structure.⁶²

Seven disulfide bridges were found in each monomer of the structure, conserving structural features of other class II PLA₂s, including the catalytic network constituted by His48, Tyr52, Tyr73, and Asp99^{8,14} and the residues involved in Ca^{2+} coordination (Tyr28, Gly30, Gly32, and Asp49).^{8,13,14} Even in the presence of a great amount of calcium ions, no Ca^{2+} was found in the calcium binding loop region. On the other hand, calcium ions were observed interacting with two equivalent regions in BthTX-II monomers (Fig. 1 – Supporting information). This finding may be related to the high concentration of calcium chloride used in the crystallization experiment

**Figure 4**

BthTX-II/Ca²⁺ crystallographic structure. Calcium ions are shown in yellow. [Color figure can be viewed in the online issue, which is available at wileyonlinelibrary.com.]

and probably have no biological significance. Additionally, the possibility of water molecules in the same positions was checked and discarded since their temperature factors and electronic density maps were in disagreement with other water molecules.

Comparison between apo BthTX-II and its complexed form

Superposition of apo BthTX-II and BthTX-II/Ca²⁺ dimeric forms resulted in C^α atom r.m.s. deviations of 0.39 and 0.55 Å for A and B monomers, respectively. Additionally, superposition of the two BthTX-II/Ca²⁺ monomers showed that they are similar (r.m.s.d. = 0.77 Å). The same occurred with the monomers of apo BthTX-II structure which showed an r.m.s.d. of 0.73 Å. The calcium binding loop of BthTX-II/Ca²⁺ structure is kept in the same orientation as the one observed for the apo form of the protein (Fig. 5). This observation explains why no Ca²⁺ was found interacting with this region since Côrrea *et al.* have reported that this loop presents a distorted conformation in the apo form of BthTX-II, a feature that impairs Ca²⁺ coordination.⁶¹

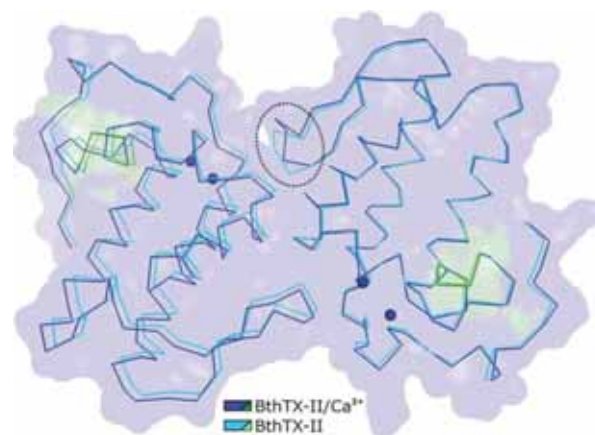
Comparison of apo and complexed BthTX-II structures indicated that some side chains present different rotameric configurations, despite the apparent absence of a relationship between these findings and the presence of calcium ions in some regions. These differences may be related to the different resolutions presented by the two structures (2.19 and 2.10 Å for apo and complexed forms, respectively). The region comprising the residues 77–81 from monomer B of BthTX-II/Ca²⁺ present a higher r.m.s.d. when compared to the same region of the apo form of BthTX-II (encircled in Fig. 5). Given the 10.5

Å distance between the calcium ion and the closest atom of BthTX-II/Ca²⁺ monomer B (oxygen from the main chain of Glu78), it is unlikely that calcium ion led to this distortion. No other significant differences were observed between apo and cocrystallized structures (Fig. 5), suggesting that calcium ions do not induce any alteration in the tertiary or even in the quaternary conformation of the protein under study.

Comparison between BthTX-II forms and other PLA₂s

In order to get insights that could explain why BthTX-II is not catalytic, comparative studies between the amino acid sequence of this protein and other classic and myotoxic Asp49-PLA₂s from the Crotalinae subfamily were performed showing that the residues of their catalytic network (e.g. His48, Asp49, Tyr52, and Asp99) and the ones responsible for calcium coordination (e.g. Tyr28, Gly30, and Gly32) are fully conserved.^{46,59,60} Therefore, it was expected that any Asp49-PLA₂ would present catalytic activity. Since no clue was ascertained by only sequence alignment analyses, the X-ray crystallographic structures were superposed.

A three-dimensional analyses of the calcium binding loop region demonstrated that residue 31 of the myotoxic Asp49-PLA₂s (PrTX-III and BthTX-II) presents a different conformation when compared to the classic Asp49-PLA₂s [Fig. 6(A)] and to Lys49-PLA₂s.⁶¹ An inspection of this region in two crystallographic structures of enzymatically-active snake venom Asp49-PLA₂s bound to calcium^{92,93} and which, like BthTX-II, presents a tryptophan in position 31 of their amino acid

**Figure 5**

Superposition of apo and calcium complexed BthTX-II crystallographic structures. Regions in green indicate the calcium binding loops and the encircled area indicates the region with highest r.m.s.d. between the two structures. Blue spheres correspond to calcium ions from BthTXII/Ca²⁺ crystallographic structure. [Color figure can be viewed in the online issue, which is available at wileyonlinelibrary.com.]

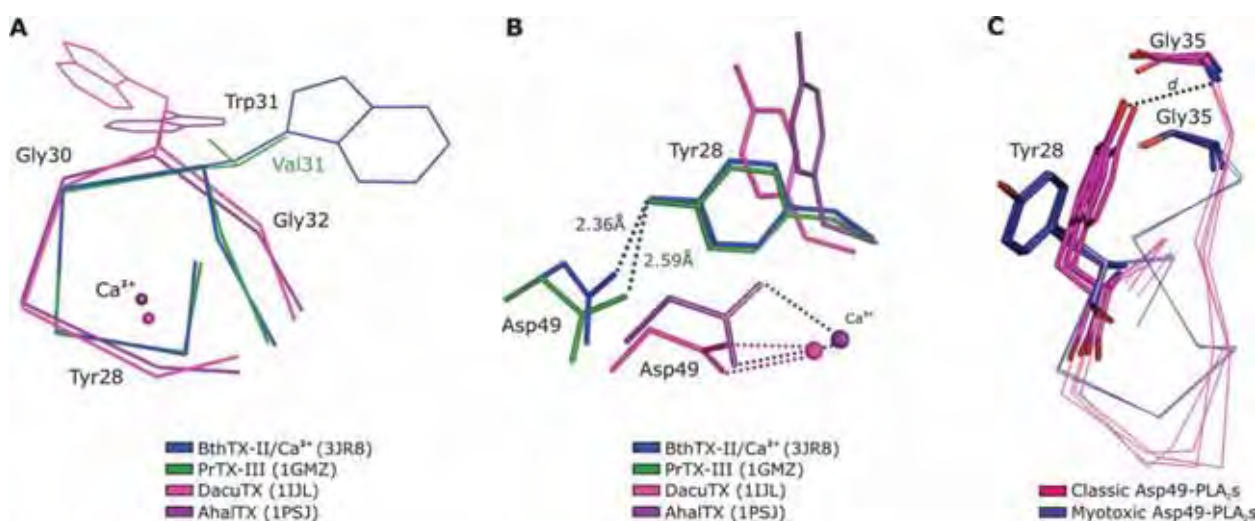


Figure 6

Inspection of the calcium-binding-loop region from some Viperidae snake venom PLA₂s. (A) Superposition of the calcium binding loop from two myotoxic Asp49-PLA₂s (BthTX-II/Ca²⁺ in blue and PrTX-III⁶² in green) and two acidic and nonmyotoxic Asp49-PLA₂s (Aha1TX⁹² in purple and DacuTX⁹³ in pink) shows the presence of tryptophan in position 31 does not impair calcium coordination. (B) Tyr28 and Asp49 residues' configurations in myotoxic and nonmyotoxic Asp49-PLA₂s. Orientation of Tyr28 in myotoxic Asp49-PLA₂s leads to the establishment of a hydrogen bond between O_η from this residue and atom O_δ from Asp49, and consequently impairs Ca²⁺ coordination by both O_δ from Asp49. (C) O_η from Tyr28 side chain and Gly35 amino group configurations for classic Asp49-PLA₂s (magenta) and myotoxic Asp49-PLA₂s (blue) structures. Distance (*d*) between O_η of Tyr28 and the amino group of Gly35 for classic Asp49-PLA₂s is shown ($3.1 < d < 3.5$). The classic Asp49-PLA₂s are represented by Aha1TX, an acidic phospholipase A₂ from *Agkistrodon halys pallas* venom (Aha1TX),⁹² a PLA₂ from *Daboia russelli pulchella* venom⁹⁴ and an acidic phospholipase A₂ from *Deinagkistrodon acutus* (DacuTX).⁹³ The myotoxic Asp49-PLA₂s (blue) are represented by BthTX-II⁶¹ and PrTX-III.⁶² [Color figure can be viewed in the online issue, which is available at wileyonlinelibrary.com.]

sequences indicates that the presence of this residue in position 31 does not impair Ca²⁺ coordination [Fig. 6(A,B)]. Interestingly, the sequence from the region 25 to 35 of the myotoxic BthTX-II is identical to the sequence of the acidic PLA₂ from the venom of *Agkistrodon halys pallas*⁹² (later renamed as *Gloydus halys*; named Aha1TX in Fig. 6). Therefore, the calcium binding loop distortion and its consequent inability to bind calcium ion cannot be attributed only to the presence of specific residues in the primary sequence of myotoxic Asp49-PLA₂s.

Nevertheless, two interesting features regarding the calcium binding loop distortion are observed: (i) a hydrogen bond is established between the O_δ from Asp49 and the O_η from Tyr28⁶¹ in the myotoxic BthTX-II and PrTX-III structures whereas both O_δ atoms from Asp49 side chain are responsible for Ca²⁺ coordination in classic Asp49-PLA₂s^{8,14,95} [Fig. 6(B)], and (ii) an interaction between O_η from Tyr28 and the Gly35 amino group with a conserved distance range in classic Asp49-PLA₂s ($3.1 < d < 3.5$ Å) [Fig. 6(C); Table II]. These patterns that allow a subdivision between classic and myotoxic Asp49-PLA₂s are due to the different side-chain orientation of Asp49 and residues of the calcium binding loop region [Fig. 6(B,C)].

The Tyr28-Gly35 interaction observed in classic Asp49-PLA₂s may provide structural stability for the Ca²⁺ binding loop since residues considered essential for the cofactor coordination are kept in favorable orientations when

this interaction is present. On the other hand, when the distance *d* is not preserved (Fig. 6; Table II), a great distortion in the calcium-binding-loop region occurs and impairs Ca²⁺ coordination. This observation is in agreement with Zhou *et al.*⁹⁶ who proposed the absence of this interaction as being responsible for the Ca²⁺ binding loop disarrangement in Ser49-PLA₂ Ecarpholin S from *Echis carinatus sochureki* venom.

An alternative dimer may explain specific features of myotoxic Asp49-PLA₂s

Snake venom PLA₂s are capable of exerting different biological activities (e.g. catalytic, myotoxic, neurotoxic,

Table II

Distance (*d*) from O_η Atom of Tyr28 to Gly35 Amino Group in Asp49-PLA₂s Structures

	Protein (PDB identification code)	<i>d</i> (Å)
classic Asp49-PLA ₂ s	BthA-I-PLA ₂ (1U73) ⁸³	3.07
	Acid-PLA ₂ from <i>G. halys</i> ^a (1PSJ) ⁷⁸	3.50
	Acid-PLA ₂ from <i>D. acutus</i> (1IJL) ⁷⁹	3.49
	DPLA ₂ (1FB2) ⁸²	3.51
	β2-Bungarotoxin (1BUN) ⁸⁴	3.51
	Bovine pancreatic PLA ₂ (1G4I) ⁸⁵	3.28
myotoxic Asp49-PLA ₂ s	PrTX-III (1GMZ) ⁶²	7.87
	BthTX-II (20QD) ⁶¹	7.64

^aformerly *Agkistrodon halys pallas*.

Table IIIInterfacial Area and Solvation Free Energy for BthTX-II, BthTX-II/ Ca^{2+} , PrTX-III, and DacuTX Crystallographic Structures^a

Proteins/Dimer type	Interfacial area (\AA^2)	$\Delta^{\text{f}}G$ (kcal/mol) ^b
BthTX-II (2OQD)		
Crystallographic dimer	456.5	-2.7
Biological dimer	669.5	-13.5
BthTX-II/Ca^{2+} (3JR8)		
Crystallographic dimer	422.5	-1.5
Biological dimer	632.6	-14.5
PrTX-III (1GMZ)		
Crystallographic dimer	522.3	0.3
Biological dimer	639.9	-10.4
DacuTX (1IJL)		
Biological /crystallog. dimer	992.7	-15.6

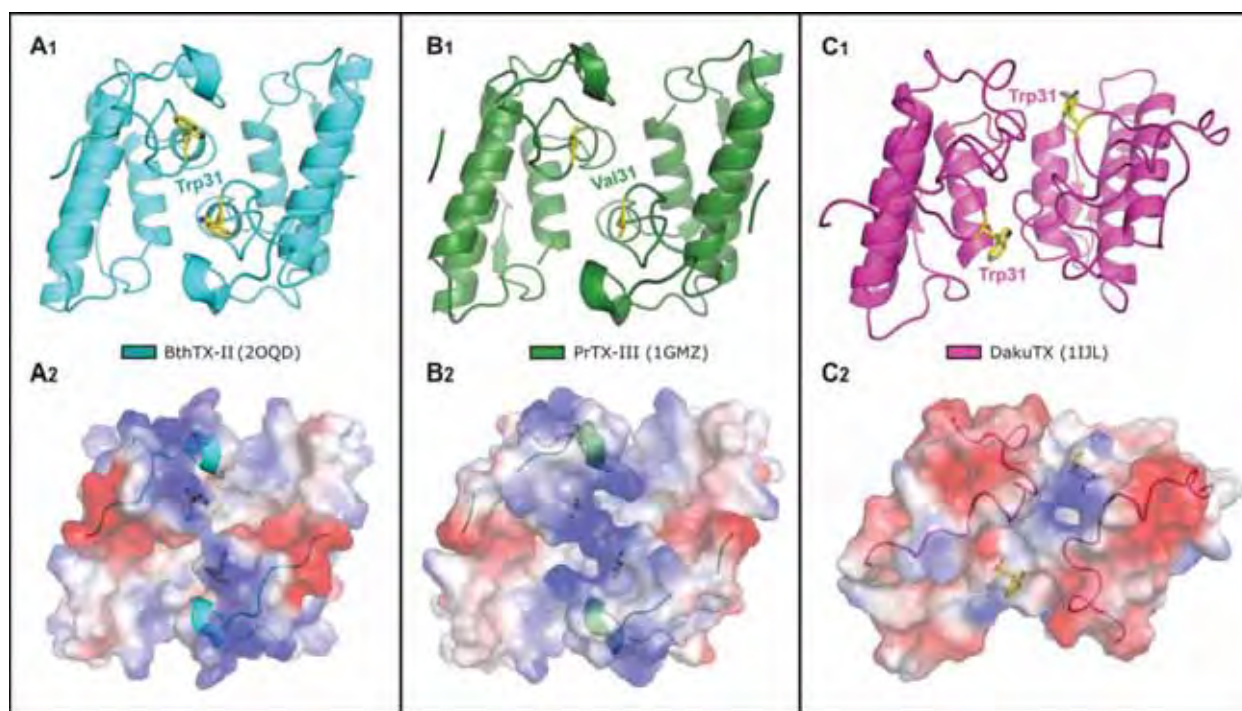
^aValues given by the online interactive tool PISA⁹³ available at the European Bioinformatics Institute server (<http://www.ebi.ac.uk>). $\Delta^{\text{f}}G$ indicates the solvation free energy gain upon formation of the interface, in kcal/mol. The value is calculated as difference in total solvation energies of isolated and interfacing structures.

^bNegative $\Delta^{\text{f}}G$ corresponds to hydrophobic interfaces, or positive protein affinity. This value does not include the effect of satisfied hydrogen bonds and salt bridges across the interface. Interface area in \AA^2 , calculated as difference in total accessible surface areas of isolated and interfacing structures divided by two.

hypotensive, anticoagulant, bactericidal, and edema-inducing, among others). A large number of structures of

these proteins has been solved, many of which present different quaternary assemblies despite possessing conserved tertiary structures.^{56,61,84,86,91,97-103} Therefore, the key to understanding the mechanisms underlying their biological activities may be found by examining their oligomeric assemblies.¹⁰⁴

Comparison of BthTX-II and PrTX-III structures with a dimeric Asp49-PLA₂ from *Deinagkistrodon acutus*⁹³ (named as DacuTX), whose structure presents a tryptophan in position 31 and Ca^{2+} coordinated by Asp49 and residues of its calcium binding loops, suggested that the cause of such distortion could be related to the oligomeric assembly adopted by myotoxic Asp49-PLA₂s toxins. As previously described, BthTX-II and PrTX-III crystallographic structures have a two-fold axis symmetry that adopts a quaternary structure resembling the Lys49-PLA₂ "conventional dimer". On the other hand, submission of these structures to PISA program⁷⁶ analyses indicated another quaternary assembly as the probable biological dimer for the myotoxins under analysis (Table III; Fig. 7) (the crystallographic structure of AhalTX was not used in this specific analysis because it is monomeric). In this suggested biological configuration, residues 31 of

**Figure 7**

Biological oligomeric assemblies adopted by BthTX-II (A₁), PrTX-III (B₁), and DacuTX (C₁) apo structures. A₁ also represents BthTX-II/ Ca^{2+} dimeric configuration as indicated by PISA program analyses.⁷⁶ Residues 31 are disposed side by side and towards the C-terminal region in myotoxic Asp49-PLA₂s (A₂ and B₂), establishing a direct route of communication between the calcium binding loop and the C-termini of these myotoxic proteins. A₂, B₂, and C₂ represent surface electrostatic charge distribution for the proteins under analysis. Basic surface charge distribution is observed along the C-terminal regions of the myotoxic proteins BthTX-II and PrTX-III (A₂ and B₂, respectively). The C-terminal region (amino acids 111 to 133) of BthTX-II, PrTX-III, and DacuTX shown in panels A₂, B₂, and C₂, respectively, are drawn in cartoon. [Color figure can be viewed in the online issue, which is available at wileyonlinelibrary.com.]

Table IVPositively Charged Residues (Arginine, Lysine, and Histidine) Distribution along the C-Terminal Region^a of svPLA₂s

Myotoxic PLA ₂ s ^b	Cgod2 6	Tgra1 7	Tfla1 5	Ooki2 6	MjTX-I 6	BthTX-I 7	Basp1 6	BthTX-II 7	PrTX-III 8
Catalytic PLA ₂ s ^b	Tfla5 3	Bsch2 3	Ooki1 3	BthA-1 3	Catr1 3	Bery1 2	Apisps2 5	Cgod3 5	Pmuc1 5

^aResidues numbered between 111–133 in Lys49-PLA₂s and the ones corresponding to this sequence in Asp49-PLA₂s were evaluated.^bProtein codes can be checked in Table V.

both monomers from the myotoxic Asp49-PLA₂s are part of the interface and oriented towards their C-terminal region [Fig. 7(A,B)]. As a consequence of this configuration, a direct connection between their calcium binding loops and C-termini of these myotoxins is established [Fig. 7(A,B)]. Additionally, it is important to highlight that the residues 31 of myotoxic Asp49-PLA₂s are disposed side by side and towards their C-termini, a feature that probably conveys mechanical support for them [Fig. 7(A,B)]. Analyses of DacuTX structure shows that despite they present residues tryptophan 31 of both monomers in the interface, their calcium binding loops are not side by side and no connection between these residues and the C-termini of the protein is established [Fig 7(C)].

The C-terminal region of Lys49-PLA₂s has already been demonstrated to be responsible for myotoxicity expression in these proteins.^{34,44,47–55} Given that the myotoxic Asp49-PLA₂s can be grouped into the same clade of Lys49-PLA₂s (Fig. 8), it is reasonable to hypothesize that their myotoxicity may also arise from their C-termini. Additionally, Francis *et al.* had already suggested that the residues between Thr112 and Pro121 from BthTX-II primary sequence are the responsible for its myotoxic activity.^{30,59} Supporting these suggestions, analysis of the C-terminal region showed BthTX-II and PrTX-III present a high content of positively charged residues in their C-termini (Table IV) [Fig. 7(A,B)]. This pattern is also observed in Lys49-PLA₂s and is thought to be the responsible for their myotoxicity³⁴ (Table IV).

The hypothesis proposed above is based on a structure-function relationship. It justifies the calcium binding loop distortion in myotoxic Asp49-PLA₂s since BthTX-II and PrTX-III are not catalytically active and also based on the need for this distortion to stabilize their dimeric assembly and their C-termini. Additionally, in this configuration their C-termini are disposed side by side, a feature that has already been demonstrated to be important for myotoxic activity expression in Lys49-PLA₂s.⁵⁶

Evolutionary inferences about snake venom phospholipases A₂ and phylogenetic relationships of myotoxic Asp49-PLA₂s

The results presented herein indicate that BthTX-II is able to damage myotubes but does not present catalytic activity. Interestingly, this toxin is an Asp49-PLA₂ and conserves the residues of the catalytic network and the ones responsible for Ca²⁺ coordination.^{59,61} In order to

get insights into this apparent paradox and clarify the phylogenetic relationships of BthTX-II and other myotoxic Asp49-PLA₂s, phylogenetic studies on snake venom PLA₂s from the Crotalinae subfamily were performed. Evolutional and phylogenetic studies of snake venom PLA₂s from the Viperidae family based on distance methods and using a few amino acid sequences had already been performed.^{36,105} However, the phylogenetic relationships of myotoxic Asp49-PLA₂s remained unclear highlighting the importance of new studies. Herein, we present a Bayesian phylogenetic analysis for snake venom phospholipases A₂ (Fig. 8) using almost all amino acid sequences from the Crotalinae subfamily (Viperidae family) available in the NCBI databank (Table V) (only redundant sequences were discarded). Furthermore, the sequence of Gln49-PLA₂ from *Gloydus ussuriensis* was also included in the analysis after being manually extracted from the article.¹⁰⁶

The phylogenetic tree presented here (Fig. 8) shows two main monophyletic clades (A and B) that have a common ancestor. For the first time, Asp49-PLA₂s are shown to be part of both clades indicating an aspartate residue occupying position 49 of the ancestor since the data of Ohno *et al.*¹⁰⁵ and of Wei *et al.*³⁶ were inconclusive about which residue occupied this position. The key difference between the Clades A and B remain on the activity exerted by proteins grouped under these branches. Proteins grouped together in Clade A present catalytic activity whereas the ones grouped in Clade B are capable of inducing local myonecrosis. The most basal sequences of Clade B are the myotoxic Asp49-PLA₂s, including BthTX-II (Bjar3) and PrTX-III (Bpir3). These results indicate that myotoxic Asp49-PLA₂s have a closer phylogenetic relationship to Lys49-PLA₂s than to classic Asp49-PLA₂s since they form a monophyletic clade with Lys49-PLA₂s (Fig. 8). These data are consistent with our findings for BthTX-II since this protein presents pronounced myotoxic activity but not catalysis.

The most basal sequences of Clade A (with exception of Bsch2) and all the sequences present in Clade B present a basic pI (Table V), suggesting a basic PLA₂ (and an Asp49 as previously shown) as the ancestor for snake venom phospholipases A₂ from the Crotalinae subfamily. On the other hand, most of the sequences of Clade A present an acidic pI (Table V), suggesting that phospholipidic activity expression is favored by this biochemical property. Interestingly, we can observe that sequences from the genera *Agkistrodon* and *Trimesurus* (Apisps2,

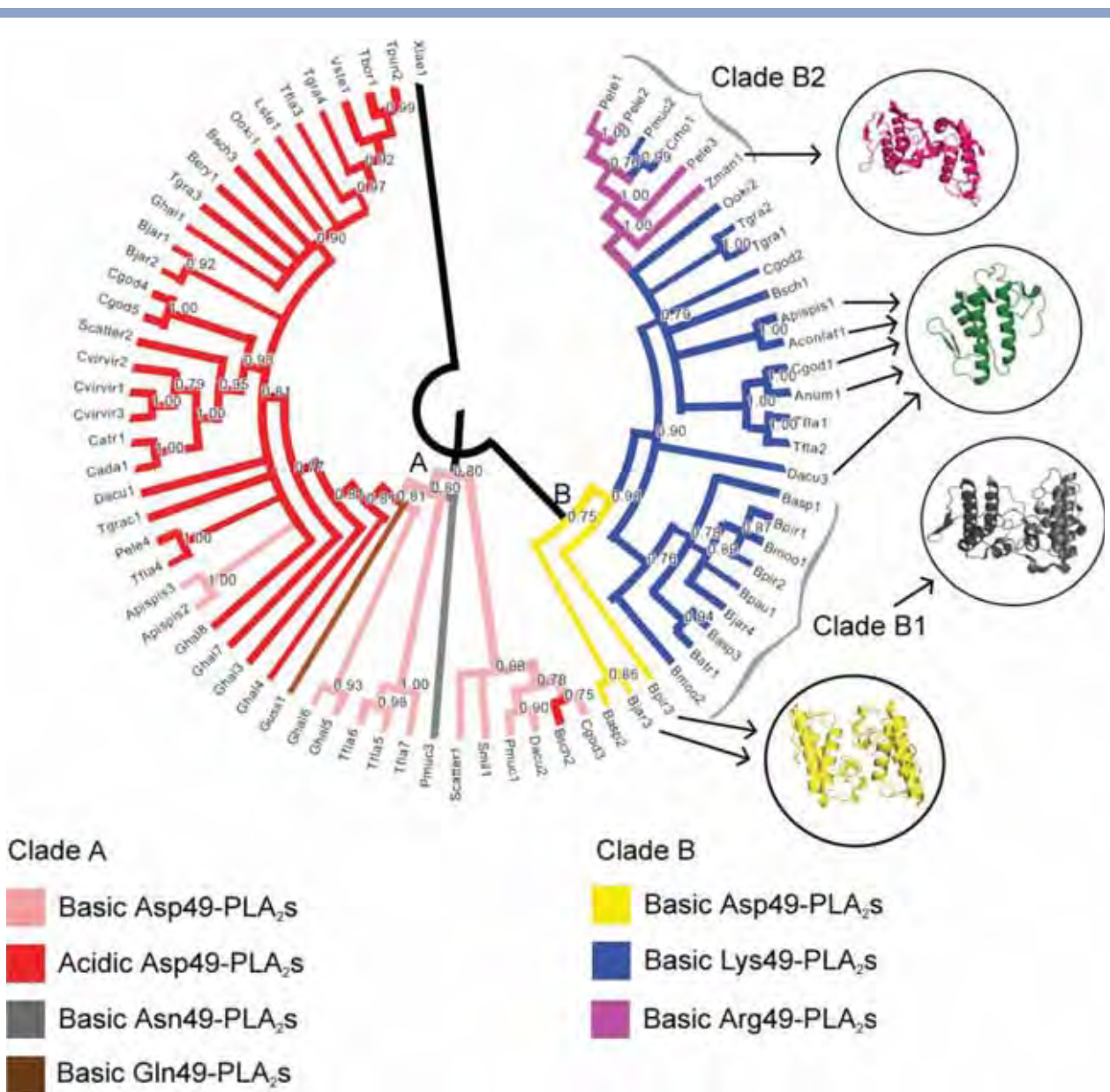


Figure 8

Phylogenetic tree of phospholipases A₂ amino acid sequences from Viperidae family (Crotalinae subfamily) snake venom. The branch color corresponds to the group to which each sequence belongs. Posterior probability values after 3,000,000 cycles are indicated in internodes. Internodes with a posterior probability value less than 0.75 were collapsed. The identification codes of the sequences are shown in Table V. Internodes with posterior probability values less than 0.75 were collapsed. Minimum *e*-value of 3.10⁻⁴⁴. Displayed oligomeric configurations are represented by apo BthTX-II (yellow), apo PrTX-I (grey), Dacu3 (green), and Zman1 (pink) structures. The biological dimer suggested by PISA⁷⁶ was used for PrTX-I and BthTX-II structures' illustrations. The representative dimeric assemblies of BthTX-II and Zman1 are the same. Proteins indicated as monomers (in green) are result of crystallographic studies and may not reflect the true biological conformation of the toxins under physiological conditions since they were crystallized in acidic pHs or in the presence of a great amount of salt (factors that can be responsible for dimer dissociation in svPLA₂s).

Apispis3, Tbor1 and Tpun2) (Fig. 8) experienced a reversal of their net charge that restored a basic pI. This may be a result of specific evolutionary pressure on phospholipases A₂ of these two snake genera. A basic pI, on the other hand, seems to be important for expression of the

myotoxic activity since all myotoxic proteins present in this phylogenetic tree possess this characteristic (Guss1, Pmuc3 and all the sequences grouped together in Clade B) (Table V) [Fig. 8(A,B)]. However, there are a few acidic Asp49-PLA₂s characterized as myotoxic proteins^{107,108}

Table V
Identification Codes, Theoretical Isoelectric Points, NCBI, and PDB Entry Codes that Correspond to the Phospholipases A₂ from Crotalinae Subfamily present in the Phylogenetic Tree of Figure 8

Class	Snake	Protein	Identification code	NCBI entry code	PDB entry code	Isoelectric point ^a	
Clade B	Lys49	<i>Agkistrodon contortrix latinctus</i>	Myotoxin	Aconlat1	1S8G/1S8H/1S8I	8.48	
		<i>Agkistrodon piscivorus piscivorus</i>	APP-K49	Apiapis1	1PPA	8.48	
		<i>Atropoides nummifer</i>	Myotoxin II	Anum1	17433156	2A0Z	8.28
		<i>Bothriechis schlegelii</i>	Bsc-K49	Bsch1	25453450	-	8.61
		<i>Bothrops asper</i>	M1-3-3 protein	Basp3	6492260	-	8.86
		<i>Bothrops asper</i>	Myotoxin II	Basp1	166215047	1CLP/1Y4L	8.87
		<i>Bothrops atrox</i>	Myotoxin I	Batr1	40888878	-	8.48
		<i>Bothrops jararacussu</i>	Bothropstoxin-I (BthTX-I)	Bjar4	265051	2H8I/3CXI/3HZD/3I03	8.87
		<i>Bothrops moojeni</i>	Myotoxin II (MjTX-II)	Bmo02	17865560	1XXS	8.61
		<i>Bothrops moojeni</i>	Myotoxin I (MjTX-I)	Bmo01	17368325	-	8.61
		<i>Bothrops pirajai</i>	BnsP-7	Bpau1	239338675	1PA0	8.61
		<i>Bothrops pirajai</i>	Piratoxin-I (PrTX-I)	Bpir1	17433154	2Q2J/2OK9/3CYL	8.61
		<i>Bothrops pirajai</i>	Piratoxin-II (PrTX-II)	Bpir2	17368328	1OLL	8.72
		<i>Calloselasma rhodostoma</i>	G6K49	Crho1	27151658	-	8.48
		<i>Cerrophidion godmani</i>	Pgo-K49	Cgod2	26397687	-	8.48
		<i>Cerrophidion godmani</i>	Myotoxin II (GODMT-II)	Cgod1	3122600	1G0D	8.15
		<i>Deinagkistrodon acutus</i>	Dac-K49II	Dacu3	26397573	1MC2/1MG6	8.36
		<i>Ovophis okinavensis</i>	Phospholipase A ₂ homolog PLA ₂ -03	Ooki 2	26006828	-	7.76
		<i>Protobothrops mucrosquamatus</i>	TMV-K49	Pmuc2	129468	-	8.48
		<i>Trimeresurus flavoviridis</i>	Basic protein I/II (BP-I/BP-II)	Tfla1	400717	-	8.72
		<i>Trimeresurus flavoviridis</i>	Basic protein II	Tfla2	222955	-	8.87
		<i>Trimeresurus gramineus</i>	PLA ₂ -VII	Tgra2	20177995	-	8.43
		<i>Trimeresurus gramineus</i>	PLA ₂ -V	Tgra1	3914265	-	8.28
		<i>Bothrops asper</i>	Myotoxin III	Basp2	166214965	-	8.28
		<i>Bothrops jararacussu</i>	Bothropstoxin-II (BthTX-II)	Bjar3	1171971	20QD/3JF8	8.02
		<i>Bothrops pirajai</i>	Piratoxin-III (PrTX-III)	Bpir3	17865540	1GMZ	7.87
		<i>Protobothrops elegans</i>	Phospholipase A ₂	Pele3	84578889	-	8.48
		<i>Protobothrops elegans</i>	Phospholipase A ₂	Pele2	84578891	-	8.48
		<i>Protobothrops elegans</i>	Phospholipase A ₂	Pele1	84578893	-	8.48
		<i>Zhaeria mangshanensis</i>	Zhaermitatoxin	Zman1	115502551	2PH4	8.61

(Continued)

Table V
(Continued)

Clade A	Class	Snake	Protein	Identification code	NCBI entry code	PDB entry code	Isoelectric point ^a	
Classical Asp49		<i>Agkistrodon piscivorus piscivorus</i>	APP-D-49	Apispis2	2851578	1VAP	8.15	
		<i>Bothriechis schlegelii</i>	acidic phospholipase A ₂	Bsch3	59726986	-	4.23	
		<i>Bothriechis schlegelii</i>	N6 basic phospholipase A ₂	Bsch2	38230125	-	6.74	
		<i>Bothrops erythromelas</i>	BE-I-PLA ₂	Bery1	86450426	-	4.51	
		<i>Bothrops jararacussu</i>	BthA-1	Bjar1	25140377	1U73/1UMV/1Z76/1ZL7/1ZLB	-	5.21
		<i>Bothrops jararaca</i>	Bj-PLA ₂	Bjar2	3914258	-	4.41	
		<i>Cerrophidion godmani</i>	DTE6b phospholipase A ₂	Cgod5	59727030	-	4.60	
		<i>Cerrophidion godmani</i>	N6 basic phospholipase A ₂	Cgod3	38230123	-	7.86	
		<i>Cerrophidion godmani</i>	NTE6a phospholipase A ₂	Cgod4	59727008	-	4.82	
		<i>Crotalus adamanteus</i>	Acid Phospholipase A ₂	Cada1	129507	-	4.91	
		<i>Crotalus atrox</i>	Phospholipase A ₂	Catr1	25108915	1PP2	4.47	
		<i>Crotalus viridis viridis</i>	Acid Phospholipase A ₂	Cvirir1	28893826	-	5.21	
		<i>Crotalus viridis viridis</i>	Acid Phospholipase A ₂	Cvirir3	28893822	-	4.76	
		<i>Crotalus viridis viridis</i>	Acid Phospholipase A ₂	Cvirir2	28893824	-	4.47	
		<i>Deinagkistrodon acutus</i>	Phospholipase A ₂	Dacu2	97180272	-	8.16	
		<i>Deinagkistrodon acutus</i>	Acid Phospholipase A ₂ (DacuTX)	Dacu1	90265326	11JL	4.53	
		<i>Gloydius halys</i>	Phospholipase A ₂	Ghal1	2460035	-	4.66	
		<i>Gloydius halys</i>	Phospholipase A ₂ BA2	Ghal3	27151650	-	4.80	
		<i>Gloydius halys</i>	Phospholipase A ₂ BA1	Ghal4	27151649	-	4.80	
		<i>Gloydius halys</i>	Phospholipase A ₂	Ghal7	27151651	-	4.67	
		<i>Gloydius halys</i> ^b	Acid Phospholipase A ₂ (AhalTX) ^b	Ghal8	129399	1M8R/1M8S	4.67	
		<i>Gloydius halys</i>	Phospholipase A ₂	Ghal5	27151648	1PSJ/1BK9	8.35	
		<i>Gloydius halys</i>	B-PLA ₂ phospholipase A ₂	Ghal6	27151647	-	8.28	
		<i>Lachesis stenophrys</i>	LSPA-1	Lste1	76363284	1B4W/1CIJ/1JIA	4.76	
		<i>Ovophis okinavensis</i>	Phospholipase A ₂	Ooki1	1769398	-	4.66	
		<i>Protobothrops elegans</i>	Phospholipase A ₂	Pele4	84578888	-	5.89	
		<i>Protobothrops mucrosquamatus</i>	Trimucrotroxin	Pmuc1	26006835	-	8.02	
		<i>Sistrurus catenatus tergeminus</i>	Phospholipase A ₂	Scatter2	45934756	-	4.78	
		<i>Sistrurus catenatus tergeminus</i>	N6b basic phospholipase A ₂	Scatter1	38230127	-	7.86	
		<i>Sistrurus miliaris</i>	Phospholipase A ₂	Smil1	166012664	-	7.76	
		<i>Trimeresurus borneensis</i>	Phospholipase A ₂	Tbor1	38230145	-	5.20	
		<i>Trimeresurus flavoviridis</i>	Phospholipase A ₂	Tfla5	28202237	-	7.76	
		<i>Trimeresurus flavoviridis</i>	TFV PL-X	Tfla7	129499	-	8.07	
		<i>Trimeresurus flavoviridis</i>	Phospholipase A ₂	Tfla3	436249	-	4.58	
		<i>Trimeresurus flavoviridis</i>	Phospholipase A ₂	Tfla4	436247	-	6.75	
		<i>Trimeresurus flavoviridis</i>	Phospholipase A ₂	Tfla6	28202238	-	7.87	
		<i>Trimeresurus gracilis</i>	Acid Phospholipase A ₂	Tgrac1	59727071	-	4.53	
		<i>Trimeresurus gramineus</i>	PLA ₂ -III	Tgra3	3914270	-	4.56	
		<i>Trimeresurus gramineus</i>	PLA ₂ -II	Tgra4	3914268	-	4.76	
		<i>Trimeresurus puniceus</i>	G6D49 phospholipase A ₂	Tpun2	38230137	-	5.20	
		<i>Viridovipera stejnegeri</i>	PLA ₂ -V	Vste1	13959432	-	4.57	
	Asn 49		<i>Protobothrops mucrosquamatus</i>	TM-N49	Pmuc3	77021843	-	8.16
	Gln49		<i>Gloydius ussuriensis</i>	Gln49-PLA ₂	Guss1	^c	-	7.80
	Outgroup		<i>Xenopus laevis</i>	Oto.conin-22	Xlae1	385670	-	5.02

^aCalculated by the DAMBE software.⁹⁸

^bformerly as *Agkistrodon halys pallas* (AhalTX).

^cSequence manually extracted from the article.⁹⁵

that have not yet been entirely sequenced and hence are not present in our analysis. Although it is very difficult to determine their phylogenetic position without their complete amino acid sequences, we suspect that these sequences will be grouped in Clade A, as catalytic acidic proteins that gained myotoxic function.

As previously noted, Clade B is formed only by myotoxic proteins, most of which are Lys49-PLA₂s. Many studies have shown that the C-terminal portion of Lys49-PLA₂s is responsible for their myotoxicity expression^{34,44,47} through the insertion of positively charged residues in the muscle membrane.³⁴ Given the large content of positively charged residues in the C-termini of myotoxic Asp49-PLA₂s and Lys49-PLA₂s (Table IV), it may be inferred that this feature was already present in the common ancestor of all sequences that form Clade B. However, an inspection of the possible quaternary assemblies exhibited by these proteins showed that they can present different oligomeric configurations, despite exerting the same biological function, as we can observe for Clades B1, B2 and for other proteins (Fig. 8). Therefore, it is possible to infer that different and specific myotoxic sites may be present among proteins that compose Clade B, although the myotoxic activity is caused by the C-terminal region. This observation is in agreement with dos Santos *et al.*⁵⁶ whose findings led to the proposal of a myotoxic site exclusive to bothropic Lys49-PLA₂s since all sequences grouped together in Clade B1 are from the *Bothrops* genus and are represented by the same oligomeric assembly.

CONCLUDING REMARKS

BthTX-II has long been known to be a bothropic snake venom compound. However, the characterization of its pharmacological properties has been misunderstood for many years. This study provides an important and novel contribution to better knowledge of this myotoxic Asp49-PLA₂. For the first time it has been shown that BthTX-II does not present catalytic activity, thus refuting the notion that all Asp49-PLA₂s are enzymes. Moreover, it has also been demonstrated that myotoxic Asp49-PLA₂s have a stronger phylogenetic relationship with Lys49-PLA₂s than with the classic Asp49-PLA₂s, as evidenced by phylogenetic analyses and by other experiments which demonstrated they do not present catalytic activity but are myotoxic, as other proteins from branch B (Fig. 8).

Recently, Bonfim *et al.* showed that BthTX-II presents a higher myotoxic effect than BthTX-I (a Lys49 PLA₂ from *Bothrops jararacussu* snake venom) and attributed the additional potency to an indirect effect related to the catalytic activity exerted by this protein.⁶³ On the other hand, our experiments have demonstrated that BthTX-II is able to induce practically the same level of muscle damage in the absence of calcium as the Lys49-PLA₂ BthTX-I.⁸⁹ Additionally, BthTX-II was demonstrated to

cause the same level of myotoxicity at 30 min in the presence and absence of Ca²⁺ when 50 µg/mL of the toxin is tested in myotube cells [Fig. 3(C)], another piece of evidence that calcium is not required for its activity. Phylogenetic and crystallographic studies were performed and support this finding. Therefore, based on our results, it is possible to infer that Branch B of the phylogenetic tree groups only sequences of myotoxic and probably noncatalytic proteins whereas Branch A is formed by catalytic snake venom PLA₂s that can also exhibit additional pharmacological properties.

This work highlights the necessity of considering the biological quaternary assembly when functionally analyzing snake venom PLA₂s. Any clue based only on primary sequence analyses cannot be conclusive since even PLA₂s that perform common activities (e.g. myotoxicity) present different quaternary assemblies, as evidenced by analysis of oligomeric configurations exhibited by myotoxins grouped under Branch B of our phylogenetic study. Furthermore, the placement of BthTX-II in the myotoxic clade and the high content of positively charged residues along its C-terminal region indicate the need for experimental studies to prove whether this function is also exerted by residues of its C-terminal region as is already known for Lys49-PLA₂s.

In conclusion, this study provides new and strong evidences about the myotoxicity and noncatalytic activity of BthTX-II. It also supplies new insights that explain the role of Trp31, the importance of its distortion for BthTX-II activity and highlights the connection between the C-terminal and the calcium binding loop regions of BthTX-II and PrTX-III myotoxic Asp49-PLA₂s.

Atomic coordinates

The coordinates were deposited in the Protein Data Bank with identification code 3JR8.

ACKNOWLEDGMENTS

This work was supported by CARIPARO, FAPESP, CNPq, INCTTOX, and LNLS. We would like to thank Prof. Cesare Montecucco and Prof. Pedro Padilha for their support during the development of this work.

REFERENCES

1. van Deenen LLM, de Haas GH, Heemskerk CHT. Hydrolysis of synthetic mixed-acid phosphatides by phospholipase A from human pancreas. *Biochim Biophys Acta* 1963;67:295–304.
2. Berk PD, Stump DD. Mechanisms of cellular uptake of long chain free fatty acids. *Mol Cell Biochem* 1999;192:17–31.
3. Gijon MA, Leslie CC. Regulation of arachidonic acid release and cytosolic phospholipase A2 activation. *J Leukoc Biol* 1999;65:330–336.
4. Austin SC, Funk CD. Insight into prostaglandin, leukotriene, and other eicosanoid functions using mice with targeted gene disruptions. *Prostaglandins Other Lipid Mediat* 1999;58:231–252.
5. Bingham CO, III, Austen KF. Phospholipase A2 enzymes in eicosanoid generation. *Proc Assoc Am Physicians* 1999;111:516–524.

6. Balsinde J, Balboa MA, Dennis EA. Identification of a third pathway for arachidonic acid mobilization and prostaglandin production in activated P388D1 macrophage-like cells. *J Biol Chem* 2000;275:22544–22549.
7. Moolenaar WH, Kranenburg O, Postma FR, Zondag GC. Lysophosphatidic acid: G-protein signalling and cellular responses. *Curr Opin Cell Biol* 1997;9:168–173.
8. Arni RK, Ward RJ. Phospholipase A2—a structural review. *Toxicon* 1996;34:827–841.
9. Renetseder R, Dijkstra BW, Huizinga K, Kalk KH, Drenth J. Crystal-structure of bovine pancreatic phospholipase-A2 covalently inhibited by para-bromo-phenacyl-bromide. *J Mol Biol* 1988;200:181–188.
10. Yu BZ, Berg OG, Jain MK. The divalent cation is obligatory for the binding of ligands to the catalytic site of secreted phospholipase A2. *Biochemistry* 1993;32:6485–6492.
11. Six DA, Dennis EA. The expanding superfamily of phospholipase A(2) enzymes: classification and characterization. *Biochim Biophys Acta* 2000;1488:1–19.
12. Kudo I, Murakami M. Phospholipase A2 enzymes. *Prostaglandins Other Lipid Mediat* 2002;68–69:3–58.
13. White SP, Scott DL, Otwinowski Z, Gelb MH, Sigler PB. Crystal structure of cobra-venom phospholipase A2 in a complex with a transition-state analogue. *Science* 1990;250:1560–1563.
14. Scott DL, White SP, Otwinowski Z, Yuan W, Gelb MH, Sigler PB. Interfacial catalysis: the mechanism of phospholipase A2. *Science* 1990;250:1541–1546.
15. Schaloske RH, Dennis EA. The phospholipase A2 superfamily and its group numbering system. *Biochim Biophys Acta* 2006;1761:1246–1259.
16. Heinrikson RL, Krueger ET, Keim PS. Amino acid sequence of phospholipase A2-alpha from the venom of *Crotalus adamanteus*. A new classification of phospholipases A2 based upon structural determinants. *J Biol Chem* 1977;252:4913–4921.
17. Calvete JJ, Juarez P, Sanz L. Snake venomomics. Strategy and applications. *J Mass Spectrom* 2007;42:1405–1414.
18. Andraio-Escarso SH, Soares AM, Fontes MR, Fuly AL, Correa FM, Rosa JC, Greene LJ, Giglio JR. Structural and functional characterization of an acidic platelet aggregation inhibitor and hypotensive phospholipase A(2) from *Bothrops jararacussu* snake venom. *Biochem Pharmacol* 2002;64:723–732.
19. Beers SA, Buckland AG, Koduri RS, Cho W, Gelb MH, Wilton DC. The antibacterial properties of secreted phospholipases A2: a major physiological role for the group IIA enzyme that depends on the very high pI of the enzyme to allow penetration of the bacterial cell wall. *J Biol Chem* 2002;277:1788–1793.
20. Bon C, Changeux JP, Jeng TW, Fraenkel-Conrat H. Postsynaptic effects of crotoxin and of its isolated subunits. *Eur J Biochem* 1979;99:471–481.
21. Chang CC, Lee JD, Eaker D, Fohlman J. Short communications the presynaptic neuromuscular blocking action of taipoxin. A comparison with beta-bungarotoxin and crotoxin. *Toxicon* 1977;15:571–576.
22. Gerrard JM, Robinson P, Narvey M, McNicol A. Increased phosphatidic acid and decreased lysophosphatidic acid in response to thrombin is associated with inhibition of platelet aggregation. *Biochem Cell Biol* 1993;71:432–439.
23. Condrea E, Yang CC, Rosenberg P. Lack of correlation between anticoagulant activity and phospholipid hydrolysis by snake venom phospholipases A2. *Thromb Haemost* 1981;45:82–85.
24. Gutiérrez JM, Lomonte B. Phospholipase A2 myotoxins from *Bothrops* snake venoms. In: Kini RM, editor. *Phospholipases A2 Enzymes: Structure, Function, and Mechanism*. Chichester: Wiley; 1997. p 321–352.
25. Lloret S, Moreno JJ. Oedema formation and degranulation of mast cells by phospholipase A2 purified from porcine pancreas and snake venoms. *Toxicon* 1993;31:949–956.
26. Paramo L, Lomonte B, Pizarro-Cerda J, Bengoechea JA, Gorvel JP, Moreno E. Bactericidal activity of Lys49 and Asp49 myotoxic phospholipases A2 from *Bothrops asper* snake venom—synthetic Lys49 myotoxin II-(115-129)-peptide identifies its bactericidal region. *Eur J Biochem* 1998;253:452–461.
27. Rosenberg P. Phospholipases. In: Shyer WT, Mebs D, editors. *Handbook of toxinology*. New York: Dekker; 1990. p 67–277.
28. Kini RM. Structure-function relationships and mechanism of anticoagulant phospholipase A2 enzymes from snake venoms. *Toxicon* 2005;45:1147–1161.
29. Barbosa PS, Martins AM, Havt A, Toyama DO, Evangelista JS, Ferreira DP, Joazeiro PP, Beriam LO, Toyama MH, Fonteles MC, Monteiro HS. Renal and antibacterial effects induced by myotoxin I and II isolated from *Bothrops jararacussu* venom. *Toxicon* 2005;46:376–386.
30. Francis B, Gutierrez JM, Lomonte B, Kaiser, II. Myotoxin II from *Bothrops asper* (Terciopelo) venom is a lysine-49 phospholipase A2. *Arch Biochem Biophys* 1991;284:352–359.
31. Geoghegan P, Angulo Y, Cangelosi A, Diaz M, Lomonte B. Characterization of a basic phospholipase A2-homologue myotoxin isolated from the venom of the snake *Bothrops neuwiedii* (yarara chica) from Argentina. *Toxicon* 1999;37:1735–1746.
32. Gutierrez JM, Chaves F, Gene JA, Lomonte B, Camacho Z, Schosinsky K. Myonecrosis induced in mice by a basic myotoxin isolated from the venom of the snake *Bothrops nummifer* (jumping viper) from Costa Rica. *Toxicon* 1989;27:735–745.
33. Gutierrez JM, Lomonte B. Phospholipase A2 myotoxins from *Bothrops* snake venoms. *Toxicon* 1995;33:1405–1424.
34. Lomonte B, Angulo Y, Calderon L. An overview of lysine-49 phospholipase A2 myotoxins from crotalid snake venoms and their structural determinants of myotoxic action. *Toxicon* 2003;42:885–901.
35. Mebs D, Kuch U, Coronas FIV, Batista CVF, Gumprecht A, Possani LD. Biochemical and biological activities of the venom of the Chinese pitviper *Zhafermia mangshanensis*, with the complete amino acid sequence and phylogenetic analysis of a novel Arg49 phospholipase A(2) myotoxin. *Toxicon* 2006;47:797–811.
36. Wei JF, Wei XL, Chen QY, Huang T, Qiao LY, Wang WY, Xiong YL, He SH. N49 phospholipase A2, a unique subgroup of snake venom group II phospholipase A2. *Biochim Biophys Acta* 2006;1760:462–471.
37. Gutierrez JM, Lomonte B, Cerdas L. Isolation and partial characterization of a myotoxin from the venom of the snake *Bothrops nummifer*. *Toxicon* 1986;24:885–894.
38. Nishioka Sde A, Silveira PV. A clinical and epidemiologic study of 292 cases of lance-headed viper bite in a Brazilian teaching hospital. *Am J Trop Med Hyg* 1992;47:805–810.
39. Otero R, Gutierrez J, Beatriz Mesa M, Duque E, Rodriguez O, Luis Arango J, Gomez F, Toro A, Cano F, Maria Rodriguez L, Caro E, Martinez J, Cornejo W, Mariano Gomez L, Luis Uribe F, Cardenas S, Nunez V, Diaz A. Complications of *Bothrops*, *Porthidium*, and *Bothriechis* snakebites in Colombia. A clinical and epidemiological study of 39 cases attended in a university hospital. *Toxicon* 2002;40:1107–1114.
40. Gutierrez JM, Theakston RD, Warrell DA. Confronting the neglected problem of snake bite envenoming: the need for a global partnership. *PLoS Med* 2006;3:e150.
41. Cardoso JL, Fan HW, Franca FO, Jorge MT, Leite RP, Nishioka SA, Avila A, Sano-Martins IS, Tomy SC, Santoro ML, Chudzinski AM, Castro SCB, Kamiguti AS, Kelen EMA, Hirata MH, Miranda RMS, Theakston RDG, Warrell DA. Randomized comparative trial of three antivenoms in the treatment of envenoming by lance-headed vipers (*Bothrops jararaca*) in Sao Paulo, Brazil. *Q J Med* 1993;86:315–325.
42. Milani R, Jorge MT, DeCampos FPF, Martins FP, Bousso A, REFAU>Cardoso JLC, Ribeiro LA, Fan HW, Franca FOS, SanoMartins IS, Cardoso D, Fernandez IDOF, Fernandes JC, Aldred VL, Sandoval MP, Puerto G, Theakston RDG, Warrell DA. Snake bites by the jararacucu (*Bothrops jararacussu*): clinicopatho-

- logical studies of 29 proven cases in Sao Paulo State, Brazil. QJM-Mon J Assoc Physicians 1997;90:323–334.
43. Lomonte B, Leon G, Angulo Y, Rucavado A, Nunez V. Neutralization of *Bothrops asper* venom by antibodies, natural products and synthetic drugs: contributions to understanding snakebite envenomings and their treatment. *Toxicon* 2009;54:1012–1028.
 44. Ward RJ, Chioato L, de Oliveira AH, Ruller R, Sa JM. Active-site mutagenesis of a Lys49-phospholipase A₂: biological and membrane-disrupting activities in the absence of catalysis. *Biochem J* 2002;362 (Part 1):89–96.
 45. Maraganore JM, Merutka G, Cho W, Welches W, Kezdy FJ, Henrikson RL. A new class of phospholipases A₂ with lysine in place of aspartate 49. Functional consequences for calcium and substrate binding. *J Biol Chem* 1984;259:13839–13843.
 46. dos Santos JI, Fernandes CA, Magro AJ, Fontes MR. The intriguing phospholipases A₂ homologues: relevant structural features on myotoxicity and catalytic inactivity. *Protein Pept Lett* 2009;16:887–893.
 47. Chioato L, de Oliveira AHC, Ruller R, Sa JM, Ward RJ. Distinct sites for myotoxic and membrane-damaging activities in the C-terminal region of a Lys(49)-phospholipase A(2). *Biochem J* 2002;366:971–976.
 48. Chioato L, Aragao EA, Ferreira TL, de Medeiros AI, Faccioli LH, Ward RJ. Mapping of the structural determinants of artificial and biological membrane damaging activities of a Lys49 phospholipase A(2) by scanning alanine mutagenesis. *Biochim Et Biophys Acta-Biomemb* 2007;1768:1247–1257.
 49. Nunez CE, Angulo Y, Lomonte B. Identification of the myotoxic site of the Lys49 phospholipase A(2) from *Agkistrodon piscivorus piscivorus* snake venom: synthetic C-terminal peptides from Lys49, but not from Asp49 myotoxins, exert membrane-damaging activities. *Toxicon* 2001;39:1587–1594.
 50. Ward RJ, Alves AR, Ruggiero Neto J, Arni RK, Casari G. A SequenceSpace analysis of Lys49 phospholipases A₂: clues towards identification of residues involved in a novel mechanism of membrane damage and in myotoxicity. *Protein Eng* 1998;11:285–294.
 51. Cintra-Francischinelli M, Pizzo P, Angulo Y, Gutierrez JM, Montecucco C, Lomonte B. The C-terminal region of a Lys49 myotoxin mediates Ca²⁺ influx in C2C12 myotubes. *Toxicon* 2010;55:590–596.
 52. Calderon L, Lomonte B. Immunochemical characterization and role in toxic activities of region 115–129 of myotoxin II, a Lys49 phospholipase A₂ from *Bothrops asper* snake venom. *Arch Biochem Biophys* 1998;358:343–350.
 53. Calderon L, Lomonte B. Inhibition of the myotoxic activity of *Bothrops asper* myotoxin II in mice by immunization with its synthetic 13-mer peptide 115–129. *Toxicon* 1999;37:683–687.
 54. Lomonte B, Pizarro-Cerda J, Angulo Y, Gorvel JP, Moreno E. Tyr->Trp-substituted peptide 115–129 of a Lys49 phospholipase A(2) expresses enhanced membrane-damaging activities and reproduces its in vivo myotoxic effect. *Biochim Biophys Acta* 1999;1461:19–26.
 55. Lomonte B, Angulo Y, Santamaria C. Comparative study of synthetic peptides corresponding to region 115–129 in Lys49 myotoxic phospholipases A₂ from snake venoms. *Toxicon* 2003;42:307–312.
 56. dos Santos JI, Soares AM, Fontes MR. Comparative structural studies on Lys49-phospholipases A(2) from *Bothrops* genus reveal their myotoxic site. *J Struct Biol* 2009;167:106–116.
 57. Homsí-Brandeburgo MI, Queiroz LS, Santo-Neto H, Rodrigues-Simioni L, Giglio JR. Fractionation of *Bothrops jararacussu* snake venom: partial chemical characterization and biological activity of bothropstoxin. *Toxicon* 1988;26:615–627.
 58. Gutierrez JM, Nunez J, Diaz C, Cintra AC, Homsí-Brandeburgo MI, Giglio JR. Skeletal muscle degeneration and regeneration after injection of bothropstoxin-II, a phospholipase A₂ isolated from the venom of the snake *Bothrops jararacussu*. *Exp Mol Pathol* 1991;55:217–229.
 59. Pereira MF, Novello JC, Cintra AC, Giglio JR, Landucci ET, Oliveira B, Marangoni S. The amino acid sequence of bothropstoxin-II, an Asp-49 myotoxin from *Bothrops jararacussu* (Jararacucu) venom with low phospholipase A₂ activity. *J Protein Chem* 1998;17:381–386.
 60. Toyama MH, Costa PD, Novello JC, de Oliveira B, Giglio JR, da Cruz-Hofling MA, Marangoni S. Purification and amino acid sequence of MP-III 4R D49 phospholipase A₂ from *Bothrops pirajai* snake venom, a toxin with moderate PLA₂ and anticoagulant activities and high myotoxic activity. *J Protein Chem* 1999;18:371–378.
 61. Correa LC, Marchi-Salvador DP, Cintra AC, Sampaio SV, Soares AM, Fontes MR. Crystal structure of a myotoxic Asp49-phospholipase A₂ with low catalytic activity: insights into Ca²⁺-independent catalytic mechanism. *Biochim Biophys Acta* 2008;1784:591–599.
 62. Rigden DJ, Hwa LW, Marangoni S, Toyama MH, Polikarpov I. The structure of the D49 phospholipase A₂ piratoxin III from *Bothrops pirajai* reveals unprecedented structural displacement of the calcium-binding loop: possible relationship to cooperative substrate binding. *Acta Crystallogr D Biol Crystallogr* 2003;59 (Part 2):255–262.
 63. Bonfim VL, de Carvalho DD, Ponce-Soto LA, Kassab BH, Marangoni S. Toxicity of phospholipases A₂ D49 (6-1 and 6-2) and K49 (Bj-VII) from *Bothrops jararacussu* venom. *Cell Biol Toxicol* 2009;25:523–532.
 64. Fuly AL, Soares AM, Marcussi S, Giglio JR, Guimaraes JA. Signal transduction pathways involved in the platelet aggregation induced by a D-49 phospholipase A₂ isolated from *Bothrops jararacussu* snake venom. *Biochimie* 2004;86:731–739.
 65. McPherson A. Introduction to macromolecular crystallography. Hoboken: Wiley-Liss; 2003. 237 p.
 66. Otwinowski Z, Minor W. Processing of X-ray diffraction data collected in oscillation mode. *Macromol Crystallogr A* 1997;276:307–326.
 67. Brunger AT. Free R value: a novel statistical quantity for assessing the accuracy of crystal structures. *Nature* 1992;355:472–475.
 68. Murshudov GN, Vagin AA, Dodson EJ. Refinement of macromolecular structures by the maximum-likelihood method. *Acta Crystallogr D Biol Crystallogr* 1997;53 (Part 3):240–255.
 69. Emsley P, Cowtan K. Coot: model-building tools for molecular graphics. *Acta Crystallogr D Biol Crystallogr* 2004;60(Part 12, Part 1):2126–2132.
 70. Brunger AT, Adams PD, Clore GM, DeLano WL, Gros P, Grosse-Kunstleve RW, Jiang JS, Kuszewski J, Nilges M, Pannu NS, Read RJ, Rice LM, Simonson T, Warren GL. Crystallography & NMR system: a new software suite for macromolecular structure determination. *Acta Crystallogr Sect D-Biol Crystallogr* 1998;54:905–921.
 71. Harding MM. Geometry of metal-ligand interactions in proteins. *Acta Crystallogr D Biol Crystallogr* 2001;57 (Part 3):401–411.
 72. Harding MM. The geometry of metal-ligand interactions relevant to proteins. II. Angles at the metal atom, additional weak metal-donor interactions. *Acta Crystallogr D Biol Crystallogr* 2000;56 (Part 7):857–867.
 73. Fraústo da Silva JJR, Willians RJP. The Biological Chemistry of the Elements—The Inorganic Chemistry of Life. Oxford University Press: Oxford; 1991. 561 p.
 74. Laskowski RA, MacArthur MW, Moss DS, Thornton JM. Procheck—a program to check the stereochemical quality of protein structures. *J Appl Crystallogr* 1993;26:283–291.
 75. Jones TA, Bergdoll M, Kjeldgaard M. O: a macromolecule modeling environment. In: Bugg C, Ealick SE, editors. Crystallographic and Modeling Methods in Molecular Design. New York: Springer-Verlag; 1990. p 189–195.
 76. Krissinel E, Henrick K. Inference of macromolecular assemblies from crystalline state. *J Mol Biol* 2007;372:774–797.
 77. DeLano WL. The PyMOL molecular graphics system. San Carlos, CA: DeLano Scientific LLC; 2002.
 78. Schwartz AS, Pachter L. Multiple alignment by sequence annealing. *Bioinformatics* 2007;23:e24–e29.

79. Huelsenbeck JP, Ronquist F. MRBAYES: Bayesian inference of phylogenetic trees. *Bioinformatics* 2001;17:754–755.
80. Maddison WP, Maddison DR. Mesquite: a modular system for evolutionary analysis. Version 2.72. 2009. Available at: <http://mesquiteproject.org/mesquite2.72/mesquite/mesquite.html>.
81. Kaiser, II, Gutierrez JM, Plummer D, Aird SD, Odell GV. The amino acid sequence of a myotoxic phospholipase from the venom of *Bothrops asper*. *Arch Biochem Biophys* 1990;278:319–325.
82. Lomonte B, Gutierrez JM. A new muscle damaging toxin, myotoxin II, from the venom of the snake *Bothrops asper* (terciopelo). *Toxicon* 1989;27:725–733.
83. Cintra AC, Marangoni S, Oliveira B, Giglio JR. Bothropstoxin-I: amino acid sequence and function. *J Protein Chem* 1993;12:57–64.
84. Arni RK, Ward RJ, Gutierrez JM, Tulinsky A. Structure of a calcium-independent phospholipase-like myotoxic protein from *Bothrops asper* venom. *Acta Crystallogr D Biol Crystallogr* 1995;51 (Part 3):311–317.
85. Soares AM, Rodrigues VM, Homs-Brandeburgo MI, Toyama MH, Lombardi FR, Arni RK, Giglio JR. A rapid procedure for the isolation of the Lys-49 myotoxin II from *Bothrops moojeni* (caissaca) venom: biochemical characterization, crystallization, myotoxic and edematogenic activity. *Toxicon* 1998;36:503–514.
86. Watanabe L, Soares AM, Ward RJ, Fontes MRM, Arni RK. Structural insights for fatty acid binding in a Lys49-phospholipase A(2): crystal structure of myotoxin II from *Bothrops moojeni* complexed with stearic acid. *Biochimie* 2005;87:161–167.
87. Angulo Y, Gutierrez JM, Soares AM, Cho W, Lomonte B. Myotoxic and cytolytic activities of dimeric Lys49 phospholipase A(2) homologues are reduced, but not abolished, by a pH-induced dissociation. *Toxicon* 2005;46:291–296.
88. Murakami MT, Vicoti MM, Abrego JRB, Lourenzoni MR, Cintra ACO, Arruda EZ, Tomaz MA, Melo PA, Arni RK. Interfacial surface charge and free accessibility to the PLA(2)-active site-like region are essential requirements for the activity of Lys49 PLA(2) homologues. *Toxicon* 2007;49:378–387.
89. Cintra-Francischinelli M, Pizzo P, Rodrigues-Simioni L, Ponce-Soto LA, Rossetto O, Lomonte B, Gutierrez JM, Pozzan T, Montecucco C. Calcium imaging of muscle cells treated with snake myotoxins reveals toxin synergism and presence of acceptors. *Cell Mol Life Sci* 2009;66:1718–1728.
90. Matthews BW. Solvent content of protein crystals. *J Mol Biol* 1968;33:491–497.
91. Murakami MT, Arruda EZ, Melo PA, Martinez AB, Calil-Elias S, Tomaz MA, Lomonte B, Gutierrez JM, Arni RK. Inhibition of myotoxic activity of *Bothrops asper* myotoxin II by the anti-trypanosomal drug suramin. *J Mol Biol* 2005;350:416–426.
92. Wang XQ, Yang J, Gui LL, Lin ZJ, Chen YC, Zhou YC. Crystal structure of an acidic phospholipase A2 from the venom of *Agkistrodon halys pallas* at 2.0 Å resolution. *J Mol Biol* 1996;255:669–676.
93. Gu L, Zhang H, Song S, Zhou Y, Lin Z. Structure of an acidic phospholipase A2 from the venom of *Deinagkistrodon acutus*. *Acta Crystallogr D Biol Crystallogr* 2002;58 (Part 1):104–110.
94. Chandra V, Kaur P, Jasti J, Betzel C, Singh TP. Regulation of catalytic function by molecular association: structure of phospholipase A2 from *Daboia russelli pulchella* (DPLA2) at 1.9 Å resolution. *Acta Crystallogr D Biol Crystallogr* 2001;57 (Part 12):1793–1798.
95. Scott DL, Otwinowski Z, Gelb MH, Sigler PB. Crystal structure of bee-venom phospholipase A2 in a complex with a transition-state analogue. *Science* 1990;250:1563–1566.
96. Zhou X, Tan TC, Valiyaveetil S, Go ML, Kini RM, Velazquez-Campoy A, Sivaraman J. Structural characterization of myotoxic ecarpholin S from *Echis carinatus* venom. *Biophys J* 2008;95:3366–3380.
97. Arni RK, Fontes MR, Barberato C, Gutierrez JM, Diaz C, Ward RJ. Crystal structure of myotoxin II, a monomeric Lys49-phospholipase A2 homologue isolated from the venom of *Cerrophidion* (*Bothrops*) *godmani*. *Arch Biochem Biophys* 1999;366:177–182.
98. Magro AJ, Murakami MT, Marcussi S, Soares AM, Arni RK, Fontes MR. Crystal structure of an acidic platelet aggregation inhibitor and hypotensive phospholipase A2 in the monomeric and dimeric states: insights into its oligomeric state. *Biochem Biophys Res Commun* 2004;323:24–31.
99. Magro AJ, Soares AM, Giglio JR, Fontes MR. Crystal structures of BnSP-7 and BnSP-6, two Lys49-phospholipases A(2): quaternary structure and inhibition mechanism insights. *Biochem Biophys Res Commun* 2003;311:713–720.
100. Marchi-Salvador DP, Correa LC, Magro AJ, Oliveira CZ, Soares AM, Fontes MR. Insights into the role of oligomeric state on the biological activities of crotoxin: crystal structure of a tetrameric phospholipase A2 formed by two isoforms of crotoxin B from *Crotalus durissus terrificus* venom. *Proteins* 2008;72:883–891.
101. Murakami MT, Melo CC, Angulo Y, Lomonte B, Arni RK. Structure of myotoxin II, a catalytically inactive Lys49 phospholipase A(2) homologue from *Atropoides nummifer* venom. *Acta Crystallogr Sect F: Struct Biol Cryst Commun* 2006;62:423–426.
102. Murakami MT, Gabdoulkhalov A, Genov N, Cintra ACO, Betzel C, Arni RK. Insights into metal ion binding in phospholipases A(2): ultra high-resolution crystal structures of an acidic phospholipase A(2) in the Ca²⁺ free and bound states. *Biochimie* 2006;88:543–549.
103. Marchi-Salvador DP, Fernandes CA, Silveira LB, Soares AM, Fontes MR. Crystal structure of a phospholipase A(2) homologue complexed with p-bromophenacyl bromide reveals important structural changes associated with the inhibition of myotoxic activity. *Biochim Biophys Acta* 2009;1794:1583–1590.
104. Magro AJ, Fernandes CA, dos Santos JI, Fontes MR. Influence of quaternary conformation on the biological activities of the Asp49-phospholipases A2s from snake venoms. *Protein Pept Lett* 2009;16:852–859.
105. Ohno M, Chijiwa T, Oda-Ueda N, Ogawa T, Hattori S. Molecular evolution of myotoxic phospholipases A2 from snake venom. *Toxicon* 2003;42:841–854.
106. Chang Y, Li Y, Bao Y, An L. Neurotoxic activity of Gln49 phospholipase A(2) from *Gloydus ussuriensis* snake venom. *J Appl Toxicol* 2007;27:447–452.
107. Rodrigues RS, Izidoro LFM, Teixeira SS, Silveira LB, Hamaguchi A, Homs-Brandeburgo MI, Selistre-de-Araujo HS, Giglio JR, Fuly AL, Soares AM, Rodrigues VM. Isolation and functional characterization of a new myotoxic acidic phospholipase A(2) from *Bothrops pauloensis* snake venom. *Toxicon* 2007;50:153–165.
108. Santos-Filho NA, Silveira LB, Oliveira CZ, Bernardes CB, Menaldo DL, Fuly AL, Arantes EC, Sampaio SV, Mamede CC, Beletti ME, de Oliveira F, Soares AM. A new acidic myotoxic, anti-platelet and prostaglandin I₂ inducer phospholipase A2 isolated from *Bothrops moojeni* snake venom. *Toxicon* 2008;52:908–917.

ANEXO IV

Outras atividades desenvolvidas durante o período de Doutorado:

1. Cristalização e resultados preliminares de difração de raios X da B_jussuMP-I (uma metaloprotease de classe I do veneno da serpente *Bothrops jararacussu*). Estes estudos estavam previstos no projeto inicial, porém não conseguimos elucidar a estrutura da proteína devido à baixa resolução dos dados de difração de raios X obtidos (4,5 Å);
2. Cristalização e resultados preliminares de difração de raios X da B_jussuMP-II (uma metaloprotease de classe III do veneno da serpente *Bothrops jararacussu*). Estes estudos estavam previstos no projeto inicial, porém não conseguimos elucidar a estrutura da proteína também devido à baixa resolução dos dados de difração de raios X obtidos;
3. Cristalização e resultados preliminares de difração de raios X de uma L-aminoxidase do veneno de *Bothrops jararacussu*. Estes estudos estavam previstos no projeto inicial, porém não conseguimos elucidar a estrutura da proteína devido à baixa resolução dos dados de difração de raios X obtidos (4,0 Å);
4. Estudos de docking e dinâmica molecular do complexo formado entre a metaloprotease Neuwiedase e o inibidor vegetal *p*-cumarato. Este trabalho foi realizado em nosso laboratório em colaboração com a profa. Veridiana Melo, da UFU (Universidade Federal de Uberlândia) (artigo em fase de redação);
5. Estudos de modelagem teórica de uma L-aminoxidase de *Bothrops pauloensis* realizado em nosso laboratório como parte de uma colaboração com o prof. Dr. Andreimar Martins Soares. Este trabalho foi publicado no periódico *Biochimie*, em 2009 (Rodrigues *et al.*, 2009);
6. Redação do artigo “Comparative structural studies on Lys49-phospholipases A₂ from *Bothrops* genus reveal their myotoxic site” relativo aos dados obtidos no meu mestrado (publicado no periódico *Journal of Structural Biology* – dos Santos *et al.*, 2009)
7. Primeira autora do artigo de revisão sobre as características relevantes para a miotoxicidade e ausência de atividade catalítica em Lys49-PLA₂s, publicado no periódico *Protein & Peptide Letters* (dos Santos *et al.*, 2009);
8. Co-autora do artigo de revisão sobre a importância da estrutura quaternária para manifestação de diferentes tipos de atividades biológicas pelas Asp49-PLA₂s de venenos de serpentes, publicado no periódico *Protein & Peptide Letters* (Magro *et al.*, 2009).



Research paper

Structural and functional properties of Bp-LAAO, a new L-amino acid oxidase isolated from *Bothrops pauloensis* snake venom

Renata S. Rodrigues^{a,1}, Juliana F. da Silva^{b,1}, Johara Boldrini França^a, Fernando P.P. Fonseca^c, Antônio R. Otaviano^a, Flávio Henrique Silva^c, Amélia Hamaguchi^a, Angelo J. Magro^d, Antônio Sérgio K. Braz^e, Juliana I. dos Santos^d, Maria Inês Homs-Brandeburgo^a, Marcos R.M. Fontes^d, André L. Fuly^f, Andreimar M. Soares^{b,*}, Veridiana M. Rodrigues^{a,*}

^aInstituto de Genética e Bioquímica, Universidade Federal de Uberlândia, UFU, Pará 1720, CEP 38400-902 Uberlândia, MG, Brazil

^bDepartamento de Análises Clínicas, Toxicológicas e Bromatológicas, Faculdade de Ciências Farmacêuticas de Ribeirão Preto, Universidade de São Paulo, FCFRP-USP, Ribeirão Preto, SP, Brazil

^cDepartamento de Genética e Evolução, Universidade Federal de São Carlos, UFSCar, São Carlos, SP, Brazil

^dDepartamento de Física e Biofísica, Instituto de Biociências, Universidade Estadual Paulista Júlio de Mesquita Filho, UNESP, Botucatu, SP, Brazil

^eDepartamento de Genética, Instituto de Biociências, Universidade Estadual Paulista Júlio de Mesquita Filho, UNESP, Botucatu, SP, Brazil

^fDepartamento de Biologia Celular e Molecular (GCM), Instituto de Biologia, Universidade Federal Fluminense, UFF, Niterói, RJ, Brazil

ARTICLE INFO

Article history:

Received 21 August 2008

Accepted 11 December 2008

Available online 24 December 2008

Keywords:

Bothrops (neuwiedi) pauloensis

L-Amino acid oxidase

cDNA library

Molecular dynamics simulation

Phylogenetic analysis

ABSTRACT

An L-amino acid oxidase (Bp-LAAO) from *Bothrops pauloensis* snake venom was highly purified using sequential chromatography steps on CM-Sepharose, Phenyl-Sepharose CL-4B, Benzamidine Sepharose and C18 reverse-phase HPLC. Purified Bp-LAAO showed to be a homodimeric acidic glycoprotein with molecular weight around 65 kDa under reducing conditions in SDS-PAGE. The best substrates for Bp-LAAO were L-Met, L-Leu, L-Phe and L-Ile and the enzyme showed a strong reduction of its catalytic activity upon L-Met and L-Phe substrates at extreme temperatures. Bp-LAAO showed leishmanicidal, antitumoral and bactericidal activities dose dependently. Bp-LAAO induced platelet aggregation in platelet-rich plasma and this activity was inhibited by catalase. Bp-LAAO-cDNA of 1548 bp codified a mature protein with 516 amino acid residues corresponding to a theoretical isoelectric point and molecular weight of 6.3 and 58 kDa, respectively. Additionally, structural and phylogenetic studies identified residues under positive selection and their probable location in Bp-LAAO and other snake venom LAAOs (svLAAOs). Structural and functional investigations of these enzymes can contribute to the advancement of toxicology and to the elaboration of novel therapeutic agents.

© 2009 Elsevier Masson SAS. All rights reserved.

1. Introduction

Snake venoms cause a variety of different biological effects as they are a mixture of simple and complex substances, such as biologically active peptides and proteins [1–5], but their biochemical characteristics change according to the snake species studied.

The Viperidae family is responsible for most and more serious ophidian accidents reported, not only in Brazil but also in other

Abbreviations: Bp-LAAO, *Bothrops (neuwiedi) pauloensis* L-amino acid oxidase; CFU, colony-forming unit; FAD, flavin adenine dinucleotide; LAAO, L-amino acid oxidase; PNGase, peptide N-glycosidase; RP-HPLC, reverse-phase high performance liquid chromatography; svLAAO, snake venom L-amino acid oxidase.

* Corresponding authors. Tel.: +55 34 32182203x22; fax: +55 32182203x24.

E-mail addresses: andreims@fcfrp.usp.br (A.M. Soares), veridiana@ingeb.ufu.br (V.M. Rodrigues).

¹ These authors contributed equally to this work.

western countries. Their venoms are usually composed of a complex mixture of proteins, enzymes, peptides and inorganic components. The proteins belong to multiple families, such as phospholipases A₂, disintegrins, metalloproteases, serine proteases, nerve growth factor (NGF), L-amino acid oxidases and others.

L-Amino acid oxidases (LAAOs) are widely distributed in the venomous snake families Viperidae, Crotalidae and Elapidae [6]. Besides those from snake venoms, different LAAOs have been isolated from sea animals, including achacin, from the mucus of the giant snail, *Achatina fulica* Férussac, escapin [7], from the ink of the sea hare *Aplysia californica*, and APIT [8] from *Aplysia punctata*, as well as from bacteria, fungi and plants [9].

LAAOs (E.C.1.4.3.2) are flavoenzymes that catalyze oxidative deamination of L-amino acids to form corresponding α -keto acids, hydrogen peroxide and ammonia. They are usually homodimeric FAD-binding glycoproteins with molecular mass around 110–150 kDa. They are responsible for the yellow color of snake venoms, containing

flavin as the prosthetic group. LAAOs are thought to contribute to the toxicity of the venom due to the production of hydrogen peroxide during the oxidation reaction [10]. They can also present antimicrobial, antiprotozoal, leishmanicidal or anticoagulant activity, induce or inhibit platelet aggregation, are cytotoxic and antiproliferative on tumor cells [1,11–19].

In the last 10–15 years, LAAOs have gained interest due to their effects on various microorganisms [11–13], blood components (platelets) [11,14–19], bacteria [10–12,18,20] and cells, including cancer cells [5,21–23].

LAAOs can be found in venoms of several snake species, including *Bothrops pauloensis*, described by Amaral [24] as *Bothrops neuwiedi pauloensis*, as one out of 12 subspecies of *B. neuwiedi* [25]. Following the systematic revision of *B. neuwiedi* complex by Silva [26], the 12 subspecies resulted in seven distinct species as accepted by the Brazilian Society of Herpetology [27].

Recently, snake venom LAAOs have become an interesting object for structural and molecular biology studies. Although little is known about their primary and tertiary structures, through the analysis of their putative amino acid sequences, it is possible to determinate the FAD-binding and N-glycosylation sites, as well as to compare them phylogenetically. This paper reports the isolation of a new *l*-amino acid oxidase from *B. pauloensis* snake venom (Bp-LAAO) and its biochemical, functional and structural characterization.

2. Materials and methods

2.1. Reagents and venom

B. pauloensis snake venom, vacuum dried and stored at 4 °C, was kindly supplied by the biologist Luiz H.A. Pedrosa (FMRP-USP, Ribeirão Preto, SP, Brazil). CM-Sepharose, Phenyl-Sepharose CL-4B and Benzamidine Sepharose were purchased from Amersham Life Science Inc. All other reagents used for chemical and biological characterization were of analytical grade and purchased from Sigma Chem. Co. or Gibco BRL.

2.2. Purification of LAAO from *B. pauloensis*

B. pauloensis crude venom (500 mg) was applied on a CM-Sepharose column (2.0 × 20 cm), previously equilibrated with 0.05 M ammonium bicarbonate (AMBI), pH 7.8. Elution was carried out using the same buffer at a flow rate of 20 mL/h, collecting 3 mL/min. The resulting fractions were assayed for their enzymatic activity and the active fraction was concentrated by ultrafiltration (AMICON YM 30,000). After that, the sample (28 mg) was applied on a Phenyl-Sepharose CL-4B column (1.0 × 10 cm) equilibrated with 10 mM Tris–HCl buffer plus 4 M NaCl, pH 8.5. Elution occurred at room temperature, with 10 mL of the same buffer, followed by decreasing concentrations of NaCl (3, 2, 1 and 0.5 M) in 10 mM Tris–HCl buffer, pH 8.5, ending the elution process with water. The active fraction was concentrated by ultrafiltration (AMICON YM 30,000) and 12 mg were applied on a Benzamidine-Sepharose column (1.8 × 4.5 cm) equilibrated with 0.02 M sodium phosphate buffer, pH 7.8 and eluted with glycine buffer (0.02 M, pH 3.2) at a flow rate of 3.0 mL/min. The final sample was named Bp-LAAO. For the purity assay, 1 mg of Bp-LAAO was applied into a C18 RP-HPLC column (0.46 × 15.0 cm), equilibrated with 0.1% (v/v) trifluoroacetic acid (TFA) followed by an acetonitrile gradient from 28% to 60% (v/v) in 0.1% TFA for 25 min. All chromatographic procedures were performed at room temperature. For N-terminal sequencing, about 5 µg of the purified protein was run on a 12.5% SDS-PAGE gel and electroblotted onto a polyvinylidene difluoride membrane (ProBlott™, Perkin–Elmer Applied Biosystems Division,

Washington, UK). After staining with Coomassie Brilliant Blue, the protein band of interest was cut out and subjected to Edman degradation in a gas phase PPSQ-23A Shimadzu Sequence apparatus as recommended by the manufacturer.

2.3. Protein determination and *l*-amino acid oxidase assay

Protein concentration was determined by the method previously described by Itzhaki and Gill [28]. LAAO activity was measured by an adaptation of the method previously described by Ponnudurai et al. [29]. In this assay, the oxidative deamination of *l*-leucine produced hydrogen peroxide, which was reduced, in the presence of horseradish peroxidase, by *o*-phenylenediamine to produce a colored oxidized product, which was spectrophotometrically monitored at 490 nm. Briefly, 10 µL of the enzyme (1 µg/µL) was incubated at 25 °C with 490 µL of a solution containing 200 µg of *o*-phenylenediamine, 10 nmol of *l*-Leu, and 10 µg of horseradish peroxidase (HRP) in 10 mM Tris–HCl buffer at pH 7.2. The reaction was stopped by addition of 0.5 mL of 10% (m/v) citric acid. One unit (1 U) of enzyme activity was defined as the amount of enzyme able to produce 1 µmol of hydrogen peroxide/min, under the described conditions. In order to find out the affinity for different substrates, other amino acids (10 nmol) were assayed at different temperatures under the same experimental conditions.

2.4. Biochemical characterization

The sample was also assayed for purity by 12% (w/v) SDS-PAGE, in Tris–glycine buffer pH 8.4 for 120 min at 10 mA and 200 V. For determination of *N*-linked sugars, the enzyme was submitted to PNGase F treatment under non-denaturing conditions. Briefly, 15 µg of Bp-LAAO in phosphate buffer (50 mM, pH 7.5) was treated with 1 µL of PNGase F (0.08 U/mL) and incubated at 37 °C for 4 h. Native PAGE and enzymatic assays were subsequently carried out to evaluate the activity of the deglycosylated Bp-LAAO.

2.5. Antitumor activity

Human breast (SKBR-3) (ATCC HTB-30) and acute T cell leukemia (Jurkat) (TIB-152™) cancer cell lines were maintained on RPMI 1640 medium supplemented with 2 mM *l*-glutamine, 1.5 g/L sodium bicarbonate, 4.5 g/L glucose, 10 mM HEPES, 1.0 mM sodium pyruvate, 10% fetal bovine serum, 100 U/mL penicillin, and 100 µg/mL streptomycin. All cell culture reagents were purchased from Gibco. All cell lines were maintained at 37 °C in 5% CO₂ and 95% air with more than 95% humidity. Tumor cytotoxic activity of LAAO was assayed with 3-(4,5-dimethylthiazol-2-yl)-2,5-diphenyltetrazolium bromide (MTT) staining as previously described by Mosmann [30]. Tumor cells cultivated in appropriate flasks and maintained in continuously exponential growth were detached with 0.05% trypsin plus 0.02% EDTA in calcium-free phosphate-buffered saline (PBS) and washed three times with RPMI medium at 500 × g/15 min/10 °C. Cells were disposed in 96-well plates at a density of 1 × 10⁵ cells per well. After 24 h, the medium was removed and fresh medium, with or without different concentrations of LAAO (0.1, 0.5, and 1.0 µg/mL), was added to the wells and incubated for 24 h. Jurkat cells (4 × 10⁴/well) were also incubated for 24 h with 5 mM exogenous H₂O₂. Cytotoxic rate was calculated as follows: % of cytotoxicity of compounds = 1 – Abs drug treated / Abs control × 100.

In some experiments, cytotoxic activity was determined on Erlich ascitic tumor (EAT) cells grown in the peritoneal cavity of Swiss mice [31]. EAT cells were suspended in Tyrode–Ringer buffer (4 × 10⁶ cells in the final volume of 1 mL) and incubated with several concentrations of LAAO (0.1, 0.5, and 1.0 µg/mL) for 60 min.

100 μ L of Trypan blue solution (1% in saline) was then added and the unviable stained cells, as well as unstained cells, were independently counted using a hemocytometer. Catalase was incubated with EAT cells and Bp-LAAO (1.0 μ g/mL) for 60 min and assayed for the antitumor activity.

2.6. Leishmanicidal activity

Leishmania strains and culture conditions: promastigote forms of all *Leishmania* species used in our experiments (*Leishmania amazonensis*—MPRO/BR/72/M1841-LV-79; *Leishmania braziliensis*—MHOM/BR/75/M2904; *Leishmania major*—LV-39, clone 5-Rho-SU/59/P; and *Leishmania donovani*—clone LV9-3 from MHOM/ET/67/HU3) were grown in M199 medium (Gibco) supplemented with 40 mM Hepes (pH 7.4), 0.1 mM adenine, 7.7 mM hemin, 10% (v/v) heat-inactivated fetal calf serum (FCS), 50 U/mL penicillin, and 50 μ g/mL streptomycin. Cultures were incubated at 26 °C, and cells were kept at densities ranging between 5×10^5 and 3×10^7 parasites/mL. Viability strains were evaluated from motility, and cell density was determined using a hemocytometer. Cytotoxic effect of the Bp-LAAO on *Leishmania* viability: parasites (3×10^6 /well) were incubated in M199 medium supplemented with 10% heat-inactivated FCS in the presence or absence of Bp-LAAO (0.2–5 μ g/mL) for 4 h. Promastigotes of *L. major* were incubated with Bp-LAAO (5 μ g/mL) or (5 mM) exogenous H₂O₂ and catalase (0.1 mg/mL) for 12 h at 25 °C in a microplate assay, in order to abolish the action of hydrogen peroxide. Parasites were then pulsed with 0.5 μ Ci/well [³H]thymidine, and the incorporation of radioisotope by viable cells was accessed after 16 h in a β -counter [32]. Values of EC₅₀ were obtained from a sigmoid dose–response curve using the GraphPad Prism Software.

2.7. Bactericidal activity

Approximately 10^5 Colony-Forming Units (CFU) of *Escherichia coli* (ATCC-25923) and *Staphylococcus aureus* (ATCC-1556) were incubated with 2 mL of Mueller–Hinton medium at 37 °C for 24 h. After growth, aliquots containing approximately 4×10^5 CFU of each bacterium were incubated with increasing concentrations of Bp-LAAO (5, 15 and 25 μ g) for 24 h at 37 °C. The bactericidal activity was measured by the decreasing of absorbance at 600 nm. Catalase was incubated with *E. coli* and *S. aureus* and Bp-LAAO (25 μ g/mL) and assayed for bactericidal activity.

2.8. Platelet aggregation

This assay was carried out as previously described by Fuly et al. [33]. Platelet-rich plasma (PRP) was prepared from citrated human blood by centrifugation (360 \times g/12 min) at room temperature. The platelet aggregation was measured for 5 min by turbidimetric assay using whole blood Lumi-Aggregometer (Chrono-Log Corporation). Assays were performed at 37 °C in siliconized glass cuvettes using 200 μ L of PRP, under stirring, and aggregation was triggered after pre-incubation for 2 min with aliquots of the purified enzyme. Control experiments were carried out using only the platelet agonists collagen (5 μ g/mL) or ADP (10 μ g/mL). Different doses of catalase (0–500 μ g/mL) were previously incubated with Bp-LAAO (25 μ g/mL) for 30 min at room temperature and assayed for platelet aggregation.

2.9. Screening and isolation of LAAO from a venom gland cDNA library

Venom gland from *B. pauloensis* adult snake was dissected 3 days after venom extraction, when transcription is most stimulated

[34]. The pair of venom glands was homogenized under liquid nitrogen and total RNA was extracted by the Trizol method. From this total RNA, the mRNA was purified using magnetic separation kit (Promega, USA) and 3 μ g of mRNA were used in CloneMiner cDNA Library Construction Kit (Invitrogen, UK). First and second cDNA strands were synthesized as described by the manufacturer protocols and size fractionation of cDNA was carried out through 1 mL column previously packed with Sephacryl S-500 resin, with the eluted fractions pooled until 300 ng of cDNA was obtained. The cDNA was precipitated with ethanol and then resuspended in 50 μ L of sterile milli-Q water and submitted to PCR. The primers used were designed according to the N-terminal sequence, as determined for the toxin and also through multiple alignments with other similar toxins, LAAO forward (ATGAATGTCTTCTTTATGTTCTC), LAAO reverse (CTCAGAAGCAGCATTACATC), LAAO internal forward (GGAATCTGAGTCCTGGAGC), LAAO internal reverse (CGCTTCTTTGGCGGAAGGG). After amplification of the obtained cDNA, the PCR products were analyzed regarding the amplified size by means of gel electrophoresis on 1% agarose. The gel was stained with ethidium bromide (0.3 mg/mL) and revealed under UV light. Purification of the PCR bands was performed using the Wizard SV Gel and PCR clean up system (Promega) kit, according to the manufacturer specifications. The Ins T/A clone PCR Product Kit (Fermentas) was used for rapid cloning of PCR products in pTZ57R/T plasmids. The bacteria were selected on a medium containing ampicillin and visualized after adding IPTG and X-Gal in the culture medium. After selection, the colonies of recombinant bacteria were assayed by PCR and gel electrophoresis for cloning confirmation. The PCR products were purified and submitted to sequencing, using the kit DYEnamic ET Terminator Automated Sequencing Kit (GE Healthcare, UK) on MEGA-BACE 1000 automated DNA sequencer (GE Healthcare, UK). The Base Caller Cimarron 3.12 software was used to analyze the electropherograms and generate the sequences, which were then aligned in the software Bioedit version 7.0.5.3.

2.10. Identification of homologous sequences

Homologous sequences were obtained from NCBI database (<http://www.ncbi.nlm.nih.gov>) using the algorithm BLASTP and the Bp-LAAO sequence as query. BLOSUM45 matrix was used for scoring the sequence alignments, with the other algorithm parameters set as default. The minimum *e*-value presented by the selected sequences was $9e-143$. The selected homologous proteins and their respective database identification codes are shown in Table 2.

2.11. Sequences alignment, phylogenetic analysis and identification of amino acid residues under positive evolutionary pressure

The alignment of the selected sequences was performed by program AMAP v.2.0 [35]. Phylogenetic analysis was executed using the programs TREE-PUZZLE v.5.2 [36], MrBayes v.3.1.2 [37], and MEGA v.4.0.2 [38]. TREE-PUZZLE phylogenetic tree was generated based on the Neighbor-joining method [39] and quartet sampling (10 000 puzzling steps) [40]. Bayesian MCMC analysis was executed by program MrBayes 3.1.2 running 75 900 cycles. The phylogenetic tree built by the program MEGA v.4.0.2 was generated by Neighbor-joining method, with complete deletion option and 2000 replications for bootstrap test [41]. Evolutionary distances of all phylogenetic trees were computed using the JTT matrix-based method [42]. The LAAOs from *Monodelphis domestica* and *Mus musculus* were defined as out groups. All protein sequences utilized in the phylogenetic analysis and their respective four-letter identification codes are shown in Table 2.

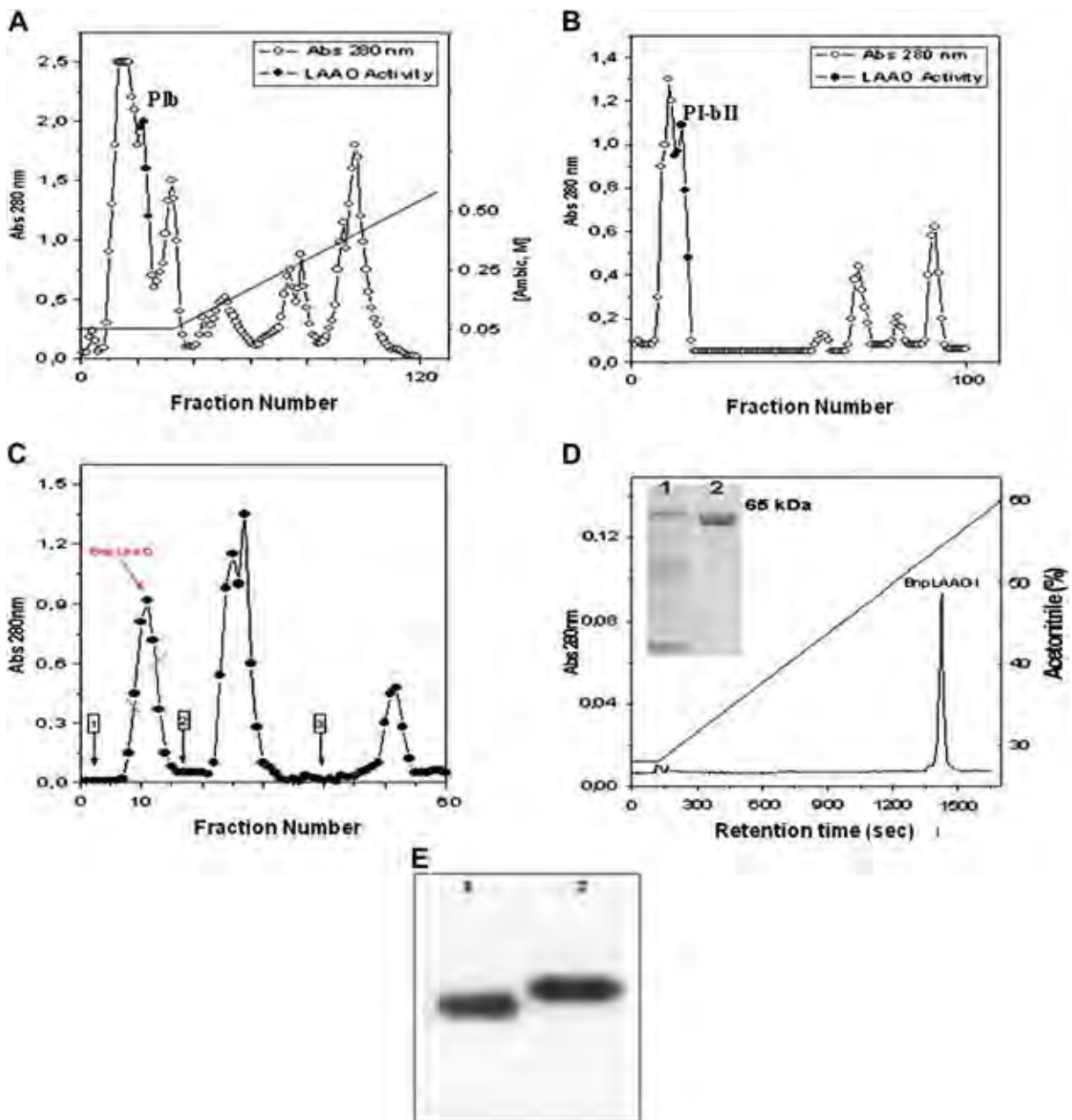


Fig. 1. Isolation and biochemical characterization of Bp-LAAO. (A) Ionic chromatography of *Bothrops pauloensis* venom on a CM-Sepharose column, previously equilibrated with ammonium bicarbonate buffer (0.05 M, pH 7.8) and eluted at the flow rate of 30 mL/h with the same buffer. (B) PIb was rechromatographed on a Phenyl-Sepharose column, previously equilibrated with 0.01 M Tris-HCl plus 4.0 M NaCl, pH 8.5, at room temperature and then eluted with a decreasing concentration gradient from 4 to 0 M NaCl plus 0.01 M Tris-HCl, pH 8.5, and finished with water. (C) The active fraction (LAAO) was rechromatographed on a Benzamidine-Sepharose column, previously equilibrated and eluted with Milli-Q water (1), followed by 0.02 M sodium phosphate, pH 7.8 (buffer 2) and glycine buffer (0.02 M, pH 3.2) (buffer 3) at flow rate of 3 mL/min. (D) Chromatography profile by RP-HPLC of Bp-LAAO. SDS-PAGE at 12% (w/v) in Tris-glycine buffer, pH 8.4. Lanes: 1 – molecular weight markers; 2 – Bp-LAAO (5 µg). (E) Native PAGE (12%) of Bp-LAAO stained by enzymatic activity. Lanes: 1 – Bp-LAAO after treatment with PNGase F; 2 – native Bp-LAAO.

The amino acid residues under positive evolutionary pressure of the svLAAO sequences from Viperidae, Elapidae and Viperidae/Elapidae phylogenetic groups were identified using the program MrBayes v.3.1.2 and the specific commands 'set nucmodel = codon nst = 2 omega = 3', 'report possel = yes'. Each chain was run for 60 000 cycles. The sump and sumt commands were used to tabulate posterior probabilities of positive selection of each amino acid site, and to build consensus trees. Results of estimations obtained before the process reached convergence were discarded. Only the amino acid residues with at least 95% probability of positive selection were considered for analysis.

2.12. Protein modeling

The crystallographic model of *Calloselasma rhodostoma* svLAAO (PDB code 2iid_chain A) was selected as template for the initial theoretical Bp-LAAO structural model, according data obtained from the based-threading method program HHpred [43], available at the Max-Planck Institute for Developmental Biology server (<http://toolkit.tuebingen.mpg.de/hhpred>). The initial theoretical Bp-LAAO structural model was generated by the program MODELLER 8v2 [44] using the selected template.

Table 1
Substrate specificity of L-amino acid oxidase from *Bothrops pauloensis* venom.

Amino acid	Specific activity (U/mg)	Amino acid	Specific activity (U/mg)
Met	580	Glu	140
Leu	575	Val	110
Phe	545	Ala	60
Ile	480	Pro	0
Arg	340	Thr	0
His	335	Ser	0
Trp	310	Cys	0
Tyr	140		

2.13. Molecular dynamics simulation

The output model from program MODELLER 8v2 was submitted to a molecular dynamics (MD) simulation executed by the program GROMACS (Groningen Machine for Chemical Simulation) v.3.3.1 [45,46] in the presence of explicit water molecules [47], using an Intel Core 2 Quad x64 equipped with a Ubuntu 8.04 Linux operational system. Protonation states of charged groups were set according to pH 7.0. Counter ions were added to neutralize the system and the GROMOS 96 53a6 force field [48] was chosen to perform the MD simulation. The minimum distance between any atom of the protein and the box wall was 1.0 nm. An energy minimization (EM) using a steepest descent algorithm was performed to generate the starting configuration of the system. After this step, 200 ps of MD simulation with position restraints applied to the protein (PRMD) were executed in order to relax the system gently. Then, 5 ns of unrestrained MD simulation were calculated to evaluate the stability of the structures. All the MD simulations were carried out in a periodic truncated dodecahedron box under constant temperature (298 K) and pressure (1.0 bar) maintained by the coupling to an external heat and an isotropic. FAD topology and coordinates were generated by the Dundee PRODRG2.5 Server (beta) (http://davapc1.bioch.dundee.ac.uk/cgi-bin/prodrg_beta).

2.14. Evaluation of the theoretical Bp-LAAO structural models

Overall stereochemical quality of the theoretical models of Bp-LAAO was checked with the programs PROCHECK v.3.5.4

Table 2
Homologue sequences to Bp-LAAO selected in the NCBI database.

Sequence (four-letter identification code ^a)	Species or subspecies	Snake family	Database code
L-Amino acid oxidase (Bjar)	<i>Bothrops jararacussu</i>	Viperidae	gi 82127391
Bp-LAAO (Bpau)	<i>Bothrops pauloensis</i>	Viperidae	gi 195927838
L-Amino acid oxidase (Bmoo)	<i>Bothrops moojeni</i>	Viperidae	gi 82127389
L-Amino acid oxidase (Crho)	<i>Calloselasma rhodostoma</i>	Viperidae	gi 20141785
L-Amino acid oxidase (Crho2)	<i>Calloselasma rhodostoma</i>	Viperidae	gi 157883889
L-Amino acid oxidase (Cada)	<i>Crotalus adamanteus</i>	Viperidae	gi 6093636
Apoxin-1 (Catr)	<i>Crotalus atrox</i>	Viperidae	gi 124106294
L-Amino acid oxidase (Eoce)	<i>Echis ocellatus</i>	Viperidae	gi 205275159
L-Amino acid oxidase (Gblo)	<i>Gloydius blomhoffi</i>	Viperidae	gi 75570145
L-Amino acid oxidase (Ghal)	<i>Gloydius halys</i>	Viperidae	gi 82088273
L-Amino acid oxidase (Scat)	<i>Sistrurus catenatus edwardsi</i>	Viperidae	gi 109254996
L-Amino acid oxidase (Tste)	<i>Trimeresurus stejnegeri</i>	Viperidae	gi 33355627
L-Amino acid oxidase (Vste)	<i>Viridovipera stejnegeri</i>	Viperidae	gi 82090465
L-Amino acid oxidase (Bfas)	<i>Bungarus fasciatus</i>	Elapidae	gi 126035653
L-Amino acid oxidase (Bmul)	<i>Bungarus multicinctus</i>	Elapidae	gi 126035649
L-Amino acid oxidase precursor (Dves)	<i>Demansia vestigiata</i>	Elapidae	gi 166216291
L-Amino acid oxidase (Nscu)	<i>Notechis scutatus scutatus</i>	Elapidae	gi 123913796
L-Amino acid oxidase (Ohan)	<i>Ophiophagus hannah</i>	Elapidae	gi 126035644
L-Amino acid oxidase (Oscu)	<i>Oxyuranus scutellatus</i>	Elapidae	gi 123916680
L-Amino acid oxidase (Paus)	<i>Pseudechis australis</i>	Elapidae	gi 123916679
Hypothetical protein LOC417039 (Ggal)	<i>Gallus gallus</i>	–	gi 150247106
L-Amino acid oxidase (Mgal)	<i>Meleagris gallopavo</i>	–	gi 169730353
Hypothetical protein similar to L-amino acid oxidase 1 (Mdom)	<i>Monodelphis domestica</i>	–	gi 126330514
L-Amino acid oxidase 1 (Mmus)	<i>Mus musculus</i>	–	gi 31981608

^a Identification code used for phylogenetic analysis.

[49] and ProSA-web (<https://prosa.services.came.sbg.ac.at/prosa.php>) [50].

3. Results

In this work, the purification of Bp-LAAO was successfully carried out by three chromatographic steps (Fig. 1). After the first chromatography on a CM-Sepharose, the active fraction, referred to as PIb, was identified by means of enzymatic assays (Fig. 1A). PIb fraction was concentrated and subsequently placed on a Phenyl-Sepharose CL-4B column (Fig. 1B). LAAO activity was detected in the second fraction, named PI-bII. The active pool (PI-bII) was resolved into other four fractions on a Benzamide-Sepharose column (Fig. 1C). The active fraction, named Bp-LAAO, was still analyzed for purity by reverse-phase HPLC chromatography (Fig. 1D). Bp-LAAO presented a molecular mass of approximately 65 kDa in SDS-PAGE (Fig. 1D). Bp-LAAO deglycosylation was confirmed by PAGE, when the enzyme was treated with PNGase (Fig. 1E). The Bp-LAAO enzymatic activity was not modified after deglycosylation, suggesting that the sugar portion is not crucial for its activity (results not shown).

The affinity of Bp-LAAO to different substrates was accessed for further biochemical characterization. The enzyme showed higher affinity to the hydrophobic amino acids L-Met, L-Leu, L-Phe and L-Ile. For other amino acids, the catalytic affinity was very low (Ala, Val, Glu and Tyr) or inexistent (L-Pro, L-Thr, L-Ser and L-Cys) (Table 1). Bp-LAAO had its activity gradually diminished under heating until 45 °C. After heating at 60 °C and 70 °C for 10 min, 80% and 100% of its activity were lost, respectively. After freezing at –70 °C for 24 h, the enzyme lost 75% of its enzymatic activity. After lyophilization, only about 12% of its activity was kept.

Bp-LAAO dose dependently induced cytotoxicity in human breast (SKBR-3), acute T cell leukemia (Jurkat) cancer and Erlich ascitic tumor (EAT) cell lines. The cytotoxicity of Bp-LAAO upon EAT cells was inhibited by catalase (Fig. 2A).

To study the cytotoxicity of Bp-LAAO, it was examined the effect of this enzyme and exogenous H₂O₂ on cell viability in the presence or absence of catalase. Jurkat cells (4 × 10⁴/well) incubated with 1.0 µg/mL Bp-LAAO underwent cell death after 24 h of incubation, similar to cells incubated with 5 mM H₂O₂ (results not shown).

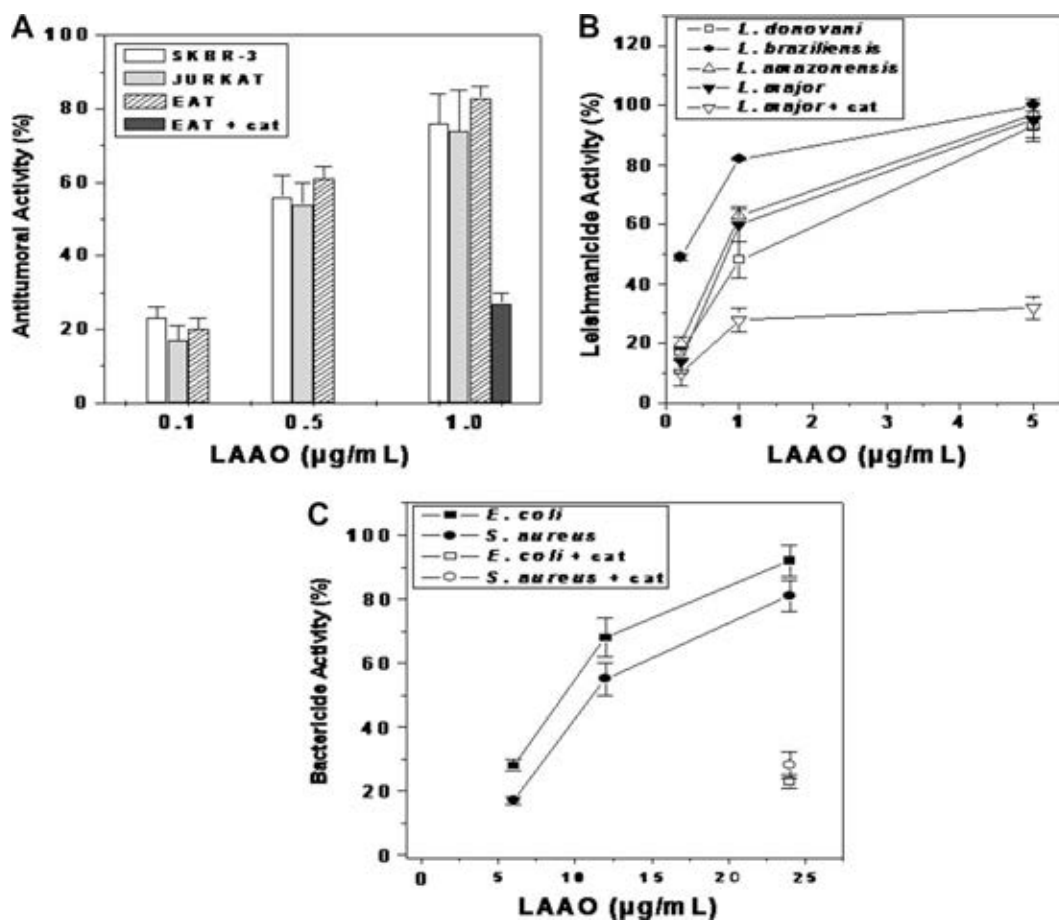


Fig. 2. Biochemical properties of Bp-LAAO. (A) Antitumor activity of Bp-LAAO upon different cell lines. Different concentrations (0.1, 0.5 and 1.0 µg/mL) of Bp-LAAO were incubated with human breast cancer cells (SKBR-3), acute T cell leukemia (JURKAT) and Erlich ascitic tumor (EAT) cell lines. The activity (Bp-LAAO + EAT) was reduced in the presence of catalase (100 µg/mL). Data are expressed as means \pm SD ($n = 03$). Control wells were cultivated in the presence of culture medium alone. (B) Leishmanicidal dose-dependent effect induced by the Bp-LAAO upon *Leishmania* sp. parasite. This activity (Bp-LAAO + *L. major*) was reduced in the presence of catalase (100 µg/mL). Data are expressed as means \pm SD ($n = 3$). (C) Bactericidal activity of Bp-LAAO enzyme on *Escherichia coli* and *Staphylococcus aureus*. Bp-LAAO (5, 15 and 25 µg) was incubated with 4×10^5 CFU of each bacterium for 24 h at 37 °C. After incubation, the bacterial growth was spectrophotometrically measured at 600 nm. Results were expressed as means \pm SD ($n = 03$).

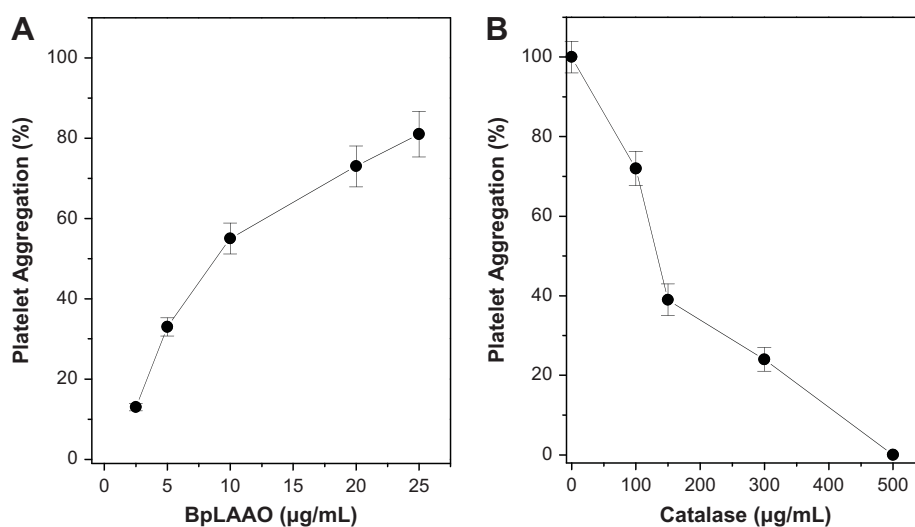


Fig. 3. Platelet aggregation induced by Bp-LAAO. (A) Dose-dependent platelet aggregation by Bp-LAAO on platelet-rich plasma (PRP). Platelets were stirred at 37 °C with different concentrations of LAAO (2.5–25 µg/mL). Maximal platelet aggregation, taken as 100% effect, was obtained with collagen (5 µg/mL) or ADP (10 µg/mL) and compared to values obtained with LAAO. (B) PRP was incubated at 37 °C for 2 min with different concentrations of catalase (0–500 µg/mL). LAAO was then added to trigger platelet aggregation. The induction did not occur when PRP and LAAO were incubated with catalase. 80% platelet aggregation was obtained with a supramaximal concentration of LAAO (25 µg/mL) in the absence of catalase. Results are expressed as means \pm SEM of two individual experiments ($n = 4$).

M N V F F M F S L L F L A A L G S C A D D
 ATGAATGTCCTTTTATGTTCTCACTGTTGTTCTTGGCTGCCCTTGGGAAGCTGTGCAGATGAC
G N P L E E C F R E T D Y E E F L E I A K
 GGAAACCCCTAGAGGAATGCTTCCGAGAACTGACTATGAGGAATTTCTAGAGATCGCCAAA
N G L S A T S N P K H V V I V G A G M S G
 AATGGTCTGAGCGACATCAAACCCGAAACATGTTGTGATTGTAGGTGCAGGAATGCTGGG
L S A A Y V L A N A G H Q V T V L E A S K
 CTTAGTGCAGCCTATGTTCTTCAAATGCTGGACATCAGGTGACAGTTCTTGAAGCCAGTAAA
 R A G G R V R T Y R N D K E G W Y A N L G
 CGTGCAGGACGAGTGGAGCTTATCGAAATGACAAAGAAGGCTGGTATGCCAATCTCGGG
 P M R L P E K H R I V R E Y I R K F G L Q
 CCCATGCGTTTACCTGAGAAACACAGGATTGTCGGGAATATATCAGAAAGTTTGGTCTGCAG
 L N E F S Q E N E N A W Y F I K N I R K R
 TTGAATGAATTTCTCAGGAAAATGAGAATGCATGGTATTTTATCAAAAACATCAGGAAGAGA
 V G E V N K D P G V L E Y P V K P S E V G
 GTAGGGGAAGTCAATAAAGACCCCTGGTGTGTTTGAATATCCCGTGAAGCCTTCAGAAGTAGGC
 K S A G Q L Y E E S L Q K A V E E L R R T
 AAAAGTGTGGACAGCTATATGAAGAGTCCCTCCAAAAGGCTGTAGAAGAATTAAGAAGGACT
N C S Y M L N K Y D T Y S T K E Y L L K E
 AACTGCAGCTACATGCTAAATAAATATGACACCTACTCAACGAAGGAGtATCTACTTAAAGAA
 G N L S P G A V D M I G D L L N E D S G Y
 GGAAATCTGAGTCTGGAGCTGTAGATATGATTGGAGACTTACTGAATGAAGATTCTGGCTAT
 Y V S F I E S L K H D D I F A Y E K R F D
 TATGTGCTTTTATTGAAAGCCTGAAACATGATGATATCTTTGCTTATGAAAAAAGATTGAT
 E I V G G M D K L P T S M Y Q A I Q E K V
 GAAATGTGGTGGAAATGGATAAGTTGCCTACATCCATGTATCAAGCCATTCAGGAAAAGGTG
 R L N V R V I K I Q Q D V K E V T V T Y Q
 CGTTTGAATGCCAGTAATCAAGATACAGCAGGATGTCAAGGAAGTACAGTGCATATCAA
 T S A K E T L S V T A D Y V I V C T T S R
 ACCTCAGCAAAGGAGACGTTATCTGTGACAGCTGATTATGTCATTGTATGCACTACGTcaAGG
 A A R R I K F E P P L P P K K A H A L R S
 GCCGCGCTGCATCAAGTTTGAACCCCTTCCGCCAAAGAAAGCGCATGCTTTGCGGTCT
 V H Y R S G T K I F L T C T K K F W E D D
 GTCCACTACAGAAGTGGCACCAAGATCTTCTCACTTGCCTAAGAAATTTGGCCTAACCAT
 G I H G G K S T T D L P S R F I Y Y P N H
 GGCATTCATGGTGGGAAGTCCACAACCTGATCTTCCATCCCGATTCTACTACCCTAACCAT
 N F P S G V G V I I A Y G I G D D A N F F
 AACTTCTAGTGGAGTTGGGGTTATTATAGCCTATGGCATTGGTGTATGCCAATTTCTTT
 Q A L D F K D C G D I V I N D L S L I H Q
 CAAGCTCTGATTTCAAGGACTGTGGTATATTGTCATTAATGACCTTTCATTGATCCATCAG
 L P K E E I Q A F C R P S M I Q R W S L D
 CTGCCAAAGGAAGAGATCCAGGCCTTCTGTCGTCCTCAATGATTCAAAGATGGAGCCTGGAT
 K Y A M G G I T T F T P Y Q F Q H F S E A
 AAGTATGCTATGGGTGGTATAACCACCTTCACTCCCTACCAGTTTCAACATTTTAGTGAAGCG
 L T A P V D R I Y F A G E Y T A Q A H G W
 CTCCTGCACTGTAGACAGAATCTACTTTGCAGGGGAGTATACAGCCCAAGCTCATGGTTGG
 I D S T I K S G L T A A R D V N R A S E N
 ATTGACAGCACAATTAAGTCAAGGCTGACAGCAGCAAGAGATGTGAATCGTGCTTCTGAGAAT
 R I P G P S T A E A C M Q A F P I
 CGGATCCCGGGCCGTCGACTGCAGAGGCTGCATGCAAGCTTTCCTATA

Fig. 4. Sequence of cDNA and deduced amino acid residues from Bp-LAAO (GenBank EU870608). Amino acid residues directly sequenced from the protein (underlined). cDNA sequence was obtained by amplification of PCR products starting from the snake gland of mRNA using specific oligonucleotides. N-glycosylation site is in box.

Addition of 100 U/mL catalase effectively abolished the effect of H₂O₂, resulting in a level of viability similar to that of controls.

Leishmania spp. had slightly different susceptibilities to Bp-LAAO, as observed for the EC₅₀ of 1.48 µg/mL (±0.07) against *L. amazonensis*, 1.59 µg/mL (±0.06) against *L. donovani* and 1.03 µg/mL (±0.003) against *L. braziliensis* and 1.29 µg/mL (±0.02) against *L. major*. Bp-LAAO induced a dose-dependent mortality of promastigote forms of different *Leishmania* species. *L. braziliensis* was the most susceptible species to the toxic effect of Bp-LAAO. In the presence of catalase, *L. major* showed approximately 70% survival (Fig. 2B). Promastigotes showed H₂O₂ susceptibility, as observed when the commercial product (5 mM) was added (100% death) (results not shown).

Bp-LAAO dose-dependently suppressed the growth of Gram-negative (*E. coli*) and Gram-positive (*S. aureus*) bacteria, with effects

more pronounced on *E. coli* (Fig. 2C). The bactericidal effect of Bp-LAAO (25 µg/mL) was also inhibited by catalase. Bp-LAAO was able to induce platelet aggregation in platelet-rich plasma at doses of 2.5–25 µg/mL (Fig. 3A). The induction did not occur when PRP and LAAO were incubated with catalase (Fig. 3B).

The product from amplification by PCR produced a cDNA fragment of 1548 bp that codifies for a mature protein of 516 amino acid residues, corresponding to a theoretical pI of 6.3 and molecular weight of 58 kDa. Several clones with inserts of the same size were sequenced and showed identical nucleotide sequence. With the glycosylation prediction software, NetNGlyc (<http://www.cbs.dtu.dk/services/NetNGlyc/>), one putative N-glycosylation site was detected (Fig. 4).

All phylogenetic trees generated by the programs TREE-PUZZLE v.5.2, MrBayes v.3.1.2, and MEGA v.4.0.2 showed the same topology

and statistical support for the calculated nodes. Remarkably, the svLAAOs from viperids and elapids were clearly divided in two monophyletic groups (Fig. 5). However, the svLAAO from *Ophiophagus hannah* was grouped in a separated branch with two LAAOs from *Gallus gallus* and *Meleagris gallopavo*, respectively (Fig. 5). The amino acid residues under positive evolutionary pressure of the svLAAO sequences from Viperidae, Elapidae and Viperidae/Elapidae phylogenetic groups are shown in Table 3.

The initial theoretical Bp-LAAO structural model calculated by program MODELLER 8v2 presented a good stereochemical quality with 99.1% of its amino acid residues in the core and additionally allowed regions of Ramachandran plot [49]. Furthermore, all residues have negative potential energies and the Z-score of the model is -11.21 [50]. The final theoretical Bp-LAAO structural model showed an r.m.s.d. (root mean square deviation) stabilization after approximately 1500 ps of molecular dynamics simulation, with

a slight positional deviation of the atoms (~ 0.1 nm). Similarly to the initial model, the final theoretical Bp-LAAO structural model shows that 97.9% of the residues are in the core and additionally allowed regions. On the same way, all residues of this model present negative potential energies and Z-score of -10.52 . All these data indicate the high stability degree of the structure after the molecular dynamics simulation, demonstrating the final theoretical Bp-LAAO structural model is feasible (Fig. 6).

4. Discussion

L-Amino acid oxidases are widely expressed in snake venoms and catalyze the oxidative deamination of L-amino acids, producing the corresponding α -ketoacids, hydrogen peroxide and ammonia. They are usually homodimeric, FAD-binding glycoproteins, with molecular mass around 110–150 kDa when measured by gel

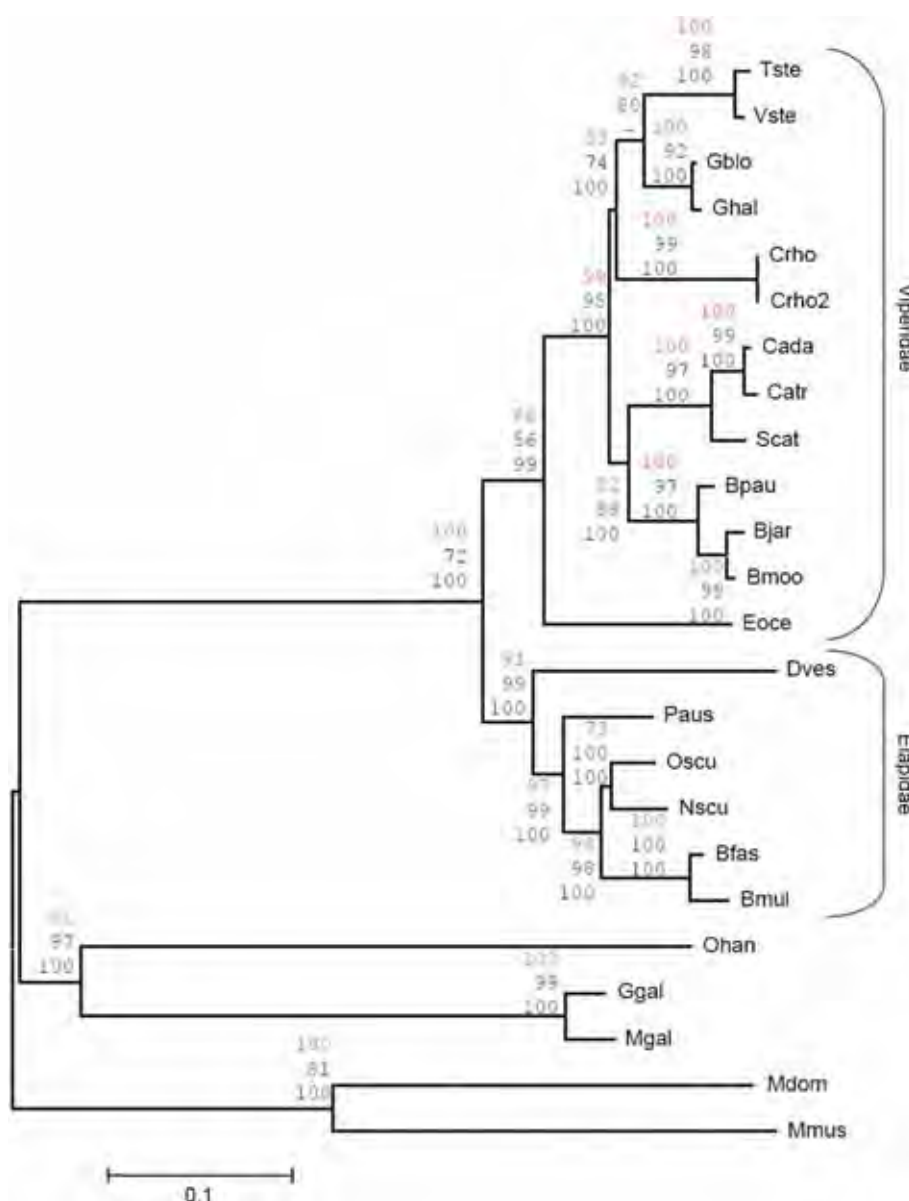


Fig. 5. Evolutionary relationships of LAAOs. The evolutionary history was inferred using the Neighbor-joining method. Phylogenetic analyses were conducted in MEGA4. The evolutionary distances were computed using the JTT matrix-based method. In red, blue and black are showed respectively the MEGA4 bootstrap test (2000 replicates), TREE-PUZZLE quartet sampling (10 000 puzzling steps) and MrBayes Bayesian MCMC analysis (75 900 cycles). The svLAAOs were grouped in two monophyletic branches (Viperidae and Elapidae groups). (For interpretation of the references to color in this text, the reader is referred to the web version of this article.)

Table 3

Positions with at least 95% probability of positive selection in the svLAAOs from Viperidae, Elapidae and Viperidae/Elapidae groups, according to the program MrBayes v.3.1.2. Sequence alignment was performed by the program AMAP v.2.0. Bp-LAAO residues shown in the table occupy the correspondent positions of the residues under positive selection of the other svLAAOs.

<i>Viperidae</i>								
S17	N72	Q126	E176	L239	V286	S302	G408	K467
C18	Q76	S131	Q180	G256	K287	A317	E424	D468
D20	K84	E135	A182	K260	E288	E323	E425	Q479
G22	A86	I141	E184	Q267	T292	D357	A428	A480
T32	D96	R147	R187	Q270	Q294	H360	R431	T493
S46	K97	G149	R188	E271	S296	S382	M434	R496
A47	E98	V157	S192	K272	A297	Q400	K442	R500
H53	G99	E159	M194	R274	E299	D403	E461	
I56	E111	V167	L225	L275	T300	F404	A462	
S62	G124	G172	I236	R278	L301	K405	P466	
<i>Elapidae</i>								
N23	A47	Q76	R121	Q824	E288	G342	K351	E424
<i>Viperidae/Elapidae</i>								
G16	Q76	Q126	G172	Q267	A297	T350	E425	V467
N23	K84	S131	E176	Q270	E299	K351	A428	D468
K42	A86	E135	Q180	L275	T300	G391	R431	Q479
S46	R91	R147	A182	R278	L301	A396	M434	A480
A47	D96	G149	R197	Q284	S302	Q400	G447	T493
H53	K97	V157	L225	E288	A317	F404	S460	R500
S62	R121	E159	K260	T292	K321	L417	A461	
N72	G124	V167	T263	S296	G342	E424	V467	

filtration under non-denaturing conditions. However, the molecular mass of svLAAOs is around 50–70 kDa when assayed by SDS-PAGE, both under reducing and non-reducing conditions. Thus, most of the svLAAOs are homodimeric glycoproteins associated by non-covalent bonds with *pI* of approximately 4.4–8.2 [8,12,29,44,51–61].

In the present work, we isolated a new LAAO from *B. pauloensis* snake venom by using three chromatographic steps (CM-Sepharose, Phenyl-Sepharose CL-4B and Benzamidine Sepharose) and finally the active fraction was still analyzed for purity by reverse-phase HPLC chromatography. Bp-LAAO presented molecular weight of approximately 65 kDa in SDS-PAGE and deglycosylation was

confirmed by PAGE, when the enzyme was treated with PNGase F. The enzymatic activity was not modified after deglycosylation suggesting that the sugar portion is not crucial for its activity. This effect was also observed by svLAAOs from *Bothrops jararaca* [62], *Bothrops pirajai* [20], *Bothrops moojeni* [15] and *Bothrops alternatus* [11].

Before the 1990s, svLAAOs were mainly used for identifying amino acid optical isomers and for preparing α -keto acids [6,61]. Usually, the oxidizing activity is determined using L-Leu as substrate. In the case of viperid venoms, hydrophobic amino acids are the best substrates for LAAOs [6,11,12,20,58]. The best substrate for *B. pauloensis* LAAO is in good accordance with other studied svLAAOs. Hydrophobic amino acids (L-Met, L-Leu, L-Phe, L-Trp and L-Ile) were the best substrates and L-Pro, L-Thr, L-Cys and L-Ser are not oxidized (Table 1). This catalytic preference can be explained by differences of side-chain binding sites in the enzyme responsible for substrate specificity [29]. The functional and structural characterization of these svLAAOs will contribute to the development of biotechnological agents, as already demonstrated in other studies [9,11,12,20,55,61].

The use of snake venoms as tumor growth inhibitors has raised several studies. There are controversial works in the literature, but LAAOs isolated from the venoms of various snake species are described as enzymes with antitumor and apoptotic effects in various types of cells [63,64]. Bp-LAAO induced dose-dependent cytotoxicity in SKBR-3, Jurkat and EAT cell lines. This type of inhibitory effect on tumor growth caused by LAAO has been demonstrated in earlier works with different cell lines, including human promyelocytic leukemia HL-60 [56,65], HeLa [66], glioma [64], human ovary carcinoma A2780 [65], endothelial cells from the human umbilical cord [65], mouse NR-3 endothelial cells [65] and murine EL-4 lymphoma cells [67]. However, reports evaluating the effect of LAAO on tumor growth *in vivo* are rare.

Leishmaniasis is an endemic tropical disease in South America with few therapeutic approaches. *Leishmania* causes a spectrum of diseases ranging from self-healing ulcers to disseminated and often fatal infections, depending on the species involved and host's immune response [68]. Interestingly, in this work, *L. braziliensis* was more susceptible to the toxic effects of Bp-LAAO. Using catalase as a scavenger for H₂O₂, we obtained partial abolition of anti-*Leishmania major* activity, suggesting that the action could be ascribed to H₂O₂ production. Indeed, if one was able to target a H₂O₂ generator, as Bp-LAAO, towards the parasitophorous vacuole, this would represent a highly specific treatment not only for leishmaniasis, but also for other intracellular parasites [54].

In our work, exogenous H₂O₂ was also able to induce antitumor and leishmanicidal effect, however the amount of H₂O₂ generated by Bp-LAAO may be different from exogenous H₂O₂. According to Zhang et al. [10] *Agkistrodon halys* LAAO (AHP-LAO) inhibited the growth of *E. coli* with a half inhibitory concentration (IC₅₀) of 2.0 μ g/mL which produced 0.21 mM H₂O₂ for 2.5 h, while H₂O₂ itself did with the IC₅₀ of 8.5 mM. They demonstrated that the effective antibacterial action of AHP-LAO could result from the binding of AHP-LAO to *E. coli* cells by fluorescence detection. They showed that the enzyme binds to the cell surface of bacteria and so generates high peroxide concentrations in the local area thus inhibiting bacterial growth with a small portion of the enzyme. Like LAAOs from *A. halys* [10], *B. alternatus* [11], *Crotalus durissus cascavella* [12], *B. pirajai* [20], and *B. moojeni* [15], *B. pauloensis* LAAO exhibits antimicrobial activity inhibiting the growth of both Gram-positive (*S. aureus*) and negative (*E. coli*) bacteria. Inhibition of the antibacterial activity by catalase confirms the role of hydrogen peroxide in the process.

Ehara et al. [7] also revealed that achacin showed significant bacterial-binding activity against *E. coli* and *S. aureus* by Western

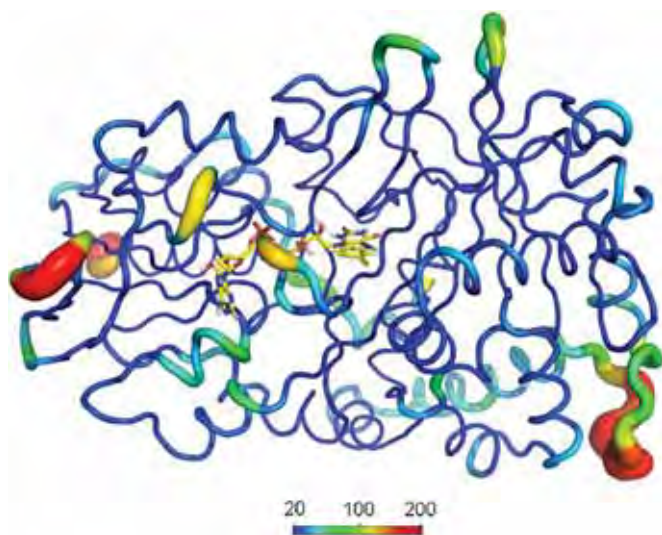


Fig. 6. B-factor ribbon diagram of the theoretical Bp-LAAO structural model obtained after molecular dynamics simulation. The color scale and ribbon width indicate the temperature/mobility of the backbone atoms of Bp-LAAO final model (blue: cold = low temperature = static/immobile regions; red = high temperature = variable/mobile regions). The FAD cofactor is represented by colored sticks. Illustration generated by program PyMOL [52]. (For interpretation of the references to color in this text, the reader is referred to the web version of this article.)

blotting. As a result, the production of highly localized concentration of H_2O_2 in or near the binding interfaces may elicit a potent antibacterial effect. Toyama and collaborators, contrary, show that H_2O_2 produced by CascaLAAO induced bacterial membrane rupture, and that binding to bacterial membrane does not seem to play an important role [12]. It is relevant that antibacterial action of LAAOs including Bp-LAAO is elicited by H_2O_2 generated from L-amino acid as substrate, since it is remarkably reduced in the presence of H_2O_2 of catalase. Although the detailed mode of antibacterial action of H_2O_2 is not fully understood, H_2O_2 could induce oxidative stress to the targeted cells, initiate cell membrane and cytoplasmatic disorganization and consequently cause cell death [12,54].

Bp-LAAO induced platelet aggregation and catalase also inhibited this effect. Snake venom LAAOs can inhibit or activate platelet aggregation [14]. The activation or inhibition functions of svLAAOs

on platelets are largely associated to their ability to produce H_2O_2 since catalase inhibits these effects. Some reports suggested that the interaction between activated platelet integrin $\alpha_{IIb}\beta_3$ and fibrinogen was inhibited by the continuous generation of H_2O_2 [14,16]. On the other hand, LAAOs from other snakes have been reported to have opposite effect on platelet aggregation through formation of H_2O_2 [20,22,32,61].

It is still unclear how H_2O_2 functions in LAAO-induced platelet aggregation. Several recent studies showed that H_2O_2 production might not be fully responsible for the biological activities of LAAOs. Li et al. [69] showed that H_2O_2 production alone is insufficient to induce platelet aggregation and both H_2O_2 production and binding to platelet membrane proteins might be involved in its action.

Sequences obtained from PCR products were identified by similarity searches on existing databases, resulting in the identification of transcripts codifying for putative svLAAO. Bp-LAAO-cDNA

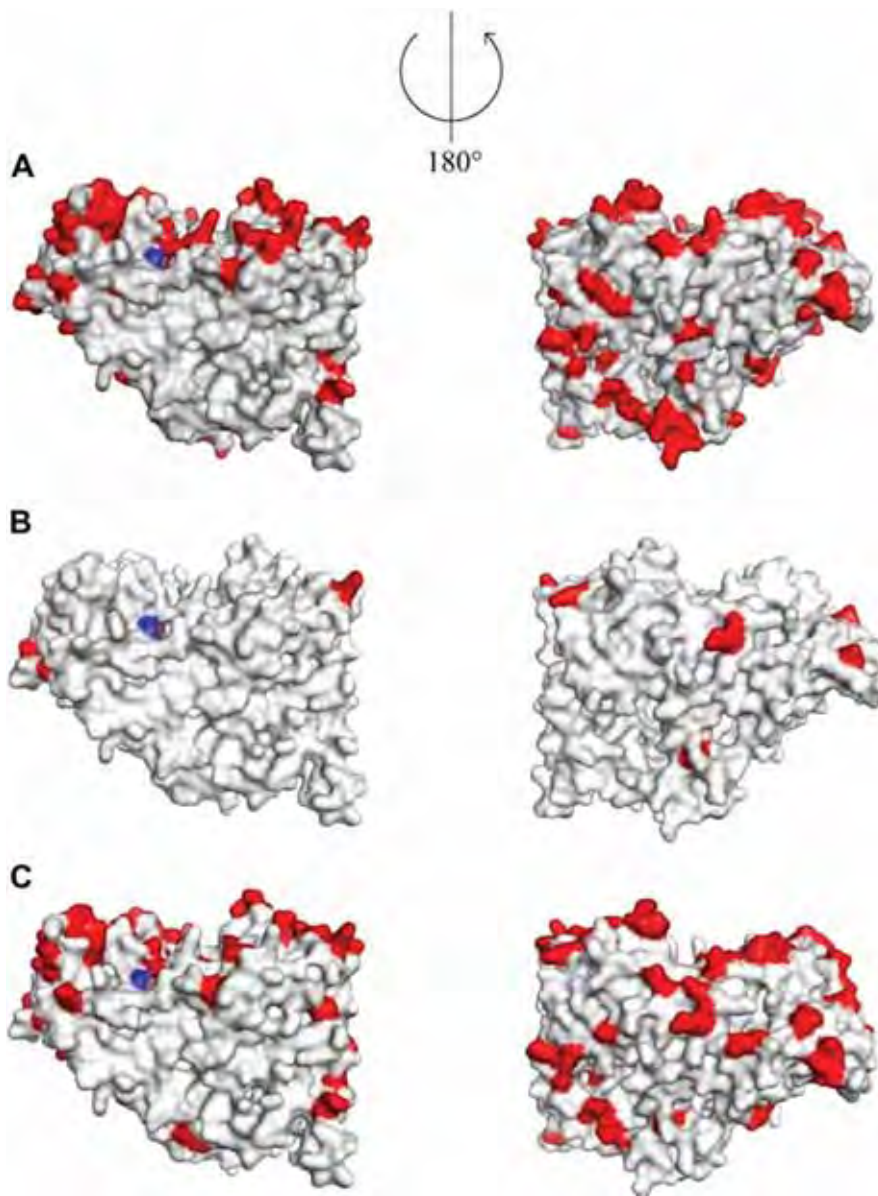


Fig. 7. Surface representation of the final theoretical Bp-LAAO structural model indicating in red the correspondent position of the residues under positive selection identified in the svLAAOs from Viperidae (A), Elapidae (B) and Viperidae/Elapidae (C) groups. (For interpretation of the references to color in this text, the reader is referred to the web version of this article.)

of 1583 bp codified a mature protein with 516 amino acid residues (Accession Number GenBank: EU870608). Primary structure analysis indicated that Bp-LAAO is a member of the flavin-containing protein family, which was confirmed by full-length spectrum scan analysis.

The phylogenetic analysis of the selected Bp-LAAO-homologue sequences showed an evident separation between svLAAOs from viperids and elapids (Fig. 5). Indeed, the topologies of the phylogenetic trees indicate the svLAAOs analyzed present a remarkable correlation with speciation, demonstrating the genes correspondent to these sequences are orthologous. On the other hand, the svLAAO from *O. hannah* was grouped with LAAOs from *G. gallus* and *M. gallopavo*, as also described by Jin et al. [51]. This fact highlights the gene of svLAAO from *O. hannah* is paralogous in relation to those which codify the other svLAAOs included in the phylogenetic analyses. Hence, it is highly probable that this svLAAO gene from *O. hannah* emerged from a recent duplication of a gene encoding for an endogenous snake LAAO. This hypothesis is strengthened by the absence of other orthologous genes to svLAAO from *O. hannah* in other snake species. Furthermore, the svLAAO from *O. hannah* may present distinct characteristics in comparison to the other svLAAOs analyzed.

Additionally to the phylogenetic analysis, the amino acid residues under positive evolutionary pressure in the Viperidae and Elapidae monophyletic groups were identified. In order to improve this study, the search for amino acid residues with positive selection was performed in the Viperidae and Elapidae groups separately and in a great group formed by the sequences from both monophyletic branches (Viperidae/Elapidae group). The analyses showed 70 amino acid residues from Viperidae/Elapidae group present a positive selection, whereas 87 and 9 residues from Viperidae and Elapidae groups show this characteristic, respectively. Bp-LAAO residues listed in Table 3 and shown in red (For interpretation of the references to color in this text, the reader is referred to the web version of this article.) in Fig. 7 occupy the correspondent positions of the residues with positive selection of the other svLAAOs. These results show the svLAAOs from viperids are exposed to most intense evolutionary pressures than their correspondent toxins in elapids, suggesting Viperidae and Elapidae svLAAOs present group-specific activities. Interestingly, all residues under positive selection are sited predominantly at one single face of the final theoretical Bp-LAAO structural model (Fig. 7). Consequently, it is very probable these residues are involved in recognition of specific sites and/or molecules, increasing the affinity of the svLAAOs for determined substrates and even the potency of the biological activities played by these toxins. This molecular recognition apparatus must be particularly important for snakes from Viperidae family, whose svLAAOs are particularly submitted to selection as cited above.

In conclusion, we isolated the first L-amino acid oxidase from *B. pauloensis* (Bp-LAAO), which shares a high degree of sequence identity and a common evolutionary origin with Viperidae svLAAOs. Furthermore, Bp-LAAO was able to induce platelet aggregation and showed leishmanicidal, antitumor and bactericidal activities. Some functional and structural studies with svLAAOs have demonstrated their high biotechnological potential for design of novel therapeutic agents.

Acknowledgements

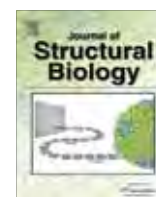
The authors gratefully acknowledge the financial support by Fundação de Amparo à Pesquisa de Minas Gerais (FAPEMIG) and São Paulo (FAPESP), and Conselho Nacional de Desenvolvimento Científico e Tecnológico (CNPq), Brazil. We gratefully thank Prof. Dr. Auro Nomizo (FCFRP-USP) and Prof. Dr. Marta C. Monteiro

(UNICENTRO) by collaboration in antitumor and antiparasite experiments, respectively.

References

- [1] F.S. Markland, Snake venoms and the hemostatic system, *Toxicon* 36 (1998) 1749–1800.
- [2] S. Braud, C. Bon, A. Wisner, Snake venom proteins acting on hemostasis, *Biochimie* 82 (2000) 851–859.
- [3] R.J. Lewis, M.L. Garcia, Therapeutic potential of venom peptides, *Nat. Rev. Drug Discov.* 2 (2003) 790–802.
- [4] Q. Lu, J.M. Clemetson, K.J. Clemetson, Snake venoms and hemostasis, *J. Thromb. Haemost.* 3 (2005) 791–799.
- [5] M.M.V. Santos, C.D. Sant'Ana, J.R. Giglio, R.J. Silva, S.V. Sampaio, A.M. Soares, D. Fecchio, Antitumoural effect of an L-amino acid oxidase isolated from *Bothrops jararaca* snake venom, *Basic Clin. Pharmacol. Toxicol.* 102 (2008) 533–542.
- [6] N.H. Tan, L-Amino acid oxidases and lactate dehydrogenases, in: G.S. Bailey (Ed.), *Enzymes from Snake Venom*, Alaken Inc., Fort Collins, Colorado, 1998, pp. 579–598.
- [7] T. Ehara, S. Kitajima, N. Kanzawa, T. Tamiya, T. Tsuchiya, Antimicrobial action of achacin is mediated by L-amino acid oxidase activity, *FEBS Lett.* 531 (2002) 509–512.
- [8] D. Butzke, R. Hurwitz, B. Thiede, S. Goedert, T. Rudel, Cloning and biochemical characterization of APIT, a new L-amino acid oxidase from *Aplysia punctata*, *Toxicon* 46 (2005) 479–489.
- [9] X.Y. Du, K.J. Clemetson, Snake venom L-amino acid oxidases, *Toxicon* 40 (2002) 659–665.
- [10] H. Zhang, M. Teng, L. Niu, Y. Wang, Y. Wang, Q. Liu, Q. Huang, Q. Hao, Y. Dong, P. Liu, Purification, partial characterization, crystallization and structural determination of AHP-LAAO, a novel L-amino-acid oxidase with cell apoptosis-inducing activity from *Agkistrodon halys pallas* venom, *Acta Crystallogr. D: Biol. Crystallogr.* 60 (2004) 974–977.
- [11] R.G. Stábéli, B. Marcussi, G.B. Carlos, R.C.L.R. Pietro, H.S. Selistre-de-Araújo, J.R. Giglio, E.B. Oliveira, A.M. Soares, Platelet aggregation and antibacterial effects of an L-amino acid oxidase purified from *Bothrops alternatus* snake venom, *Bioorg. Med. Chem.* 12 (2004) 2881–2886.
- [12] M.H. Toyama, D.O. Toyama, L.F.D. Passero, M.D. Laurenti, C.E. Corbett, T.Y. Tomokane, F.V. Fonseca, E. Antunes, P.P. Joazeiro, L.O.S. Beriam, M.A.C. Martins, H.S.A. Monteiro, M.C. Fonteles, Isolation of a new L-amino acid oxidase from *Crotalus durissus cascavella* venom, *Toxicon* 47 (2006) 47–57.
- [13] S.C. Franca, S. Kashima, P.G. Roberto, M. Marins, F.K. Tielci, J.O. Pereira, S. Astolfi-Filho, R.G. Stábéli, A.J. Magro, M.R.M. Fontes, S.V. Sampaio, A.M. Soares, Molecular approaches for structural characterization of *Bothrops* L-amino acid oxidases with anti protozoal activity: cDNA cloning, comparative sequence analysis, and molecular modeling, *Biochem. Biophys. Res. Commun.* 355 (2007) 302–306.
- [14] Y. Sakurai, H. Takatsuka, A. Yoshioka, T. Matsui, M. Suzuki, K. Titani, Y. Fujimura, Inhibition of human platelet aggregation by L-amino acid oxidase purified from *Naja naja kaouthia* venom, *Toxicon* 39 (2001) 1827–1833.
- [15] R.G. Stábéli, C.D. Sant'Ana, P.H. Ribeiro, T.R. Costa, F.K. Tielci, M.G. Pires, A. Nomizo, S. Albuquerque, N.R. Malta-Neto, M. Marins, S.V. Sampaio, A.M. Soares, Cytotoxic L-amino acid oxidase from *Bothrops moojeni*: biochemical and functional characterization, *Int. J. Biol. Macromol.* 41 (2007) 132–140.
- [16] H. Takatsuka, Y. Sakurai, A. Yoshioka, T. Kokubo, Y. Usami, M. Suzuki, Molecular characterization of L-amino acid oxidase from *Agkistrodon halys blomhoffii* with special reference to platelet aggregation, *Biochim. Biophys. Acta* 1544 (2001) 267–277.
- [17] M. Samel, H. Vija, G. Rönnholm, J. Siigur, N. Kalkkinen, E. Siigur, Isolation and characterization of an apoptotic and platelet aggregation inhibiting L-amino acid oxidase from *Vipera berus berus* (common viper) venom, *Biochim. Biophys. Acta* 1764 (2006) 707–714.
- [18] K. Tõnismägi, M. Samel, K. Trummal, G. Rönnholm, J. Siigur, N. Kalkkinen, E. Siigur, L-Amino acid oxidase from *Vipera lebetina* venom: isolation, characterization, effects on platelets and bacteria, *Toxicon* 48 (2006) 227–237.
- [19] Q. Wei, Q.M. Lu, Y. Jin, R. Li, J.F. Wei, W.Y. Wang, Y.L. Xiong, Purification and cloning of a novel C-type lectin-like protein with platelet aggregation activity from *Trimeresurus mucrosquamatus* venom, *Toxicon* 40 (2002) 1331–1338.
- [20] L.F. Izidoro, M.C. Ribeiro, G.R. Souza, C.D. Sant'Ana, A. Hamaguchi, M.I. Homs-Brandeburgo, L.R. Goulart, R.O. Belebani, A. Nomizo, S.V. Sampaio, A.M. Soares, V.M. Rodrigues, Biochemical and functional characterization of an L-amino acid oxidase isolated from *Bothrops pirajai* snake venom, *Bioorg. Med. Chem.* 14 (2006) 7034–7043.
- [21] S.M. Suhr, D.S. Kim, Comparison of the apoptotic pathways induced by L-amino acid oxidase and hydrogen peroxidase, *J. Biochem.* 125 (1999) 305–309.
- [22] S.A. Ali, S. Stoeva, A. Abbasi, J.M. Alam, R. Kayed, M. Faigle, B. Neumeister, W. Voelter, Isolation, structural, and functional characterization of an apoptosis-inducing L-amino acid oxidase from leaf-nosed viper (*Eristocophis macmahoni*) snake venom, *Arch. Biochem. Biophys.* 15 (2000) 216–226.

- [23] P. Sun, X.D. Ren, H.W. Zhang, X.H. Li, S.H. Cai, K.H. Ye, X.K. Li, Serum from rabbit orally administered cobra venom inhibits growth of implanted hepatocellular carcinoma cells in mice, *World J. Gastroenterol.* 9 (2003) 2441–2444.
- [24] A. Amaral, A general consideration of snake poisoning and observations of neotropical pit vipers, *Contrib. Harvard Inst. Trop. Biol.* 2 (1925) 1–64.
- [25] M. Jansen, First records of *Bothrops pauloensis* Amaral, 1925 (Serpentes: Viperidae) in Bolivia, *Kemppifiana* 2 (1) (2006) 66–71.
- [26] V.X. Silva, The *Bothrops neuwiedi* complex, in: *The Venomous Reptiles of the Western Hemisphere*, Ithaca, New York, 2004, pp. 410–422.
- [27] BSH, Lista de espécies de répteis do Brasil, Sociedade Brasileira de Herpetologia (SBH), 2005, Available from: www.sberpetologia.org.br/checklist/repteis.html.
- [28] R.F. Itzhaki, D.M. Gill, A micro-biuret method for estimating proteins, *Anal. Biochem.* 9 (1964) 401–410.
- [29] G. Ponnudurai, M.C. Chung, N.H. Tan, Purification and properties of the amino acid oxidase from Malayan pit viper (*Calloselasma rhodostoma*) venom, *Arch. Biochem. Biophys.* 313 (1994) 373–378.
- [30] T.J. Mosmann, Rapid colorimetric assay for cellular growth and survival: application to proliferation and cytotoxicity assays, *J. Immunol. Methods* 65 (1983) 55–63.
- [31] S. Chwetsoff, S. Tsunasawa, F. Sakiyama, A. Menez, Nigexine, a phospholipase A₂ from cobra venom with cytotoxic properties not related to esterase activity. Purification, amino acid sequence, and biological properties, *J. Biol. Chem.* 264 (1989) 13289–13297.
- [32] R.G. Stabeli, S.F. Amui, C.D. Sant'ana, M.G. Pires, A. Nomizo, M.C. Monteiro, P.R. Romão, R. Guerra-Sa, C.A. Vieira, J.R. Giglio, M.R. Fontes, A.M. Soares, *Bothrops moojeni* myotoxin-II, a Lys49-phospholipase A₂ homologue: an example of function versatility of snake venom proteins, *Comp. Biochem. Physiol.* 142C (2006) 371–381.
- [33] A.L. Fuly, O.L. Machado, E.V. Alves, C.R. Carlini, Mechanism of inhibitory action on platelet activation of a phospholipase A₂ isolated from *Lachesis muta* (Bushmaster) snake venom, *Thromb. Haemost.* 78 (1997) 1372–1380.
- [34] D. Rotenberg, E.S. Bamberg, E. Kochva, Studies on ribonucleic acid synthesis in the venom glands of *Vipera palaestinae*, *Biochem. J.* 121 (1971) 609.
- [35] A.S. Schwartz, L. Pachter, Multiple alignment by sequence annealing, *Bioinformatics* 23 (2007) 24–29.
- [36] H.A. Schmidt, K. Strimmer, M. Vingron, A. von Haeseler, TREE-PUZZLE: maximum likelihood phylogenetic analysis using quartets and parallel computing, *Bioinformatics* 18 (2002) 502–504.
- [37] J.P. Huelsenbeck, F. Ronquist, MRBAYES: Bayesian inference of phylogenetic trees, *Bioinformatics* 17 (2001) 754–755.
- [38] K. Tamura, J. Dudley, M. Nei, S. Kumar, MEGA4: Molecular Evolutionary Genetics Analysis (MEGA) software version 4.0, *Mol. Biol. Evol.* 24 (2007) 1596–1599.
- [39] N. Saitou, M. Nei, The neighbor-joining method: a new method for reconstructing phylogenetic trees, *Mol. Biol. Evol.* 4 (1987) 406–425.
- [40] K. Strimmer, A. von Haeseler, Quartet puzzling: a quartet maximum likelihood method for reconstructing tree topologies, *Mol. Biol. Evol.* 13 (1996) 964–969.
- [41] J. Felsenstein, Confidence limits on phylogenies: an approach using the bootstrap, *Evolution* 39 (1985) 783–791.
- [42] D.T. Jones, W.R. Taylor, J.M. Thornton, The rapid generation of mutation data matrices from protein sequences, *Comput. Appl. Biosci.* 8 (1992) 275–282.
- [43] J. Söding, A. Biegert, A.N. Lupas, The HHpred interactive server for protein homology detection and structure prediction, *Nucleic Acids Res.* 33 (2005) 244–248.
- [44] M.A. Marti-Renom, A. Stuart, A. Fiser, R. Sánchez, F. Melo, A. Sali, Comparative protein structure modeling of genes and genomes, *Annu. Rev. Biophys. Biomol. Struct.* 29 (2000) 291–325.
- [45] H.J.C. Berendsen, D. van der Spoel, R. van Drunen, GROMACS: a message-passing parallel molecular dynamics implementation, *Comput. Phys. Commun.* 91 (1995) 43–56.
- [46] E. Lindahl, B. Hess, R. van der Spoel, GROMACS 3.0: a package for molecular simulation and trajectory analysis, *J. Mol. Model.* 7 (2001) 306–317.
- [47] H.J.C. Berendsen, J.P.M. Postma, W.F. van Gunsteren, J. Hermans, Interaction models for water in relation to protein hydration, in: B. Pullman (Ed.), *Intermolecular Forces*, D. Reidel Publishing Company, Dordrecht, 1981, pp. 331–342.
- [48] C. Oostenbrink, T.A. Soares, N.F.A. van der Vegt, W.F. van Gunsteren, Validation of the 53A6 GROMOS force field, *Eur. Biophys. J.* 34 (2005) 273–284.
- [49] R.A. Laskowski, M.W. MacArthur, D.S. Moss, J.M. Thornton, PROCHECK: a program to check the stereochemical quality of protein structures, *J. Appl. Crystallogr.* 26 (1993) 283–291.
- [50] M. Wiederstein, M.J. Sippl, ProSA-web: interactive web service for the recognition of errors in three-dimensional structures of proteins, *Nucleic Acids Res.* 35 (2007) W407–W410.
- [51] Y. Jin, W.H. Lee, L. Zeng, Y. Zhang, Molecular characterization of L-amino acid oxidase from king cobra venom, *Toxicon* 50 (2007) 479–489.
- [52] W.L. Delano, The PyMOL Molecular Graphics System, DeLano Scientific, San Carlos, 2002.
- [53] I.M. Moustafa, S. Foster, A.Y. Lyubimov, A. Vrielink, Crystal structure of LAAO from *Calloselasma rhodostoma* with an L-phenylalanine substrate: insights into structure and mechanism, *J. Mol. Biol.* 364 (2006) 991–1002.
- [54] A.G. Tempone, H.F. Andrade Jr., P.J. Spencer, C.O. Lourenço, J.R. Rogero, N. Nascimento, *Bothrops moojeni* venom kills *Leishmania* spp. with hydrogen peroxide generated by its L-amino acid oxidase, *Biochem. Biophys. Res. Commun.* 280 (2001) 620–624.
- [55] S. Torii, K. Yamane, T. Mashima, N. Haga, K. Yamamoto, J.W. Fox, M. Naito, T. Tsuruo, Molecular cloning and functional analysis of apoxin I, a snake venom-derived apoptosis-inducing factor with L-amino acid oxidase activity, *Biochemistry* 39 (2000) 3197–3205.
- [56] D.H.F. Souza, L.M. Eugenio, J.E. Fletcher, M. Jiang, R.C. Garratt, G. Oliva, H.S. Selistre-de-Araujo, Isolation and structural characterization of a cytotoxic L-amino acid oxidase from *Agkistrodon contortrix latincinctus* snake venom: preliminary crystallographic data, *Arch. Biochem. Biophys.* 368 (1999) 285–290.
- [57] M.Y. Ahn, B.M. Lee, Y.S. Kim, Characterization and cytotoxicity of L-amino acid oxidase from the venom of king cobra (*Ophiophagus hannah*), *Int. J. Biochem. Cell Biol.* 29 (1997) 911–919.
- [58] Y. Abe, Y. Shimoyama, H. Munakata, J. Ito, N. Nagata, K. Ohtsuki, Characterization of an apoptosis-inducing factor in Habu snake venom as a glycyrrhizin (GL)-binding protein potentially inhibited by GL *in vitro*, *Biol. Pharm. Bull.* 21 (1998) 924–927.
- [59] Y.I. Zhang, J.H. Wang, W.H. Lee, Q. Wang, H. Liu, Y.T. Zheng, Y. Zhang, Molecular characterization of *Trimeresurus stejnegeri* venom L-amino acid oxidase with potential anti-HIV activity, *Biochem. Biophys. Res. Commun.* 309 (2003) 598–604.
- [60] S. Iwanaga, T. Suzuki, Enzymes in snake venoms, in: C.Y. Lee (Ed.), *Snake Venoms*, Springer-Verlag, New York, 1979, pp. 61–158.
- [61] Q.M. Lu, Q. Wei, Y. Jin, J.F. Wei, W.Y. Wang, Y.L. Xiong, L-Amino acid oxidase from *Trimeresurus jerdonii* snake venom: purification, characterization, platelet aggregation-inducing and antibacterial effects, *J. Nat. Toxins* 11 (2002) 345–352.
- [62] C.D. Sant'Ana, D.L. Menaldo, T.R. Costa, H. Godoy, V.D.M. Muller, V.H. Aquino, S. Albuquerque, S.V. Sampaio, M.C. Monteiro, R.G. Stabeli, A.M. Soares, Antiviral and antiparasite properties of an L-amino acid oxidase from the snake *Bothrops jararaca*: cloning and identification of a complete cDNA sequence, *Biochem. Pharmacol.* 76 (2008) 279–288.
- [63] S.M. Suhr, D.S. Kim, Identification of the snake venom substance that induces apoptosis, *Biochem. Biophys. Res. Commun.* 224 (1996) 134–139.
- [64] L.K. Sun, Y. Yoshii, A. Hyodo, H. Tsurushima, A. Saito, T. Harakuni, Apoptotic effect in the glioma cells induced by specific protein extracted from Okinawa Habu (*Trimeresurus flavoviridis*) venom in relation to oxidative stress, *Toxicol. In Vitro* 17 (2003) 169–177.
- [65] S. Torii, M. Naito, T. Tsuruo, Apoxin I, a novel apoptosis inducing factor with L-amino acid oxidase activity purified from Western diamondback rattlesnake venom, *J. Biol. Chem.* 272 (1997) 9539–9542.
- [66] N. Kanzawa, S. Shintani, K. Ohta, S. Kitajima, T. Ehara, H. Kobayashi, Achacin induces cell death in HeLa cells through two different mechanisms, *Arch. Biochem. Biophys.* 422 (2004) 103–109.
- [67] R. Iijima, J. Kisugi, M. Yamazaki, L-Amino acid oxidase activity of an anti-neoplastic factor of a marine mollusk and its relationship to cytotoxicity, *Dev. Comp. Immunol.* 27 (2003) 505–512.
- [68] D.H. Molyneux, J.K. Stiles, Trypanosomatid-vector interactions, *Ann. Soc. Belg. Med. Trop.* 71 (1991) 151–166.
- [69] R. Li, S. Zhu, J. Wu, W. Wang, Q. Lu, K.J. Clemetson, L-Amino acid oxidase from *Naja atra* venom activates and binds to human platelets, *Acta Biochim. Biophys. Sin. (Shanghai)* 40 (2008) 19–26.



Comparative structural studies on Lys49-phospholipases A₂ from *Bothrops* genus reveal their myotoxic site

Juliana I. dos Santos^a, Andreimar Martins Soares^b, Marcos R.M. Fontes^{a,*}

^a Depto. de Física e Biofísica, Instituto de Biociências, UNESP, 18618-000 Botucatu, SP, Brazil

^b Depto. de Análises Clínicas, Toxicológicas e Bromatológicas, FCFRP, USP, Ribeirão Preto, SP, Brazil

ARTICLE INFO

Article history:

Received 7 November 2008

Received in revised form 26 March 2009

Accepted 17 April 2009

Available online 3 May 2009

Keywords:

Phospholipase A₂

Myotoxicity

α-Tocopherol

X-ray crystallography

Bothrops genus

Homologue phospholipase A₂ assembly

ABSTRACT

Phospholipases A₂ (PLA₂s) are membrane-associated enzymes that hydrolyze phospholipids at the *sn*-2 position, releasing lysophospholipids and free fatty acids. Phospholipase A₂ homologues (Lys49-PLA₂s) are highly myotoxic and cause extensive tissue damage despite not showing measurable catalytic activity. They are found in different snake venoms and represent one third of bothropic venom composition. The importance of these toxins during envenomation is related to the pronounced local myotoxic effect they induce since this effect is not neutralized by serum therapy. We present herein three structures of Lys49-PLA₂s from *Bothrops* genus snake venom crystallized under the same conditions, two of which were grown in the presence of α-tocopherol (vitamin E). Comparative structural analysis of these and other Lys49-PLA₂s showed two different patterns of oligomeric conformation that are related to the presence or absence of ligands in the hydrophobic channel. This work also confirms the biological dimer indicated by recent studies in which both C-termini are in the dimeric interface. In this configuration, we propose that the myotoxic site of these toxins is composed by the Lys 20, Lys115 and Arg118 residues. For the first time, a residue from the short-helix (Lys20) is suggested as a member of this site and the importance of Tyr119 residue to myotoxicity of bothropic Lys49-PLA₂s is also discussed. These results support a complete hypothesis for these PLA₂s myotoxic activity consistent with all findings on bothropic Lys49-PLA₂s studied up to this moment, including crystallographic, bioinformatics, biochemical and biophysical data.

© 2009 Elsevier Inc. All rights reserved.

1. Introduction

Phospholipases A₂ (PLA₂s) are small (~14 kDa), stable, calcium-dependent, disulfide-rich enzymes. They are membrane-associated proteins and their importance is related to catalysis of membrane phospholipids at the *sn*-2 position, producing lysophospholipids and free fatty acids (van Deenen and de Haas, 1963). The fatty acids released can function as energy stores, second messengers (Berk and Stump, 1963; Gijón and Leslie, 1999) and as precursors of eicosanoids, which are potent mediators of inflammation (Austin and Funk, 1999; Bingham and Austen, 1999). On the other hand, lysophospholipids are involved in cell signaling and phospholipid remodeling, and are also associated with membrane perturbation (Balsinde et al., 1999; Molenaar et al., 1997). These proteins also present many pharmacological properties, among which have been noted neurotoxic, myotoxic, anticoagulant, bactericidal, hypotensive and edema-inducing activities (Andrião-Escarso et al., 2002; Beers et al., 2002; Bon et al., 1979; Chang et al., 1977; Gerrard and Robinson, 1993; Gutiérrez et al., 1986; Gutiérrez and Lomonte,

1997; Lloret and Moreno, 1993; Paramo et al., 1998; Rosenberg, 1990). Their ability to exhibit such a diverse spectrum of activities is intriguing since they share significant sequential and structural similarity and since these activities emerge from a single structural scaffold (Arni and Ward, 1996).

PLA₂s are also one of the enzymes involved in the production of eicosanoids. These molecules have physiological effects at very low concentrations, but they can lead to the inflammatory state at high concentrations (Needleman et al., 1986). Therefore, the study of specific PLA₂s inhibitors can be important in the production of structure-based anti-inflammatory agents. α-Tocopherol (vitamin E) regulates the production of eicosanoids by inhibition of both PLA₂ (Pentland et al., 1992) and cyclooxygenase activities (Abate et al., 2000), and has been used to slow the progression of Alzheimer and Parkinson diseases (Ebadi et al., 1996; Sano et al., 1997). Thus, it is very important to know the exact manner by which this inhibitor interacts with PLA₂s. The first attempt at this goal was the structural study of the complex formed by a dimeric PLA₂ from *Daboia russelli pulchella* and α-tocopherol (Chandra et al., 2002).

Ophidic accidents caused by snakes from the Viperidae family are characterized by drastic local myonecrosis, among other ef-

* Corresponding author. Fax: +55 14 3815 37444.

E-mail address: fontes@ibb.unesp.br (M.R.M. Fontes).

fects, which are not efficiently neutralized by serum therapy and may lead to permanent tissue loss (Gutiérrez and Lomonte, 1995). This effect is related to enzymes like PLA₂s and metalloproteases, and to PLA₂ homologues (Lys49-PLA₂s), a subclass of snake venom PLA₂s that are enzymatically inactive (Scott et al., 1992; Francis et al., 1991). The site responsible for this activity in Lys49-PLA₂s has been the subject of important efforts since this information is important to the design of efficient inhibitors for these toxins. Studies on synthetic peptides and site-directed mutagenesis strongly suggest the C-terminal region of these proteins as being responsible for expression of this activity in Lys49-PLA₂s (Chioato et al., 2002, 2007; Lomonte et al., 2003a,b; Núñez et al., 2001; Ward et al., 1998, 2002). Based on these and other studies, a model for Lys49-PLA₂s–membrane interaction was proposed by Lomonte et al. (2003a). In this model the authors suggest that the action of Lys49-PLA₂s is based on the interaction of the C-terminal positive residues with membrane anionic phospholipids. In agreement with this proposal, site-directed mutagenesis studies showed that the replacement of Arg and Lys residues by Ala in the region 117–122 of BthTX-I resulted in a significant reduction of myotoxic activity (Chioato et al., 2002).

Several crystal structures of myotoxic Lys49-PLA₂s from the *Bothrops* genus have been solved (Arni et al., 1995, 1999; de Azevedo et al., 1998; Lee et al., 2001; Magro et al., 2003; da Silva-Giotto et al., 1998; Watanabe et al., 2005) and studies to correlate them with the pharmacological site of these proteins have also been performed (Chioato et al., 2002, 2007; Lomonte et al., 2003a,b; Murakami et al., 2007; Núñez et al., 2001; Soares et al., 2001a; Soares and Giglio, 2003; Ward et al., 1998, 2002). However, the structural bases of this toxicological effect appear difficult to interpret merely by analyzing native (apo) structures. Thus, the comparison between complexed and native structures from these toxins can produce new insights into their mechanism of action and help to determine their myotoxic site. Some Lys49-PLA₂s crystallographic structures complexed with ligands are already available in the literature (Ambrosio et al., 2005; Lee et al., 2001; Murakami et al., 2005; Watanabe et al., 2005).

In this work we present three structures of Lys49-PLA₂s from *Bothrops* genus snake venom (PrTX-I and BthTX-I, isolated from *Bothrops pirajai* and *Bothrops jararacussu* venoms, respectively) crystallized under the same experimental conditions, with two of them grown in the presence of α -tocopherol. Additionally, comparative structural analysis of these and other Lys49-PLA₂s are performed showing two different patterns of oligomeric conformation (apo and complexed configurations). Based on these and other structural studies, a “myotoxic site” is suggested for these toxins.

2. Materials and methods

2.1. Crystallization

Crystallization experiments were performed with lyophilized samples of PrTX-I and BthTX-I (Jancarik and Kim, 1991; Mancuso et al., 1995) at a concentration of 12 mg/mL. Crystals of the native protein were obtained by hanging drop vapor diffusion method and the complexed ones by sitting drop method (MacPherson, 1982). For the complexed forms, the protein solution was pre-incubated with α T (Sigma–Aldrich) for two hours before the crystallization plate set-up. Better crystals were obtained with 30% (w/v) polyethylene glycol 4000, 0.2 M lithium sulfate and 0.1 M Tris–HCl, pH 7.5 (dos Santos et al., 2007; Takeda et al., 2008). Native and PrTX-I/ α T crystals were crystallized at 298 K whereas BthTX-I/ α T was obtained at 291 K.

2.2. X-ray data collection and processing

X-ray diffraction data were collected using a wavelength of 1.421 or 1.431 Å at a synchrotron-radiation source (MX1 station–LNLS, Campinas, Brazil) with a MAR CCD imaging-plate detector (MAR Research). Crystals were mounted in a nylon loop and flash cooled in a stream of nitrogen at 100 K using no cryoprotectant. Data were processed using the HKL program package (Otwinowski and Minor, 1997).

2.3. Structure determination and refinement

The crystal structures were solved by the Molecular Replacement Method using the program AMoRe (Navaza, 1994) and the coordinates of the BnSP-7 (Magro et al., 2003). The model choice was based on the best results of correlation and R-factor calculated by the AMoRe program. The models were improved, as judged by the free R-factor (Brünger et al., 1998), through rounds of crystallographic refinement using the CNS program (Brünger et al., 1998), and manual rebuilding was performed with the “O” program (Jones et al., 1990). During the refinement 432, 356 and 246 water molecules were added to the models of PrTX-I, PrTX-I/ α T and BthTX-I/ α T, respectively, using the CNS program (Brünger et al., 1998). Due to the lack of electron density in side chains, the following residues changes were made: in native PrTX-I–A monomer: Phe3Ala, Lys69Ala and Lys70Ala; and in the B monomer: Arg34Ala, Lys53Ala, Lys57Ala, Lys70Gly, Lys115Ala, Lys116Ala, Lys127Ala and Lys129Ala. For the complex PrTX-I/ α T the substitutions were—monomer A: Lys70Gly and Gln86Gly, and for monomer B: Asp79Ala and Lys129Ala. For the BthTX-I/ α T the substitutions were—monomer A: Lys36Ala, Lys69Ala, Lys70Ala, Lys78Ala and Lys122Gly, and for monomer B: Lys69Ala and Pro132Ala. Additionally, during the refinement a mismatch between the published sequence for the residue 116 of PrTX-I (Toyama et al., 1998) and its electron density became apparent, leading to the substitution Leu116Lys (Supplementary Fig. 1). α T molecules occupancies were refined using the CNS program (Brünger et al., 1998) due to lack of density for some of their atoms. The refinement statistics for the final models are shown in Table 1. The quality of the models was checked by the program Procheck (Laskowski et al., 1993) and the contacts between the proteins and the ligands were analyzed by the DIMPLOT program (Wallace et al., 1995).

2.4. Comparative analysis

Molecular comparisons of the Lys49-PLA₂ structures were performed using the “O” program (Jones et al., 1990) (only C α coordinates were considered). The structures BaspTX-II (myotoxin II from *Bothrops asper*) in its native form (Arni et al., 1995) and complexed with suramin (Murakami et al., 2005), BnSP-6 (myotoxin I from *Bothrops pauloensis*) (Magro et al., 2003), BnSP-7 (myotoxin II from *Bothrops pauloensis*) (Magro et al., 2003), BthTX-I (myotoxin I from *Bothrops jararacussu*) in its native form (da Silva-Giotto et al., 1998) and complexed with α T, MjTX-II (myotoxin II from *Bothrops moojeni*) complexed with stearic acid (Watanabe et al., 2005), PrTX-I (myotoxin I from *Bothrops pirajai*) in its native form and complexed with α T, and PrTX-II (myotoxin II from *Bothrops pirajai*) with a natural fatty acid (Lee et al., 2001) were used in the comparative analysis. All these structures (with exception of BthTX-I) are available in the Protein Data Bank (<http://www.pdb.org>). Analyses of the quaternary assemblies and interfacial contacts of the crystallographic models were performed using the online interactive tool PISA (Krissinel and Henrick, 2007) available at the European Bioinformatics Institute server (<http://www.ebi.ac.uk>). The sequence alignment for class IIA Asp49 and Lys49-PLA₂s from the Crotalinae

Table 1
X-ray data collection and refinement statistics.

	Native PrTX-I	PrTX-I/ α T	BthTX-I/ α T
Unit cell (Å)	$a = b = 55.9$ $c = 127.9$	$a = 38.9$ $b = 71.4$ $c = 44.3$ $\beta = 102.3^\circ$	$a = 38.4$ $b = 70.1$ $c = 43.9$ $\beta = 102.2^\circ$
Space group	P3 ₁ 21	P2 ₁	P2 ₁
Resolution (Å)	40–1.65 (1.71–1.65) ^a	40–1.87 (1.94–1.87) ^a	40–1.83 (1.9–1.83) ^a
Unique reflections	27251 (2648) ^a	19407 (1927) ^a	19435 (1824) ^a
Completeness (%)	94.9 (94.0) ^a	98.9 (98.2) ^a	96.2 (92.0) ^a
R _{merge} ^b (%)	8.4 (52.5) ^a	6.0 (20.6) ^a	6.8 (33.5) ^a
Radiation source	Synchrotron (LNLS - MX1)		
Data collection temperature (K)	100		
I/ σ (I)	12.0 (2.0) ^a	19.3 (3.9) ^a	22.76 (2.36) ^a
Matthews coefficient V _M (Å ³ /Da)	2.06	2.15	2.14
Molecules in asymmetric unit	2	2	2
Solvent content (%)	40.3	42.7	42.4
R _{cryst} ^c (%)	21.4	18.3	19.6
R _{free} ^d (%)	25.8	24.3	24.4
Mean B-factor (Å ²) ^e			
Overall	34.4	25.0	32.1
Protein	32.2	22.7	30.4
Sulfate ions	47.2	44.2	68.8
Tris	44.4	–	–
PEG molecule	–	29.5	41.8
α T molecules	–	34.7	47.5
Mean occupancy– α T molecules	–	0.7	0.8
R.m.s. deviations from ideal values ^e			
Bond lengths (Å)	0.014	0.016	0.013
Bond angles (°)	2.0	2.0	1.8
Ramachandran plot ^f			
Residues in most favorable region (%)	90.9	90.8	89.3
Residues in additionally allowed regions (%)	8.2	8.7	10.2
Residues in generously/not allowed regions (%)	0.5/0.5	0.0/0.5	0.0/0.5
Coordinate error (Å)			
SIGMAA (cross-validated SIGMAA) ^e	0.17 (0.21)	0.07 (0.08)	0.19 (0.20)

^a Numbers in parenthesis are for the highest resolution shell.

^b R_{merge} = $\sum_{hkl}(\sum_i(|I_{hkl,i} - \langle I_{hkl} \rangle|))/\sum_{hkl,i} \langle I_{hkl,i} \rangle$, where $I_{hkl,i}$ is the intensity of an individual measurement of the reflection with Miller indices h, k and l , and $\langle I_{hkl} \rangle$ is the mean intensity of that reflection. Calculated for $I > 3\sigma(I)$.

^c R_{cryst} = $\sum_{hkl}(|F_{obs,hkl}| - |F_{calc,hkl}|)/|F_{obs,hkl}|$, where $|F_{obs,hkl}|$ and $|F_{calc,hkl}|$ are the observed and calculated structure factor amplitudes.

^d R_{free} is equivalent to R_{cryst} but calculated with reflections (5%) omitted from the refinement process.

^e Calculated with the program CNS (Brünger et al., 1998).

^f Calculated with the program PROCHECK (Laskowski et al., 1993).

subfamily was performed using the MUSCLE program (Edgar, 2004) after a search for these sequences at NCBI (<http://www.ncbi.nlm.nih.gov>). All the figures were generated by the Py-mol program (DeLano, 2002).

Two different angles, θ_A (aperture angle) and θ_T (torsional angle) were used to quantify the oligomeric changes between apo and complexed forms. The coordinates (x, y, z) of C α atoms from α -helices h2 and h3 were used to define vectors in each monomer: (i) monomer A; vector **A**₁ (orange)—from Glu108 (h3) to Glu97 (h3); vector **A**₂ (green)—from Glu108 (h3) to Arg43 (h2), (ii) monomer B; vector **B**₁ (blue)—from Glu97 (h3) to Glu108 (h3); vector **B**₂ (black)—from Arg43 (h2) to Glu108 (h3) (Fig. 1). θ_A is the angle between **A**₁ and **B**₁ vectors (Fig. 1b) calculated by:

$$\cos \theta_A = \frac{|\vec{\mathbf{A}}_1 \cdot \vec{\mathbf{B}}_1|}{\|\vec{\mathbf{A}}_1\| \cdot \|\vec{\mathbf{B}}_1\|}$$

θ_T is the angle between the normal (vector **n**) of plane α (beige) and the vector **B**₁ (Fig. 1c) calculated by:

$$\sin \theta_T = \frac{|\vec{\mathbf{n}} \cdot \vec{\mathbf{B}}_1|}{\|\vec{\mathbf{n}}\| \cdot \|\vec{\mathbf{B}}_1\|},$$

where **n** (red vector—Fig. 1c) is calculated by the vector cross product between **A**₁ and **A**₂.

3. Results

3.1. Overall structure of native PrTX-I and the complexes PrTX-I/ α -tocopherol and BthTX-I/ α -tocopherol

All crystals were obtained under the same crystallization conditions (two different temperatures were used) (dos Santos et al., 2007; Takeda et al., 2008) and diffracted X-rays in the range of 1.87–1.65 Å resolution. Both complexed crystals are isomorphous and belong to P2₁ space group whereas native PrTX-I crystals belong to P3₁21 (dos Santos et al., 2007; Takeda et al., 2008). Data-processing and refinement statistics are presented in Table 1.

The structures present a better stereochemical quality than expected for structures with the same resolution as indicated by the overall *G-factor* of 0.1–0.2 (Laskowski et al., 1993). All structures are dimeric and present seven disulfide bridges in each monomer, conserving structural features of other class II PLA₂s (including the catalytic network His48, Tyr52, Tyr73 and Asp99 residues).

The examination of unit-cell packing showed two possible dimeric configurations for all these structures: (i) the first possibility is stabilized by interactions between the tips of β -wings and the residues of the N-terminal helices (Arni et al., 1995); (ii) the second is stabilized by contacts between the putative calcium-binding loops and C-termini forming a connection route between the active sites of both monomers (Murakami et al., 2007). The former is

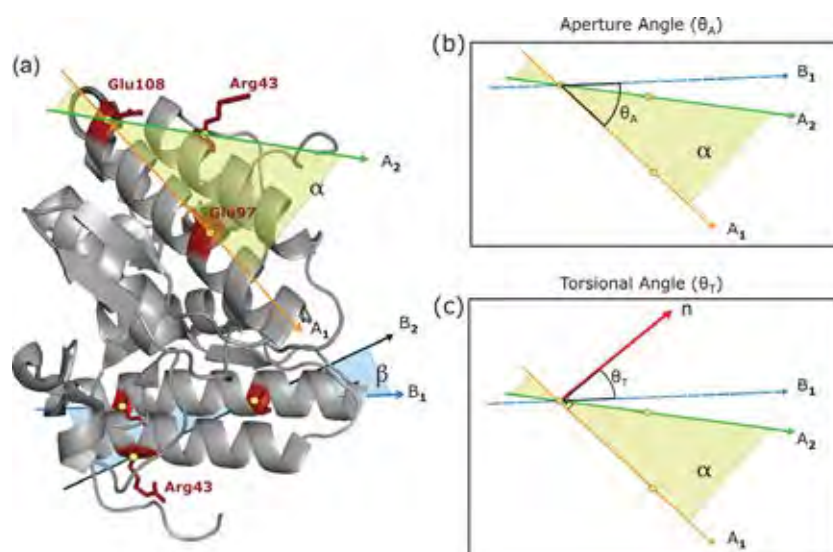


Fig. 1. Model characterizing the oligomeric changes for apo and complexed structures using two different angles. θ_A (aperture angle) indicates the aperture value between monomers defined by the vectors A_1 (orange) and B_1 (blue); θ_T (torsional angle) indicates the torsion angle between the planes α (beige) and β (blue) occupied by h2 and h3 α -helices of the monomers A and B, respectively (see Section 2 for more details). (For interpretation of color mentioned in this figure the reader is referred to the web version of the article.)

called “conventional dimer” since the most of Lys49-PLA₂s structures was solved in this configuration (Magro et al., 2003) and the latter, “alternative dimer”. The choice of the configuration with the highest probability of occurring in solution was based on the interface area and free energy values calculated by the PISA program (Krissinel and Henrick, 2007) (Table 2). Additionally, recent studies using small angle X-ray scattering experiments (Murakami et al., 2007) and functional aspects were considered in this choice (see item 4.1).

Specific analysis of the “active site” region showed that only water molecules were found in this region for native PrTX-I (in both monomers), in contrast to the complexed structures where α -tocopherol (α T) molecules were also present (Fig. 2). Additionally, the following ions or molecules were found interacting with other regions of the proteins: sulfate and Tris (2-amino-2-(hydroxymethyl) propane-1,3- diol) for native PrTX-I (Supplementary Fig. 2); sulfates and a polyethylene glycol 4000 (PEG 4000) for complexed structures (Supplementary Fig. 2). α T molecules interact with residues from the N-terminal, short helix, Ca²⁺ binding loop, “active site” and C-terminal regions. For each one of the complexed structures a PEG molecule interacts with one monomer surface stabilizing the Lys7 residue by hydrogen bonds. Application of crystallographic symmetry shows that this PEG interacts with the

other monomer leading to a displacement of Trp77. Sulfate ions interact with C-terminus residues (Lys115 and Arg 118) and Lys20 (Supplementary Fig. 2) in the three structures solved, although they present a lower occupation in apo PrTX-I. For the complexed structures only α T molecules occupancies were refined.

3.2. Comparison between native and complexed Lys49-PLA₂s

Superposition of PrTX-I/ α T monomers and BthTX-I/ α T monomers resulted in C ^{α} atom r.m.s. deviations of 0.82 and 0.76 Å, respectively, while for native PrTX-I this value was 1.04 Å. These values were compared to other Lys49-PLA₂s already deposited in the Protein Data Bank (Supplementary Table 1). A pattern was observed for apo forms, which presented an r.m.s.d. around 1.0 Å. These higher values for native forms occur mainly due to differences in their C-termini (Fig. 3d; (Supplementary Table 2—r.m.s.d. of approximately 2.0 Å)), demonstrating higher conformational plasticity of this region.

Analysis of dimeric interfaces shows that the structures presented are kept in this conformation mainly by hydrophobic interactions, although some hydrogen bonds are also observed. Furthermore, new interactions are established when the α T bound structures are formed. For native PrTX-I, three hydrogen bonds are

Table 2

Interface area and solvation free energy analyses for both oligomeric conformations (conventional and alternative) of Lys49-PLA₂s.

	Lys49-PLA ₂	Alternative dimer		Conventional dimer	
		Interface area (Å ²)	Δ^iG (kcal/mol)	Interface area (Å ²)	Δ^iG (kcal/mol)
Apo	BaspTX-II	500.9	−11.2	365.5	−0.3
	BnSP-7	622.9	−10.3	494.2	−1.3
	BnSP-6	604.1	−9.6	505.1	−1.7
	PrTX-I	667.5	−12.9	475.3	−0.9
Complexed	PrTX-I/ α T	518.6	−11.6	361.9	−0.4
	BthTX-I/ α T	503.7	−11.8	379.9	0.1
	MjTX-II/stearic acid	485.6	−8.1	331.1	0.1
	BaspTX-II/suramin	526.1	−10.3	361.3	0
	PrTX-II/fatty acid	692.7	−17.7	429.6	1.4

Δ^iG indicates the solvation free energy gain upon formation of the interface, in kcal/mol. The value is calculated as difference in total solvation energies of isolated and interfacing structures. Negative Δ^iG corresponds to hydrophobic interfaces, or positive protein affinity. This value does not include the effect of satisfied hydrogen bonds and salt bridges across the interface. Interface area in Å², calculated as difference in total accessible surface areas of isolated and interfacing structures divided by two.

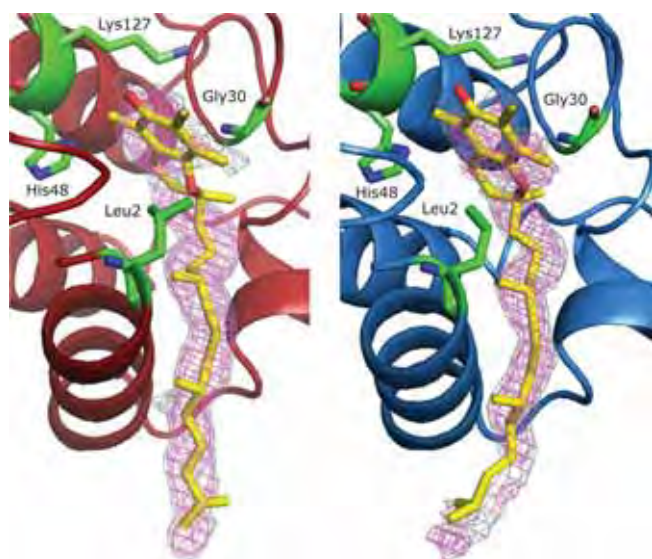


Fig. 2. Electron density omit map for the region corresponding to PrTX-I/ α T (red) and BthTX-I/ α T (blue) hydrophobic channel. α -tocopherol molecules (yellow) and the residues (green) His48, Lys49 (from “active site” regions), Gly30 (from the Ca^{2+} binding loops), and Leu2 (from N-termini) are shown. Simulated annealing was run with starting temperature of 1000 K with ligands omitted from the model. The maps were calculated with coefficients $|F_{\text{obs}}| - |F_{\text{calc}}|$ and contoured at 1.5 (grey) and 2.0 (pink) standard deviations. (For interpretation of color mentioned in this figure the reader is referred to the web version of the article.)

observed between its monomers (Asn17:Tyr119, Asn17:His120 and Val31:Lys69) whereas for PrTX-I/ α T and BthTX-I/ α T complexes Asn17:Tyr119 is maintained and a new interchain hydrogen bond (Tyr119:Tyr119) is established (Fig. 4). This interaction is also

present in all complexed Lys49-PLA₂s compared herein. In order to better characterize the oligomeric changes occurred in Lys49-PLA₂s bound to a ligand, a model based on two different angles was developed (Fig. 1—see item 2.4 for more details). Based on this analysis, two different groups could be observed (Table 3): (i) apo proteins, and (ii) complexed proteins. One exception was observed for each group (see item 4.2).

4. Discussion

4.1. Biological dimer for bothropic Lys49-PLA₂s

The oligomeric assembly appears to be a fundamental issue for the biological activity of many PLA₂s. A large number of these intriguing proteins has been solved and, although they present very similar tertiary structures, many of them have totally different biological activities and quaternary structures (Arni et al., 1995; Magro et al., 2004; Soares et al., 2004). Therefore, the key of this molecular puzzle may be related to their oligomeric assembly, as observed in several studies (Angulo et al., 2005; Corrêa et al., 2008; Magro et al., 2004; Marchi-Salvador et al., 2008; Murakami et al., 2007).

Bothropic Lys49-PLA₂s are dimeric proteins as shown by electrophoresis, spectroscopic (da Silva-Giotto et al., 1998; Arni et al., 1999), small angle X-ray scattering (Murakami et al., 2007) and dynamic light scattering experiments (data not shown). Furthermore, the dimeric state is also found *in vivo*, and it is stable even upon heating in the presence of β -mercaptoethanol (da Silva-Giotto et al., 1998; Soares et al., 2000). pH-induced dissociation studies also demonstrated a considerable decrease of membrane-damaging activity after the dimeric dissociation (Angulo et al., 2005). Several crystal structures of bothropic Lys49-PLA₂s have been solved (Arni et al., 1995, 1999; de Azevedo et al., 1999; Lee et al., 2001;

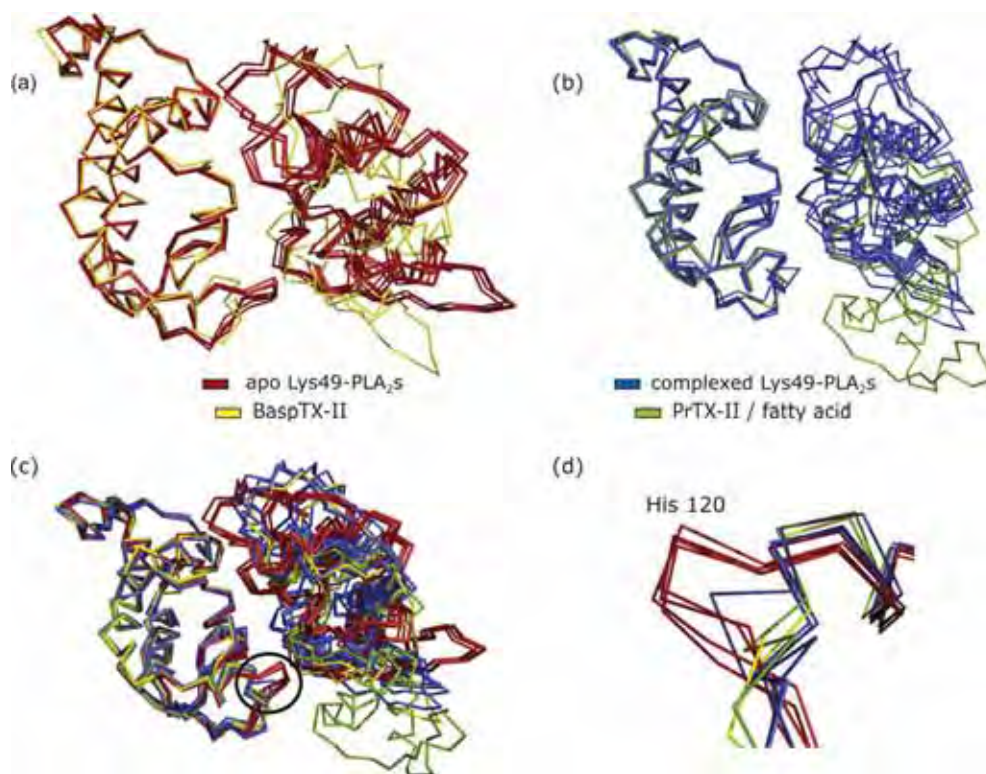


Fig. 3. Different patterns of quaternary assembly for apo (a) and complexed (b) Lys49-PLA₂s dimeric structures. BaspTX-II shows a deviation from the apo pattern (a) and PrTX-II/fatty acid shows a deviation from the complexed pattern (b). (c) Superposition of the two different patterns of oligomerization by one of their monomers shows a significant difference in their C-termini. (d) C-terminal region with significant displacement.

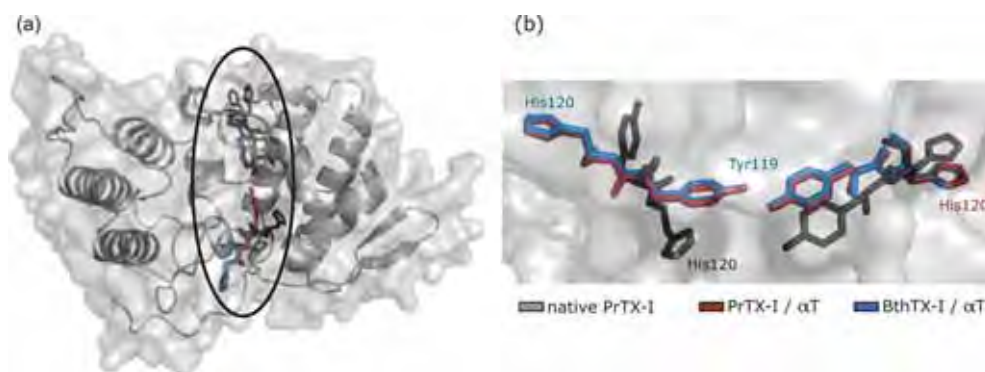


Fig. 4. (a) Superposition of the three Lys49-PLA₂s structures solved showing the localization of Tyr119 from both monomers in each structure. (b) Detailed view of Tyr119 intermolecular hydrogen bond present in α -tocopherol complexed structures. This bond occurs after the reorientation in their C-termini induced by ligand binding.

Table 3

Aperture (θ_A) and torsional (θ_T) angles for Lys49-PLA₂s.

	Lys49-PLA ₂	θ_T (torsional angle)	θ_A (aperture angle)
Apo	BaspTX-II	44°	22°
	BnSP-7	60°	6°
	BnSP-6	60°	6°
	BthTX-I	61°	6°
	PrTX-I	60°	7°
	Complexed	PrTX-I/ α T	41°
BthTX-I/ α T		40°	11°
MjTX-II/stearic acid		52°	20°
BaspTX-II/suramin		51°	15°
PrTX-II/fatty acid		81°	23°

Magro et al., 2003; da Silva-Giotto et al., 1998; Watanabe et al., 2005) and a common dimer conformation has been considered the biological unit, denominated as conventional dimer in the present work.

In 2005, the crystal structure of the complex formed by suramin (a symmetric polysulfonated naphthylurea) and the Lys49-PLA₂ BaspTX-II revealed that one ligand molecule binds simultaneously to both monomers of the protein in a similar mode, which lacks a twofold axis symmetry (Murakami et al., 2005) (Fig. 5). This mode of binding is only possible for an alternative dimeric assembly, where the hydrophobic surfaces surrounding the entrance to the active sites form the dimer interface. If the conventional dimer had been used to solve this structure a great portion of the ligand

would be exposed to the solvent (Fig. 5). Small angle X-ray scattering experiments and molecular dynamic simulations also showed this “alternative dimer” is the configuration found in aqueous solution for the Lys49-PLA₂ BthTX-I (Murakami et al., 2007). Similarly to the BaspTX-II/suramin structure, the choice of the alternative dimer appears to be relevant to the hydrophobic character of the α T ligands. These molecules (α T) present a higher buried surface area and a larger number of hydrophobic interactions with the monomers when the alternative dimer is chosen (Fig. 5); otherwise, a large portion of this ligand would be in contact with the solvent.

In order to clarify the correct assembly of bothropic Lys49-PLA₂s, nine crystal structures of these toxins were revised and the presence of the alternative dimer was a common feature for all the proteins analyzed, including both α T complexes (Table 2; Fig. 3a,b). Moreover, the dimeric interface contacts for both possible conformations were analyzed using bioinformatic tools showing that all Lys49-PLA₂s present larger interface area and negative solvation free energy values for the alternative dimer, indicating that this dimer has a higher probability to occur in solution (Table 2).

In summary, we suggest that the alternative dimer represents the true biological assembly for Lys49-PLA₂s based on the results discussed above.

4.2. Lys49-PLA₂s: apo and complexed configurations

Da Silva-Giotto et al. (1998) observed two quaternary conformations (“open” and “closed”) for BthTX-I where the β -wing re-

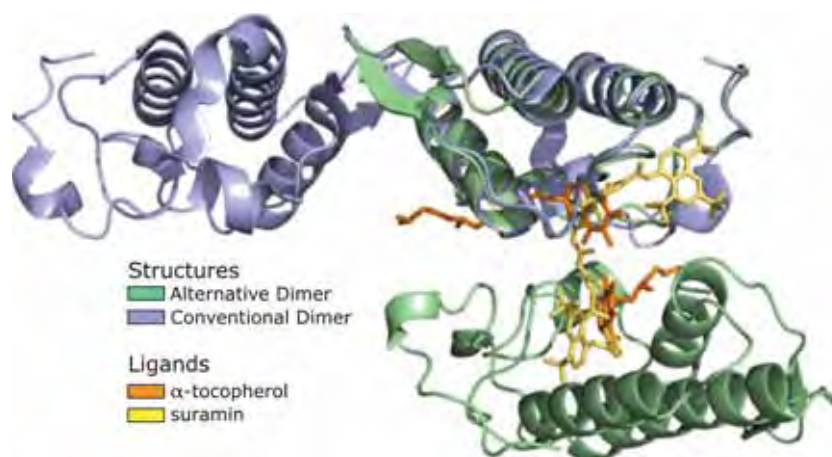


Fig. 5. Two possible dimeric configurations for Lys49-PLA₂s: alternative (green) and conventional dimers (purple). Suramin (yellow) and α -tocopherol (orange) are shown interacting with the alternative dimer. (For interpretation of color mentioned in this figure the reader is referred to the web version of the article.)

gions act as a molecular hinge allowing the characterization of these two different conformations by an aperture angle. More recently, Magro et al. (2003) compared seven Lys49-PLA₂ structures and showed there are not only two conformations but at least six different ones as a consequence of the high flexibility between the monomers. However, when the alternative dimer is considered for Lys49-PLA₂ structures, their oligomeric conformation can be divided into two classes: apo and complexed structures. This conclusion is based on the following observations.

Firstly, the superposition of monomers from each structure shows lower r.m.s.d. values for complexed structures in comparison to apo ones (Supplementary Table 2). This is due to an increase of symmetry when a ligand is present at the “active site”/hydrophobic channel since it induces a better order of their C-termini. The disorder in apo Lys49-PLA₂ C-termini has been already described (Magro et al., 2003), and interestingly this fact is remarkable only for one of the two C-termini of apo structures. This finding can be clearly observed in the case of PrTX-I and BthTX-I which have both apo and complexed structures available (Supplementary Table 2). Considering the existence of a connection route between the C-terminal and the hydrophobic channel regions in

the alternative dimer, the conformational changes experienced by the Ca²⁺ binding loop after ligand binding (Supplementary Fig. 3) appear to be the main reason for the C-terminus rearrangement in the complexed forms (Supplementary Table 2; Fig. 3c,d; Fig. 4). This reorganization of the C-terminal region leads to the establishment of the already mentioned interchain hydrogen bond between Tyr119 residues, which is a common feature for the complexed Lys49-PLA₂s and might be an important characteristic for the myotoxicity of these toxins. Site-directed mutagenesis experiments support this hypothesis since a significant decrease in the myotoxic activity was observed after Y119A mutant was tested *in vivo* (Chioato et al., 2007).

Secondly, the θ_A (aperture angle) and θ_T (torsional angle) model support the subdivision of bothropic Lys49-PLA₂s in apo and complexed forms (Table 3), which may represent two states of these toxins: “inactive” and “active” (see last item of Section 4). The myotoxic sites tend to be aligned in the same plane (side by side) in the complexed forms (active state), as indicated by lower torsional angles for these structures (Table 3). This conformation may help the active Lys49-PLA₂s to better attach the membrane.

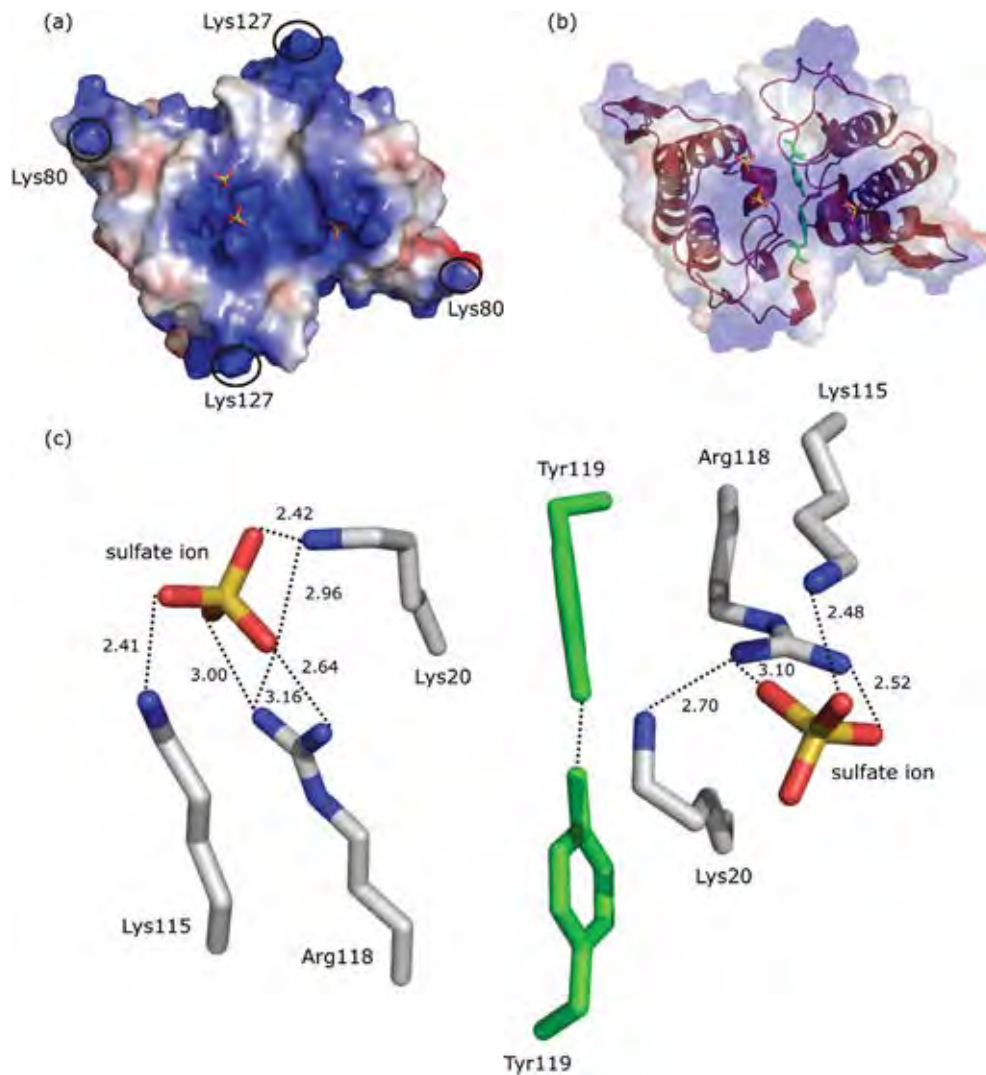


Fig. 6. Myotoxic site for bothropic Lys49-PLA₂s. (a) Surface charge distribution for PrTX-I/αT (blue, basic regions; red, acidic regions). Sulfate ions are shown interacting with the “myotoxic sites”. Lys80 and Lys127 residues with secondary importance for the myotoxic activity are also shown. (b) Semi-transparent electrostatic surface shows the disposition of both Tyr119 residues and their proximity to the “myotoxic sites”. (c) Distance (Å) between the residues of the “myotoxic sites” and atoms from the sulfate ions (these ions simulate the polar head of phospholipids).

Although apo and complexed structures could be classified in different conformational groups, BasPTX-II (Arni et al., 1995) and PrTX-II/fatty acid (Lee et al., 2001) were exceptions to this rule. The former was described as an apo structure, but according to our analyses it appears to be a complex (Table 2, Supplementary Table 1 (space group), Supplementary Table 2 (C-termini analysis) and Table 3). This probably occurred due to the limited resolution of data (2.8 Å) which made it difficult to find a fatty acid in the hydrophobic channel. No explanation for the PrTX-II/fatty acid deviation was found, except the fact it was the only complexed dimeric structure whose crystallization experiments were performed without the addition of ligands (an electron density was found in the hydrophobic channels and thus modeled as fatty acids).

4.3. Establishment of interactions between Lys49-PLA₂s and muscle membranes

Different studies pointed out the C-terminal region of Lys49-PLA₂s as being responsible for their myotoxic activity (Ambrosio et al., 2005; Chioato et al., 2002, 2007; Lomonte et al., 2003b; Núñez et al., 2001; Ward et al., 2002), especially the residues 115–116 to 129. Site-directed mutagenesis experiments demonstrated that the residues Pro37, Tyr117, Arg118, Tyr119, Lys122 and Phe125 are important to this function (Chioato et al., 2002, 2007). Lomonte and colleagues also showed the role of C-terminus in myotoxicity by experiments with synthetic peptides, revealing that residues 115–119 interact with heparin, a potent inhibitor of the myotoxic activity of Lys49-PLA₂s (Lomonte et al., 1994).

X-ray crystallographic analysis of bovine pancreatic PLA₂s suggested the importance of ions interacting with specific regions of these enzymes (Bahnsen, 2005). This author showed that interactions of phosphate ions can indicate the region(s) of these proteins that interact with membranes since they can simulate the phospholipid polar head group. PrTX-I/αT, BthTX-I/αT and other complexed structures of snake venom Lys49-PLA₂s exhibit ions interacting with specific residues; otherwise, all apo structures available in PDB do not present them. αT-bound structures present ions interacting with C-termini (Lys 115 and Arg118) and with the Lys20 residue which, according to Bahnsen's studies (2005), may represent the “myotoxic site” of bothropic Lys49-PLA₂s (Fig. 6).

In contrast, the Lys115 and Lys116 residues of the apo PrTX-I present lack of electron density confirming the high flexibility of the C-termini in the apo form. This can represent an “inactive state” of the myotoxic site while the complexed forms, in which the Lys115 and 116 have a well-defined position, correspondent to the “active state”.

Furthermore, the observations of basic residues and charge distribution along the electrostatic surface lead us to hypothesize that there are residues with secondary importance to muscle membrane damage (residues highlighted in Fig. 6a). These residues (Lys80 and Lys 127) can help in membrane “anchoring” after interactions with the primary site (Lys20, Lys115 and Arg118) are established.

Amino acid sequence alignment of Lys49-PLA₂s showed that the residues Lys20, Lys115, Arg118 and Tyr119 are conserved among all Lys49-PLA₂s from *Bothrops* genus (Fig. 7; Supplementary Table 3). It is also interesting to highlight that the Arg118 and Tyr119 residues are exclusive for bothropic venom (with exception of the Lys49-PLA₂ from *Deinagkistrodon acutus*). Moreover, the residues of the “secondary site” (Lys80 and Lys127) are also conserved among all Lys49-PLA₂s.

4.4. Evidences of an evolutive mechanism of action for Lys49-PLA₂s activity

Ambrosio and co-workers (2005) suggested a possible mechanism of “collaboration” between Asp49 and Lys49-PLA₂s activities in which the fatty acids released by Asp49-PLA₂s can be used for Lys49-PLA₂s activity. Our analyses pointed out two patterns of oligomeric assembly, being the presence/absence of ligands with high structural similarity in the hydrophobic channel (e.g. the long chain αT, fatty acids and PEG 4000 molecules) the main reason for this classification. Based on these facts, the following sequence of events supports this hypothesis: (i) the catalytic action of Asp49-PLA₂s in membranes leads to liberation of lysophospholipids and fatty acids; (ii) the released fatty acids interact with the hydrophobic channel of Lys49-PLA₂s inducing structural changes in the toxin (Fig. 3) (Lys49-PLA₂s change from the “inactive” to the “active state”—represented by apo and complexed structures, respectively); (iii) the conformational changes allow the dimeric Lys49-

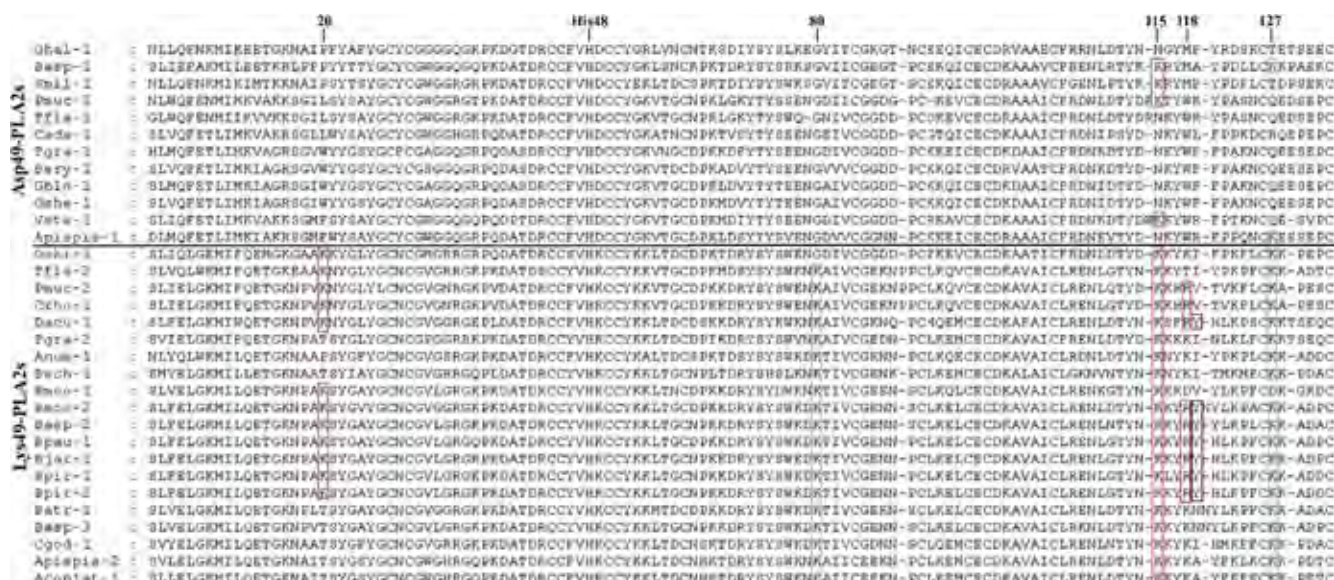


Fig. 7. Amino acid sequence alignment of Asp49 and Lys49-PLA₂s from Crotalinae subfamily snake venoms (codes used in the alignment and NCBI entries are shown in Supplementary Table 3). Residues from the “myotoxic site” (Lys20, Lys115 and Arg118) (in red) and Tyr119 (in black) are highlighted. Residues with possible secondary importance for myotoxicity (Lys80 and Lys127) are shown in blue. (For interpretation of color mentioned in this figure the reader is referred to the web version of the article.)

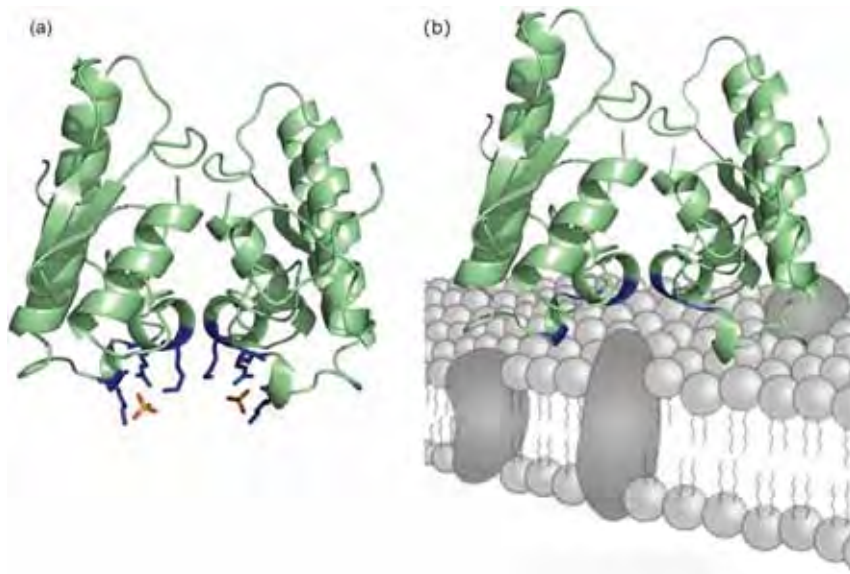


Fig. 8. “Myotoxic sites” of Lys49-PLA₂ interacting with membrane phospholipids. (a) Residues from the myotoxic sites (shown in dark blue) interacting with sulfate ions. The oxygen atoms from these ions can simulate the negatively charged atoms from phospholipids head group. (b) A model for membrane-bothropic Lys49-PLA₂s interaction. (For interpretation of color mentioned in this figure the reader is referred to the web version of the article.)

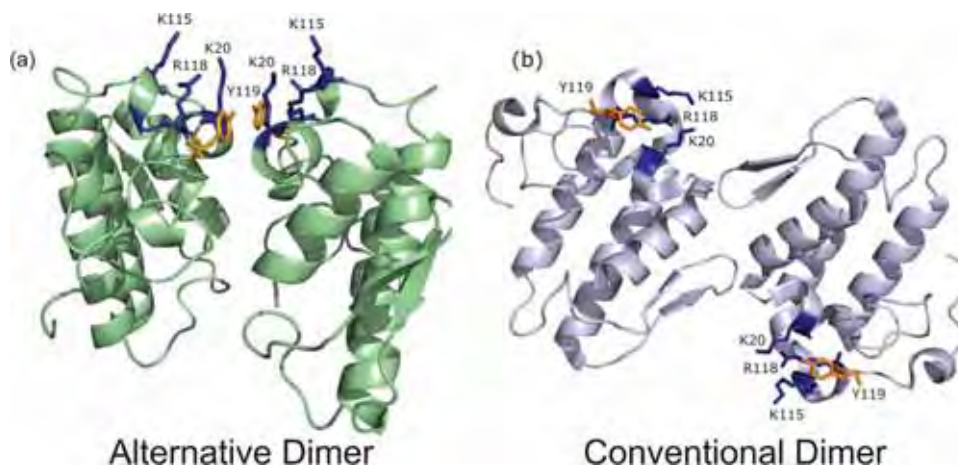


Fig. 9. “Myotoxic sites” disposition are represented for both alternative and conventional dimers of bothropic Lys49-PLA₂s. (a) Myotoxic sites (residues shown in dark blue) are disposed side by side and Tyr119 (orange) from both monomers can make a hydrogen bond in the alternative dimer. (b) Myotoxic sites (residues shown in dark blue) are disposed in the opposite sides and Tyr119 (orange) disposition do not allow their interaction if the alternative dimer is considered. (For interpretation of color mentioned in this figure the reader is referred to the web version of the article.)

PLA₂s to interact with the membrane using both “myotoxic sites” at the same time resulting in a better “anchoring” (Fig. 8) (the myotoxic sites tend to be aligned side by side in the complexed forms, as indicated by lower torsional angles for these structures (Table 3)).

These facts also support the configuration of the so-called “alternative dimer” as the biological unit since both “myotoxic sites” are arranged side by side. In contrast, they would act separately if the “conventional dimer” was considered (Fig. 9), showing no advantage for a dimeric conformation. Furthermore, the hypothesis of activation of Lys49-PLA₂s by the presence of fatty acid molecules at the phospholipase “active site” and hydrophobic channel justifies the conservation of these regions in Lys49-PLA₂s despite their catalytic inactivity. Chemical modification studies also support this idea since alkylation of His48 residue by *p*-bromophenacyl bromide dramatically reduced the myotoxic activity of both Lys49 and Asp49-PLA₂s (Soares et al., 2001a,b; Soares and Gi-

lio, 2003), demonstrating the interdependency of both “active” and “myotoxic” sites. Consequently, we suggest the “connectivity” between the two sites mentioned is a fundamental rule for the myotoxic function of Lys49-PLA₂s since it allows the transition of the “inactive” to the “active” state after ligand binding.

5. Concluding remarks

Why Lys49-PLA₂s appear to be specific to muscle membranes is not yet clear. It could be related to interaction with specific receptors or acceptors exposed on the surface of muscle membranes (Lomonte et al., 2003b) or to the presence of membrane lipid rafts with specific composition for this type of tissue (Simons and Toomre, 2000). Although this question remains to be answered, experiments employing synthetic peptides to simulate the C-terminal region showed that D-amino acids retained both activities of the natural L-enantiomer, suggesting that its mechanism of action does

not involve the recognition of a proteic receptor/acceptor site on muscle cells, but possibly binds to other structures, such as negatively-charged membrane phospholipids (Lomonte et al., 2003b) as proposed in the present study.

In conclusion, for the first time, a comprehensive hypothesis consistent with all findings for bothropic Lys49-PLA₂s studied up to this moment is proposed: (i) dimeric conformation for Lys49-PLA₂s (Arni et al., 1999; Murakami et al., 2007; da Silva-Giotto et al., 1998), (ii) “alternative” dimeric conformation (Murakami et al., 2005), (iii) connection between the “active site”/hydrophobic channel and C-terminus (Ambrosio et al., 2005), (iv) presence of fatty acid at the hydrophobic channel (Lee et al., 2001), (v) presence of sulfate ions bound to the toxin (Bahnsen, 2005) (vi) site-directed mutagenesis experiments for C-terminal residues (Chioato et al., 2002, 2007; Ward et al., 2002), and (vii) experiments employing synthetic peptides as a mimetic of the C-terminus (Lomonte et al., 2003b; Núñez et al., 2001). The proposals raised herein can guide new experiments and, if confirmed, will be of fundamental importance since it will allow structure-based inhibitors design to complement serum therapy.

5.1. Atomic coordinates

The coordinates were deposited in the Protein Data Bank with identification codes 2Q2J, 3CYL and 3CXI.

Acknowledgements

The authors thank Drs. N. Lemke and R.M. Fernandez for helping with the calculations of the angles model, Dr. A.J. Magro and C.A.H. Fernandes for the comments on the manuscript, and A.A.S. Takeda and Rafael J. Borges for helping with figures preparation. This work was supported by FAPESP, CNPq, and LNLS.

Appendix A. Supplementary data

Supplementary data associated with this article can be found, in the online version, at doi:10.1016/j.jsb.2009.04.003.

References

- Abate, A., Yang, G., Dennery, P.A., Oberle, S., Schroder, H., 2000. Synergistic inhibition of cyclooxygenase-2 expression by vitamin E and aspirin. *Free Rad. Biol. Med.* 29, 1135–1142.
- Ambrosio, A.L.B., Nonato, M.C., Selistre-de-Araújo, H.S., Arni, K., Ward, R.J., Ownby, C.H., de-Souza, D.H.F., Garratt, R.C., 2005. A molecular mechanism for Lys49-phospholipase A₂ activity based on ligand-induced conformational change. *J. Biol. Chem.* 280, 7326–7335.
- Andrião-Escarso, S.H., Soares, A.M., Fontes, M.R.M., Fuly, A.L., Correa, F.M., Rosa, J.C., Greene, L.J., Giglio, J.R., 2002. Structural and functional characterization of an acidic platelet aggregation inhibitor and hypotensive phospholipase A₂ from *Bothrops jararacussu* snake venom. *Biochem. Pharmacol.* 64, 723–732.
- Angulo, Y., Gutiérrez, J.M., Soares, A.M., Cho, W., Lomonte, B., 2005. Myotoxic and cytolytic activities of dimeric Lys49 phospholipase A₂ homologues are reduced, but not abolished, by a pH-induced dissociation. *Toxicon* 46, 291–296.
- Arni, R.K., Ward, R.J., 1996. Phospholipase A₂—a structural review. *Toxicon* 34, 827–841.
- Arni, R.K., Ward, R.J., Gutiérrez, J.M., Tulinsky, A., 1995. Structure of a calcium-independent phospholipase-like myotoxic protein from *Bothrops asper* venom. *Acta Crystallogr. D Biol. Crystallogr.* 51, 311–317.
- Arni, R.K., Fontes, M.R.M., Barberato, C., Gutiérrez, J.M., Díaz-Oreiro, C., Ward, R.J., 1999. Crystal structure of myotoxin II, a monomeric Lys49-phospholipase A₂ homologue isolated from the venom of *Cerrophidion (Bothrops) godmani*. *Arch. Biochem. Biophys.* 366, 177–182.
- Austin, A.C., Funk, C.D., 1999. Insight into prostaglandin, leukotriene, and other eicosanoid functions using mice with targeted gene disruptions. *Prostaglandins Other Lipid. Mediat.* 58, 231–252.
- Bahnsen, B.J., 2005. Structure, function and interfacial allostereism in phospholipase A₂: insight from the anion-assisted dimer. *Arch. Biochem. Biophys.* 433, 96–106.
- Balsinde, J., Balboa, M.A., Insel, P.A., Dennis, E.A., 1999. Regulation and inhibition of phospholipases A₂. *Annu. Rev. Pharmacol. Toxicol.* 39, 175–189.
- Beers, S.A., Buckland, A.G., Koduri, R.S., Cho, W., Gelb, M.H., Wilton, D.C., 2002. The antibacterial properties of secreted phospholipases A₂. A major physiological role for the group IIA enzyme that depends on the very high pI of the enzyme to allow penetration of the bacterial cell wall. *J. Biol. Chem.* 277, 1788–1793.
- Berk, P.D., Stump, D.D., 1963. Mechanisms of cellular uptake of long chain free fatty acids. *Mol. Cell Biochem.* 192, 17–31.
- Bingham 3rd, C.O., Austen, K.F., 1999. Phospholipase A₂ enzymes in eicosanoid generation. *Proc. Assoc. Am. Physicians* 111, 516–524.
- Bon, C., Changeux, J.O., Jeng, T.W., Fraenkel-Conrat, H., 1979. Postsynaptic effects of Crotoxin and its isolated subunits. *Eur. J. Biochem.* 99, 471–481.
- Brünger, A.T., Adams, P.D., Clore, G.M., Delano, W.L., Gros, P., Grosse-Kunstleve, R.W., Jiang, J.S., Kuszewski, J., Nilges, M., Pannu, N.S., Read, R.J., Rice, L.M., Simonson, T., Warren, G.L., 1998. Crystallography and NMR system: a new software suite for macromolecular structure determination. *Acta Crystallogr. D Biol. Crystallogr.* 54, 905–921.
- Chandra, V., Jasti, J., Kaur, P., Betzel, C., Srinivasan, A., Singh, T.P., 2002. First structural evidence of a specific inhibition of phospholipase A₂ by α -tocopherol (vitamin E) and its implications in inflammation: crystal structure of the complex formed between phospholipase A₂ and α -tocopherol at 1.8 Å resolution. *J. Mol. Biol.* 320, 215–222.
- Chang, C.C., Lee, J.D., Eaker, D., Fohlman, J., 1977. Short communications the presynaptic neuromuscular blocking action of taipoxin. A comparison with p-bungarotoxin and crotoxin. *Toxicon* 15, 571–576.
- Chioato, L., de Oliveira, A.H., Ruller, R., Sá, J.M., Ward, R.J., 2002. Distinct sites for myotoxic and membrane-damaging activities in the C-terminal region of a Lys49-phospholipase A₂. *Biochem. J.* 366, 971–976.
- Chioato, L., Aragão, E.A., Ferreira, T.L., Medeiros, A.I., Faccioli, L.H., Ward, R.J., 2007. Mapping the structural determinants of artificial and biological membrane damaging activities of a Lys49 phospholipase A₂ by scanning alanine mutagenesis. *Biochim. Biophys. Acta* 1768, 1247–1257.
- Corrêa, L.C., Marchi-Salvador, D.P., Cintra, A.C., Sampaio, S.V., Soares, A.M., Fontes, M.R.M., 2008. Crystal structure of a myotoxic Asp49-phospholipase A₂ with low catalytic activity: insights into Ca(2+)-independent catalytic mechanism. *Biochim. Biophys. Acta* 1784, 591–599.
- da Silva-Giotto, M.T., Garratt, R.C., Oliva, G., Mascarenhas, Y.P., Giglio, J.R., Cintra, A.C.O., de Azevedo Jr., W.F., Arni, R.K., Ward, R.J., 1998. Crystallographic and spectroscopic characterization of a molecular hinge: conformational changes in bothropstoxin I, a dimeric Lys49-phospholipase A₂ homologue. *Proteins* 30, 442–454.
- de Azevedo Jr., W.F., Ward, R.J., Canduri, F., Soares, A.M., Giglio, J.R., Arni, R.K., 1998. Crystal structure of piratoxin-I: a calcium-independent, myotoxic phospholipase A₂-homologue from *Bothrops pirajai* venom. *Toxicon* 36, 1395–1406.
- de Azevedo Jr., W.F., Ward, R.J., Gutiérrez, J.M., Arni, R.K., 1999. Structure of a Lys49-phospholipase A₂ homologue isolated from the venom of *Bothrops nummifer* (jumping viper). *Toxicon* 37, 371–384.
- DeLano, W.L., 2002. The PyMOL Molecular Graphics System. DeLano Scientific LLC, San Carlos, CA, USA.
- dos Santos, J.I., Marchi-Salvador, D.P., Fernandes, C.A.H., Silveira, L.B., Soares, A.M., Fontes, M.R.M., 2007. Preliminary X-ray crystallographic studies of a Lys49-phospholipase A₂ homologue from *Bothrops pirajai* venom complexed with p-bromophenacyl bromide and α -tocopherol inhibitors. *Protein Pept. Lett.* 14, 698–701.
- Ebadi, M., Srinivasan, S.K., Baxi, M.D., 1996. Oxidative stress and anti-oxidant therapy in Parkinson's disease. *Prog. Neurobiol.* 48, 1–19.
- Edgar, R.C., 2004. MUSCLE: multiple sequence alignment with high accuracy and high throughput. *Nucleic Acids Res.* 32, 1792–1797.
- Francis, B., Gutiérrez, J.M., Lomonte, B., Kaiser, I.I., 1991. Myotoxin II from *Bothrops asper* (Terciopelo) venom is a lysine-49 phospholipase A₂. *Arch. Biochem. Biophys.* 284, 352–359.
- Gerrard, J.M., Robinson, P., 1993. Increased phosphatidic acid and decreased lysophosphatidic acid in response to thrombin is associated with inhibition of platelet aggregation. *Biochem. Cell Biol.* 71, 432–439.
- Gijón, M.A., Leslie, C.C., 1999. Regulation of arachidonic acid release and cytosolic phospholipase A₂ activation. *J. Leukoc. Biol.* 65, 330–336.
- Gutiérrez, J.M., Lomonte, B., 1995. Phospholipase A₂ myotoxins from *Bothrops* snake venoms. *Toxicon* 33, 1405–1424.
- Gutiérrez, J.M., Lomonte, B., 1997. Phospholipase A₂ myotoxins from *Bothrops* snake venoms. In: Kini, R.M. (Ed.), *Venom Phospholipases A₂ Enzymes. Structure, Function and Mechanism*. Wiley, New York, pp. 321–352.
- Gutiérrez, J.M., Lomonte, B., Cerdas, L., 1986. Isolation and partial characterization of a myotoxin from the venom of the snake *Bothrops nummifer*. *Toxicon* 24, 885–894.
- Jancarik, J., Kim, S.H., 1991. Sparse matrix sampling: a screen method for crystallization of proteins. *J. Appl. Crystallogr.* 24, 409–411.
- Jones, T.A., Bergdoll, M., Kjeldgaard, M., 1990. O: a macromolecule modeling environment. In: Ealick, S., Bugg, C.E. (Eds.), *Crystallographic and Modeling Methods in Molecular Design*. New York, Springer-Verlag, pp. 189–195.
- Krissinel, E., Henrick, K., 2007. Inference of macromolecular assemblies from crystalline state. *J. Mol. Biol.* 372, 774–797.
- Laskowski, R.A., MacArthur, M.W., Moss, D.S., Thornton, J.M., 1993. PROCHECK: a program to check the stereochemical quality of protein structures. *J. Appl. Crystallogr.* 26, 283–291.
- Lee, W.H., da Silva-Giotto, M.T., Marangoni, S., Toyama, M.H., Polikarpov, I., Garratt, R.C., 2001. Structural basis for low catalytic activity in Lys49 phospholipases A₂—a hypothesis: the crystal structure of piratoxin II complexed to fatty acid. *Biochemistry* 40, 28–36.

- Lloret, S., Moreno, J.J., 1993. Oedema formation and degranulation of mast cells by phospholipase A2 purified from porcine pancreas and snake venoms. *Toxicon* 31, 949–956.
- Lomonte, B., Tarkowski, A., Bagge, U., Hanson, L.A., 1994. Neutralization of the cytolytic and myotoxic activities of phospholipases A₂ from *Bothrops asper* snake venom by glycosaminoglycans of the heparin/heparan sulfate family. *Biochem. Pharmacol.* 47, 1509–1518.
- Lomonte, B., Angulo, Y., Calderón, L., 2003a. An overview of Lys49-phospholipase A2 myotoxins from crotalid snake venoms and their structural determinants of myotoxic action. *Toxicon* 42, 885–901.
- Lomonte, B., Yamileth, A., Santamaría, C., 2003b. Comparative study of synthetic peptides corresponding to region 115–129 in Lys49 myotoxic phospholipases A2 from snake venoms. *Toxicon* 42, 307–312.
- MacPherson, A., 1982. *Preparation and Analysis of Protein Crystals*. Wiley, New York.
- Magro, A.J., Soares, A.M., Giglio, J.R., Fontes, M.R.M., 2003. Crystal structures of BnSP-7 and BnSP-6, two Lys49-phospholipases A2: quaternary structure and inhibition mechanism insights. *Biochem. Biophys. Res. Commun.* 311, 713–720.
- Magro, A.J., Murakami, M.T., Marcussi, S., Soares, A.M., Arni, R.K., Fontes, M.R.M., 2004. Crystal structure of an acidic platelet aggregation inhibitor and hypotensive phospholipase A2 in the monomeric and dimeric states: insights into its oligomeric state. *Biochem. Biophys. Res. Commun.* 323, 24–31.
- Mancuso, L.C., Correa, M.M., Vieira, C.A., Cunha, O.A.B., Lachatt, J.J., Selistre-de-Araújo, H.S., Owby, C.L., Giglio, J.R., 1995. Fractionation of *Bothrops pirajai* snake venom: isolation and characterization of piratoxin-I, a new myotoxic protein. *Toxicon* 33, 615–626.
- Marchi-Salvador, D.P., Corrêa, L.C., Magro, A.J., Oliveira, C.Z., Soares, A.M., Fontes, M.R.M., 2008. Insights into the role of oligomeric state on the biological activities of crotoxin: crystal structure of a tetrameric phospholipase A(2) formed by two isoforms of crotoxin B from *Crotalus durissus terrificus* venom. *Proteins* 72, 883–891.
- Molenaar, W.H., Kranenburg, O., Postma, F.R., Zondag, G.C.M., 1997. Lysophosphatidic acid: G-protein signalling and cellular responses. *Curr. Opin. Cell Biol.* 9, 168–173.
- Murakami, M.T., Arruda, E.Z., Melo, P.A., Martinez, A.B., Calil-Elias, S., Tomaz, M.A., Lomonte, B., Gutiérrez, J.M., Arni, R.K., 2005. Inhibition of myotoxic activity of *Bothrops asper* myotoxin II by the anti-trypanosomal drug suramin. *J. Mol. Biol.* 350, 416–426.
- Murakami, M.T., Viçoti, M.M., Abrego, J.R.B., Lourenzoni, M.R., Cintra, A.C.O., Arruda, E.Z., Tomaz, M.A., Melo, P.A., Arni, R.K., 2007. Interfacial surface charge and free accessibility to the PLA2-active site-like region are essential requirements for the activity of Lys49 PLA2 homologues. *Toxicon* 49, 378–387.
- Navaza, J., 1994. AMoRe: an automated package for molecular replacement. *Acta Crystallogr. A* 50, 157–163.
- Needleman, P., Turk, J., Jakschik, B.A., Morrison, A.R., Lefkowitz, J.B., 1986. Arachidonic acid metabolism. *Annu. Rev. Biochem.* 55, 69–102.
- Núñez, C.E., Yamileth, A., Lomonte, B., 2001. Identification of the myotoxic site of the Lys49 phospholipase A2 from *Agkistrodon piscivorus piscivorus* snake venom: synthetic C-terminal peptides from Lys49, but not from Asp49 myotoxins, exert membrane-damaging activities. *Toxicon* 39, 1587–1594.
- Otwinowski, Z., Minor, W., 1997. Processing of X-ray diffraction data collected in oscillation mode. *Methods Enzymol.* 276, 307–326.
- Paramo, L., Lomonte, B., Pizarro-Cerda, J., Bengoechea, J.A., Gorvel, J.P., Moreno, E., 1998. Bactericidal activity of Lys49 and Asp49 myotoxic phospholipases A2 from *Bothrops asper* snake venom—synthetic Lys49 myotoxin II-(115–129)-peptide identifies its bactericidal region. *Eur. J. Biochem.* 253, 452–461.
- Pentland, A.P., Morrison, A.R., Jacobs, S.C., Hruza, L.L., Hebert, J.S., Packer, L., 1992. Tocopherol analogues suppress arachidonic acid metabolism via phospholipase inhibition. *J. Biol. Chem.* 267, 1603–1608.
- Rosenberg, P., 1990. Phospholipases. In: Shier, W.T., Mebs, D. (Eds.), *Handbook of Toxicology*. New York, Marcel Dekker, pp. 67–277.
- Sano, M., Ernesto, C., Thomas, R.G., Klauber, M.R., Schafer, K., Grundman, M., Woodbury, P., Gowdon, J., Cotman, C.W., Pfeiffer, E., Schneider, L.S., Thal, L.J., 1997. A controlled trial of selegiline, alpha-tocopherol, or both as treatment for Alzheimer's disease. The Alzheimer's Disease Cooperative Study. *N. Engl. J. Med.* 336, 1216–1222.
- Scott, D., Achari, A., Vidal, J.C., Sigler, P.B., 1992. Crystallographical and biochemical studies of the (inactive) Lys49 phospholipase A₂ from the venom of *Agkistrodon piscivorus piscivorus*. *J. Biol. Chem.* 267, 22645–22657.
- Simons, K., Toomre, D., 2000. Lipid rafts and signal transduction. *Nat. Rev. Mol. Cell Biol.* 1, 31–39.
- Soares, A.M., Giglio, J.R., 2003. Chemical modifications of phospholipases A2 from snake venoms: effects on catalytic and pharmacological properties. *Toxicon* 42, 855–868.
- Soares, A.M., Guerra-Smarka, R., Borja-Oliveira, C.R., Rodrigues, V.M., Rodrigues-Simioni, L., Rodrigues, V., Fontes, M.R.M., Lomonte, B., Gutiérrez, J.M., Giglio, J.R., 2000. Molecular cloning and functional characterization of BnSP-7, a myotoxin Lys-49 phospholipase A₂ homologue, from *Bothrops neuwiedi pauloensis* venom. *Arch. Biochem. Biophys.* 378, 201–209.
- Soares, A.M., Andrião-Escarso, S.H., Bortoleto, R.K., Rodrigues-Simioni, L., Arni, R.K., Ward, R.J., Gutiérrez, J.M., Giglio, J.R., 2001a. Dissociation of enzymatic and pharmacological properties of piratoxins-I and -III, two myotoxic phospholipases A₂ from *Bothrops pirajai* snake venom. *Arch. Biochem. Biophys.* 387, 188–196.
- Soares, A.M., Mancin, A.C., Cecchini, A.L., Arantes, E.C., Franca, S.C., Gutiérrez, J.M., Giglio, J.R., 2001b. Effects of chemical modifications of crotoxin B, the phospholipase A₂ subunit of crotoxin from *Crotalus durissus* snake venom, on its enzymatic and pharmacological activities. *Int. J. Biochem. Cell Biol.* 33, 877–888.
- Soares, A.M., Fontes, M.R.M., Giglio, J.R., 2004. Phospholipase A2 myotoxins from *Bothrops* snake venoms: structure function relationship. *Curr. Org. Chem.* 8, 1677–1690.
- Takeda, A.A.S., dos Santos, J.I., Marchi-Salvador, D.P., Soares, A.M., Fontes, M.R.M., 2008. Crystallization and preliminary X-ray crystallographic studies of a myotoxic Lys49-phospholipase A2 from *Bothrops jararacussu* venom complexed with α -tocopherol inhibitor. *Open Crystallogr. J.* 1, 6–9.
- Toyama, M.H., Soares, A.M., Vieira, C.A., Novello, J.C., Oliveira, B., Giglio, J.R., Marangoni, S., 1998. Amino acid sequence of piratoxin-I, a myotoxin from *Bothrops pirajai* snake venom, and its biological activity after alkylation with *p*-bromophenacyl bromide. *J. Protein Chem.* 17, 713–718.
- van Deenen, L.L.M., de Haas, G.H., 1963. The substrate specificity of phospholipase A2. *Biochem. Biophys. Acta* 70, 538–553.
- Wallace, A.C., Laskowski, R.A., Thornton, J.M., 1995. LIGPLOT: a program to generate schematic diagrams of protein–ligand interactions. *Prot. Eng.* 8, 127–134.
- Ward, R.J., Rodrigues Alves, A., Ruggiero Neto, J., Arni, R.K., Casari, G., 1998. A sequence space analysis of phospholipase A2. *Protein Eng.* 11, 285–294.
- Ward, R.J., Chioato, L., de Oliveira, A.H.C., Ruller, R., Sá, J.M., 2002. Active-site mutagenesis of a Lys49-phospholipase A2: biological and membrane-disrupting activities in the absence of catalysis. *Biochem. J.* 362, 89–96.
- Watanabe, L., Soares, A.M., Ward, R.J., Fontes, M.R.M., Arni, R.K., 2005. Structural insights for fatty acid binding in a Lys49-phospholipase A2: crystal structure of myotoxin II from *Bothrops moojeni* complexed with stearic acid. *Biochimie* 87, 161–167.

The Intriguing Phospholipases A₂ Homologues: Relevant Structural Features on Myotoxicity and Catalytic Inactivity

Juliana I. dos Santos, Carlos A.H. Fernandes, Angelo J. Magro and Marcos R.M. Fontes*

Departamento de Física e Biofísica, Instituto de Biociências, UNESP, Botucatu/ SP, Brazil

Abstract: Phospholipases A₂ homologues are found in the venom of Crotalinae snakes, being their main action related to myonecrosis induction. Although many studies on these toxins had already been performed, their mechanism of action remains unclear. Here, important aspects about these toxins are reviewed, including their correct biological assembly and how essential is the natural substitution D49K for their catalytic inactivity.

Keywords: Phospholipase A₂ homologues, snake venom, oligomeric conformation, quaternary structure, myotoxicity, X-ray crystallography.

INTRODUCTION

Homologues phospholipases A₂ (PLA₂s), also known as Lys49-PLA₂s, are a subgroup of PLA₂s characterized by the natural substitution D49K [1]. These proteins are incapable of binding Ca²⁺ ion, the essential co-factor for PLA₂s catalysis [2], what results in their disability to promote phospholipid hydrolysis [3]. Despite this, they induce myonecrosis, among other pharmacological effects, which is not efficiently neutralized by serum therapy [4].

The first Lys49-PLA₂ was isolated in 1984 from the venom of *Agkistrodon piscivorus piscivorus* by Maragarone *et al.* [1] and, since then, a great number of these proteins have been found in several Asian and New World viperid species. Currently, almost thirty described amino acid sequences of these proteins can be found in the National Center for Biotechnology Information (NCBI) databases and eighteen crystallographic structures of native (apo) and complexed forms are available in the Protein Data Bank (PDB). Furthermore, other variant forms of snake venom PLA₂s with alanine, arginine, asparagine, cysteine, glutamine, and serine at position 49 have been identified recently [5-10].

In this review, we will discuss three main topics about Lys49-PLA₂s: i) important features for their myotoxicity, ii) how essential is the natural substitution D49K for their catalytic inactivity and, iii) the relevance of the quaternary assembly for their activity.

LYS49-PLA₂S MYOTOXICITY: A HISTORICAL APPROACH

The myotoxic effect induced by Lys49-PLA₂s was firstly detected by Gutierrez *et al.* [11] using plasma creatine kinase release assay, histological and ultrastructural techniques. In 1994, Lomonte *et al.* [12] observed cytolytic action of myotoxin II from *Bothrops asper* on a variety of cell types in culture, including skeletal muscle myoblasts. These authors

suggested that the region responsible for this effect, further implicating in myotoxicity, is composed of basic and hydrophobic amino acid residues.

Studies with different polyanions showed heparin derivatives can inhibit the myotoxic activity of bothropstoxin I (BthTX-I), a Lys49-PLA₂ from *Bothrops jaracussu* snake venom [13]. Moreover, studies using synthetic peptides with different amino acid sequence compositions demonstrated the peptide whose sequence corresponds to the C-terminal segment (115-129) of myotoxin II from *Bothrops asper* venom interacts with heparin [14]. This segment is rich in basic, aromatic and hydrophobic residues, demonstrating conformity with the data formerly obtained [14]. Other experiments with C-terminal synthetic peptides showed similar results and pointed out the importance of a hydrophobic residue at position 121 for membrane disorganization [15,16]. Thus, it is possible to suggest that the electrostatic interactions between cationic residues of Lys49-PLA₂s C-termini and negatively charged groups of phospholipidic membranes are important for sarcolemma disruption [2]. Indeed, other site-directed mutagenesis experiments demonstrated the substitution of Tyr117, Arg118, Tyr119, Lys122, and Phe125 by Ala residues resulted in a significant reduction of Lys49-PLA₂s myotoxic activity [17,18].

In 1998, a Lys49-PLA₂ (BthTX-I) was crystallized by da Silva-Giotto and colleagues in two different conformations ("open" and "closed") [19]. After comparison of these two structures, the authors suggested a mechanism of action for Lys49-PLA₂s based on the flexibility between their monomers [19]. According to them, the dimer interface might act as a hinge, allowing a relative displacement of the C-terminal region along membrane phospholipids bilayers. It leads to C-terminal specific residues insertion in the membrane and to its consequently disorganization [19]. Additional crystallographic studies with Lys49-PLA₂s proposed a fatty acid bound in the active site of these toxins leads to a significant additional exposure of hydrophobic amino acids at the surface of the C-terminal region, increasing the interaction of Lys49-PLA₂s with muscle membranes [20].

*Address correspondence to this author at the Departamento de Física e Biofísica, Instituto de Biociências, UNESP, Botucatu/SP, Brasil, 18.618-000; Tel: +55-14-3811-6254; Fax: +55-14-3815-3744; E-mail: fontes@ibb.unesp.br

LYS49-PLA₂S LACK OF CATALYTIC ACTIVITY: ANY INFLUENCE OF THE QUATERNARY STRUCTURE?

Initially, Lys49-PLA₂s were believed to be inactive proteins upon membrane phospholipids due to their incapacity to bind the cofactor Ca²⁺. This inability had been directly attributed to the natural substitution D49K, which prevents the stabilization of the tetrahedral intermediate formed in the Ca²⁺-dependent catalytic reaction carried out by Asp49-PLA₂s [3]. Structural studies support this hypothesis demonstrating the ε-amino group of Lys49 occupies the position of the coordinated Ca²⁺ ion in Asp49-PLA₂s structures [3, 21-23]. Furthermore, site-directed mutagenesis with porcine [24] and bovine [25] pancreatic PLA₂s showed D49K mutant suffers a severe reduction in its ability to bind Ca²⁺ with a concomitant loss of catalytic activity.

Despite of the apparent catalytic inactivity of these molecules, some *in vitro* studies have provided evidences of a limited PLA₂ activity for Lys49-PLA₂s [26-32]. Later, these results were criticized since they were performed with crude toxins and, for this reason, possible traces of Asp49-PLA₂s could be responsible by the residual enzymatic activity observed [3]. In contrast, experiments with recombinant PLA₂s have demonstrated Lys49-PLA₂s were unable to catalyze artificial substrates *in vitro* [33]. On the other hand, it has been observed an extensive release of natural fatty acids after exposure of radiolabelled cell cultures to Lys49-PLA₂s [32,34]. However, it is important to emphasize the origin of these fatty acids is questionable since it is impossible to establish if they were released by a direct action of Lys49-PLA₂s or by an indirect activation of endogenous cellular lipases via Ca²⁺ intracellular influx.

Site-directed mutagenesis experiments with a Lys49-PLA₂ showed K49D mutant remained catalytically inactive, demonstrating the single D49K replacement is not crucial for the lack of enzymatic activity in these toxins [33], and suggesting the catalytic inactivity of these homologues PLA₂s

may be related to other structural features. Lee *et al.* [35] studied the structure of the complex formed between a Lys49-PLA₂ from *Bothrops pirajai* venom complexed with a fatty acid and proposed that Lys122 (conserved in all Lys49-PLA₂s but rare in Asp49-PLA₂s) interacts with the carbonyl of Cys29. This interaction hyperpolarizes the peptide bond between Cys29 and Gly30, leading to an increased affinity for the fatty acid head group. In an ultimate instance, it precludes the hydrophobic channel making impossible any other molecule to bind in this region, thus preventing the occurrence of catalysis. Strengthening this hypothesis, Magro *et al.* [36], after analyses of eight dimeric Lys49-PLA₂s structures, observed Lys122 interacts with Cys29 in both monomers only in structures which present ligands in their hydrophobic channels. Otherwise, for apo structures it was observed an alternative conformation for Lys122 in one or both monomers.

In addition to residues Lys49 and Lys122, sequence alignment analysis indicates other residues that are conserved among Lys49-PLA₂s but not in Asp49-PLA₂s. (Fig. 1, Table 1). This shows Lys49-PLA₂s present other particularities that may be responsible their catalytic inactivity - these conserved residues can, for example, induce a different oligomeric conformation in these toxins. Examination of Asp and Lys49-PLA₂s quaternary structures solved by X-ray crystallographic techniques support these observations since it shows their oligomeric conformations are different. Therefore, careful analyses regarding these observations can validate this hypothesis and might help to explain their catalytic inactivity.

BOTHROPIC LYS49-PLA₂S: THE CORRECT ASSEMBLY PROBLEM

The oligomeric assembly appears to be a fundamental issue for the biological activity of many PLA₂s. A large number of these intriguing proteins has been solved and, although they present similar tertiary structures, many of



Figure 1. Amino acid sequence alignment of Asp49 and Lys49-PLA₂s from Crotalinae subfamily snake venoms (codes used in the alignment and NCBI entries are shown in Table 1). Residues conserved among Lys49-PLA₂s but not in Asp49-PLA₂s are highlighted.

Table 1. NCBI Entry Codes for Asp49 and Lys49-PLA₂s Used in the Alignment Presented in Fig. 1

	Protein*	NCBI ID Code	Species or Subspecies
Asp49-PLA ₂ s	Ghal-1	P14421	<i>Gloydus halys</i>
	Basp-1	P20474	<i>Bothrops asper</i>
	Smil-1	ABY77926	<i>Sistrurus miliaris</i>
	Pmuc-1	Q91506	<i>Protobothrops mucrosquamatus</i>
	Tfla-1	1202299A	<i>Trimeresurus flavoviridis</i>
	Cada-1	P00623	<i>Crotalus adamanteus</i>
	Tgra-1	P81479	<i>Trimeresurus gramineus</i>
	Bery-1	ABC96692	<i>Bothrops erythromelas</i>
	Gblo-1	P20249	<i>Gloydus blomhoffi</i>
	Gshe-1	AAR11860	<i>Gloydus shedaensis</i>
	Vste-1	AAP48901	<i>Viridovipera stejnegeri</i>
	Apispis-1	A53872	<i>Agkistrodon piscivorus piscivorus</i>
Lys49-PLA ₂ s	Ooki-1	Q92152	<i>Ovophis okinavensis</i>
	Tfla-2	BAA01561	<i>Trimeresurus flavoviridis</i>
	Pmuc-2	P22640	<i>Protobothrops mucrosquamatus</i>
	Arho-1	Q9PVF3	<i>Calloselasma rhodostoma</i>
	Dacu-1	O57385	<i>Deinagkistrodon acutus</i>
	Tgra-2	P70090	<i>Trimeresurus gramineus</i>
	Anum-1	P82950	<i>Atropoides nummifer</i>
	Bsch-1	P80963	<i>Bothriechis schlegelii</i>
	Bmoo-1	P82114	<i>Bothrops moojeni</i>
	Bmoo-2	Q9I834	<i>Bothrops moojeni</i>
	Basp-2	P24605	<i>Bothrops asper</i>
	Bpau-1	AAO27453	<i>Bothrops pauloensis</i>
	Bjar-1	AAB25286	<i>Bothrops jararacussu</i>
	Bpir-1	P58399	<i>Bothrops pirajai</i>
	Bpir-2	P82287	<i>Bothrops pirajai</i>
	Batr-1	AAR97287	<i>Bothrops atrox</i>
	Basp-3	AAF14241	<i>Bothrops asper</i>
	Cgod-1	AAL39066	<i>Cerrophidion godmani</i>
	Apispis-2	P04361	<i>Agkistrodon piscivorus piscivorus</i>
	Aconlat-1	AAC59887	<i>Agkistrodon contortrix laticinctus</i>

*Abbreviations for snake venom PLA₂s used in the alignment

them have totally different biological activities and quaternary structures [23,37,38]. Therefore, the key to this molecular puzzle may be related to their oligomeric assembly, as observed in several studies [37,39-42].

Bothropic Lys49-PLA₂s, the most studied proteins of this group, are dimeric as shown by electrophoresis, spectroscopic [19,43], small angle X-ray scattering [39] and dynamic light scattering experiments (data not shown). The dimeric conformation has been also found *in vivo* [43], and it

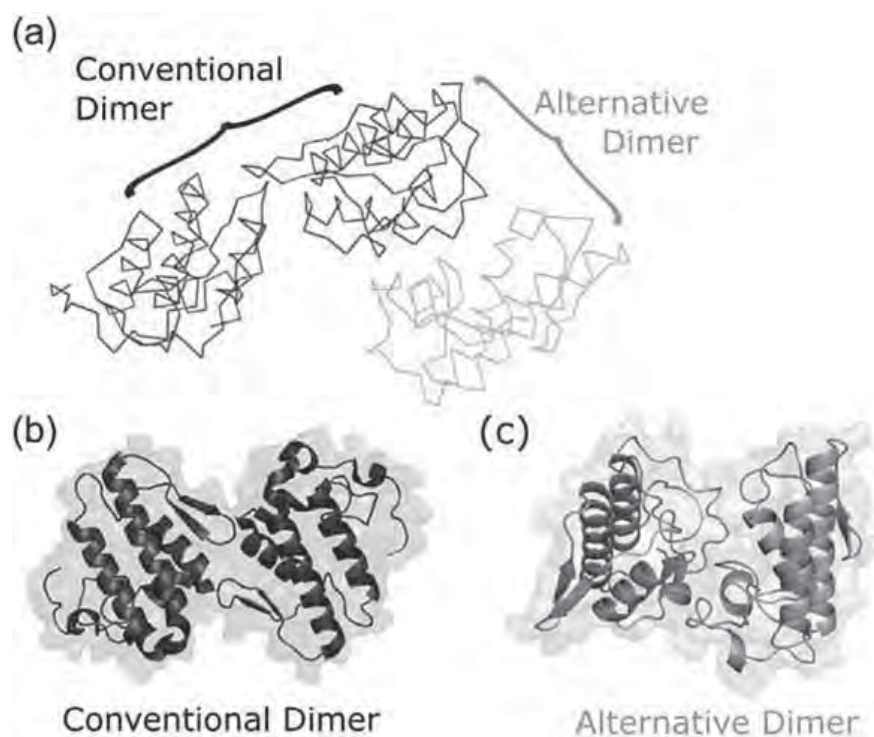


Figure 2. (a) Possible quaternary assemblies for Lys49-PLA₂s structures. (b) “Conventional dimer”. (c) “Alternative dimer”.

is stable even upon heating in the presence of 1% SDS [19,44].

The first structure of a Lys49-PLA₂ from *Bothrops* genus was solved in 1995 [23] and, since then, several crystal structures of Lys49-PLA₂s from the same genus have been solved [19,23,35,36,43,45,46]. A common dimeric conformation was found for all these structures, which is stabilized by interactions between the tips of β -wings and the residues of the N-terminal helices, leading to a relative flexibility between their monomers [19,36] (Fig. 2b). Spectroscopic investigations performed by da Silva-Giotto and colleagues [19] support the existence of this oligomeric conformation in solution. Otherwise, in 2005, Murakami and co-workers [47] crystallized BaspTX-II (myotoxin II from *Bothrops asper*) with suramin (a symmetric polysulfonated naphthylurea) and observed that a suramin molecule binds to both monomers of the protein simultaneously, being these interactions only allowed if a novel Lys49-PLA₂ quaternary conformation is considered (Fig. 2c). This “alternative dimeric assembly” is stabilized by contacts between the putative calcium-binding loop and C-terminal regions, and its dimeric interface is formed by the hydrophobic surfaces surrounding the entrance to the active sites (Fig. 2c). If the “conventional dimer” had been used to solve this structure, it would not be energetically favorable since a great portion of the ligand would be exposed to the solvent [47]. The same problem was faced when dos Santos *et al.* [48] solved the first Lys49-PLA₂ crystal structure complexed with α -tocopherol (α T). In this case, the choice for the “alternative dimer” was relevant when the hydrophobic character of α T ligands were considered [49].

In order to determine if this new conformation (“alternative dimer”) was induced by ligand binding or is a possibility for all bothropic Lys49-PLA₂s, the structures of these proteins available in the PDB (Protein Data Bank – <http://www.pdb.org>) (Table 2) were inspected by crystallographic symmetry application. The “alternative dimer” was demonstrated to be a possible oligomeric conformation for all the proteins analyzed [49].

Aiming to get more information in this scenario, bioinformatics analyses were performed using the on-line PISA program [50] (Protein Interfaces, Surfaces and Assemblies; http://www.ebi.ac.uk/msd-srv/prot_int/pistart.html). Despite the variability of results, all Lys49-PLA₂s present larger interface area and negative solvation free energy values for the “alternative dimer”, indicating this dimer is more stable in solution [49] (Table 3). Small angle X-ray scattering experiments and molecular dynamics simulations with BthTX-I also indicate the “alternative dimer” as the most probable conformation in aqueous solution [39].

Considering experiments and bioinformatics analyses with Lys49-PLA₂s indicate two possibilities for their oligomeric conformation, determination of the dimer that represents the biological unit is of fundamental importance; otherwise any experiment or inference based on structural analysis can point in a wrong direction. As soon as this problem becomes solved, it will be possible to perform structure-based inhibitors design to develop complementary therapies since the muscle damage induced by these proteins is not efficiently neutralized by serum therapy administration.

Table 2. Bothropic Lys49-PLA₂s Crystallographic Structures Available in the Protein Data Bank (PDB)

Lys49-PLA ₂	PDB code	Snake specie	Reference
BaspTX-II	1CLP	<i>Bothrops asper</i>	Arni <i>et al.</i> , 1995 ²³
BnSP-7	1PA0	<i>Bothrops pauloensis</i>	Magro <i>et al.</i> , 2003 ³⁶
BnSP-6	1PC9	<i>Bothrops pauloensis</i>	Magro <i>et al.</i> , 2003 ³⁶
PrTX-I	2Q2J	<i>Bothrops pirajai</i>	dos Santos <i>et al.</i> , 2009 ⁴⁹
BthTX-I complexed with PEG 400	2H8I	<i>Bothrops jararacussu</i>	Murakami <i>et al.</i> , 2007 ³⁹
MjTX-II complexed with stearic acid	1XXS	<i>Bothrops moojeni</i>	Watanabe <i>et al.</i> , 2005 ⁴⁵
BaspTX-II complexed with suramin	1Y4L	<i>Bothrops asper</i>	Murakami <i>et al.</i> , 2005 ⁴⁷
PrTX-II complexed with fatty acid	1QLL	<i>Bothrops pirajai</i>	Lee <i>et al.</i> , 2001 ³⁵
PrTX-I complexed with alpha-tocopherol	3CYL	<i>Bothrops pirajai</i>	dos Santos <i>et al.</i> , 2008 ⁴⁹
BthTX-I complexed with alpha-tocopherol	3CXI	<i>Bothrops jararacussu</i>	dos Santos <i>et al.</i> , 2008 ⁴⁹

Table 3. Interface Area and Solvation Free Energy Analyses for Both Possible Oligomeric Conformations (Conventional and Alternative) of Lys49-PLA₂s Calculated by PISA Program [50]

Lys49-PLA ₂	Alternative Dimer		Conventional Dimer	
	Interface área(A ²)	Δ ¹ G (Kcal/M)	Interface área(A ²)	Δ ¹ G (Kcal/M)
BaspTX-II	500.9	-11.2	365.5	-0.3
BnSP-7	622.9	-10.3	494.2	-1.3
BnSP-6	604.1	-9.6	505.1	-1.7
PrTX-I	667.5	-12.9	475.3	-0.9
BthTX-I/PEG 400	891.8	-15.2	493.7	-0.6
MjTX-II/stearic acid	485.6	-8.1	331.1	0.1
BaspTX-II/suramin	526.1	-10.3	361.3	0
PrTX-II/fatty acid	692.7	-17.7	429.6	1.4
PrTX-I/αT	518.6	-11.6	361.9	-0.4
BthTX-I/αT	503.7	-11.8	379.9	0.1

Δ¹G indicates the solvation free energy gain upon formation of the interface, in kcal/M. The value is calculated as difference in total solvation energies of isolated and interfacing structures. Negative Δ¹G corresponds to hydrophobic interfaces, or positive protein affinity. This value does not include the effect of satisfied hydrogen bonds and salt bridges across the interface. **Interface area** in Å², calculated as difference in total accessible surface areas of isolated and interfacing structures divided by two.

REFERENCES

- [1] Maragarone, J.M.; Merutka, G.; Cho, W.; Welches, W.; Kezdy, F.J.; Heinrikson, R.L. A new class of phospholipase A₂ with lysine in place of aspartate 49. *J. Biol. Chem.*, **1984**, 259(22), 13839-13843.
- [2] Lomonte, B.; Angulo, Y.; Calderon, L. An overview of Lys49-phospholipase A₂ myotoxins from crotalid snake venoms and their structural determinants of myotoxic action. *Toxicon*, **2003**, 42(8), 885-901.
- [3] Holland, D.R.; Clancy, L.L.; Muchmore, S.W.; Ryde, T.J.; Einspahr, H.M.; Finzel, B.C.; Heinrikson, R.L.; Watenpaugh, K.D. The crystal structure of a lysine 49 phospholipase A₂ from the venom of the cottonmouth snake at 2.0Å resolution. *J. Biol. Chem.*, **1990**, 265(29), 17649-17656.
- [4] Gutiérrez, J. M.; Lomonte, B. Phospholipase A₂ myotoxins from *Bothrops* snake venoms (1995). *Toxicon*, **1995**, 33(11), 1405-1424.
- [5] Liu, C.S.; Kuo, P.Y.; Chen, J.M.; Chen, S.W.; Chang, C.H.; Tseng, C.C.; Tzeng, M.C.; Lo, T.B. Primary structure of an inactive mutant of phospholipase A₂ in the venom of *Bungarus fasciatus* (banded krait). *J. Biochem.*, **1992**, 112(5), 707-713.
- [6] Mebs, D.; Kuch, U.; Coronas, F.I.; Batista, C.V.; Gumprecht, A.; Possani, L.D. Biochemical and biological activities of the venom of the Chinese pitviper *Zhaovermia mangshanensis*, with the complete amino acid sequence and phylogenetic analysis of a novel Arg49 phospholipase A₂ myotoxin. *Toxicon*, **2006**, 47(7), 797-811.
- [7] Hua, P.; Liu, X.L.; Ou-Yang, L.L.; Yang, G.Z.; Zhou, Y.C.; Li, Z.P.; Wu, X.F. Diversity of cDNAs encoding phospholipase A₂ from *Agkistrodon halys* Pallas venom, and its expression in *E. coli*. *Toxicon*, **1998**, 36(8), 1155-1163.
- [8] Jabeen, T.; Singh, N.; Singh, R.K.; Jasti, J.; Sharma, S.; Kaur, P.; Srinivasan, A.; Singh, T.P. Crystal structure of a heterodimer of phospholipase A₂ from *Naja naja sagittifera* at 2.3 Å resolution reveals the presence of a new PLA₂-like protein with a novel Cys

- 32-Cys 49 disulphide bridge with a bound sugar at the substrate-binding site. *Proteins*, **2006**, 62(2), 329-337.
- [9] Bao, Y.; Bu, P.; Jin, L.; Hongxia, W.; Yang, Q.; An, L. Purification, characterization and gene cloning of a novel phospholipase A₂ from the venom of *Agkistrodon blomhoffii ussurensis*. *Int. J. Biochem. Cell. B.*, **2005**, 37(3), 558-565.
- [10] Polgar, J.; Magnenat, E.M.; Peitsch, M.C.; Wells, M.C.; Clemetson, K.J. Asp-49 is not an absolute prerequisite for the enzymic activity of low-M(r) phospholipases A₂: purification, characterization and computer modelling of an enzymically active Ser-49 phospholipase A₂, ecarpholin S, from the venom of *Echis carinatus sochureki* (saw-scaled viper). *Biochem. J.*, **1996**, 319(3), 961-968.
- [11] Gutiérrez, J.M.; Lomonte, B.; Cerdas, L. Isolation and partial characterization of a myotoxin from the venom of the snake *Bothrops nummifer*. *Toxicon*, **1986**, 24(9), 885-894.
- [12] Lomonte, B.; Tarkowski, A.; Hanson, L.Å. Broad cytolytic specificity of myotoxin II, a lysine-49 phospholipase A₂ of *Bothrops asper* snake venom. (1994). *Toxicon*, **1994**, 32(11), 1359-1369.
- [13] Melo, P.A.; Homs-Brandeburgo, M.I.; Giglio, J.R.; Suarez-Kurtz, G. Antagonism of the myotoxic effect of *Bothrops jararacussu* venom and bothropstoxin by polyanions. *Toxicon*, **1993**, 31(3), 87-95.
- [14] Lomonte, B.; Moreno, E.; Tarkowski, A.; Hanson, L.Å.; Maccarana, M. Neutralizing interaction between heparins and myotoxin II, a lysine 49 phospholipase A₂ from *Bothrops asper* snake venom. Identification of a heparin-binding and cytolytic toxin region by the use of synthetic peptides and molecular modeling. *J. Biol. Chem.*, **1994**, 269(47), 29867-29873.
- [15] Núñez, C.E.; Angulo, Y.; Lomonte, B. Identification of the myotoxic site of the Lys49 phospholipase A₂ from *Agkistrodon piscivorus piscivorus* snake venom: synthetic C-terminal peptides from Lys49, but not from Asp49 myotoxins, exert membrane-damaging activities. *Toxicon*, **2001**, 39(10), 1587-1594.
- [16] Lomonte, B.; Angulo, Y.; Santamaría, C. Comparative study of synthetic peptides corresponding to region 115-129 in Lys49 myotoxic phospholipases A₂ from snake venoms. *Toxicon*, **2003**, 42(3), 307-312.
- [17] Ward, R.J.; Chioato, L.; Oliveira, A.H.C.; Ruller, R.; Sá, J.M. Active-site mutagenesis of a Lys49-phospholipase A₂: biological and membrane-disrupting activities in the absence of catalysis. *Biochem. J.*, **2002**, 362(1), 89-96.
- [18] Chioato, L.; Aragão, E.A.; Ferreira, T.L.; Medeiros, A.I.; Faccioli, L.H.; Ward, R.J. Mapping the structural determinants of artificial and biological membrane damaging activities of a Lys49 phospholipase A₂ by scanning alanine mutagenesis. *Biochim. Biophys. Acta*, **2007**, 1768(5), 1247-1257.
- [19] da Silva-Giotto, M.T.; Garratt, R.C.; Oliva, G.; Mascarenhas, Y.P.; Giglio, J.R.; Cintra, A.C.; de Azevedo, Jr., W.F.; Arni, R.K.; Ward, R.J. Crystallographic and spectroscopic characterization of a molecular hinge: conformational changes in bothropstoxin I, a dimeric Lys49-phospholipase A₂ homologue. *Proteins*, **1998**, 30(4), 442-454.
- [20] Ambrosio, A.L.B.; Nonato, M.C.; Selistre de Araujo, H.S.; Arni, R.; Ward, R.J.; Ownby, C.H.; de Souza, D.H.F.; Garratt, R.C. A molecular mechanism for Lys49-phospholipase A₂ activity based on ligand-induced conformational change. *J. Biol. Chem.*, **2005**, 280(8), 7326-7335.
- [21] Arni, R.K.; Ward, R.J. Phospholipase A₂-a structural review. *Toxicon*, **1996**, 34(8), 827-841.
- [22] Scott, D.L.; Achari, A.; Vidal, J.C.; Sigler, P.B. Crystallographic and biochemical studies of the (inactive) Lys49 phospholipase A₂ from the venom of *Agkistrodon piscivorus piscivorus*. *J. Biol. Chem.*, **1992**, 267(31), 22645-22657.
- [23] Arni, R.K.; Ward, R.J.; Gutierrez, J.M.; Tulinsky, A. Structure of a calcium-independent phospholipase-like myotoxic protein from *Bothrops asper* venom. *Acta Cryst. D.*, **1995**, 51(3), 311-317.
- [24] van den Bergh, C.J.; Slotboom, A.J.; Verheij, H.M.; de Haas, G.H. The role of aspartic acid-49 in the active site of phospholipase A₂. A site-specific mutagenesis study of porcine pancreatic phospholipase A₂ and the rationale of the enzymatic activity of lysine49 phospholipase A₂ from *Agkistrodon piscivorus piscivorus*' venom. *Eur. J. Biochem.*, **1988**, 176(2), 353-357.
- [25] Li, Y.; Yu, B.; Zhu, H.; Jain, M.; Tsai, M. Phospholipase A₂ engineering. Structural and functional rules of the highly conserved active site residue aspartate-49. *Biochemistry*, **1994**, 33(49), 14714-14722.
- [26] Yoshizumi, K.; Liu, S.Y.; Miyata, T.; Saita, S.; Ohno, M.; Iwanaga, S.; Kihara, H. Purification and amino acid sequence of basic protein I, a lysine-49-phospholipase A₂ with low activity, from the venom of *Trimeresurus flavoviridis* (Habu snake). *Toxicon*, **1990**, 28(1), 43-54.
- [27] Liu, S.Y.; Yoshimizu, K.; Oda, N.; Ohno, M.; Tokunaga, F.; Iwanaga, S.; Kihara, H. Purification and amino acid sequence of basic protein II, a lysine-49-phospholipase A₂ with low activity, from *Trimeresurus flavoviridis* venom. *J. Biochem.*, **1990**, 107(3), 400-408.
- [28] Shimohigashi, Y.; Tani, A.; Matsumoto, H.; Nakashima, K.; Yamaguchi, Y. Lysine-49-phospholipases A₂ from *Trimeresurus flavoviridis* venom are membrane-acting enzymes. *J. Biochem.*, **1995**, 118(5), 1037-1044.
- [29] Rodrigues-Simioni, L.; Prado-Franceschi, J.; Cintra, A.C.O.; Giglio, J.R.; Jiang, M.S.; Fletcher, J.E. No role for enzymatic activity or dantrolene-sensitive Ca²⁺ stores in the muscular effects of bothropstoxin, a Lys49 phospholipase A₂ myotoxin. *Toxicon*, **1995**, 33(11), 1479-1489.
- [30] Yamaguchi, Y.; Shimohigashi, Y.; Chiwata, T.; Tani, A.; Chijiwa, T.; Lomonte, B.; Ohno, M. Lys-49-phospholipases A₂ as active enzyme for beta-arachidonoyl phospholipid bilayer membranes. *Biochem. Mol. Biol. Int.*, **1997**, 43(1), 19-26.
- [31] Mancin, A.C.; Soares, A.M.; Giglio, C.A.; Andriao-Escarso, S.H.; Giglio, J.R. The histamine releasers cromamine, protamine and compound 48/80 activate specific proteases and phospholipases A₂. *Biochem. Mol. Biol. Int.*, **1997**, 42(6), 1171-1177.
- [32] Soares, A.M.; Oshima-Franco, Y.; Vieira, C.A.; Leite, G.B.; Fletcher, J.E.; Jiang, M.S.; Cintra, A.C.O.; Giglio, J.R.; Rodrigues-Simioni, L. Mn(2+) ions reduce the enzymatic and pharmacological activities of bothropstoxin-I, a myotoxic Lys49 phospholipase A₂ homologue from *Bothrops jararacussu* snake venom. *Int. J. Biochem. Cell Biol.*, **2002**, 34(6), 668-677.
- [33] Ward, R.J.; Chioato, L.; de Oliveira, A.H.C.; Ruller, R.; Sá, J.M. Active-site mutagenesis of a Lys49-phospholipase A₂: biological and membrane-disrupting activities in the absence of catalysis. *Biochem. J.*, **2002**, 362(1), 89-96.
- [34] Fletcher, J.E.; Hubert, M.; Wieland, S.J.; Gong, Q.H.; Jiang, M.S. Similarities and differences in mechanisms of cardiotoxins, melittin and other myotoxins. *Toxicon*, **1996**, 34(11-12), 1301-1311.
- [35] Lee, W.H.; da Silva Giotto, M.T.; Marangoni, S.; Toyama, M.H.; Polikarpov, I.; Garratt, R.C. Structural basis for low catalytic activity in Lys49 phospholipases A₂-a hypothesis: the crystal structure of piratoxin II complexed to fatty acid. *Biochemistry*, **2001**, 40(1), 28-36.
- [36] Magro, A.J.; Soares, A.M.; Giglio, J.R.; Fontes, M.R.M. Crystal structures of BnSP-7 and BnSP-6, two Lys49-phospholipases A₂: quaternary structure and inhibition mechanism insights. *Biochem. Biophys. Res. Commun.*, **2003**, 311(3), 713-720.
- [37] Magro, A.J.; Murakami, M.T.; Marcussi, S.; Soares, A.M.; Arni, R.K.; Fontes, M.R.M. Crystal structure of an acidic platelet aggregation inhibitor and hypotensive phospholipase A₂ in the monomeric and dimeric states: insights into its oligomeric state. *Biochem. Biophys. Res. Commun.*, **2004**, 323(1), 24-31.
- [38] Soares, A.M.; Fontes, M.R.M.; Giglio, J.R. Phospholipase A₂ myotoxins from *Bothrops* snake venoms: structure function relationship. *Curr. Org. Chem.*, **2004**, 8(17), 1677-1690.
- [39] Murakami, M.T.; Viçoti, M.M.; Abrego, J.R.B.; Lourenzoni, M.R.; Cintra, A.C.O.; Arruda, E.Z.; Tomaz, M.A.; Melo, P.A.; Arni, R.K. Interfacial surface charge and free accessibility to the PLA₂-active site-like region are essential requirements for the activity of Lys49 PLA₂ homologues. *Toxicon*, **2007**, 49(3), 378-387.
- [40] Corrêa, L.C.; Marchi-Salvador, D.P.; Cintra, A.C.; Sampaio, S.V.; Soares, A.M.; Fontes, M.R.M. Crystal structure of a myotoxic Asp49-phospholipase A₂ with low catalytic activity: Insights into Ca²⁺-independent catalytic mechanism. *Biochim. Biophys. Acta*, **2008**, 1784(4), 591-599.
- [41] Angulo, Y.; Gutiérrez, J.M.; Soares, A.M.; Cho, W.; Lomonte, B. Myotoxic and cytolytic activities of dimeric Lys49 phospholipase A₂ homologues are reduced, but not abolished, by a pH-induced dissociation. *Toxicon*, **2005**, 46(3), 291-296.
- [42] Marchi-Salvador, D.P.; Corrêa, L.C.; Magro, A.J.; Oliveira, C.Z.; Soares, A.M.; Fontes, M.R.M. Insights into the role of oligomeric state on the biological activities of crotoxin: Crystal structure of a tetrameric phospholipase A(2) formed by two isoforms of crotoxin

- B from *Crotalus durissus terrificus* venom. *Proteins*, **2008**, 72(3), 883-891.
- [43] Arni, R.K.; Fontes, M.R.M.; Barberato, C.; Gutiérrez, J.M.; Díaz-Oreiro, C.; Ward, R.J. Crystal Structure of myotoxin II, a monomeric Lys49-phospholipase A₂ homologue isolated from the venom of *Cerrophidion (Bothrops) godmani*. *Arch. Biochem. Biophys.*, **1999**, 366(2), 177-182.
- [44] Soares, A.M.; Guerra-Smarka, R.; Borja-Oliveira, C.R.; Rodrigues, V.M.; Rodrigues-Simioni, L.; Rodrigues, V.; Fontes, M.R.M.; Lomonte, B.; Gutiérrez, J.M.; Giglio, J.R. Structural and functional characterization of BnSP-7, a Lys49 myotoxic phospholipase A₂ homologue from *Bothrops neuwiedi pauloensis* venom. *Arch. Biochem. Biophys.*, **2000**, 378(2), 201-209.
- [45] Watanabe, L.; Soares, A.M.; Ward, R.J.; Fontes, M.R.M.; Arni, R.K. Structural insights for fatty acid binding in a Lys49-phospholipase A₂: crystal structure of myotoxin II from *Bothrops moojeni* complexed with stearic acid. *Biochimie*, **2005**, 87(2), 161-167.
- [46] de Azevedo, W.F.Jr.; Ward, R.J.; Gutiérrez, J.M.; Arni, R.K. Structure of a Lys49-phospholipase A₂ homologue isolated from the venom of *Bothrops nummifer* (jumping viper). *Toxicon*, **1999**, 37(2), 371-384.
- [47] Murakami, M.T.; Arruda, E.Z.; Melo, P.A.; Martinez, A.B.; Calil-Elias, S.; Tomaz, M.A.; Lomonte, B.; Gutiérrez, J.M.; Arni, R.K. Inhibition of myotoxic activity of *Bothrops asper* myotoxin II by the anti-trypanosomal drug suramin. *J. Mol. Biol.*, **2005**, 350(3), 416-426.
- [48] dos Santos, J.I.; Marchi-Salvador, D.P.; Fernandes, C.A.H.; Silveira, L.B.; Soares, A.M.; Fontes, M.R.M. Preliminary X-ray crystallographic studies of a Lys49-phospholipase A₂ homologue from *Bothrops pirajai* venom complexed with p-bromophenacyl bromide and α-tocopherol inhibitors. *Protein Pept. Lett.*, **2007**, 14(7), 698-701.
- [49] dos Santos, J.I.; Soares, A.M.; Fontes, M.R.M. Comparative structural studies on Lys49-phospholipases A₂ from *Bothrops* genus reveal their myotoxic site. *J. Struct. Biol.*, **2009**, [accepted] (doi 10.1016/j.jsb.2009.04.003).
- [50] Krissinel, E.; Henrick, K. Inference of macromolecular assemblies from crystalline state. *J. Mol. Biol.*, **2007**, 372(3), 774-797.

Influence of Quaternary Conformation on the Biological Activities of the Asp49-phospholipases A₂s from Snake Venoms

Angelo J. Magro, Carlos A.H. Fernandes, Juliana I. dos Santos and Marcos R.M. Fontes*

Departamento de Física e Biofísica, Instituto de Biociências, UNESP, Botucatu/SP, Brasil

Abstract: One of the main components of snake venoms are the Asp49-phospholipases A₂, also known as svPLA₂s. The study of these toxins is a matter of great scientific interest due to their wide variety of biological effects. In this work we present strong evidences found in literature and other aspects which strengthen the importance of quaternary assembly for understanding the activities and molecular evolution of svPLA₂s.

Keywords: Phospholipase A₂, oligomerization, quaternary conformation, snake venom.

INTRODUCTION

Snake venoms comprise a complex mixture of pharmacological components able to affect several biological systems. One of the main components of snake venoms are the phospholipases A₂ (PLA₂s - EC 3.1.1.4), which are small and stable molecules (14-18 kDa) found in a great diversity of organisms and biological fluids [1]. These enzymes promote the hydrolysis of the *sn*-2 acyl groups of membrane phospholipids (*sn*-3 glycerophospholipids), releasing free fatty acids and lysophospholipids, such as arachidonic acid [1,2]. The products of phospholipid hydrolysis may subsequently take part in many biological processes. Arachidonic acid molecules, for example, can be converted to eicosanoids which serve as secondary messengers in a wide range of physiological and pathological processes such as sleep regulation, immune responses, inflammation, and pain perception [3]. Otherwise, the lysophospholipids can serve as precursors for lipid mediators involved in cell proliferation, survival and migration and in many inflammatory processes [4,5].

Initially, PLA₂s were classified in three main groups according to their amino acid sequence [6], but, in 1994, Dennis [7] established the first systematic group numbering system classifying these enzymes in four groups. This classification was reviewed some years later and the PLA₂s were reclassified in eleven groups on the basis of disulfide bonding pattern and amino acid sequences similarity [8]. With the expansion of molecular biology techniques, a great number of new PLA₂s was discovered and a revision in the classification of these molecules became necessary. Recently, the PLA₂s were classified in fifteen different groups that can be divided in five kinds of enzymes: secreted PLA₂s (sPLA₂s), cytosolic PLA₂s (cPLA₂s), Ca⁺⁺-independent PLA₂s (iPLA₂s), PAF acetylhydrolases (PAF-AH) and lysosomal PLA₂s [1]. The sPLA₂ group has sixteen subgroups and includes the phospholipases A₂ from snake venoms (svPLA₂s) [1]. The svPLA₂s from Elapidae and Viperidae (pit vipers)

families, the most important when considering envenomation and their effects, belong, respectively, to IA and IIA/IIB groups. This classification is based on sequence similarity, position of disulfide bonds and *loops* insertions. The snake venom sPLA₂ classified in groups IA and IIA have seven disulfide bonds: six of them are conserved in both Elapidae and Viperidae families, whereas the disulfide bonds Cys11/Cys77 and Cys51/Cys133 are only found in elapids and viperids, respectively. Moreover, the group IIB sPLA₂s of snake venoms have only six disulfide bonds, lacking the Cys61/Cys91 bond [1,9].

The catalytic site of PLA₂s is composed by a histidine residue (His48; according to the numbering system proposed to PLA₂s by Renetseder *et al.* [10]) in close proximity to both conserved Asp99 and Asp49. A detailed description of the PLA₂ catalytic mechanism of phospholipid hydrolysis was proposed by Scott *et al.* [11,12]. This mechanism was based on structural studies of PLA₂s from classes IA and III in the native and complexed states with transition-state analogues. In this catalytic model (known as single-water mechanism), His48 Nδ1 atom is stabilized by the carboxyl oxygen atom of Asp99, which is hydrogen bonded to the hydroxyl oxygen atom of Tyr52. After the phospholipid binding, His48 Nδ1 atom abstracts a proton from a structurally conserved water molecule initiating the nucleophilic attack of *sn*-2 position of the substrate forming a tetrahedral oxyanion intermediate. This tetrahedral intermediate is stabilized by the Ca⁺⁺ cofactor which, by its turn, is kept in position due to interactions with the carboxyl oxygen atom(s) of Asp49, carbonyl main chain oxygen atoms of the Ca⁺⁺-binding loop (region 25-33) and two structurally conserved solvent water molecules [12]. A disulfide bond (Cys27/Cys44) ensures the correct relative orientation of the calcium binding loop in relation to the amino acids that form the catalytic region. Upon collapse of the tetrahedral intermediate and release of hydrolysis products, three water molecules move into the active site [11]. An alternative mechanism (know as assisting-water mechanism) was proposed suggesting that two different water molecules are involved in the formation and breakdown, respectively, of the tetrahedral intermediate [13-15]. In this model, a water molecule coordinated by the Ca⁺⁺ ion generates the nucleophilic attack

*Address correspondence to this author at the Departamento de Física e Biofísica, Instituto de Biociências, UNESP, Caixa Postal 510, Botucatu/SP, Brasil, 18618-000; Tel: +55 14 3811 6254; Fax: +55 14 3815 3744; E-mail: fontes@ibb.unesp.br

[15]. This catalytic water is also stabilized by a second water molecule H-bonded to the His48/Asp99 dyad. A detailed description of this alternative mechanism was discussed by Rogers *et al.* [13], Yu *et al.* [14] and Bahnson [15]. Indeed, this catalytic mechanism is supported by the crystal structure of a His48Gln mutant of a human group IIA PLA₂ [16]. This mutant retained a significant residual catalytic activity and its structure displayed a catalytic region and a calcium-binding loop with no significant structure perturbation. According to the assisting-water mechanism, a glutamine residue would function similarly to His48. However, Bahnson [15] showed these findings do not necessarily discard the importance of previous structural models complexed with transition-state analogues. Interestingly, the assisting-water mechanism predicts two tetrahedral intermediates and the structures that served to propose the single water mechanism are entirely consistent with the second tetrahedral intermediate of the assisted-water mechanism. Despite eventual differences between the single-water and water-assisted mechanisms, several biochemical studies demonstrated the Ca⁺⁺ ion is an obligatory co-factor for sPLA₂s catalysis. Studies of its substitution by other divalent ions (Cd⁺⁺, Sr⁺⁺, Ba⁺⁺, Mg⁺⁺) showed cadmium, in contrast to other ions, was able to keep the substrate bound to the enzyme, although only Ca⁺⁺ supports the catalytic activity [17]. This can be explained by different coordination geometries assumed by the tetrahedral intermediate due to the presence of the Cd⁺⁺ and Ca⁺⁺ ions, which determine the electrophilic behavior of the catalytic site [17]. However, later experiments demonstrated Ni⁺⁺ and Co⁺⁺ ions support a significant catalytic hydrolysis of phospholipid with determined headgroups [14]. These results can be also attributed to differences in coordination geometry and indicate a noteworthy plasticity of the active site environment [14].

The canonical protein fold PLA₂s from snake venoms includes a motif highly conserved in all class I/II enzymes defined by two long antiparallel α -helices linked by disulphide bonds in conjunction to a Ca⁺⁺-binding loop (helices 2 and 3, residues 37-54 and 90-109), with a distance between the helical axes of about 10 Å [9]. Although these two α -helices do not display a clear amphipathic character, the hydrophilic amino acid side chains are generally exposed to the solvent and the hydrophobic residues point into the protein core, excepting the amino acids that form the catalytic network: His48, Asp49, Asp99 and Tyr52. The other conserved structural features, the N-terminal helix, the β -wing region, the Ca⁺⁺-binding loop, the "elapid loop" (an insertion of two or three amino in region 52-65 present only in class IA enzymes), the short helix and the C-terminal loop can adopt different relative orientations, especially the C-terminal loop, a very flexible region [9, 18] (Fig. 1).

In addition to their catalytic action, a wide variety of pharmacological activities has been described for snake venom PLA₂s, such as pre- [19,20] or post-synaptic neurotoxicity [21], myotoxicity [22], cardiotoxicity [23], bactericidal [24], platelet aggregation inhibition [25], edema [26], hemolysis [27], anti-coagulation [28], convulsion [29] and hypotension [30]. Nevertheless the amount of available data, the mechanism(s) involved in these biological and pharmacological activities is still poorly known. Thus, despite the different degrees of identity between the svPLA₂s, it is very

reasonable to accept the several biological activities presented by these molecules are also related to their oligomeric conformations in solution. Based in some relevant crystallographic structures deposited in the RCSB Protein Data Bank, we present in this review strong evidences found in literature and other aspects corroborating the importance of the quaternary conformation for understanding the activities and molecular evolution of Asp49-PLA₂s from snake venoms.

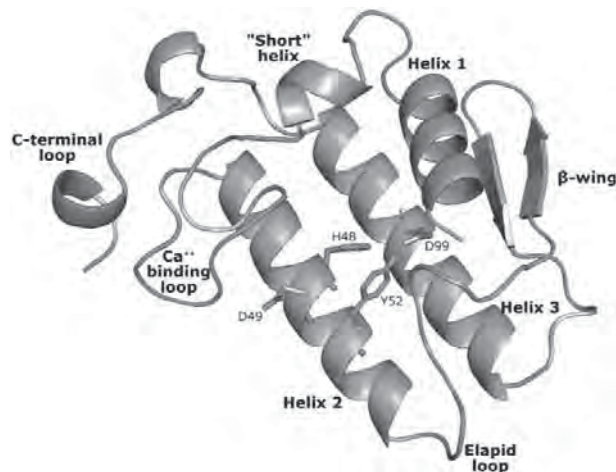


Figure 1. Cartoon representation highlighting the main structural features found in snake venom Asp49-PLA₂s. Illustration generated by program PyMOL [31].

OLIGOMERIZATION IN ELAPIDAE AND VIPERIDAE SVPLA₂S

It is well known that oligomeric proteins are profusely found in nature. It has been calculated the average oligomeric state of cellular proteins is tetrameric [32], and a recent survey suggests that 35% or more of the proteins in a cell are oligomeric [33]. However, the proportion of oligomeric protein structures deposited in the RCSB Protein Data Bank (<http://www.pdb.org>) is significantly lower [34]. This fact may simply indicate the experimental constraints favoring the structural determination of small monomeric proteins. Nonetheless possible experimental restrictions, it is very significant that a great number of elapid and bothropic Asp49-PLA₂ crystallographic structures found in the RCSB Protein Data Bank are oligomers constituted by two or more subunits, as exemplified in Table 1. Thus, it is very probable the oligomerization of svPLA₂s plays an essential role for their biological activities.

Carredano *et al.* [35] described the three-dimensional structure of *Notechis* II-5, a neurotoxic Asp49-PLA₂s from *Notechis scutatus scutatus* venom, which was the first dimeric elapid svPLA₂s solved by protein crystallography. This crystallographic model was determined at 3 Å resolution and, according to the authors, the main structural differences between the two molecules present in the asymmetric unit are located at the Ca⁺⁺-binding loop. Although the authors focused the probable structural characteristics related to the neurotoxic activity of *Notechis* II-5, none possible influence of oligomerization on the biological activities of this toxin was pointed out. In contrast, some aspects de-

Table 1. Examples of Oligomeric Asp49-PLA₂s from Snake Venoms Found in the RCSB Protein Data Bank

Asp49-PLA ₂	Space Group	Molecules in ASU*	Family	Species	PDB code
PLA ₂	H3	2	Elapidae	<i>Bungarus caeruleus</i>	1U4J
MIPLA2	C2(C121)	4	Elapidae	<i>Micropechis ikaheka</i>	1PWO
MIPLA3	P4 ₁	2	Elapidae	<i>Micropechis ikaheka</i>	1OZY
MIPLA4	I4 ₁	6	Elapidae	<i>Micropechis ikaheka</i>	1P7O
PLA ₂	P4 ₁	2	Elapidae	<i>Naja naja sagittifera</i>	1S6B
<i>Notechis</i> II-5	P2 ₁ 2 ₁ 2 ₁	2	Elapidae	<i>Notechis scutatus scutatus</i>	2NOT
OHV APLA ₂	C2(C121)	3	Elapidae	<i>Ophiophagus hannah</i>	1GP7
Agkistrodoxin	P2 ₁ 2 ₁ 2 ₁	6	Viperidae	<i>Agkistrodon halys</i> Pallas	1BJJ
BthA-I	P2 ₁ (P12 ₁ 1)	2	Viperidae	<i>Bothrops jararacussu</i>	1U73
BthA-I	P2 ₁ (P12 ₁ 1)	2	Viperidae	<i>Bothrops jararacussu</i>	1Z76
BthTX-II	C2(C121)	2	Viperidae	<i>Bothrops jararacussu</i>	2OQD
PrTX-III	C2 (C121)	2	Viperidae	<i>Bothrops pirajai</i>	1GMZ
Crotoxin B	P2 ₁ 2 ₁ 2 ₁	4	Viperidae	<i>Crotalus durissus terrificus</i>	2QOG
PLA ₂	C222 ₁	2	Viperidae	<i>Daboia russelli pulchella</i>	1FB2
PLA ₂	C222 ₁	2	Viperidae	<i>Daboia russelli pulchella</i>	1KPM
PLA ₂	C222 ₁	3	Viperidae	<i>Daboia russelli pulchella</i>	1JQ9
Vipoxin	P2 ₁ 2 ₁ 2 ₁	2	Viperidae	<i>Vipera ammodytes ammodytes</i>	1JLT
Vipoxin	P2 ₁ 2 ₁ 2	2	Viperidae	<i>Vipera ammodytes meridionalis</i>	1AOK

* Asymmetric unit cell.

scribed in an article of Zhang *et al.* [36] suggest the probable importance of oligomerization for elapid svPLA₂s. These authors showed the crystal asymmetric unit of a cardiotoxic class I PLA₂ (OHV APLA₂) from *Ophiophagus hannah* was constituted by three molecules (A, B, and C), with two main types of intermolecular interactions (A/B and B/C) presenting a two-fold non-crystallographic symmetry. The pancreatic loop, the calcium-binding loop, and the N-terminal helix are involved in the interactions between the molecules A and B, whereas the segments Cys11 – Ala23 and Ser109 – Asn113 are responsible by the interactions which involve the molecules B and C. Even though two kinds of intermolecular contacts are clearly identified, it is most probable the molecules A and B form the dimer more stable, since the contact area between these molecules is significantly larger (1606 Å²) in relation to the interface of the molecules B and C (995 Å²). The oligomeric conformation of OHV APLA₂ also reveals the active sites and the hydrophobic channels of the monomers are buried in the interior of the dimer, as well as most of the residues near the entrance of the hydrophobic channels. Based on these structural features, the authors suggested that the dimer of OHV APLA₂ is an inhibited form, which probably protects the snake from its own venom, or a storage method to improve the solubility of the toxin in the venom gland at high concentrations. This hypothesis was also proposed by other authors in order to justify the dimeric conformation of some svPLA₂s [37-43]. Even this hypothesis does not make a direct association between any biological

activity of OHV APLA₂ and its oligomeric state, other remarks point to this direction. A signal of the probable importance of OHV APLA₂ quaternary conformation are the position and contacts of the pancreatic loop, which is located near the entrance of the hydrophobic channel and was proposed to take part in the interface recognition sites (IRS) [44]. As described in this work, extensive intermolecular interactions, including several hydrophobic interactions and two hydrogen bonds with the main-chain atom N of a neighbor glycine, help to stabilize the pancreatic loop of OHV APLA₂. Consequently, the stabilization of the pancreatic loop due to oligomerization may be essential for OHV APLA₂, allowing the binding of this molecule to its substrates. After the complexation, it is possible that eventual structural alterations promote the separation of the dimer, with the exposition of the hydrophobic channels and active sites of the monomers.

Lok *et al.* [45] proposed the oligomeric conformation of elapid isoenzymes MiPLA2, MiPLA3 and MiPLA4 from *Micropechis ikaheka* venom is important for the pharmacological activities played by these molecules. Indeed, it is known that higher levels of oligomerization in isoenzymes are related to higher potency of action. In the specific case of *M. ikaheka* isoenzymes the potency of each toxin seems to be defined by the spatial arrangement of the C-terminal regions: the least potent MiPLA3 is a dimer whose terminal loops are located in opposite sides, whereas MiPLA4 is a

trimer with a highly exposed region formed by neighbor C-termini and MiPLA2 (the most potent isoenzyme) is constituted by two dimers where the final segments of the monomers protrude creating an wide and complex interfacial architecture. The authors suggested this explanation about the different potency of the isoenzymes based on the fact the C-terminal regions present the most significant structural differences between the molecules. According to the authors, this structural aspect indicates the C-terminus is probably the main pharmacological site of *M. ikaheka* isoenzymes. The presence of a proline bracket in the C-terminus of MiPLA2 also support the probable functional role of this region; it was observed that proline residues flank interaction sites and protect the integrity and conformation of active sites [46]. Additionally, primary sequence and binding affinity of M-type receptor – a molecule found at cellular membranes of some preys of *M. ikaheka* [47,48] – indicate the C-terminus may also contain the M-type receptor binding motif. Further, in *M. ikaheka* isoenzymes, the C-termini are placed close to the Ca⁺⁺-binding loop, in agreement with a previous work which demonstrated the residues in the vicinity of this loop are involved in M-type receptor binding [47].

Interestingly, Singh *et al.* [49] suggested that ligands may influence the oligomeric conformation of svPLA₂s. The authors showed the presence of two molecules of mannose induced the dimerization of *Bungarus caeruleus* PLA₂. These carbohydrate molecules are located at the dimeric surface of the crystallographic model and present extensive interactions with various residues of the monomers, including the catalytically important Asp49. Probably, this structural feature is responsible by the lack of catalytic activity of *Bungarus caeruleus* PLA₂ in presence of mannose. Thus, these findings indicate inhibitory molecules may also suppress some svPLA₂ activities modifying the quaternary conformation of these toxins.

The analysis of some Asp49-PLA₂ toxins from Viperidae family strengthens the significance of oligomerization for this class of molecules. Vipoxin from *Vipera ammodytes meridionalis* was the first determined venom toxin structure formed by an alkaline Asp49-PLA₂ and an acidic protein inhibitor molecule, both constituted by 122 amino acids [50]. The alkaline Asp49-PLA₂ subunit is a potent neurotoxic phospholipase, with LD₁₀₀ = 1-3 µg/20 g mouse [51]. However, the inhibitory subunit of vipoxin is able to reduce the phospholipase activity of the active molecule *in vitro* by up to 60% [52]. Although the inhibition of the Asp49-PLA₂ by its associated subunit molecule is an interesting remark, the authors pointed out other particular characteristics as the main feature of the complex. In the active subunit of vipoxin structure, the conformation of the Ca⁺⁺-coordination site is different in comparison to those from bovine [44] and human [53] PLA₂s. In the former molecules the three backbone carbonyl oxygens of Tyr28, Gly30 and Gly32 and the carboxylate group of Asp49 form a Ca⁺⁺-coordination site, whereas in the vipoxin the same conformation is not observed since the backbone carbonyl oxygens of Tyr28 and Gly32 are involved in intermolecular contacts with the inhibitory subunit. This alteration of the Ca⁺⁺-binding loop is probably the basis for the absence of Ca⁺⁺ at this vipoxin structure. Despite this structural modification, the vipoxin from *Vipera ammodytes meridionalis* still preserves a low enzymatic activity. In fact,

the authors emphasize the binding of Ca⁺⁺ would change the conformation of both vipoxin subunits, weakening the stability of the complex. Interestingly, Corrêa *et al.* [54] also observed the lack of Ca⁺⁺ and a distortion in the Ca⁺⁺-binding loop of BthTX-II myotoxin, a low catalytic Asp49-PLA₂ from *Bothrops jararacussu* venom. The separation of the molecules which compose the vipoxin complex causes an irreversible loss of enzymatic activity of the PLA₂ subunit after a determined period of time [55]. Aleksiev and Tchobanov (1976) [52] also observed the disconnection between the PLA₂ and inhibitory subunits caused the same effect on the neurotoxic activity of the vipoxin complex. Therefore, it is evident the quaternary association between active molecule and inhibitor provides a structural stability of the complex, upholding the neurotoxicity at the expense of phospholipase activity. Other important result of the binding of the inhibitor is the change in the target of physiological attack: the complex exhibits postsynaptic neurotoxicity, while the isolated enzyme is a presynaptic toxin. Similar findings were found by Banumathi *et al.* [56], responsible by the structure determination at 1.4 Å of the vipoxin complex from *Vipera ammodytes ammodytes*.

In 2001, Chandra *et al.* [57] determined the structure of a *Daboia russelli pulchella* PLA₂, which presented a novel quaternary conformation. The quaternary arrangement of the dimer shows the monomers are linked in a manner that the binding surfaces are fully accessible. However, the conformations of Trp31 in the monomers differ drastically due to strong intramolecular and intermolecular interactions presented by this residue. Such interactions cause in one of the monomers a displacement of the Trp31 side chain, which hinders the opening of the hydrophobic binding channel and impairs the binding of substrate molecules. On the other hand, the Trp31 side chain of the other monomer points to an opposite direction, leaving the access to the hydrophobic binding channel open for substrate diffusion. These structural features of *Daboia russelli pulchella* PLA₂ shed light on the probable reasons which determine the low enzymatic activities presented by some oligomeric PLA₂s. Structural studies of complexes of *Daboia russelli pulchella* PLA₂ with inhibitory molecules, as the natural compounds α-tocopherol [58] and aristolochic acid [59] and designed peptides [60,61], confirmed the native oligomeric conformation is the correct assembly and demonstrated this toxin is a dimer in solution by the execution of dynamic light scattering experiments. Moreover, these works with inhibitors explained why the cited inhibitory molecules can suppress only a maximum of 50% of the *Daboia russelli pulchella* PLA₂ phospholipase activity. This occurs, as mentioned above, in function of the Trp31 side chain conformation, which allows the access of inhibitory molecules to the putative catalytic site of *Daboia russelli pulchella* PLA₂ just in one of the monomers.

Magro *et al.* [62] crystallized BthA-I, an acidic Asp49-PLA₂ from *Bothrops jararacussu* venom, both in monomeric and dimeric forms. This svPLA₂, which is three to four times more active catalytically than BthTX-II (found in the venom of the same species) and other basic Asp49-PLA₂s from bothropic venoms, presents a great variety of pharmacological action, as time-independent oedema induction, hypotensive response in rats and platelet aggregation inhibition [63].

It was demonstrated the catalytic, desintegrin, and pharmacological activities were abolished by chemical modification with p-bromophenacyl bromide (pBPB), which covalently binds to His48 of the catalytic site [63]. Curiously, the structure of BthA-I/pBPB determined by Magro *et al.* [64] was showed to be dimeric. Furthermore, the quaternary structure of BthA-I may present a regulatory role, hence determining the occurrence or potency of some biological activities of this svPLA₂. This control would be possible by the access or hindering of determined sites to the solvent, since it was proposed certain pharmacological and toxic actions of svPLA₂s, as anticoagulant and platelet-inhibition activities, are not related to enzymatic activity [65,66]. In addition, Rigden *et al.* [67] explained the clearly sigmoidal character of the catalytic reaction held by the svPLA₂ PrTX-III from *Bothrops pirajai* in terms of an active (R) and an inactive (T) conformational state. The R-state was suggested as a substrate-binding induced dimer which presents the Ca⁺⁺-binding loops and C-terminal regions at the interface. This possible dimeric conformation would be determined by structural changes at the Ca⁺⁺-binding loop, with posterior modifications of the C-terminal transmitted via the disulfide bridges Cys27-Cys125 and Cys50-Cys133. After the structural alteration in one molecule, the other monomer would be similarly affected, in a typical mechanism of cooperative substrate binding.

Interestingly, oligomerization for neurotoxic viperid svPLA₂s seems to be especially relevant. Tang *et al.* [68] showed the asymmetric unit of an orthorhombic crystal of the presynaptic neurotoxin agkistrotoxin (ATX) from *Agkistrodon halys* Pallas was occupied by three pairs of molecules. The authors proposed these dimeric associations driven by hydrophobic interactions constituted a self-protection mechanism characterized by the protection of the interfacial recognition sites and entrances of the hydrophobic channels of both ATX molecules. The obstruction of these regions prevents the binding of the neurotoxin to non-targeting substrates and increases the affinity for specific acceptors on the presynaptic membranes. Regarding to crotoxin B (CB), the neurotoxic subunit of crotoxin from *Crotalus durissus terrificus*, Marchi-Salvador *et al.* [69] suggested that the tetrameric crystallographic model of this toxin seems to be biologically significant due to three main reasons: (i) SDS-PAGE results revealed the non-reduced crotoxin B may be a dimer or tetramer in solution; (ii) the DLS experiments confirmed the presence of these two molecular associations in solution and showed the tetrameric form is highly predominant at the crystallization conditions of the toxin (protein concentration = 6.0 mg/mL; T = 291 K); (iii) the solvation and dissociation free energy variations calculated for the tetrameric crystallographic with the program model show that this assembly is stable in solution. Indeed, the authors noted their experimental model of crotoxin B is formed by two heterodimers composed of a pair of isoforms (CB1 and CB2) (Fig. 2). Thus, it was proposed the crotoxin B may bind to the presynaptic membrane as a tetramer or a dimer. Therefore, the CB1 and CB2 isoforms probably are complementary parts of a functional molecular complex, whose quaternary conformation is essential to the biological activities performed by CB, particularly in relation to the neurotoxic activity. This hypothesis is supported by the localiza-

tion of the most probable CB regions related to the neurotoxic activity (N and C-terminal regions, Ca⁺⁺-binding loops and β -wings) at the surface of the heterodimers and tetramer, hence indicating these structural assemblies are able to hold the toxic effects. Moreover, the quaternary conformations resulted from the CB1/CB2 association may even enhance the neurotoxicity of the toxin CB by the formation of new binding sites not found on the isolated monomers. Consequently, it is possible to suppose the CB1 and CB2 isoforms and even other CB isoforms possibly evolved in order to allow the assembling of oligomeric structures capable to carry out and maximizing the neurotoxic activity of crotoxin.

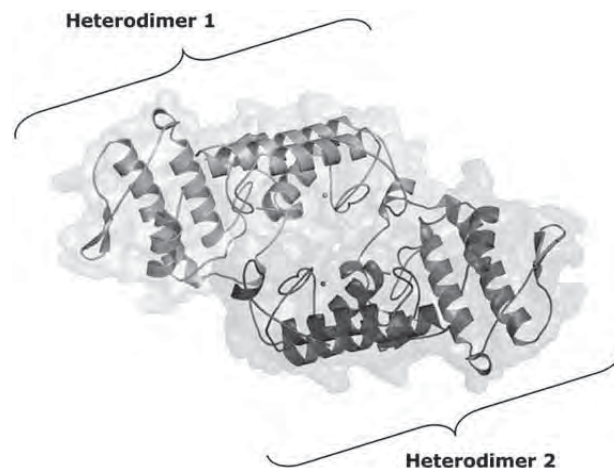


Figure 2. Quaternary assembly of crotoxin B crystallographic model. The complete structure is formed by two heterodimers composed of a pair of isoforms (CB1 and CB2). Illustration generated by program PyMOL [31].

INTERFACIAL CHARACTERISTICS OF SOME OLIGOMERIC SVPLA₂S

The characteristics and amino acid composition of the interfaces of supposed oligomeric proteins is other interesting approach to support oligomerization *in vivo*. On this basis, it was demonstrated the hydrophobic interactions play an important role in defining oligomeric interfaces. According to some authors, around two-thirds of the residues in inter-subunit interfaces are nonpolar [70,71]. Otherwise, Miller [71] indicated approximately one-fifth of the residues at oligomeric interfaces are polar. This incidence of polar residues shows the hydrogen bonds and salt bridges are also important for the stabilization of oligomeric proteins. Early studies suggested that there is about one hydrogen bond per 200 Å² of subunit interface [70]. In order to verify if the interfaces of oligomeric svPLA₂s meet these characteristics, we analyzed four crystallographic structures using the on-line program PISA (Protein Interfaces, Surfaces and Assemblies) [72] available at the European Bioinformatics Institute (http://www.ebi.ac.uk/msd-srv/prot_int/pistart.html): MIPLA2 from *Micropechis ikaheka*, vipoxin from *Vipera ammodytes meridionalis* [45], PLA₂ from *Daboia russelli pulchella* [57], and crotoxin B from *Crotalus durissus terrificus* [69]. These Asp49-PLA₂s from snake venoms were chosen due to the influence of oligomerization on their biological and biochemical properties, as attested by the

Table 2. Interfacial Characteristics of Some Important Oligomeric svPLA₂s Using the Program PISA [72]

Asp49-PLA ₂ (PDB Code)		Species	Interface Area (Å ²)	Polar Residues (%)	Hydrophobic Residues (%)	Hydrogen Bonds	Salt Bridges
MIPLA2 (1PWO)		<i>Micropechis ikaheka</i>	1083.5	26 (43.3)	16 (26.6)	6	4
Vipoxin (1AOK)		<i>Vipera ammodytes meridionalis</i>	1467.3	37 (45.1)	26 (31.7)	13	3
PLA ₂ (1FB2)		<i>Daboia russelli pulchella</i>	558.3	11 (33.3)	15 (45.4)	2	-
Crotoxin B (2QOG)*	Dimer 1	<i>Crotalus durissus terrificus</i>	777.2	27 (55.1)	12 (25.5)	11	4
	Dimer 2		781.8	28 (56.0)	12 (24.0)	6	2

* Two heterodimers composed by a pair of isoforms form the tetrameric crystallographic model of crotoxin B [69].

authors. In contrast to the above mentioned interfacial amino acid composition expected for stable oligomers, the interfaces of these experimental structures show a high proportion of polar residues in relation to the hydrophobic ones, with exception of PLA₂ from *Daboia russelli pulchella* (Table 2). The svPLA₂s with predominance of polar residues at their interfaces present several hydrogen bonds and salt bridges (Table 2). Thus, in comparison to the proposed density of hydrogen bonds for stable interfaces (1/200 Å²), these oligomers show a remarkable high density of hydrogen bonds, as observed in vipoxin (1/112.3 Å²) and in one of the dimers which compose the crotoxin B tetramer (1/70.2 Å²). For this reason, we suppose the concentration of polar residues at surface protein sites is able to induce the oligomerization of many svPLA₂s by the formation of a well-structured net of hydrogen bonds and salt bridges. On the other hand, it is important to underline that oligomerization also may occur in determined molecules with predominance of interfacial hydrophobic residues, as suggested by the analysis of PLA₂ from *Daboia russelli pulchella* (Table 2).

FINAL REMARKS

The study of protein oligomerization is an important research field due to the implications of this subject for a great variety of scientific questions. Several mechanisms can induce the formation of oligomers, indicating oligomerization evolves through different evolutionary routes. Genetically, oligomeric species could be created from monomeric proteins through some combination of a few genetic events [73-75], which involve substitutions, insertions, and deletions of amino acid residues. These mutations could affect the electrostatic or geometric properties of a surface patch, or the length or geometry of an inter-domain linker, resulting in oligomeric alteration of a protein. In the case of svPLA₂s, numerous indications suggest the notable influence of oligomerization on the biological and pharmacological activities played by these toxins. The analysis of some important oligomeric svPLA₂s has indicated the interfacial polar residues are probably responsible by the oligomerization of these toxins. Thus, we suppose the increase of the concentration of surface polar residues could be the main evolutionary event related to oligomerization of many svPLA₂s.

REFERENCES

- [1] Schaloske, R.H.; Dennis, E.A. The phospholipase A₂ superfamily and its group numbering system. *Biochim. Biophys. Acta*, **2006**, *1761*(11), 1246-1259.
- [2] van Deenen, L.L.M.; de Haas, G.J. The substrate specificity of phospholipase A₂. *Biochim. Biophys. Acta*, **1963**, *70*(1), 538-553.
- [3] Tsuboi, K.; Sugimoto, Y.; Ichikawa, A. Prostanoid receptor subtypes. *Prostaglandins Other Lipid Mediat.*, **2002**, *68-69*(1), 535-556.
- [4] Moolenaar, W.H.; van Meeteren, L.A.; Giepmans, B.N. The ins and outs of lysophosphatidic acid signaling. *Bioessays*, **2004**, *26*(8), 870-881.
- [5] Prescott, S.M.; Zimmerman, G.A.; Stafforini, D.M.; McIntyre, T.M. Platelet-activating factor and related lipid mediators. *Annu. Rev. Biochem.*, **2000**, *69*(1), 419-445.
- [6] Davidson, F.F.; Dennis, E.A. Evolutionary relationships and implications for the regulation of phospholipase A₂ from snake venom to human secreted forms. *J. Mol. Evol.*, **1990**, *31*(3), 228-238.
- [7] Dennis, E.A. Diversity of group types, regulation, and function of phospholipase A₂. *J. Biol. Chem.*, **1994**, *269*(18), 13057-13060.
- [8] Six, D.A.; Dennis, E.A. The expanding superfamily of phospholipase A(2) enzymes: classification and characterization. *Biochim. Biophys. Acta*, **2000**, *1488*(1-2), 1-19.
- [9] Arni, R.K.; Ward, R.J. Phospholipase A₂ - a structural review. *Toxicol.*, **1996**, *34*(8), 827-828.
- [10] Renetseder, R.; Brunie, S.; Dijkstra, B.W.; Drenth, J.; Singler, P.B. A comparison of the crystal structures of phospholipase A₂ from bovine pancreas and *Crotalus atrox* venom. *J. Biol. Chem.*, **1985**, *260*(21), 11627-11634.
- [11] Scott, D.L.; Otwinowski, Z.; Gelb, M.H.; Singler, P.B. Crystal structure of bee-venom phospholipase A₂ in a complex with a transition-state analogue. *Science*, **1990**, *250*(4987), 1563-1566.
- [12] Scott, D.L.; White, S.P.; Otwinowski, Z.; Yuan, W.; Gelb, M.H.; Singler, P.B. Interfacial catalysis: the mechanism of phospholipase A₂. *Science*, **1990**, *250*(4987), 1541-1546.
- [13] Rogers, J.; Yu, B.Z.; Serves, S.V.; Tsivgoulis, G.M.; Sotiropoulos, D.M.; Ioannou, P.V.; Jain, M.K. Kinetic basis for the substrate specificity during hydrolysis of phospholipids by secreted phospholipase A₂. *Biochemistry*, **1996**, *35*(29), 9375-9384.
- [14] Yu, B.Z.; Rogers, J.; Nicol, G.R.; Theopold, K.H.; Seshadri, K.; Vishweshwara, S.; Jain, M.K. Catalytic significance of the specificity of divalent cations as KS* and kcat* cofactors for secreted phospholipase A₂. *Biochemistry*, **1998**, *37*(36), 12576-12587.
- [15] Bahnson, B.J. Structure, function and interfacial allostereism in phospholipase A₂: insight from the anion-assisted dimer. *Arch. Biochem. Biophys.*, **2005**, *433*(1), 96-106.
- [16] Edwards, S.H.; Thompson, D.; Baker, S.F.; Wood, S.P.; Wilton, D.C. The crystal structure of the H48Q active site mutant of human group IIA secreted phospholipase A₂ at 1.5 Å resolution provides an insight into the catalytic mechanism. *Biochemistry*, **2002**, *41*(52), 15468-15476.
- [17] Yu, B.Z.; Berg, O.G.; Jain, M.K. The divalent cation is obligatory for the binding of ligands to the catalytic site of secreted phospholipase A₂. *Biochemistry*, **1993**, *32*(25), 6485-6492.
- [18] Ward, R.J.; de Azevedo, Jr. W.F.; Arni, R.K. At the interface: crystal structures of phospholipases A₂. *Toxicol.*, **1998**, *36*(11), 1623-1633.
- [19] Chang, C.C.; Lee, J.D.; Eaker, D.; Fohlman, J. The presynaptic neuromuscular blocking action of taipoxin. A comparison with β-bungarotoxin and crotoxin. *Toxicol.*, **1977**, *15*(6), 571-576.

- [20] Westerlund, B.; Nordlund, P.; Uhlin, U.; Eaker, D.; Eklund, H. The three-dimensional structure of notexin, a presynaptic neurotoxic phospholipase A₂ at 2.0 Å resolution. *Febs Lett.*, **1993**, *301*(2), 159-164.
- [21] Bon, C.; Changeux, J.P.; Jeng, T.W.; Fraenkel-Conrat, H. Postsynaptic effects of crotoxin and of its isolated subunits. *Eur. J. Biochem.*, **1979**, *99*(3), 471-481.
- [22] Gutiérrez, J.M.; Nunez, J.; Diaz, C.; Cintra, A.C.O.; Homs-Brandeburgo, M.I.; Giglio, J.R. Skeletal muscle degeneration and regeneration after injection of bothropstoxin-II, a phospholipase A₂ isolated from the venom of the snake *Bothrops jararacussu*. *Exp. Mol. Pathol.*, **1991**, *55*(3), 217-229.
- [23] Fletcher, J.E.; Rapuano, B.E.; Condrea, E.; Yang, C.C.; Rosenberg, P. Relationship between catalysis and toxicological properties of three phospholipases A₂ from elapid snake venoms. *Toxic. Appl. Pharmacol.*, **1981**, *59*(2), 375-388.
- [24] Paramo, L.; Lomonte, B.; Pizarro-Cerda, J.; Bengoechea, J.A.; Gorvel, J.P.; Moreno, E. Bactericidal activity of Lys49 and Asp49 myotoxic phospholipases A₂ from *Bothrops asper* snake venom-synthetic Lys49 myotoxin II-(115-129)-peptide identifies its bactericidal region. *Eur. J. Biochem.*, **1998**, *253*(2), 452-461.
- [25] Yuan, Y.; Jackson, S.P.; Mitchell, C.A.; Salem, H.H. Purification and characterisation of a snake venom phospholipase A₂: a potent inhibitor of platelet aggregation. *Thromb. Res.*, **1993**, *70*(6), 471-481.
- [26] Lloret, S.; Moreno, E. Oedema formation and degranulation of mast cells by phospholipase A₂ purified from porcine pancreas and snake venoms. *Toxicon*, **1993**, *31*(8), 949-956.
- [27] Condrea, E.; Yang, C.C.; Rosenberg, P. Lack of correlation between anticoagulant activity and phospholipid hydrolysis by snake venom phospholipases A₂. *Thromb. Haemost.*, **1981**, *45*(1), 82-85.
- [28] Rosenberg, P.; Condrea, E.; Rapuano, B.E.; Soons, K.R.; Yang, C.C. Dissociation of pharmacological and enzymatic activities of snake venom phospholipases A₂ by modification of carboxylate groups. *Biochem. Pharmacol.*, **1983**, *32*(23), 3525-3530.
- [29] Fletcher, J.E.; Rapuano, B.E.; Condrea, E.; Yang, C.C.; Ryan, M.; Rosenberg, P. Comparison of a relatively toxic phospholipase A₂ from *Naja nigricollis* snake venom with that of a relatively nontoxic phospholipase A₂ from *Hemachatus haemachatus* snake venom-II: pharmacological properties in relationship to enzymatic activity. *Biochem. Pharmacol.*, **1980**, *29*(11), 1565-1574.
- [30] Huang, H.C. Release of slow reacting substance from the guinea-pig lung by phospholipases A₂ of *Vipera russelli* snake venom. *Toxicon*, **1984**, *22*(3), 359-372.
- [31] Delano, W.L. *The PyMOL Molecular Graphics System*, 1st ed.; DeLano Scientific: Palo Alto, **2002**.
- [32] Goodsell, D.S. Inside a living cell. *Trends Biochem. Sci.*, **1991**, *16*(6), 203-206.
- [33] Goodsell, D.S.; Olson, A.J. Structural symmetry and protein function. *Annu. Rev. Biophys. Biomol. Struct.*, **2000**, *29*(1), 105-153.
- [34] Jones, S.; Thornton, J.M. Principles of protein-protein interactions. *Proc. Natl. Acad. Sci. USA*, **1996**, *93*(1), 13-20.
- [35] Carredano, E.; Westerlund, B.; Persson, B.; Saarinen, M.; Ramaswamy, S.; Eaker, D.; Eklund, H. The three-dimensional structures of two toxins from snake venom throw light on the anticoagulant and neurotoxic sites of phospholipase A₂. *Toxicon*, **1998**, *36*(1), 75-92.
- [36] Zhang, H.L.; Xu, S.J.; Wang, Q.Y.; Song, S.Y.; Shu, Y.Y.; Lin, Z.J. Structure of a cardiotoxic phospholipase A₂ from *Ophiophagus hannah* with the "pancreatic loop". *J. Struct. Biol.*, **2002**, *138*(3), 207-215.
- [37] Brunie, S.; Bolin, J.; Gewirth, D.; Sigler, P.B. The refined crystal structure of dimeric phospholipase A₂ at 2.5 Å. Access to a shielded catalytic center. *J. Biol. Chem.*, **1985**, *260*(17), 9742-9749.
- [38] Suzuki, A.; Matsueda, E.; Yamane, T.; Ashida, T.; Kihara, H.; Ohno, M. Crystal structure analysis of phospholipase A₂ from *Trimeresurus flavoviridis* (Habu snake) venom at 1.5 Å resolution. *J. Biochem.*, **1995**, *117*(4), 730-740.
- [39] Zhao, K.; Zhou, Y.; Lin, Z. Structure of basic phospholipase A₂ from *Agkistrodon halys* Pallas: implications for its association, hemolytic and anticoagulant activities. *Toxicon*, **2000**, *38*(7), 901-916.
- [40] Fremont, D.H.; Anderson, D.H.; Wilson, I.A.; Dennis, E.A.; Xuong, N.H. Crystal structure of phospholipase A₂ from Indian cobra reveals a trimeric association. *Proc. Natl. Acad. Sci. USA*, **1993**, *90*(1), 342-346.
- [41] Segelke, B.W.; Nguyen, D.; Chee, R.; Xuong, N.H.; Dennis, E.A. Structures of two novel crystal forms of *Naja naja naja* phospholipase A₂ lacking Ca²⁺ reveal trimeric packing. *J. Mol. Biol.*, **1998**, *279*(1), 223-232.
- [42] Gu, L.; Wang, Z.; Song, S.; Shu, Y.; Lin, Z. Crystal structures of an acidic phospholipase A₂ from the venom of *Naja kaouthia*. *Toxicon*, **2002**, *40*(7), 917-922.
- [43] Jabeen, T.; Sharma, S.; Singh, N.; Singh, R.K.; Kaur, P.; Perbandt, M.; Betzel, Ch.; Srinivasan, A.; Singh, T.P. Crystal structure of a calcium-induced dimer of two isoforms of cobra phospholipase A₂ at 1.6 Å resolution. *Proteins*, **2005**, *59*(4), 856-863.
- [44] Dijkstra, B.W.; Kalk, K.H.; Hol, W.G.J.; Drenth, J. Structure of bovine pancreatic phospholipase A₂ at 1.7 Å resolution. *J. Mol. Biol.*, **1981**, *147*(1), 97-123.
- [45] Lok, S.M.; Gao, R.; Rouault, M.; Lambeau, G.; Gopalakrishnakone, P.; Swaminathan, K. Structure and function comparison of *Micropechis ikaheka* snake venom phospholipase A₂ isoenzymes. *Febs J.*, **2005**, *272*(5), 1211-1220.
- [46] Kini, R.; Evans, H.J. A hypothetical structural role for proline residues in the flanking segments of protein-protein interaction sites. *Biochem. Biophys. Res. Commun.*, **1995**, *212*(3), 1115-1124.
- [47] Lambeau, G.; Ancian, P.; Nicolas, J.P.; Beiboer, S.H.W.; Moinier, D.; Verheij, H.; Lazdunski, M. Structural elements of secretory phospholipases A₂ involved in the binding to M-type receptors. *J. Biol. Chem.*, **1995**, *270*(10), 5534-5540.
- [48] Cupillard, L.; Mulherkar, R.; Gomez, N.; Kadam, S.; Valentin, E.; Lazdunski, M.; Lambeau, G. Both group IB and group IIA secreted phospholipases A₂ are natural ligands of the mouse 180-kDa M-type receptor. *J. Biol. Chem.*, **1999**, *274*(11), 7043-7051.
- [49] Singh, G.; Gourinath, S.; Sarvanan, K.; Sharma, S.; Bhanumathi, S.; Betzel, Ch.; Yadav, S.; Srinivasan, A.; Singh, T.P. Crystal structure of a carbohydrate induced homodimer of phospholipase A₂ from *Bungarus caeruleus* at 2.1 Å resolution. *J. Struct. Biol.*, **2005**, *149*(3), 264-272.
- [50] Perbandt, M.; Wilson, J.C.; Eschenburg, S.; Mancheva, I.; Aleksiev, B.; Genov, N.; Willingmann, P.; Weber, W.; Singh, T.P.; Betzel, Ch. Crystal structure of vipoxin at 2.0 Å: an example of regulation of a toxic function generated by molecular evolution. *Febs Lett.*, **1997**, *412*(3), 573-577.
- [51] Mancheva, I.; Aleksiev, B.; Kleinschmidt, T.; Braunitzer, G. In *Chemistry of Peptides and Proteins*; Voelter W., Bayer E., Ovchinnikov Y., Ivanov V., Eds.; Walter de Gruyter and Co.: Berlin, **1986**; pp. 167-176.
- [52] Aleksiev, B.; Tchobanov, B. Action on phosphatidylcholine of the toxic phospholipase A₂ from the venom of Bulgarian viper (*Vipera ammodytes ammodytes*). *Toxicon*, **1976**, *14*(6), 477-485.
- [53] Wery, J.P.; Schevitz, R.W.; Clawson, D.K.; Bobbitt, J.L.; Dow, E.R.; Gamboa, G.; Goodson Jr., T.; Hermann, R.B.; Kramer, R.M.; McClure, D.B.; Mihelich, E.D.; Putman, J.E.; Sharp, J.D.; Stark, D.H.; Teater, C.; Warrick, M.W.; Jones, N.D. Structure of recombinant human rheumatoid arthritic synovial fluid phospholipase A₂ at 2.2 Å resolution. *Nature*, **1991**, *352*(6330), 79-82.
- [54] Corrêa, L.C.; Marchi-Salvador, D.P.; Cintra, A.C.; Sampaio, S.V.; Soares, A.M.; Fontes, M.R.M. Crystal structure of a myotoxic Asp49-phospholipase A₂ with low catalytic activity: insights into Ca²⁺-independent catalytic mechanism. *Biochim. Biophys. Acta*, **2008**, *1784*(4), 591-599.
- [55] Blinov, N.O.; Tchobanov, B.P.; Grishin, E.V.; Aleksiev, B.V. Neurotoxic action of a protein complex from the venom of the Bulgarian viper (*Vipera ammodytes ammodytes*). *Compt. Rend. Acad. Bulg. Sci.*, **1979**, *32*(1), 663-666.
- [56] Banumathi, S.; Rajashankar, K.R.; Notzel, C.; Aleksiev, B.; Singh, T.P.; Genov, N.; Betzel, Ch. Structure of the neurotoxic complex vipoxin at 1.4 Å resolution. *Acta Crystallogr.*, **2001**, *D57*(11), 1552-1559.
- [57] Chandra, V.; Kaur, P.; Jasti, J.; Betzel, Ch.; Singh, T.P. Regulation of catalytic function by molecular association: structure of phospholipase A₂ from *Daboia russelli pulchella* (DPLA2) at 1.9 Å resolution. *Acta Crystallogr.*, **2001**, *D57*(12), 1793-1798.
- [58] Chandra, V.; Jasti, J.; Kaur, P.; Betzel, Ch.; Srinivasan, A.; Singh, T.P. First structural evidence of a specific inhibition of phospholipase A₂ by alpha-tocopherol (vitamin E) and its implications in inflammation: crystal structure of the complex formed between phospholipase A₂ and alpha-tocopherol at 1.8 Å resolution. *J. Mol. Biol.*, **2002**, *320*(2), 215-222.

- [59] Chandra, V.; Jasti, J.; Kaur, P.; Srinivasan, A.; Betzel, Ch.; Singh, T.P. Structural basis of phospholipase A2 inhibition for the synthesis of prostaglandins by the plant alkaloid aristolochic acid from a 1.7 Å crystal structure. *Biochemistry*, **2002**, *41*(36), 10914-10919.
- [60] Chandra, V.; Jasti, J.; Kaur, P.; Dey, S.; Perbandt, M.; Srinivasan, A.; Betzel, Ch.; Singh, T.P. Crystal structure of a complex formed between a snake venom phospholipase A(2) and a potent peptide inhibitor Phe-Leu-Ser-Tyr-Lys at 1.8 Å resolution. *J. Biol. Chem.*, **2002**, *277*(43), 41079-41085.
- [61] Chandra, V.; Jasti, J.; Kaur, P.; Dey, S.; Srinivasan, A.; Betzel, Ch.; Singh, T.P. Design of specific peptide inhibitors of phospholipase A2: structure of a complex formed between Russell's viper phospholipase A2 and a designed peptide Leu-Ala-Ile-Tyr-Ser (LAIYS). *Acta Crystallogr.*, **2002**, *D58*(10-2), 1813-1819.
- [62] Magro, A.J.; Murakami, M.T.; Marcussi, S.; Soares, A.M.; Arni, R.K.; Fontes, M.R.M. Crystal structure of an acidic platelet aggregation inhibitor and hypotensive phospholipase A₂ in the monomeric and dimeric states: insights into its oligomeric state. *Biochem. Biophys. Res. Commun.*, **2004**, *323*(1), 24-31.
- [63] Andrião-Escarso, S.H.; Soares, A.M.; Fontes, M.R.M.; Fuly, A.L.; Corrêa, F.M.A.; Rosa, J.C.; Greene, L.J.; Giglio J.R. Structural and functional characterization of an acidic platelet aggregation inhibitor and hypotensive phospholipase A(2) from *Bothrops jararacussu* snake venom. *Biochem. Pharmacol.*, **2002**, *64*(4), 723-732.
- [64] Magro, A.J.; Takeda, A.A.; Soares, A.M.; Fontes, M.R.M. Structure of BthA-I complexed with p-bromophenacyl bromide: possible correlations with lack of pharmacological activity. *Acta Crystallogr.*, **2005**, *D61*(12), 1670-1677.
- [65] Kini, R.M.; Evans, H.J. A model to explain the pharmacological effects of snake venom phospholipases A2. *Toxicon*, **1989**, *27*(6), 613-635.
- [66] Soares, A.M.; Giglio, J.R. Chemical modifications of phospholipases A2 from snake venoms: effects on catalytic and pharmacological properties. *Toxicon*, **2003**, *42*(8), 855-868.
- [67] Rigden, D.J.; Hwa, L.W.; Marangoni, S.; Toyama, M.H.; Polikarpov, I. The structure of the D49 phospholipase A2 piratoxin III from *Bothrops pirajai* reveals unprecedented structural displacement of the calcium-binding loop: possible relationship to cooperative substrate binding. *Acta Crystallogr.*, **2003**, *D59*(2), 255-262.
- [68] Tang, L.; Zhou, Y.C.; Lin, Z.J. Structure of agkistrodotoxin in an orthorhombic crystal form with six molecules per asymmetric unit. *Acta Crystallogr.*, **1999**, *D55*(12), 1986-1996.
- [69] Marchi-Salvador, D.P.; Corrêa, L.C.; Magro, A.J.; Oliveira, C.Z.; Soares, A.M.; Fontes, M.R.M. Insights into the role of oligomeric state on the biological activities of crotoxin: crystal structure of a tetrameric phospholipase A₂ formed by two isoforms of crotoxin B from *Crotalus durissus terrificus* venom. *Proteins*, **2008**, *72*(3), 883-891.
- [70] Janin, J.; Miller, S.; Chothia, C. Surface, subunit interfaces and interior of oligomeric proteins. *J. Mol. Biol.*, **1988**, *204*(1), 155-164.
- [71] Miller, S. The structure of interfaces between subunits of dimeric and tetrameric proteins. *Protein Eng.*, **1989**, *3*(2), 77-83.
- [72] Krissinel, E.; Henrick, K. Inference of macromolecular assemblies from crystalline state. *J. Mol. Biol.*, **2007**, *372*(3), 774-797.
- [73] Nooren, I.M.A.; Thornton, J.M. Structural characterization and functional significance of transient protein-protein interactions. *J. Mol. Biol.*, **2003**, *325*(5), 991-1018.
- [74] Chothia, C.; Gough, J.; Vogel, C.; Teichmann, S.A. Evolution of the protein repertoire. *Science*, **2003**, *300*(5626), 1701-1703.
- [75] Long, M.; Betrán, E.; Thornton, K.; Wang, W. The origin of new genes: glimpses from the young and old. *Nat. Rev. Genet.*, **2003**, *4*(11), 865-875.